

# The role of CIZ1 in quiescence

Olivia Grace Dobbs

PhD

University of York

Biology

June 2022

## Abstract

Mammalian cells have developed various mechanisms in order to protect themselves from damage. This includes exit from the cell cycle into a non-dividing, paused state referred to as quiescence. Quiescence is a reversible, stress-resistant state and an essential part of our physiology, with errors in its establishment linked to multiple pathologies.

Recent work has shown that the Cip1-interacting zinc finger protein 1 (CIZ1) forms RNA-dependent protein assemblies that stabilise epigenetic state at the inactive X chromosome (Xi). Loss of CIZ1 manifests as hyperproliferative lymphoid lineages in female mice, with primary embryonic fibroblasts demonstrating loss of H3K27me3 and H2AK119Ub1 at the Xi, and dispersal of the long non-coding RNA *Xist*.

Here, I show that H4K20me1 is also depleted at the Xi in female CIZ1-null cells and extend the analysis to show nucleus-wide depletion of H4K20me1 in males and females. This underpins an aberrant response of primary cell populations to quiescence triggers, via compromised nuclear condensation. Global transcriptional repression remained intact, however, a subset of genes linked with chromatin condensation and homology directed repair were perturbed. In the absence of CIZ1, nuclear decondensation upon re-entry to the cell cycle remained functional. Repeated entry and exit cycles gave rise to expanded nuclei susceptible to mechanical stress and exhibited DNA damage checkpoint activation. Together, the data show that CIZ1 is required for H4K20me1-dependent condensation and protects against aberrant nuclear expansion and instability during quiescence cycles.

Finally, in a separate but related project, I have developed an *in vitro* assay to study the requirements for CIZ1 retention at the Xi. Preliminary data shows that endogenous RNase activity and ATP hydrolysis are both required to separate and disperse CIZ1 particles from the Xi. It is hypothesised that retention of CIZ1 (and *Xist*) at the Xi is modulated through a balance of kinase and phosphatase activity.

# Table of Contents

<b>Abstract</b> .....	<b>2</b>
<b>List of Tables</b> .....	<b>8</b>
<b>List of Figures</b> .....	<b>9</b>
<b>List of Appendices</b> .....	<b>11</b>
<b>Acknowledgments</b> .....	<b>12</b>
<b>Declaration</b> .....	<b>13</b>
<b>1 Introduction</b> .....	<b>14</b>
<b>1.1 The cell cycle and quiescence</b> .....	<b>15</b>
1.1.1 Cell cycle control and arrest.....	15
1.1.2 Quiescence .....	16
1.1.3 Biological markers of quiescence.....	17
<b>1.2 Gene expression changes during quiescence entry</b> .....	<b>17</b>
1.2.1 Core quiescence program .....	18
1.2.2 The DREAM complex.....	20
1.2.3 Epigenetic status in quiescence .....	21
1.2.4 Other post-transcriptional controls .....	22
<b>1.3 Chromatin changes during quiescence entry</b> .....	<b>23</b>
1.3.1 Nuclear reorganisation and chromosome positioning .....	24
1.3.2 The condensin complex .....	25
1.3.3 H4K20 methylation and condensation.....	27
1.3.4 Quiescence and disease .....	29

<b>1.4</b>	<b>Cip1-interacting zinc finger protein 1 (CIZ1)</b>	<b>31</b>
1.4.1	The inactive X chromosome	32
1.4.2	Localisation of CIZ1 in the cell	32
1.4.3	Alternative splicing of CIZ1	33
1.4.4	CIZ1 and disease	33
<b>1.5</b>	<b>CIZ1 and quiescence</b>	<b>34</b>
<b>1.6</b>	<b>Project aims</b>	<b>36</b>
<b>2</b>	<b>Materials and Methods</b>	<b>37</b>
<b>2.1</b>	<b>Cell culture</b>	<b>37</b>
2.1.1	Cell lines	37
2.1.2	Cell maintenance	37
2.1.3	Quiescence	39
2.1.4	Detection of foci formation	39
2.1.5	Cell viability	39
2.1.6	Inhibitors	40
2.1.7	Nuclear fragility	40
<b>2.2</b>	<b>Immunofluorescence</b>	<b>40</b>
2.2.1	Detection of EdU	41
2.2.2	Permeabilised cell CIZ1 release assay	41
<b>2.3</b>	<b>Imaging</b>	<b>41</b>
2.3.1	Nuclear area and intensity analysis	41
2.3.2	Dispersal analysis	42
2.3.3	Detailed steps for Fiji analysis	42

<b>2.4</b>	<b>Western blot .....</b>	<b>43</b>
2.4.1	Whole cell lysate generation .....	43
2.4.2	Subcellular fractionation .....	43
2.4.3	Immunoprecipitation .....	43
2.4.4	Western blot analysis .....	44
2.4.5	Western blot quantification .....	44
<b>2.5</b>	<b>Graphical presentation and statistical analysis .....</b>	<b>44</b>
<b>2.6</b>	<b>Transcriptomic analysis .....</b>	<b>46</b>
2.6.1	RNA Extraction .....	46
2.6.2	Sample preparation .....	46
2.6.3	Transcriptome assembly .....	47
2.6.4	Analysis of WT and CIZ1-null genomes during quiescence entry .....	47
<b>3</b>	<b>Gene expression changes during entry to quiescence ...</b>	<b>48</b>
<b>3.1</b>	<b>Introduction .....</b>	<b>48</b>
<b>3.2</b>	<b>Aims .....</b>	<b>48</b>
<b>3.3</b>	<b>Experimental design .....</b>	<b>49</b>
<b>3.4</b>	<b>Results .....</b>	<b>49</b>
3.4.1	Murine core quiescence program .....	49
3.4.2	Changes in global gene expression on entry to quiescence are not dependent on CIZ1 .....	55
3.4.3	CIZ1-dependent genes during quiescence entry .....	58
3.4.4	DNA repair and chromatin organisation genes .....	65
<b>3.5</b>	<b>Discussion .....</b>	<b>70</b>

<b>4</b>	<b>CIZ1-dependent chromatin condensation during quiescence entry .....</b>	<b>72</b>
4.1	Introduction .....	72
4.2	Aims .....	73
4.3	Experimental design .....	74
4.4	Results .....	75
4.4.1	Chromatin condensation on entry to quiescence is impaired in CIZ1-null cells .....	75
4.4.2	Reduced H4K20me1 in CIZ1-null cells .....	80
4.4.3	Manipulation of WT and CIZ1-null cells to investigate the role of CIZ1 and H4K20 methylation in chromatin condensation during quiescence entry..	84
4.4.4	Overexpansion of CIZ1-null nuclei over multiple rounds of quiescence entry and exit.....	89
4.4.5	CIZ1-null cells are more susceptible to cell death upon serum withdrawal... ..	91
4.4.6	Generation of fragile CIZ1-null nuclei.....	93
4.5	Discussion.....	96
4.5.1	Activation of the DNA damage response .....	97
4.5.2	Chromatin condensation .....	98
4.5.3	H4K20 methylation .....	99
<b>5</b>	<b>Dispersal of CIZ1-Xi assemblies: an <i>in vitro</i> assay.....</b>	<b>101</b>
5.1	Introduction .....	101
5.2	Aims .....	102
5.3	Experimental design and assay development .....	102

<b>5.4</b>	<b>Results</b> .....	<b>104</b>
5.4.1	Requirements for CIZ1 dispersal.....	104
5.4.2	Xi chromatin remains localised.....	106
5.4.3	Titration of NaCl to refine the CIZ1 release assay .....	108
5.4.4	Extraction of putative catalytic ACP5 between 200-300mM NaCl.....	109
5.4.5	CIZ1 and ACP5 interaction.....	112
<b>5.5</b>	<b>Discussion</b> .....	<b>114</b>
<b>6</b>	<b>Discussion</b> .....	<b>117</b>
<b>6.1</b>	<b>CIZ1 as a protector of the epigenome</b> .....	<b>117</b>
6.1.1	Misbalance of histone modifiers .....	118
<b>6.2</b>	<b>The implication of chromatin condensation in disease</b> .....	<b>119</b>
<b>6.3</b>	<b>Clinical application</b> .....	<b>120</b>
<b>6.4</b>	<b>Final remarks</b> .....	<b>121</b>
<b>Appendix A</b>	.....	<b>122</b>
<b>Appendix B</b>	.....	<b>141</b>
<b>Appendix C</b>	.....	<b>161</b>
<b>Abbreviations</b>	.....	<b>162</b>
<b>References</b>	.....	<b>165</b>

## List of Tables

Table 2.1.	List of primary cell populations and cell lines.....	38
Table 2.2.	Antibodies used for immunofluorescence and Western blot.....	45
Table 3.1.	GSEA of murine core quiescence genes.....	53
Table 3.2.	GSEA of human core quiescence genes.....	53
Table 3.3.	GSEA of genes present in both human and murine core quiescence programs. ....	54
Table 3.4.	Core set of DREAM complex target genes that are inappropriately downregulated during quiescence entry in CIZ1-null cells. ....	61

## List of Figures

Figure 1.1.	Illustration of the cell cycle.....	16
Figure 1.2.	The DREAM complex. ....	20
Figure 1.3.	Methylation status of H4K20.....	22
Figure 1.4.	The condensin complexes. ....	26
Figure 1.5.	Summary of three key cellular changes during the reversible quiescence transition.....	28
Figure 1.6.	Consequences of imbalance between a cycling and quiescent state.....	30
Figure 1.7.	Murine CIZ1 schematic.....	31
Figure 1.8.	CIZ1-dependent quiescence.....	35
Figure 3.1.	Murine core quiescence genes (mCQG). ....	50
Figure 3.2.	Comparison of the human and murine quiescence programs. ....	52
Figure 3.3.	Transcriptomic analysis during entry to quiescence.....	57
Figure 3.4.	A subset of DREAM complex target genes are modulated by CIZ1.....	60
Figure 3.5.	Expression changes for the 33 I-DN DREAM complex target genes during quiescence entry. ....	64
Figure 3.6.	Elevated expression of chromatin condensation genes. ....	67
Figure 3.7.	Increased solubility of SMC2 and SMC4 in CIZ1-null cells.....	69
Figure 4.1.	Fiji analysis workflow. ....	74
Figure 4.2.	WT and CIZ1-null cells have a reduced S phase index following 24-hour SW. ....	75
Figure 4.3.	Nuclei from CIZ1-null cells fail to condense during entry to quiescence.	78
Figure 4.4.	WT and CIZ1-null nuclear area changes in response to contact inhibition. ....	79
Figure 4.5.	Loss of H4K20me1 assemblies at the Xi in female CIZ1-null PEFs. ....	81

Figure 4.6.	Global depletion of H4K20me1 in CIZ1-null PEFs.....	83
Figure 4.7.	Induction of GFP-CIZ1 in CIZ1-null PEFs.....	85
Figure 4.8.	H4K20me1-dependent chromatin condensation following SW.....	88
Figure 4.9.	Aberrant decondensation of CIZ1-null nuclei.....	90
Figure 4.10.	Cell viability over multiple rounds of SW and AB. ....	92
Figure 4.11.	Fragility and checkpoint activation upon AB in CIZ1-null cells.....	94
Figure 4.12.	Extended contact inhibition strategy. ....	95
Figure 5.1.	<i>In vitro</i> dispersal of CIZ1.....	103
Figure 5.2.	Dispersal of CIZ1 requires RNase activity and is an energy driven process. .....	105
Figure 5.3.	CIZ1 disperses away from Xi chromatin. ....	107
Figure 5.4.	CIZ1 disperses at 300mM NaCl.....	108
Figure 5.5.	Extractability of CIZ1 and ACP5. ....	111
Figure 5.6.	CIZ1 and ACP5 interaction studies.....	113

## List of Appendices

### Appendix A

PDF of peer-reviewed book chapter.

**Dobbs OG** and Coverley D. (2022) Chromatin Dynamics During Entry to Quiescence and Compromised Functionality in Cancer Cells. In Kloc M, Kubiak JZ (editors), Nuclear, Chromosomal, and Genomic Architecture in Biology and Medicine.

### Appendix B

PDF of manuscript currently in the submission process.

**Dobbs OG**, Wilson RHC, Newling K, Ainscough JFX, Coverley D. Epigenetic instability caused by absence of CIZ1 drives transformation during quiescence cycles. 2022.

### Appendix C

Gene lists generated from transcriptomic analysis.

## Acknowledgments

What an incredible experience these past 5 years have been! It's certainly been difficult but whilst I sit here reflecting on my PhD and all the people I have to thank for helping me through to the end, the highs definitely outweigh the lows.

Firstly, I would like to thank my supervisor, Dawn, for your endless support and encouragement since day one. Thank you for your advice throughout the years and the opportunities you have offered me, it has truly been inspiring to work alongside you. Thank you to the BBSRC for funding this PhD, my co-supervisor, Darren Goffin, and TAP member, Nia Bryant, for your advice and support as well as many others in the department who have helped me with different strands of work. I would also like to thank Justin Ainscough for the cells used in my work, your help and advice and for the cider supplies! Also, thank you to other members of the Coverley lab, Emma, Louisa, Gaby, Lewis and Elena for making the lab a fun work environment filled with coffee, trips to Browns and wordle competitions! Emma, thank you for putting up with me since the beginning and for repeatedly telling me everything will be ok. Louisa, thank you for the laughs, the hugs and your help both in and out of the lab. Finally to my lab sister, Gaby. I feel so sorry for everyone who has to listen to our conversations! I'm not sure how I would have made it through without you, thank you for always being there.

Thank you to the York gals, Jess, Annie, Grace and Sarah. I could not have wished for a better group of girls to spend these last few years with, from our extended lunch breaks to taking over the dancefloor in Flares. We've certainly got lots of memories! A special mention to Jess for being my partner in crime during our write up, bring on travelling! Thank you to Becky for being the most supportive best friend, my flatmate Emily for the tv and gin nights and to all my other friends who have supported me along the way.

My final thank you goes to my family. You all mean so much to me and I can't thank you enough for your love and support. Thank you for being my biggest cheerleaders and for giving me the confidence and motivation to finish. To my mum and dad, I would not have achieved any of this without you, thank you. I also have to give a special thank you to Dennis and Daisy for all the cuddles!

I would like to dedicate my thesis to my Grandad, who we sadly lost during the pandemic. You are loved and sorely missed.

## Declaration

I declare that this thesis is a presentation of original work and I am the sole author. This work has not previously been presented for an award at this, or any other, University. All sources are acknowledged as References.

Text and figures contained in Chapter 1 are part of a peer-reviewed review article where I am primary author.

**Dobbs OG** and Coverley D. (2022) Chromatin Dynamics During Entry to Quiescence and Compromised Functionality in Cancer Cells. In Kloc M, Kubiak JZ (editors), Nuclear, Chromosomal, and Genomic Architecture in Biology and Medicine

Text, figures and tables contained in Chapter 2,3 and 4 and excel files contained in Appendix C are part of a manuscript currently in the submission process where I am primary author.

**Dobbs OG**, Wilson RHC, Newling K, Ainscough JFX, Coverley D. Epigenetic instability caused by absence of CIZ1 drives transformation during quiescence cycles. 2022

My contributions to these publications have been reproduced in full.

All work generated by other authors, including data from Rosemary Wilson in Chapter 1, is explicitly stated throughout.

# 1 Introduction

Accurate cell cycle regulation is essential for maintaining tissue homeostasis and preventing disease with both too little and too much proliferation having catastrophic consequences. In fact, the majority of cells in the human body are not actively cycling but in a poised, non-proliferating state known as quiescence. It is the reversibility of quiescence that is essential for maintaining tissue homeostasis, making it a highly controlled cellular state, with a range of factors determining entry and exit. Imbalances in the transition between proliferation and quiescence in multicellular organisms can underlie a range of diseases, including excess proliferation associated with cancer (Cho et al., 2019), as well as too little proliferation that may result in cell loss and accelerated ageing and degeneration (Pack et al., 2019). As quiescence is an essential part of our normal physiology, it is important to understand the mechanisms controlling successful quiescence entry and exit and what happens when these processes go wrong.

The main focus of this thesis is to understand the quiescence transition in relation to the Cip1-interacting zinc finger protein 1 (CIZ1). CIZ1 has been associated with various pathologies, including cancer, and previous work from the Coverley lab has begun to suggest a role in the maintenance of quiescence.

This introduction will discuss several of the main cellular changes that occur during the transition to a quiescent state including global changes in gene expression and chromatin state. My research provides mechanistic insight into how CIZ1 is required for an accurate response to quiescence triggers through maintenance of the epigenetic state.

The majority of this introduction is currently in press as a peer-reviewed review article for the Springer Nature volume "Nuclear, chromosomal and genomic architecture in biology and medicine."

## 1.1 The cell cycle and quiescence

The cell cycle is a complex, highly regulated process which results in a parent cell forming two identical daughter cells. It is divided into five phases; G1, S, G2 and M, and the paused state G0, also known as quiescence (Schafer, 1998). Interphase includes G1, where cells prepare for DNA synthesis, S-phase, where the cell replicates its DNA, and the final phase G2, where the cell prepares for mitosis (Figure 1.1). Multiple, well studied control mechanisms regulate the transition between stages and the proliferation status of the cell. Cell cycle control is an important research area in relation to cancer biology (Hartwell and Kastan, 1994).

### 1.1.1 Cell cycle control and arrest

Progression through the cell cycle is controlled through the expression of cyclins, cyclin-dependent kinases (CDKs) and CDK-inhibitors (CDKIs) (Bloom and Cross, 2007, Massagué, 2004). CDKs are activated by cyclins, whose expression is controlled to allow timely function. Cyclin D is responsible for activation of CDK4/6 to allow the cell to transition from G1 to S phase (Sherr and Roberts, 2004, Morgan, 1997). Phosphorylation of the retinoblastoma protein (pRb) by CDK4/6 must occur in G1 to allow activation of E2F and therefore activation of E2F-regulated genes (Topacio et al., 2019, Bertoli et al., 2013). This also leads to expression of cyclin E that interacts with CDK2 initiating DNA replication. Cyclin A expression begins in S phase followed by cyclin B that associates with CDK1 to initiate mitosis. The activity of CDKs is also managed via CDKIs, that bind to cyclin/CDK complexes, inhibiting their function and preventing cell cycle progression (Amani et al., 2021, Pavletich, 1999).

As the cell passes through the cell cycle it encounters several cell cycle checkpoints. These enable the cell to assess whether any damage has occurred before replication (G1/S checkpoint), division (G2/M checkpoint) or to ensure successful spindle attachment (Mitotic spindle checkpoint) (Barnum and O'Connell, 2014). One way the cell has adapted to avoid over-proliferation, is to exit the cell cycle and enter a reversible, non-proliferating quiescent state (Coller et al., 2006). Typically, this is expected to happen after exit from mitosis in early/mid G1 before the restriction point (Pardee, 1974). The restriction point is known as a critical decision point before commitment to the cell cycle and once passed the cell no longer requires mitogenic stimulation. However, it is also believed that entry to quiescence can occur at other times throughout the cell cycle in response to stress. Cell types that can exit the cell cycle outside of G1 include multiple yeast strains (Laporte et al., 2011, Costello et al., 1986, Takeo et al., 1995), stem cells (Sutcu and Ricchetti, 2018) and cancer cells (Pearl Mizrahi et al., 2016, Drewinko et al., 1984). Other models suggest that when a cell exits mitosis they exist as two

subpopulations, with the decision to start the next cell cycle depending on CDK2 activity and the CDKI p21. This challenges the viewpoint that CDK2 is activated during G1 and that cells will pass through the restriction point depending on nutrient availability. Instead, it proposes that a cell's commitment is inherited from the previous cell cycle depending on CDK2 levels (Moser et al., 2018, Spencer et al., 2013). Other mechanisms of growth arrest include terminal differentiation and senescence. The main difference between these states and quiescence is the ability of a quiescent cell to re-enter the cell cycle (Pack et al., 2019).

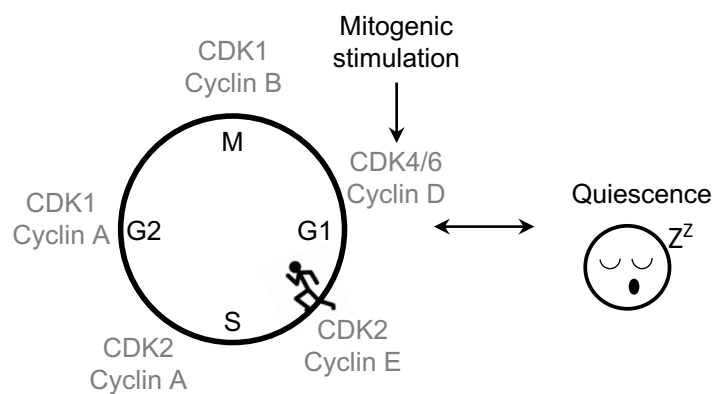


Figure 1.1. **Illustration of the cell cycle.** Activation of CDKs via cyclins is essential for cell cycle progression, annotated here at each stage. In unfavourable growth conditions, cells can exit the cell cycle and enter the reversible state, quiescence.

### 1.1.2 Quiescence

Quiescence is described as a reversible, non-proliferating cellular state (Coller et al., 2006). It is a stress-resistant state in which chromatin is compacted and gene expression suppressed, as cells exit the cell cycle. In the body, most cells are found in the quiescent state with some cell types undergoing multiple rounds of entering and exiting the cell cycle for example, fibroblasts in the process of tissue repair, lymphocytes as part of the immune response, and stem cells. The reversibility of quiescence is essential for maintaining tissue homeostasis (Yao, 2014). The transition between an active, proliferating state and quiescence is the main focus of this project.

### 1.1.3 Biological markers of quiescence

A quiescent cell is mostly recognised by what it doesn't do rather than having a distinct trait itself. For example, a quiescent cell can be identified via its inability to synthesise DNA, as it has exited the cell cycle. This can be experimentally shown by a low/negative signal for fluorescently labelled nucleotides, BrdU/EdU, which are usually incorporated into newly synthesized DNA during S phase. Quiescent cells also have reduced levels of total RNA due to decreased gene expression. Levels of cell cycle regulators can also be monitored, for example, a quiescent population will exhibit reduced CDK activity and perhaps elevated levels of CDKIs (Mitra et al., 2018).

## 1.2 Gene expression changes during quiescence entry

The prevailing view of quiescence is as a dormant phase of the cell cycle with little activity. However, recent advances have altered this view of the quiescent state to one that is actively regulated to allow for rapid re-entry to the cell cycle when needed. Transcriptional profiling studies have been conducted to follow the changes in gene expression that occur during entry to quiescence and, therefore, better our understanding of this “resting” cellular state.

As expected, when a cell exits the cell cycle, there is a global suppression of cell cycle genes (Coller et al., 2006, Cheung and Rando, 2013). These include cyclin A2, cyclin B, cyclin E2, and survivin, as well as genes involved in DNA replication to ensure a halt to cell cycle progression. Quiescent cells also exhibit a low metabolic activity; therefore genes relating to mitochondrial function are downregulated (Cheung and Rando, 2013). Despite quiescent cells being recognised for what they do not do, studies into quiescence are beginning to show that it remains an active state with upregulation of gene sets involved in transcriptional regulation and stem cell fate decisions (Cheung and Rando, 2013, Cho et al., 2019). Transient upregulation of stress-related genes is also seen upon entry to quiescence before becoming repressed, enabling a successful response to the quiescent trigger. Interestingly, the corresponding proteins remain at a high level despite eventual gene repression (Marguerat et al., 2012).

Using a yeast model, studies have quantified the transcriptome and proteome of proliferating and quiescent populations. They revealed that quiescent *Schizosaccharomyces pombe* (*S. pombe*) cells have a smaller transcriptome compared to cells that were cycling but the proteome remained at a similar size. Even though comparable in size, the proteome in quiescent cells is remodelled in a way that reflects the change in gene expression and is adapted for maintenance rather than cell growth (Marguerat et al., 2012). While most studies focus on the widespread repression of

transcription during quiescence entry and the downregulation of essential genes involved in proliferation, translation, and metabolite biogenesis, it is clear that the transition to quiescence is not a simple shut down. Quiescent cells need to have a basal level of transcription in order to survive, and active regulation is required to maintain the quiescent cell in a state that is ready to re-enter the cell cycle when instructed (Marguerat et al., 2012, McKnight et al., 2015, Roche et al., 2017).

### **1.2.1 Core quiescence program**

As exit from the cell cycle can be initiated by a range of different triggers, one question that surrounds quiescence is whether one or multiple quiescent states exist. By distinguishing whether a gene expression change is the result of the specific trigger instructing cell cycle arrest or central to quiescence itself will help understand the functionality of quiescent cells.

To begin to address this, some studies have compared quiescence triggers and profiled the expression changes that occur. In human fibroblasts, the initial gene expression changes are dependent on the trigger (serum starvation or contact inhibition), but the changes have common functions that are essential to quiescence entry, such as downregulation of pro-proliferation genes. This suggests that each trigger is capable of creating a subtly different quiescent state, possibly resulting in a heterogeneous quiescent population (Coller et al., 2006, Yao, 2014). Cells that remain in quiescence for a long period of time enter what is known to be a deeper quiescent state. Deep quiescent populations can still return to the cell cycle but often take longer due to a decreased sensitivity to the relevant triggers. The Rb-E2F network acts as a bistable switch which can be monitored to determine quiescence depth with deeper quiescence associated with a higher E2F-switching threshold (Yao et al., 2008, Kwon et al., 2017). Adult neural stem cells (NSCs) also demonstrate a range of quiescent states. A deeper, dormant quiescent state and a primed quiescent state have been modelled based on whether the cells receive BMP or BMP/FGF treatment, respectively. These two states have distinct signalling pathways and transcriptional programs with an increase in the LRIG1 protein evident in the primed quiescent state. This data suggests that the level of LRIG1 expression is an important regulator of the transition between the cell cycle and quiescence in NSCs (Marqués-Torrejón et al., 2021).

Focussing on the serum starvation method, 135 serum deprivation early response genes (SDERGs) have been identified in human fibroblasts. These include two tumour suppressor genes, SALL2 and MXI1, that also have a unique role in regulating other SDERGs. Silencing of these two genes during quiescence entry results in failed cell cycle exit and continued progression of the cell cycle (Liu et al., 2007), evidencing a clear hierarchy.

Following such initial signal-dependent changes, cells eventually develop a common quiescence programme. This is a set of gene expression changes vital to the maintenance of the long-term quiescent state and is not specific to the initial trigger. The quiescence program includes genes involved in the regulation of cell growth and division, suppression of apoptosis, suppression of differentiation, and intercellular communication. These are candidate genes that could be required for maintaining cells in a reversible, viable arrested state (Coller et al., 2006, Liu et al., 2007). What is becoming clear is that different genes are involved in the transition to quiescence compared to the maintenance of the quiescent state.

### 1.2.2 The DREAM complex

Repression of cell cycle genes is essential for quiescence entry and requires strict regulation. The dimerization partner, RB-like, E2F, and multi-vulval class B (DREAM) complex is best known for its role in quiescent cells where it is involved in the repression of pro-proliferation genes (Sadasivam and DeCaprio, 2013).

The DREAM complex is made up of a MuvB core complex along with the additional subunits p130 or p107, E2F4/E2F5, and dimerization partner 1 (DP1) (Figure 1.2). The MuvB core consists of five MuvB-like proteins; LIN9, LIN37, LIN52, LIN54, and RBBP4. Phosphorylation of the LIN52 subunit at Ser28 by the kinase DYRK1A is needed for binding of p130/E2F4 to the MuvB core and subsequent assembly of the DREAM complex (Litovchick et al., 2011). In other stages of the cell cycle, the MuvB core can assemble and function with other transcription factors such as BMYB and FOXM1 (Sadasivam and DeCaprio, 2013). The balance between different complex assemblies in response to proliferative/anti-proliferative triggers determines DREAM complex activity and the extent to which it can repress cell-cycle genes by binding to CHR promoter elements (Müller and Engeland, 2010, Müller et al., 2014) and E2F target genes (Litovchick et al., 2007).

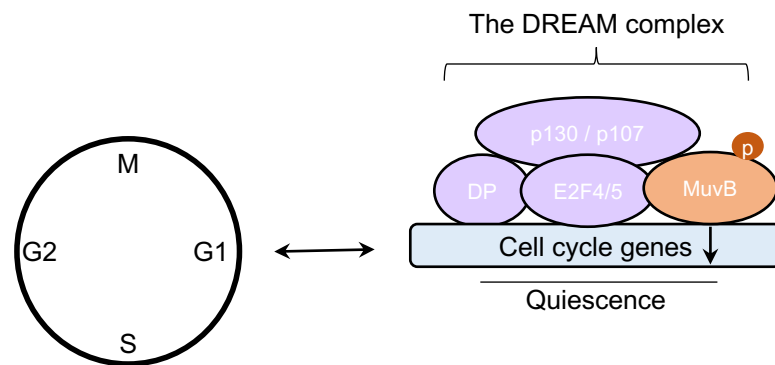


Figure 1.2. **The DREAM complex.** To enable quiescence entry, the MuvB core (orange) associates with the additional subunits; p130 or p107, E2F4/5 and DP. This complex is responsible for the repression of cell cycle genes on entry to quiescence.

### 1.2.3 Epigenetic status in quiescence

The methylation status of DNA and post-translational modification of histones determine chromatin state. Whether it is in a receptive conformation for transcription factor binding and transcriptional activation or a closed conformation resulting in transcriptional suppression. Thus, chromatin state in quiescence requires consideration.

DNA methylation occurs at cytosines in CpG sequences and plays an important role in mammalian development by modulating gene expression, typically suppressing it. However, in human fibroblasts, constant levels of DNA methylation are observed through all phases of the cell cycle, with no global changes evident in the quiescent state (Vandiver et al., 2015). Similarly, no difference in CpG methylation was observed between naive and activated T cells, further supporting the hypothesis that DNA methylation is not significantly altered in quiescence (Rawlings et al., 2011).

In contrast, specific histone post-translational modifications (PTMs) have been linked with the quiescent state and have been extensively reviewed (Bonitto et al., 2021). Most notably, on entry to quiescence, *Saccharomyces cerevisiae* (*S. cerevisiae*) exhibit a global reduction in histone acetylation as the lysine deacetylase, Rpd3, targets gene promoters of at least 50% of genes, resulting in their hypoacetylation and repression (McKnight et al., 2015). Moreover, while similar levels of H3K4me2, H3K36me2, and H3K36me3 were observed between proliferating and quiescent yeast cell populations, H3K4me3 falls upon quiescence entry. As H3K4me3 is associated with active chromatin this is not surprising, though it is also worth noting that even in quiescent cells, H3K4me3 levels are still relatively high, suggesting that features associated with transcriptionally active chromatin remain (Young et al., 2017).

In human cells, the picture is still emerging. While similar global levels of histone methylation were observed between proliferating and quiescent fibroblasts (Everitts et al., 2013), in lymphocytes and hair follicle stem cells, quiescence coincided with reduced levels of H3 lysine methylation (Baxter et al., 2004, Lee et al., 2016).

One histone PTM that is highly dynamic through the cell cycle, and attracting investigation in the context of quiescence, is methylation of histone H4 at lysine 20 (H4K20). H4K20 can exist without methylation or in a mono-, di-, or tri-methylated state, with the di- and tri- modifications dependent on the presence of monomethylation (Oda et al., 2009). Several methyltransferases have been associated with the methylation status of H4K20 including SET8 (also known as PR-Set7) responsible for H4K20me1, SUV4-20H1 responsible for H4K20me2 and SUV4-20H2 responsible for H4K20me3

(Fang et al., 2002, Schotta et al., 2004). There are currently no known demethylases for the di- and tri- methylated state, however the demethylase, PHF8, is responsible for removal of H4K20me1 (Liu et al., 2010) (Figure 1.3). H4K20me2 is present throughout the cell cycle and is the most abundant state, with H4K20me1 and H4K20me3 present at much lower levels (Pesavento et al., 2008). H4K20me1 levels fluctuate throughout the cell cycle, with the highest levels in the G2/M phase, while H4K20me3 is associated with quiescence, heterochromatic regions, and transcriptional silencing. The upregulation of H4K20me3 was found to be the most widespread change in histone modification status in quiescent human fibroblasts (Evertts et al., 2013, Jørgensen et al., 2013). Regulation of H4K20 methylation has been associated with the fidelity of the quiescence transition for both skeletal muscle stem cells (MuSCs) and NSCs. Suv4-20h1 KO mouse models demonstrate the importance of Suv4-20h1 in maintaining quiescence, with activation of MuSCs leading to eventual stem cell depletion and impaired muscle regeneration (Boonsanay et al., 2016). Conversely, SET8 is required for NSC reactivation in *Drosophila*, with loss of function delaying the transition back into cycle through decreased expression of Cdk1 and the Wnt pathway transcriptional co-activator, Ebd1 (Huang et al., 2021).

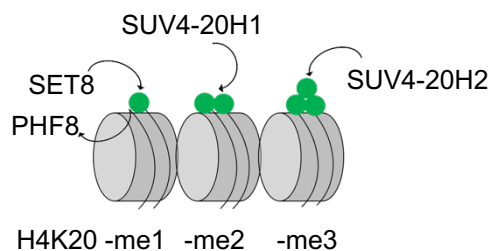


Figure 1.3. **Methylation status of H4K20.** H4K20 can exist as an unmethylated state or in a mono-, di- or tri- methylated state. The methyltransferases associated with each state are SET8, SUV4-20H1 and SUV4-20H2 for mono-, di- and trimethylation respectively. PHF8 is the demethylase associated with H4K20me1.

#### 1.2.4 Other post-transcriptional controls

Additional mechanisms implicated in differential regulation of gene expression in quiescence include RNA stability, expression and function of specific microRNAs, and RNA polymerase II (RNA Pol II). RNA Pol II remains relatively high in quiescent cells, but levels of the initiating and elongating forms become depressed (Young et al., 2017).

Several microRNAs, non-coding RNA molecules that can bind to mRNAs, have been linked with entry to quiescence. For example, miR-29 is downregulated resulting in

increased expression of its target genes, including those that code for extracellular matrix proteins (Suh et al., 2012). Another microRNA, miR-489, is upregulated in quiescent muscle stem cells and prevents cell proliferation by targeting the oncogene Dek mRNA (Cheung et al., 2012). Thus, microRNAs have been linked with both the maintenance of the quiescent state and the prevention of uncontrolled exit.

The widely accepted global reduction in RNA levels in quiescent cells disguises the fact that many RNAs are still highly expressed. This reflects a combination of active transcription and an increase in RNA stability. In fact, quiescent cells can store important RNAs that are vital to their survival when transcribed during active proliferation or the transition to the quiescent state (Young et al., 2017). Extracellular matrix organisation genes are among those that have increased stability in quiescent human fibroblasts compared to proliferating fibroblasts (and which are also upregulated) (Johnson et al., 2017).

The diverse mechanisms that regulate gene expression in quiescent cells, the sequestration of RNA as well as the histone modifications associated with active transcription, suggest that quiescent cells are in a poised state and are adapted for a quick response to environmental change, ensuring tissue homeostasis.

### **1.3 Chromatin changes during quiescence entry**

Packaging of chromatin in the nucleus is highly versatile and in quiescent cells exists in a compact, condensed form that appears different to interphase (Tokuyasu et al., 1968). Changes have been seen in both the facultative heterochromatin, which can adapt between active euchromatin and condensed heterochromatin, and in gene-poor constitutive heterochromatin (Grigoryev et al., 2004). Moreover, the spatial organisation of chromatin in the nucleus is not random and adopts configurations that are specific to quiescent cells (Cope et al., 2010, Guidi et al., 2015, Bridger et al., 2000).

Whilst the compaction of chromatin into mitotic chromosomes is well understood, the chromatin condensation that takes place upon entry to quiescence remains relatively underexplored. Chromatin condensation is clearly evident in quiescent *S. cerevisiae* (Laporte et al., 2016, Swygert et al., 2019), quiescent primary human fibroblasts (Evertts et al., 2013), and during thymocyte development (Rawlings et al., 2011).

### **1.3.1 Nuclear reorganisation and chromosome positioning**

The spatial organisation of chromatin plays a key role in gene expression by influencing the maintenance of epigenetic marks and the long-range interaction of inter- and intra-chromosomal domains. As disruption of this organisation, and other features of nuclear architecture, are closely associated with disease phenotypes such as cancer (Zink et al., 2004, Foster and Bridger, 2005), the rearrangements that occur in quiescence, and the mechanism by which they are achieved, require a more thorough and detailed analysis. A few pioneering papers have begun to shed light on this area.

#### **1.3.1.1 The role of microtubules**

Microtubules, formed of  $\alpha$ - and  $\beta$ -tubulin, are dynamic and the largest type of filament that contribute to the cell's cytoskeletal network. Their ability to polymerise and depolymerise underpins multiple cell processes, notably chromosome segregation during mitosis in all eukaryotes (Wade, 2009). However, in *S. cerevisiae* their role in the conversion of a G1 nucleus to a quiescent nucleus has been described and highlights their importance in nuclear reorganisation events. The short nuclear microtubules originating from the spindle pole body in G1, termed the 'Rabl' configuration, elongate to form a stable array across the nucleus in quiescence. As they grow, the nucleus undergoes a dramatic rearrangement, with the nucleolus moving from a position opposite the spindle pole body to one at the side of the microtubule array. Cells that are defective in forming the array have poor survival during extended periods in the quiescent state but remain able to exit the cell cycle (Laporte et al., 2013). Overall, many of the changes experienced by yeast cells as they enter quiescence are similar in mammalian cells (Laporte and Sagot, 2014) though whether this reorganisation event is conserved remains unknown.

#### **1.3.1.2 The role of nuclear myosin**

Studies of nuclear reorganisation events during quiescence entry in human fibroblasts have implicated nuclear myosin. In primary interphase nuclei, chromosomes are located in discrete chromosome territories, and their position is strictly regulated. Gene-poor chromosomes are typically located at the periphery of the nucleus, but move to a more internal position in quiescence (Bridger et al., 2000). In fact, ten chromosomes have been shown to change their position in the nucleus upon exit from the cell cycle. Repositioning is a rapid response to quiescence triggers (serum starvation), with chromosomes evident in their new position after only 15 minutes. This rapid, manipulable transition has allowed evaluation of the effect of small molecule inhibitors and has implicated nuclear myosin 1 $\beta$  in the relocation process, suggesting that chromosome movement is an active process (Mehta et al., 2010).

### 1.3.2 The condensin complex

Two major protein complexes that play a role in chromatin organisation are cohesin and condensin, both structural maintenance of chromosomes (SMC) complexes important in chromatid cohesion and chromatin condensation, respectively (Hirano, 2012, Uhlmann, 2016). In eukaryotes, two forms of the condensin complex, condensin I and II, exist (Hirano, 2012). Both consist of the two core subunits SMC2 and SMC4, plus three different additional subunits; NCAPH, NCAPD2 and NCAPG for condensin I and NCAPH2, NCAPD3 and NCAPG2 for condensin II (Gerlich et al., 2006) (Figure 1.4). The two SMC core subunits exist as a V-shaped complex and, when associated with the non-SMC subunits, form a ring-shaped structure (Yuen and Gerton, 2018). The prevailing model describing the mechanism by which condensin compacts chromatin is the 'Loop Extrusion' model, in which DNA is pushed through the ring structure from both directions to form a DNA loop that extends as more DNA is pushed through (Uhlmann, 2016, Terakawa et al., 2017). In quiescent *S. cerevisiae*, condensin has been shown to bind large chromosomal interaction domains (L-CIDs), which resemble topologically associated domains (TADs) in metazoans, forming chromatin loops between the domains, which is consistent with the loop extrusion model (Swygert et al., 2019). However, other studies are beginning to suggest that the condensin complex binds to DNA itself through DNA binding domains in the non-SMC subcomplex creating a 'safety belt' mechanism (Kschonsak et al., 2017).

Condensin complexes play a key role in chromatin condensation, which was first reported in 1997 (Hirano et al., 1997), and since then immunofluorescence studies have shown that condensin I and II are sequestered in different locations of the cell. While condensin II is located in the nucleus during interphase, condensin I is found in the cytoplasm and only able to access chromosomes after nuclear envelope breakdown in mitosis (Maeshima and Laemmli, 2003, Hirota et al., 2004). The difference in location has been theorised to underpin independent functions, with nuclear exclusion limiting the action of condensin I to a specific point in the cell cycle (Hirano, 2012). As condensin II is located in the nucleus throughout the cell cycle, it would be able to impact chromosomes during prophase before nuclear envelope breakdown, and consistent with this, deletion of NCAPD3 (Hirota et al., 2004), NCAPG2, and NCAPH2 (Ono et al., 2004) all have a dramatic effect on the prophase nucleus, with chromatin unable to condense. Condensin I then binds to chromosomes in prometaphase and anaphase and remains there throughout mitosis, contributing to their stability until after segregation (Gerlich et al., 2006). While condensin I and II work together to ensure stable condensation of chromatin into chromosomes, they can also function independently of each other, as

neither complex needs the other to associate with chromosomes (Hirota et al., 2004). Cell cycle regulators of condensin activity have been reported and Cdk1, Aurora B, Plks and protein phosphatase 2A are likely to contribute to its regulation in mitosis (Hirano, 2012).

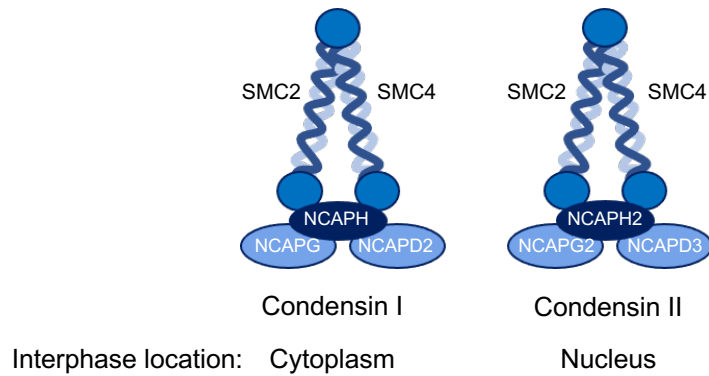


Figure 1.4. **The condensin complexes.** Condensin I and II consist of two core subunits, SMC2 and SMC4, with 3 accessory subunits that are specific to each complex. Both complexes impact chromatin condensation in mitosis however condensin I only functions following nuclear envelope breakdown due to its cytoplasmic localisation.

### 1.3.2.1 The role of the condensin complex in quiescence

Condensation of interphase chromatin into chromosomes at mitosis and the compaction of nuclei in quiescence are different events with different endpoints, yet it is plausible that the same condensation machinery underpins them both.

In quiescent yeast cells, the promotion of loops between TAD/L-CID boundaries by condensin is known to lead to the compaction of chromatin. In the same study, knockdown of the core condensin subunit SMC2 in human foreskin fibroblasts prevented chromatin condensation during entry to quiescence, demonstrating a role for condensin in both yeast and human quiescence (Swygert et al., 2019). Furthermore, a specific role for condensin II has been established in thymocyte development. Mice lacking the Kleisin- $\beta$  subunit, NCAPH2, are unable to condense their chromatin, a defect that is proposed to underlie heightened apoptosis and reduced numbers of double-positive thymocytes (Gosling et al., 2007, Gosling et al., 2008, Rawlings et al., 2011).

Interestingly, condensin has also been closely associated with the changes in gene expression that occur during quiescence entry. In condensin-depleted *S. cerevisiae*, an

increase in polymerase II occupancy is seen compared to controls that remain capable of chromatin compaction. The authors suggest that the effect of nuclear compaction in quiescence is to repress transcription and that in its absence, transcriptional de-repression can occur in quiescent cells (Swygert et al., 2019, Swygert et al., 2021).

### **1.3.3 H4K20 methylation and condensation**

The methylation status of H4K20 has been associated with the regulation of chromatin compaction and also with DNA damage repair and DNA replication (Jørgensen et al., 2013). During prophase, the H4K20me1 demethylase, PHF8, is phosphorylated and removed from chromatin resulting in the accumulation of H4K20me1. H4K20me1 is thought to play a role in mitotic chromosome condensation by providing a platform for condensin II binding via HEAT repeat clusters in two subunits, NCAPD3 and NCAPG2 (Liu et al., 2010). Similarly, the role of H4K20me1 in cell cycle progression was illustrated by manipulating its methyltransferase, SET8. Lack of SET8 and reduced H4K20me1 levels prevent cells from passing to mitosis from G2 with global chromosome condensation failure (Houston et al., 2008, Oda et al., 2009). The Lethal 3 malignant brain tumour 1 (L3MBTL1) protein can also compact chromatin by binding to H4K20me1/2 through its MBT domains (Trojer et al., 2007).

Importantly, H4K20 methylation impacts chromatin structure in other stages of the cell cycle, as well as in mitosis. As condensin II is present in the nucleus throughout the cell cycle, it is the most likely candidate for H4K20-dependent interphase roles. Loss of SET8 in embryonic stem cells results in chromatin decondensation in interphase nuclei (Oda et al., 2009), while SET8-mediated H4K20 methylation is thought to regulate chromatin decompaction during the transition from mitosis to G1, helping to guard against loss of genome integrity (Shoaib et al., 2018).

While there is a lack of information on the role of H4K20me1 during entry to quiescence, once in quiescence H4K20me3 has a documented role and has been associated with an increase in chromatin compaction (Lu et al., 2008, Evertts et al., 2013). H4K20me3 becomes more prominent in quiescent cells, and upon depletion of both SUV4-20H1 and SUV4-20H2, the enzymes responsible for converting H4K20me1 to H4K20me2 and H4K20me3, respectively, a decrease in chromatin compaction is observed along with failure to exit the cell cycle (Lu et al., 2008, Evertts et al., 2013). Overall, the available evidence, largely based on manipulating enzymes that modify H4K20, reveals a range of effects on cell cycle progression and chromatin condensation, some of which can be linked to quiescence.

Together, these data clearly illustrate quiescence as a highly complex state. Advances focussing on gene expression and chromatin organisation, in both yeast models and human studies, demonstrate the dramatic remodelling that occurs when a cell exits the cell cycle (Figure 1.5).

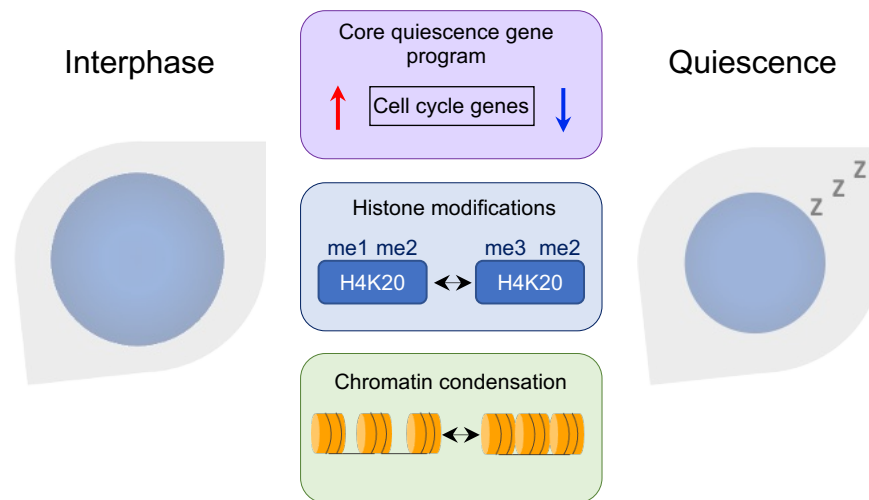


Figure 1.5. **Summary of three key cellular changes during the reversible quiescence transition.** As a cell exits the cell cycle and enters quiescence it undergoes dramatic changes, including in global gene expression, histone modifications and chromatin dynamics.

### 1.3.4 Quiescence and disease

Quiescence is a stress-resistant state which the cell can enter as part of its normal physiology to avoid the accumulation of DNA damage and over proliferation in unfavourable conditions. The cell experiences major reorganisation events during the transition from an interphase nucleus to a condensed, quiescent nucleus. Therefore, it is unsurprising that defects in the players that drive and regulate this transition have been linked with human diseases such as cancer and other diseases of ageing (Figure 1.6).

Over their lifespan, ageing stem cells can begin to lose their function and cause a misbalance between proliferation and quiescence. Hematopoietic stem cells (HSCs) can demonstrate how ageing affects functional capacity as the majority of aged HSCs have lost their regenerative capabilities and remain quiescent. This results in reduced levels of adaptive immune cells and an increased risk of anaemia and myeloid leukaemia (Pietras et al., 2011). Ageing in the muscle stem cell niche results in the cells losing their ability to remain in a quiescent state, reducing the stem cell population and thereby impacting the regenerative capacity of the muscle (Chakkalakal et al., 2012). Long-lived HSCs also accumulate sites of DNA damage over the ageing process that poses a risk to their genome integrity (Beerman et al., 2014). DNA damage response (DDR) pathways exist to efficiently manage DNA damage in all cells and promote damage repair or cell death to maintain healthy cell populations. DNA damage is particularly detrimental in quiescence as cells are unable to repair strand breaks by the accurate process of homologous recombination (HR) and instead rely on the error-prone mechanism of non-homologous end joining (NHEJ). This inaccurate form of repair leaves quiescent HSCs susceptible to mis-repaired breaks, mutations, genomic instability, and may underly haematological disorders including leukaemia (Mohrin et al., 2010, Pietras et al., 2011). Upon re-entry to the cell cycle, HSCs have been shown to upregulate DDR pathways and repair damage accumulated during quiescence to avoid further downstream effects during proliferation (Beerman et al., 2014).

Cancer cells are defined by their inability to sustain quiescence and no longer respond to anti-proliferative signals. Along with the evasion of controlled cell death by apoptosis, this results in uncontrolled cell proliferation (Roche et al., 2017). SDERGs, tumour suppressor genes that normally play a role in cell cycle exit, are downregulated, and breast cancer patients who have a reduced expression of SDERGs have a worse survival rate as well as an increased chance of cancer metastasis (Liu et al., 2007). Therefore, the global regulation of gene expression that occurs during quiescence entry is vital for the restraint of tumour cell growth. Dysregulation of the DREAM complex and its target genes have also been associated with cancer. Upregulation of the subunits that

associate with the MuvB core during the active cell cycle is commonly observed in cancer, tipping the balance towards a proliferative competent state (Iness and Litovchick, 2018, Iness et al., 2019). Similarly, inhibition of DREAM complex formation by the PCNA-associated factor (PAF), which is upregulated in various cancers, including lung adenocarcinoma, leads to failure of cell-cycle gene repression and failure to establish a quiescent state (Kim et al., 2021). In contrast, quiescence can be beneficial to cancer cell survival as a way to avoid the cytotoxic effects of chemotherapy, which typically targets actively cycling cells (Sadasivam and DeCaprio, 2013, Iness and Litovchick, 2018). This is evident in glioblastoma, an aggressive brain tumour, which consists of both proliferating and quiescent cells. Quiescence in this context allows for regrowth of the tumour following cytotoxic therapy. A risk allele associated with LRIG1 has been identified for glioblastoma and it has been proposed that these quiescent cancer cells may be in a primed state, with a high level of LRIG1, that enables cell cycle re-entry and cancer progression. However, loss of LRIG1 altogether results in failed quiescence entry and hyperproliferation of normal NSCs. This requirement for balanced expression is an important demonstration of the fine-tuning required for homeostasis (Marqués-Torrejón et al., 2021).

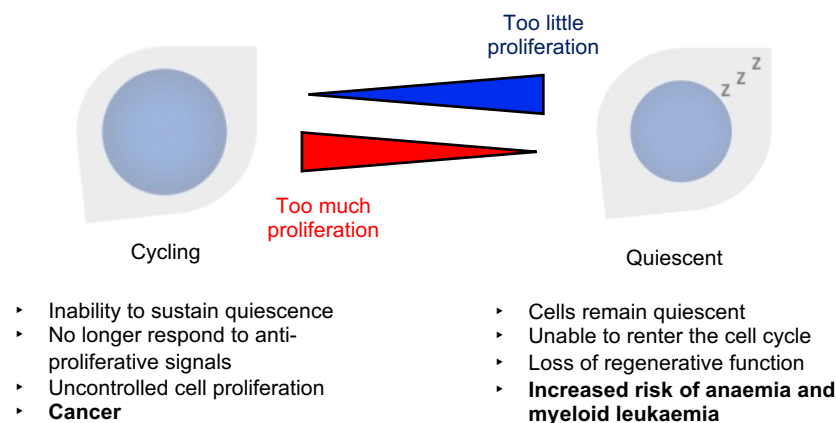


Figure 1.6. **Consequences of imbalance between a cycling and quiescent state.** Dysregulation of the quiescence transition can result in too much or too little cell proliferation and is linked with various pathologies. This highlights the importance of an accurate, regulated transition between these two states to maintain tissue homeostasis.

## 1.4 Cip1-interacting zinc finger protein 1 (CIZ1)

Cip1-interacting zinc finger protein 1, known as and referred to hereafter as CIZ1, is a nuclear protein implicated in the initiation of DNA replication (Coverley et al., 2005) and shown to interact directly with regulators of the cell cycle including p21 (Mitsui et al., 1999, Copeland et al., 2010). Cyclin E and A are two cyclins involved in pre-replication complex assembly and activation of DNA replication, respectively, through interaction with CDK2. Both these cyclins are important in regulating DNA replication and have shown to interact with CIZ1 in order to regulate the initiation of S phase (Copeland et al., 2015, Copeland et al., 2010). CIZ1 can also be phosphorylated by cyclin-A-CDK2 which inhibits its effect on DNA replication (Copeland et al., 2015). CIZ1 is also implicated in other cellular processes including apoptosis (Sun et al., 2020, Chen et al., 2019) and transcriptional regulation (den Hollander et al., 2006, Thacker et al., 2020, Lei et al., 2016).

CIZ1 encompasses two characterised domains; an N-terminal domain involved in DNA replication (Coverley et al., 2005, Copeland et al., 2010, Copeland et al., 2015) and a C-terminal domain which acts as a nuclear matrix (NM) anchor (Ainscough et al., 2007) (Figure 1.7). The nuclear matrix is a biochemically defined fraction that remains in the nucleus when lipids, soluble proteins, chromatin and in some cases RNA is removed (Berezney and Coffey, 1974).

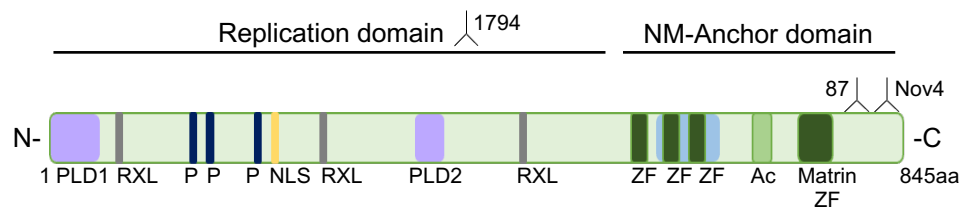


Figure 1.7. **Murine CIZ1 schematic.** The N-terminal 'Replication domain' and the C-terminal 'NM-Anchor domain' of CIZ1 are indicated as well as other important functional sites. Three C2H2-type zinc fingers and the Matrin3-type RNA-binding zinc finger (ZF, dark green), the acidic domain (Ac, green), RXL cyclin-binding motifs (RXL, grey), the nuclear localisation signal (NLS, yellow), CDK phosphorylation sites (P, dark blue), two prion-like domains (PLD, purple) and the GIY-YIG nuclease domain (blue). Epitopes for three CIZ1 antibodies are illustrated.

### **1.4.1 The inactive X chromosome**

One model for studying CIZ1 function is the inactive X chromosome (Xi). Dosage compensation in female mammals occurs when one of the two inherited X chromosomes becomes transcriptionally silenced in development (Lyon, 1961). The long non-coding RNA *Xist* expressed on the Xi initiates X chromosome inactivation and spreads in-cis to cover the entire chromosome. This results in vast chromatin alterations including facultative heterochromatin formation and gene repression (Brockdorff et al., 1992, Brown et al., 1992). A consequence of *Xist* accumulation is the recruitment of polycomb repressive complexes and deposition of the repressive histone modifications, ubiquitylation of histone H2A at lysine 119 (H2AK119Ub1) and tri-methylation of histone H3 at of lysine 27 (H3K27me3) (Brockdorff, 2017).

### **1.4.2 Localisation of CIZ1 in the cell**

CIZ1 has been associated with the RNA fraction of the nuclear matrix by interacting with the E repeats of *Xist* through its C-terminal domain (Ridings-Figueroa et al., 2017). Direct interaction between CIZ1 and *Xist* drives formation of CIZ1:RNA assemblies around the Xi (Sofi et al., 2022). The term assembly is used throughout this thesis to refer to the large CIZ1:RNA aggregates that are locally confined around the Xi. These are referred to in recent papers as supramolecular complexes (SMACs) (Markaki et al., 2021). It has been hypothesised that these assemblies are formed through liquid-liquid phase separation and represent dynamic, membrane-less condensates (Shin and Brangwynne, 2017, Sofi et al., 2022).

Loss of CIZ1 assemblies has multiple consequences in primary murine fibroblasts including loss of H3K27me3 and H2AK119Ub1 enrichment at the Xi, dispersal of *Xist* and widespread effects on polycomb-mediated control of gene expression. CIZ1 has also been linked with movement of the Xi from the nuclear periphery to a peri-nucleolar region during a brief window in mid-S phase (Stewart et al., 2019). The current data surrounding CIZ1 assemblies is starting to suggest a role as a phase-separated molecular shield that is responsible for protecting the epigenetic status of a cell by influencing the modifying enzymes' access to chromatin.

Even with CIZ1 being highly enriched at the Xi, it is also distributed throughout the nucleus in smaller aggregates in both male and female cells with its effects also appearing to be genome wide (Stewart et al., 2019, Ainscough et al., 2007). Therefore, functions that are uncovered by analysis of the Xi may apply to CIZ1 function elsewhere in the nucleus.

It is also notable that the S-phase Xi relocation process, in which CIZ1 functions, is gradually diminished with time in culture (Stewart et al., 2019), necessitating analysis in early passage cells. In order to avoid the deterioration of CIZ1-dependent processes that take place during culture adaptation, I have used cells that are within a few passages of derivation from mouse embryos throughout this project.

### **1.4.3 Alternative splicing of CIZ1**

Alternative splicing events of the CIZ1 transcript have been identified to yield over 25 variants (Rahman et al., 2010), some constitutive, some developmentally regulated and some detected only in disease contexts. Splicing events have been shown to impact the localisation of CIZ1 in the cell as well as its ability to form large assemblies (Rahman et al., 2007, Sofi et al., 2022). The three CIZ1 antibodies used throughout this thesis, primarily in Chapter 5, all detect CIZ1 assemblies at the Xi and have been validated in CIZ1-null cells. However, these antibodies can detect multiple, different forms of the denatured protein via western blot. This provides a complex picture for how CIZ1 exists naturally, due to different variants, as well as possible multimerization events, and adds a level of difficulty to analysis.

### **1.4.4 CIZ1 and disease**

Genetic depletion of CIZ1 results in viable mice with no apparent developmental differences when compared to wild-type (WT) mice. However, between 9 and 18 months, females develop fully penetrant lympho-proliferative disorder, characterised as non-Hodgkin type B-cell lymphoma, with abnormal spleen architectures, effacement of normal follicles, and infiltration of abnormal B (CD20 +ve) and reactive T (CD3 +ve) cells in all affected tissues (Ridings-Figueroa et al., 2017). This analysis did not involve any additional deliberate stimuli, however an independent analysis of a different CIZ1-null model reported leukaemia one year after retroviral infection of CIZ1-null but not WT neonates, with MOL4070A (Nishibe et al., 2013). The leukemic samples were diagnosed as acute lymphoblastic leukaemia, acute myeloid leukaemia or acute undifferentiated leukaemia. No gender information was reported in this study, but like our analysis it concluded that CIZ1 acts as a tumour suppressor involved in protecting against haematological malignancies. It should be noted that neither model was investigated for other, rarer abnormalities. Overexpression and alternatively spliced variants of CIZ1 have been associated with a range of cancers. These include medulloblastoma (Warder and Keherly, 2003), Ewings tumour (Rahman et al., 2007), breast (den Hollander et al., 2006), lung (Higgins et al., 2012), colon (Wang et al., 2014), prostate (Liu et al., 2015) and liver cancer (Wu et al., 2016). Specific targeting and reduction of CIZ1 in a colorectal cancer cell line successfully inhibited cell proliferation, indicating CIZ1 may play a role in

cancer progression (Yin et al., 2013). CIZ1 has also been linked with the neurological disorders cervical dystonia (Xiao et al., 2014), and Alzheimer's disease (Dahmcke et al., 2008). As the underpinning mechanism implicating CIZ1 in unconstrained proliferation is unknown, it is important to study the function of this protein as part of the cell cycle to develop our understanding of its apparent contribution to cancer biology.

## **1.5 CIZ1 and quiescence**

Previous data from the Coverley lab has indicated an essential role for CIZ1 during the entry to quiescence. WT and CIZ1-null tail-tip fibroblasts (TTFs) and primary embryonic fibroblasts (PEFs) were driven into quiescence by contact inhibition (CI). The response to a standardised long-term CI maintenance protocol, in which media was replenished every three-four days, was evaluated. Under these conditions, checkpoint activation was evident in the CIZ1-null population. Phosphorylation of ataxia telangiectasia mutated (pATM) was evident within the first week, while phosphorylated checkpoint kinase 1 (pCHK1) and phosphorylated histone H2AX ( $\gamma$ H2AX) emerged later. For all markers there was no difference between the two genotypes at the start of the time course (cycling), but all became progressively activated reaching 60-90% of the CIZ1-null population by the end of the 3-week time course (Figure 1.8A). Proliferating colonies eventually emerged from checkpoint activated CIZ1-null monolayers, at a rate of approximately 1 per 10,000 cells plated, after 21 days in culture, whilst WT cells remained as a stable monolayer (Figure 1.8B). This suggests that establishment of a stable, quiescent state is dependent on CIZ1 (Figure 1.8C) (Wilson, 2013).

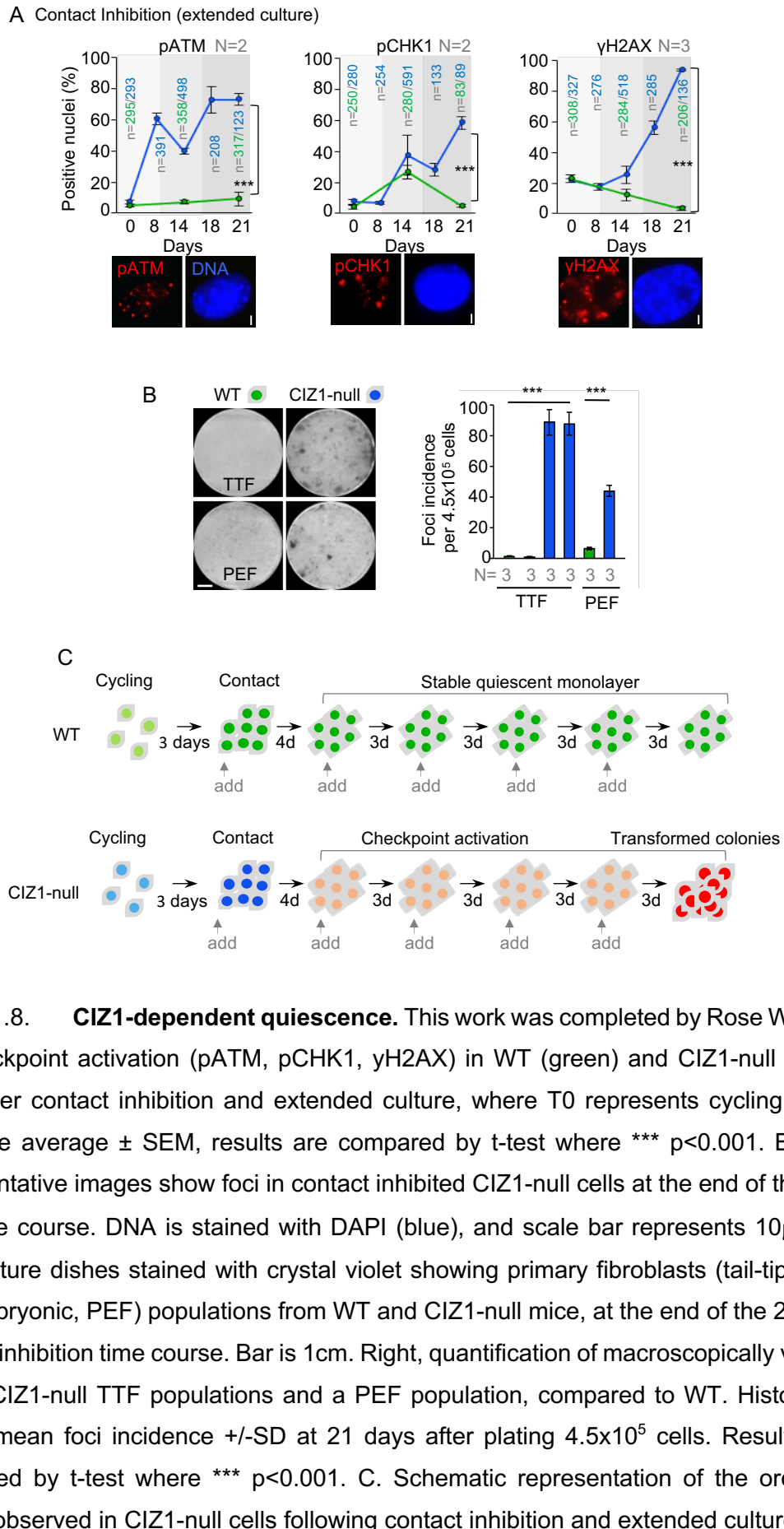


**Figure 1.8. CIZ1-dependent quiescence.** This work was completed by Rose Wilson. A. Checkpoint activation (pATM, pCHK1, γH2AX) in WT (green) and CIZ1-null (blue) cells after contact inhibition and extended culture, where T0 represents cycling cells. Data are average  $\pm$  SEM, results are compared by t-test where \*\*\*  $p < 0.001$ . Below, representative images show foci in contact inhibited CIZ1-null cells at the end of the 21-day time course. DNA is stained with DAPI (blue), and scale bar represents 10  $\mu$ m. B. 6cm culture dishes stained with crystal violet showing primary fibroblasts (tail-tip, TTF and embryonic, PEF) populations from WT and CIZ1-null mice, at the end of the 21-day contact inhibition time course. Bar is 1cm. Right, quantification of macroscopically visible foci in CIZ1-null TTF populations and a PEF population, compared to WT. Histogram shows mean foci incidence  $\pm$  SD at 21 days after plating  $4.5 \times 10^5$  cells. Results are compared by t-test where \*\*\*  $p < 0.001$ . C. Schematic representation of the order of events observed in CIZ1-null cells following contact inhibition and extended culture.

## 1.6 Project aims

The main goals of my project were to understand the role of CIZ1 in relation to the quiescence transition and the consequences of CIZ1 loss in the cell, with particular focus on its implications in cancer. To achieve this, my specific aims were:

- To profile the transcriptome of WT and CIZ1-null PEFs during entry to quiescence and to investigate if the loss of CIZ1 affects the global changes in gene expression that occur over this transition. (Chapter 3)
- Based on transcriptome findings, investigate chromatin dynamics during entry to quiescence and how these differ in the absence of CIZ1. (Chapter 4)
- To investigate the role of CIZ1 as a protector of epigenetic state and the impact on formation of a quiescent nucleus. (Chapter 4)
- To develop a permeabilised cell assay to probe the release and subnuclear movement of CIZ1. (Chapter 5)
- To exploit the permeabilised cell assay to further the understanding of the relationship between CIZ1 assemblies, kinases and phosphatases throughout the cell cycle and cancer. (Chapter 5)

## 2 Materials and Methods

### 2.1 Cell culture

#### 2.1.1 Cell lines

Wild-type (WT) and CIZ1-null primary murine embryonic fibroblasts (PEFs) and murine tail-tip fibroblasts (TTFs) were generated and kindly gifted by Justin Ainscough. All PEFs used were derived from independent embryos at days 13-14 of gestation and TTFs at 3-4 weeks, with all animal work carried out under a UK Home Office licence. CIZ1-null mice were generated from the C57BL/6 ES clone IST13830B6 (TIGM) harbouring a neomycin resistance gene trap inserted downstream from exon 1 with additional details and confirmation of *Ciz1/CIZ1* absence outlined in Ridings-Figueroa et al. 2017. Inducible cells with the designated strain name: Tg(GFP/CIZ1,LacZ)24jfxa:Gt(ROSA)26Sor<tm1.1 (rtTA,EGFP)Nagy:Ciz1Gt(IST13830B6)Tigm, harbour transactivator and responder transgenes to induce GFP-CIZ1 expression (Ridings-Figueroa et al., 2017). Experimentation on mouse cells was carried out with approval from the Animal Welfare and Ethical Review Body at the University of York. All cells throughout this project are listed in Table 2.1.

#### 2.1.2 Cell maintenance

Non-primary and primary cycling cells were cultured in Gibco™ Dulbecco's Modified Eagle Medium (DMEM, 1X), GlutaMAX, low glucose (1g/l, 21885-025) and high glucose (4.5g/l, 31966-021), respectively. Media was supplemented with 10% foetal calf serum (PAA, A15-151) and 1% penicillin/streptomycin/L-glutamine (Gibco, 10378-016) referred to throughout as high-serum media. Cells were grown at 37°C in a humid incubator with 5% CO<sub>2</sub> on Nunc™ Cell Culture Dishes (ThermoFisher Scientific, 150350) with/without 0.13-0.16mm thick glass coverslips and maintained in a rapidly cycling state unless stated otherwise. Primary cells were used at a low passage (typically between passage 2-4) due to the effects of long-term culture on primary mechanisms (Stewart et al., 2019). To split cells, media was removed, washed with pre-warmed Dulbecco's phosphate buffered saline (D-PBS, Gibco, 14190-094), and lifted by incubating with 1ml of 0.5% trypsin-EDTA acid (Gibco, 15400-054) in D-PBS at 37°C with 5% CO<sub>2</sub>. Trypsin was quenched with fresh, high-serum media (pre-warmed) and cells were split onto new plates at the required density (usually 70% for cycling, therefore a 1:3 split). For inducible cells, addition of doxycycline to media (5-10 µg/ml) was used to induce GFP-CIZ1 over 48 hours.

Table 2.1. **List of primary cell populations and cell lines.**

Strain number	Source	Genotype	Sex
13.1	Primary embryonic fibroblast (PEF)	WT (+/+)	Female (F)
13.8	PEF	WT (+/+)	F
14.4	PEF	WT (+/+)	F
45.1fc	PEF	WT (+/+)	F
45.1ff	PEF	WT (+/+)	F
13.49	PEF	WT (+/+)	F
13.31	PEF	WT (+/+)	F
13.22	PEF	WT (+/+)	F
13.32	PEF	WT (+/+)	F
14.2	PEF	CIZ1-null (-/-)	F
13.15	PEF	CIZ1-null (-/-)	F
13.17	PEF	CIZ1-null (-/-)	F
30.3ca	PEF	CIZ1-null (-/-) with inducible CIZ1 transgene	F
41.2fa	PEF	CIZ1-null (-/-) with inducible CIZ1 transgene	F
14.19	PEF	CIZ1-null (-/-)	F
13.42	PEF	CIZ1-null (-/-)	F
13.59	PEF	CIZ1-null (-/-)	F
13.2	PEF	WT (+/+)	Male (M)
13.4	PEF	WT (+/+)	M
45.1fb	PEF	WT (+/+)	M
13.20	PEF	WT (+/+)	M
13.30	PEF	WT (+/+)	M
13.6	PEF	CIZ1-null (-/-)	M
16.5de	PEF	CIZ1-null (-/-)	M
13.45	PEF	CIZ1-null (-/-)	M
13.38	PEF	CIZ1-null (-/-)	M
13.41	PEF	CIZ1-null (-/-)	M
13.43	PEF	CIZ1-null (-/-)	M
259	Tail-tip fibroblast (TTF)	WT (+/+)	M
260	TTF	CIZ1-null (-/-)	M
D001 3T3	Adapted murine fibroblast cell line	WT (+/+)	F

### **2.1.3 Quiescence**

Two well-established protocols were used to induce quiescence, serum withdrawal (SW) or contact inhibition (CI) (Mitra et al., 2018). For quiescence by SW, cells were plated at 70-80% confluency in high-serum media. Once settled and cycling, usually after 24 hours, the media was removed, cells washed in warmed D-PBS, and low-serum media added (DMEM supplemented with 0.01% FBS (PAA) and 1% Pen/Strep/Glutamine). Cells were typically harvested following a short SW (up to two hours) or a long SW (24 hours post removal). To achieve CI, cells were plated at 70-80% confluency and cultured to 100% confluency which usually occurs after three days. At the point of 100% confluency, media was changed (fresh, high-serum media) and cells were incubated for a further four days and are now called quiescent. If cells were left in culture for an extended period of time, media was changed twice a week.

#### **2.1.3.1 Multiple rounds of serum withdrawal**

To investigate the behaviour of cells as they pass in and out of quiescence the SW method was extended to include re-feed (serum add-back, AB) incubations. Following either a short period (1-2 hours) or a long period (24 hours) in low-serum media, the media was removed, and high-serum media added back to the cells. This cycle of SW (0.01% PAA media, low serum) and AB (10% PAA media, high serum) was often repeated so the population experienced either one round or multiple rounds of exiting and re-entering the cell cycle.

### **2.1.4 Detection of foci formation**

WT and CIZ1-null TTFs were plated at 70-80% confluency in 3cm plates and subjected to an extended CI protocol. After 3 weeks in culture, with media changed twice a week, the plates were washed twice in room temperature (RT) PBS followed by fixation using 4% paraformaldehyde (PFA) for 20 minutes. Foci were stained using 0.05% filtered crystal violet for 30 minutes and plates washed overnight.

### **2.1.5 Cell viability**

WT and CIZ1-null PEFs were plated at 70-80% confluency in a 24-well plate and subjected to various SW and AB times. To investigate cell death in the population, media was removed, and cells incubated with Trypan Blue stain (0.2%, Gibco, 15250061) for 5 minutes at 37°C. The stain was then removed and the number of blue cells per well manually counted using an EVOS Cell Imaging System (10X objective).

### **2.1.6 Inhibitors**

To investigate the role of H4K20me1 in nuclear condensation following SW, adherent cells were incubated with 10 $\mu$ M UNC0379 (Sigma, sml1465) for two hours in high-serum media for cycling cells or low-serum media for cells subject to SW. UNC0379 is a selective, substrate competitive inhibitor of SET8, the lysine methyltransferase that monomethylates H4K20, with an IC<sub>50</sub> of 7.3  $\mu$ M (Ma et al., 2014). Following incubation, cells were taken through the immunofluorescence protocol below.

### **2.1.7 Nuclear fragility**

Method was adapted from (Furusawa et al., 2015). Briefly, adherent cells were harvested by trypsinisation then pelleted at 2000rpm and resuspended in 200 $\mu$ l PBS/Hoechst (1:1000). Before subjecting cells to mechanical shear, a reference sample (0 passes) was taken and fixed in 4% PFA to generate a measure of cell count and integrity. Using a 1ml syringe, the remaining cell suspension was passed through a 25G needle 40 times, then fixed. Equal volumes of treated and untreated fixed cells were concentrated onto microscope slides using a cytopspin and mounted in Vectashield (Vector Labs, H-1000). The number of intact stained nuclei in 2-7 fields per independent experiment were counted, averaged, and expressed relative to control.

## **2.2 Immunofluorescence**

Adherent cells grown on glass coverslips were washed briefly in cytoskeletal buffer (CSK; 10mM PIPES/KOH pH 6.8, 100mM NaCl, 300mM sucrose, 1mM EGTA, 1mM MgCl<sub>2</sub>, 1mM DTT, 1 cOmplete™ Protease Inhibitor Cocktail per 50ml) or D-PBS with 0.1% Triton-X-100 before fixation with 4% PFA. After fixation, cells were rinsed twice with RT D-PBS then incubated for 30 minutes in bovine serum albumin (BSA) antibody buffer (0.02% SDS, 0.1% TX100, 10 mg/ml nuclease-free BSA in PBS). Coverslips were then incubated for 1-2 hours at 37°C in a humidified chamber with primary antibody (in BSA antibody buffer), followed by three washes in the BSA antibody buffer before incubating with anti-species secondary antibodies (Alexa Fluor 488 or 568) for 1 hour. Cells were washed a further three times in BSA antibody buffer prior to a 5-minute incubation in Hoechst 33258 and mounted in VectorShield (Vector, H-1000), if Hoechst was not used, coverslips were mounted in VectorShield with DAPI (Vector, H-1200). For DNA damage response antibodies (pATM), PBS was substituted by TBS in all buffers. Antibodies are listed in Table 2.2.

### **2.2.1 Detection of EdU**

To label cells in S phase, adherent cells on coverslips were incubated with 10 $\mu$ M nucleotide analogue 5-ethynyl-2'-deoxyuridine (EdU) for 30 minutes (pulse) under usual growth conditions. To visualize newly synthesized DNA, coverslips were washed briefly in CSK with 0.1% Triton-X-100 before fixation with 4% PFA for 15 minutes. Coverslips were then washed in D-PBS and EdU detected using the Click-iT<sup>®</sup> EdU Alexa Fluor<sup>®</sup> 555 nm Imaging Kit (ThermoFisher, C10338) as recommended. Briefly, coverslips were blocked with BSA Antibody buffer before incubation in a light-proof humidified chamber with Click-iT<sup>®</sup> reaction cocktail (per coverslip: 17.2  $\mu$ l 1x reaction buffer, 0.8  $\mu$ l CuSO<sub>4</sub>, 0.048  $\mu$ l Alexa Fluorazide, 2  $\mu$ l 1x reaction buffer additive) for 60 minutes. Coverslips were then washed and mounted using VectaShield with DAPI.

### **2.2.2 Permeabilised cell CIZ1 release assay**

Adherent cells grown on glass coverslips (70-80% confluency) were subjected to a 1-minute detergent wash (0.1% Triton-X-100 in CSK) followed by a high salt buffer wash (0.1% Triton-X-100 in CSK, 500mM NaCl) for 2 minutes. Cells were fixed for 15 minutes with 8% PFA and the immunofluorescence protocol followed accordingly.

## **2.3 Imaging**

Fluorescence images were captured using a Zeiss Axiovert 200M fitted with a 63X/1.40 Plan-Apochromat objective and Zeiss filter sets 2, 10, 15 (G365 FT395 LP420, BP450-490 FT510 BP515-565, BP546/12 FT580 LP590), using AxioCam 506 mono and Axiovision image acquisition software (SE64 release 4.9.1). For images where intensity differences are quantified, all samples were analysed as a set, with constant image acquisition parameters, and no image manipulation. For presentation purposes, images were enhanced using Fiji V1.0 (Schindelin et al., 2012) or Affinity Photo 1.5.2. Where intensity differences are being illustrated, all images in the set were manipulated identically. All quantification was conducted on unedited images.

### **2.3.1 Nuclear area and intensity analysis**

The nuclear area of typically 30-50 cells per coverslip was analysed using Fiji V1.0 (Schindelin et al., 2012). Channels were split to show blue (DAPI), green (FITC) and red (Rhodamine) output separately and thresholds for nuclear area were identified using the Otsu setting in the blue (DAPI) channel. Thresholds were converted to masks and all particles within the size 0.01-Infinity analysed and returned as area in pixels. Conversion to area in  $\mu$ m<sup>2</sup>, then to volume, was calculated based on the 10 $\mu$ m scale bar and assumed a spherical nucleus. Where intensity measures for other channels were

required, the DAPI mask was overlaid onto the relevant image and pixel density within the mask returned as maximum, minimum or mean density in the selected area.

### **2.3.2 Dispersal analysis**

The extent of CIZ1 dispersal was measured as the percentage area of nucleus covered using Fiji. Channels were split to show blue (DAPI), green (FITC) and red (Rhodamine) output separately and thresholds were set on each channel independently using the Otsu setting. Thresholds were converted to masks and all particles within the size 0.01-Infinity analysed and returned as area in pixels.

### **2.3.3 Detailed steps for Fiji analysis**

#### **Area analysis:**

Open tiff image

Image > Colour > Split channels

Select colour channel: blue for nuclear area, green / red for CIZ1 and Ub1

Image > Adjust > Threshold > Otsu. This should create a neat outline around the outer limit of the stain, adjustments can be made if needed. > Apply

Process > Binary > Convert to mask

Analyse > Analyse particles > change size to 0.01-Infinity, Circularity 0.00-1.00, ensure "Display results" and "add to Manager" are selected > OK

To determine extent of dispersal (%):  $(\text{Area for CIZ1 or Ub1} / \text{Area for nucleus}) * 100$

#### **Nucleus-wide fluorescence intensity on red and green channels:**

Select green or red image

Image > Overlay > Show overlay. This will overlay the mask from the blue channel.

Select the nucleus to measure > Analyse > Measure

Results will appear in results window with area and intensity measurements.

## **2.4 Western blot**

### **2.4.1 Whole cell lysate generation**

Whole cell lysates (WCL) were generated by scrape harvesting adherent cells, following two cold washes in D-PBS, in SDS-PAGE sample buffer (2% SDS, 15% glycerol, 1.7% betamercaptoethanol, 75mM Tris pH 6.8 with bromophenol blue) supplemented with 2mM PMSF.

### **2.4.2 Subcellular fractionation**

Following two cold washes in D-PBS, adherent cells were scrape harvested, supplemented with 2mM PMSF and incubated with 0.1% Triton-X-100 for 3-5 minutes on ice. Samples were then centrifuged for 2 minutes at 5000rpm, to generate a pellet fraction (insoluble material including chromatin and nuclear structural proteins). Fractions were denatured in 1X SDS-PAGE sample buffer for subsequent analysis to reveal any protein binding differences.

### **2.4.3 Immunoprecipitation**

#### ***2.4.3.1 Preparation of Protein A/G UltraLink™ Resin***

Pierce™ Protein A/G UltraLink™ Resin (Thermo Scientific, 53133) uses the recombinant Protein A/G to capture mammalian IgG. 10µl of slurry (equivalent to 5µl of Protein A/G resin) was prepared for each antibody test. The resin was subjected to centrifugation and CSK washes before the pelleted resin was resuspended in CSK buffer.

#### ***2.4.3.2 Preparation of samples and ClZ1 immunoprecipitation***

Two 15cm plates of 3T3s were washed in cold CSK buffer supplemented with DTT and protease inhibitor prior to scrape harvesting. Samples were pooled, 2mM PMSF added and incubated on ice with 0.1% Triton-X-100 for 5 minutes. Centrifugation (10,000rpm) at 4°C for 5 minutes generated a pellet and a supernatant which contained any detergent-soluble components. ClZ1 antibodies (1794 and Nov4) were added to separate aliquots of the detergent-soluble fraction and incubated for 1 hour with rotation at 4°C. During this incubation, the antibody will bind to its specific epitope if present in the sample. 10µl of prepared Protein A/G UltraLink™ Resin was added to each reaction and incubated at 4°C for another 1 hour with rotation. During this incubation, the antibody will bind to the immobilised Protein A/G. Unbound proteins were removed through centrifugation and CSK washes. The remaining pellet was resuspended in 1X SDS-PAGE sample buffer for subsequent western blot analysis.

#### **2.4.4 Western blot analysis**

Samples in SDS-PAGE sample buffer went through two cycles of heating (90°C) and vortexing prior to separation through a 4-15% gradient polyacrylamide gel (BioRad, 4561085) with 1X SDS running buffer (0.1% SDS, 192mM glycine, 25mM Tris). Gels were transferred onto a nitrocellulose membrane using the iBlot system (iBlot gel transfer stacks, Invitrogen) or a semi-dry transfer. Membranes were blocked with 5% BSA (Sigma, A3294) or 10% low fat milk (Marvel, 8066) in PBS (Sigma, P3813) with 0.1% Tween20, for 30 minutes before primary antibody incubation for 2 hours at RT or overnight at 4°C depending on the antibody, with gentle agitation. Blots were washed three times with blocking buffer then probed with HRP-conjugated anti-species secondary antibody (Jackson Immunochemicals 115-035-174 and 211-032-171) for 1 hour at RT and imaged using EZ-ECL (Biological Industries) and Syngene PXi chemiluminescence imaging system.

#### **2.4.5 Western blot quantification**

Image quantification was performed on unedited images in Fiji with background subtracted and normalised to histone H3 for loading.

### **2.5 Graphical presentation and statistical analysis**

Experiments were designed to use the minimum number of animals (independently derived PEF or TTF populations) while achieving statistically valid data, with N representing the number of independent experiments. Unless stated otherwise for nuclear area measurements and dispersal analysis, 30-50 cells from three independent coverslips were analysed at the indicated treatment times. For scoring histone post-translational modifications, or protein at the Xi, each replicate is an average of 3 independent counts or measurements per coverslip (30-50 cells each), with the average of all replicates shown. Unless stated otherwise, values represent the means  $\pm$  SEM. Asterisks indicate statistical significance (ns not significant, \*p < 0.05; \*\*p < 0.01; \*\*\*p < 0.001). Statistical analysis was carried out in GraphPad Prism using a two-tailed Student's t test, one-way ANOVA or two-way ANOVA. Significance for expression level differences between WT and CIZ1-null cycling cells for subunits of the condensin complex, cohesin complex, TOR complex and CDC73 PAF1 complex were calculated using the Wilcoxon signed rank test. Graphs were generated using GraphPad Prism Version 9.1.0 (216) or Microsoft Excel and, where indicated, measurements normalised to the relevant internal control.

Table 2.2. **Antibodies used for immunofluorescence and Western blot.**

Antibody		Concentration (IF)	Concentration (WB)	Supplier/Reference
<b>Primary Antibodies</b>				
CIZ1 N-term (1794)	Rabbit polyclonal	1:1000	-	(Coverley et al., 2005)
CIZ1 C-term (87)	Mouse polyclonal	1:20	-	Unpublished, Coverley lab
CIZ1 C-term (Nov4)	Rabbit polyclonal	1:1000		Novus Biologicals, NB100-74624
Lamin B2	Mouse monoclonal	1:100	-	Invitrogen, 33-2100
H2AK119Ub1	Rabbit monoclonal	1:10,000	-	Cell Signalling Technology, D27C4
H3K27me3	Rabbit polyclonal	1:2000	-	Cell signalling technology, C36B11
H4K20me1	Mouse monoclonal	1:1000	1:1000	Active motif, 39728
H4K20me3	Mouse monoclonal	1:1000	1:1000	Active motif, 39672
pATM	Rabbit polyclonal	1:4000	-	Abcam, 2888
SMC2	Rabbit polyclonal	-	1:1000	Biorbyt, orb542536
SMC4	Rabbit polyclonal	-	1:1000	Novus Biologicals, NBP1-86635
Histone H3	Rabbit polyclonal	-	1:10000	Abcam, ab1791
<b>Secondary Antibodies</b>				
Goat anti-rabbit IgG		1:1000	-	Invitrogen, A11011
Goat anti-mouse IgG		1:1000	-	Invitrogen, A11001
Peroxidase IgG fraction monoclonal mouse anti-rabbit		-	1:10000	Jackson Immuno, 211-032-171
Peroxidase AffiniPure goat anti-mouse		-	1:10000	Jackson Immuno, 115-035-174

## **2.6 Transcriptomic analysis**

Three independently derived populations of primary (before passage 4) PEFs from both WT (13.8, 13.1 and 14.4) and CIZ1-null (13.17, 14.2 and 13.15) female embryos were cultured to 80% confluency and RNA extracted following the protocol below. RNA samples also underwent DNase treatment (Sigma, 04716728001) and clean-up using RNA clean & concentrator-5 with Zymo-Spin IC columns (Zymo Research, R1015).

### **2.6.1 RNA Extraction**

For each cell line, cells were cultured on 6cm dishes and RNA extracted with TRIzol (Ambion, 15596-026) from either a cycling population, 24 hours after serum withdrawal or 4 days after 100% confluency. Briefly, adherent cells were washed twice with PBS, drained on a shallow angle for 2 minutes and excess PBS removed. 1mL of TRIzol was added per 28cm<sup>2</sup> and incubated for 3-5 minutes at RT with periodic agitation. Lysates were collected in clean Eppendorf tubes and stored at -80°C. Samples were defrosted and 200µl of chloroform was added per 1ml of TRIzol used for extraction followed by rigorous shaking for 15 seconds then left to incubate at RT for 2-3 minutes. Samples were centrifuged at 12000g for 15 minutes at RT allowing the RNA, protein and DNA to separate. The top RNA aqueous phase was transferred to a clean tube and equal volume of isopropanol added to precipitate the RNA. The sample was mixed through gentle inversions before a 10-minute RT incubation and 10-minute centrifugation at 12000g. Supernatant was disposed, and the RNA pellet washed with 1ml 75% ethanol per 1ml TRIzol originally used then centrifuged at the same speed for 5 minutes. The ethanol wash was removed, and the pellet centrifuged again to remove any remaining ethanol. The RNA pellet was allowed to dry for 30 seconds before resuspension in 20µl DEPC-treated water and was stored at -80°C. This created 18 samples for sequencing and subsequent analysis.

### **2.6.2 Sample preparation**

Total RNA libraries were prepared by Sally James (Technology Facility, University of York) with NEBNext® Ultra™ RNA library Prep Kit for Illumina® and enriched for mRNA using NEBNext Poly(A) mRNA Magnetic Isolation Module, which is optimized for production of libraries with 250-400bp inserts. Enriched mRNA was fragmented by heating to 95°C for 12 minutes, cDNA synthesised from random primers, followed by end repair, dA-tailing, adaptor ligation and PCR enrichment. Libraries were sequenced at the Leeds Institute for Molecular Medicine (LIMM) using Illumina 3000 system, using paired-end sequencing to generate ~50 million reads per sample.

### **2.6.3 Transcriptome assembly**

Transcriptome assembly was kindly carried out by Katherine Newling (Technology Facility, University of York). Sequence reads were trimmed to remove any adapter sequences using Cutadapt version 1.8.3 (Martin, 2012) then aligned to version GRCm38 of the mouse genome using HISAT2 (Kim et al., 2015). Transcriptomes were assembled and gene expression quantified using the Tuxedo pipeline (version 2.2.1) (Trapnell et al., 2012). Cufflinks was used to assemble transcriptomes for each sample using the GTF annotation file for the GRCm38 mouse genome (*C57BL/6*), followed by Cuffmerge to merge individual sample transcriptomes. Quantification, normalisation, and differential expression was carried out using Cuffquant, Cuffnorm, and Cuffdiff, respectively. Individual fragment counts per million (FPKM) were converted to individual transcripts per million (TPM) and extracted for biological replicates (independent PEF lines) enabling calculation of means and SEM, and comparisons between genotypes. Changes in expression levels between cell cycle stage and genotype were expressed as  $\log_2$ (fold change). False discovery rate (FDR) was controlled using the Benjamini-Hochberg method in the StatsModels library (v.0.8.0), to generate q-values.

### **2.6.4 Analysis of WT and *CIZ1*-null genomes during quiescence entry**

Genes are stated to differ in expression level when the average  $\log_2$ (fold change), between two states, passes the significance threshold, FDR  $q < 0.05$ , and is either above 1 or below -1. These thresholds are illustrated on volcano plots generated in Excel. Heat maps were generated using Spyder (v.4.1.4) (Python 3.6-8), accessed via Anaconda Navigator (v.1.9.12), using the pandas, seaborn and matplotlib modules. All Python scripts were kindly donated by Emma Stewart (Coverley lab). Transcription units which did not have a numerical value for  $\log_2$ (fold change), due to mean expression of 0 in one condition, were manually removed before generating the plots, with all non-significant changes indicated in white. Gene Set Enrichment Analysis (Subramanian et al., 2005) was performed in Python 3.6 using one-sided Fisher's Exact tests as part of the SciPy library (v.0.19.0), this script was kindly donated by Katherine Newling. Excel files containing the gene lists generated from my analysis have been provided separately.

## 3 Gene expression changes during entry to quiescence

### 3.1 Introduction

To study the quiescent state *in vitro* a number of techniques have been developed to stimulate the anti-proliferative triggers that cells experience in the body (Mitra et al., 2018). Two well-established protocols are serum withdrawal and cell contact inhibition. When a cell experiences such anti-proliferative cues, intracellular signalling (Duronio and Xiong, 2013, Cho et al., 2019, Ricard et al., 2021), instigates global changes in both gene expression and chromatin organisation to ensure a stable transition to a quiescent state.

This chapter focusses on the global gene expression changes that take place during cell cycle exit and explores the role of CIZ1 in the process. A CIZ1-dependent gene set in the cycling state has already been established (Stewart et al., 2019), with 266 genes affected by the loss of CIZ1 in primary embryonic fibroblasts (PEFs). This highlights a role for CIZ1 in regulating gene expression. Another transcriptomic study of WT and CIZ1-null lymphocytes by Emma Stewart as part of her PhD in the Coverley lab, revealed another role for CIZ1. The data showed that ~25% of the genes upregulated only in CIZ1-null lymphocytes upon antigen stimulation were DREAM complex targets. The dimerization partner, RB-like, E2F and multi-vulval class B (DREAM) complex is best known for its role in quiescent cells where it is involved in repression of cell cycle-related genes (Sadasivam and DeCaprio, 2013). These results suggest that without CIZ1 the DREAM complex is unable to perform its usual role in restraining the cell cycle. This was an informative finding as deregulation of the DREAM complex can lead to loss of cell cycle control and has been implicated in human cancers (Sadasivam and DeCaprio, 2013). It is therefore important to understand if CIZ1 loss impacts the gene expression changes that occur during the quiescence transition.

### 3.2 Aims

This chapter focuses on the generation of whole transcriptome samples to compare gene expression changes during entry to quiescence in WT and CIZ1-null cells. The aims are to investigate whether CIZ1 impacts the transcriptional program that usually takes place and to identify candidate pathways that may lead to an unstable quiescent state in CIZ1-null cells.

### 3.3 Experimental design

To minimise the effects of pathway-specific signalling and to increase focus on common downstream events, I compared changes in the transcriptome after the two quiescence triggers, serum withdrawal (SW) and contact inhibition (CI), in three independently derived populations of PEFs from both WT and CIZ1-null female embryos. High quality DNase-free RNA was isolated from early passage cells and supplied to the genomics team at the University of York Technology Facility, where Sally James ran quality checks and prepared libraries enriched for mRNA. Samples were sequenced using pair-end sequencing at the Leeds Institute for Molecular Medicine using the Illumina 3000 system. The sequence data was mapped to the mouse genome assembly GRCm38 by Katherine Newling, also part of the Technology Facility at the University of York. This returned gene expression changes for all murine genes. Thresholds were applied to generate a list of genes that were significantly changed, for example upon a particular quiescence trigger. Genes are stated to differ in expression level when the average  $\log_2(\text{fold change})$ , between two states, passes the significance threshold, FDR  $q < 0.05$ , and is either above 1 or below -1. Initially, comparisons focussed on the overlap between the two quiescence triggers for WT and CIZ1-null cells separately, moving to a comparison of the two genotypes to reveal CIZ1-dependent changes.

### 3.4 Results

#### 3.4.1 Murine core quiescence program

In human fibroblasts, a set of core quiescence genes have been identified that are both independent of the quiescence trigger and vital to maintenance of a long-term quiescent state (Coller et al., 2006, Liu et al., 2007). These are referred to as the core quiescence program and have been established by comparing three independent quiescence triggers; mitogen deprivation (serum withdrawal), contact inhibition and loss of adhesion.

In order to generate a core quiescence program for WT murine fibroblasts, genes that significantly changed expression ( $-1 > \log_2(\text{foldchange}) > 1$ ,  $q < 0.05$ ) over 24 hours of serum withdrawal (SW) or after 4-days of 100% confluency (CI) were compared (Figure 3.1A,B). Genes that were common to both quiescence techniques, represented in the overlap of the Venn diagram (Figure 3.1C), are referred to as murine core quiescence genes (mCQG), to distinguish from the human study. This results in 680 upregulated and 563 downregulated mCQG.

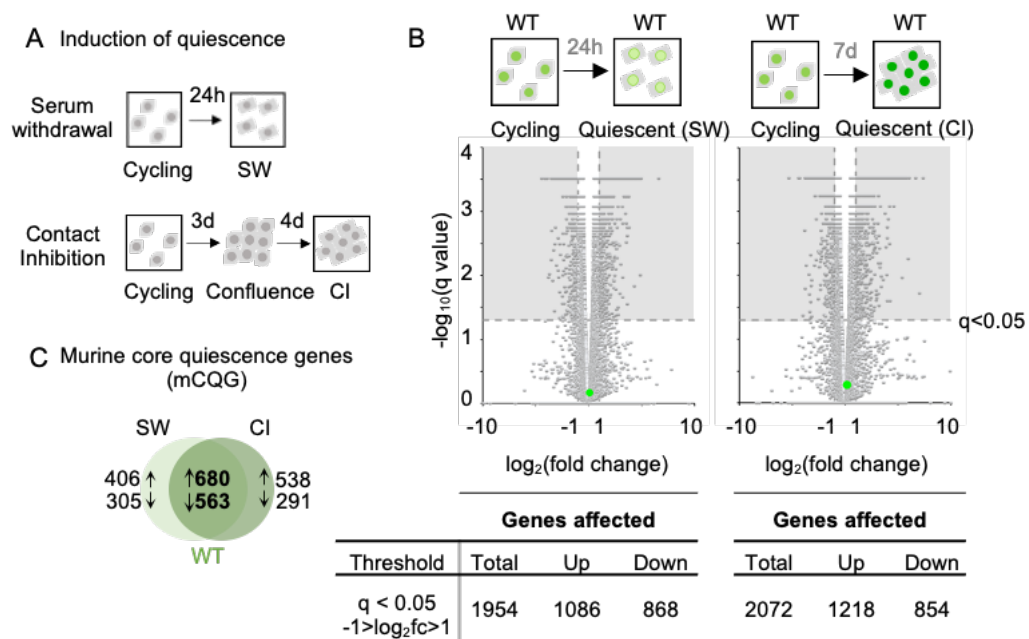


Figure 3.1. **Murine core quiescence genes (mCQG)**. A. Schematic describing two strategies for inducing quiescence, serum withdrawal (SW, 24 hours) and contact inhibition (CI, 7 days), each applied to triplicate cell populations from independent day 13 embryos, from WT mice. B. Volcano plots showing the mean fold change in transcript level against significance (q-value) for all 43834 genes in WT PEFs over the quiescence transition for both SW and CI. CIZ1 is highlighted on each plot in green. Below each plot are the number of genes that reach the threshold  $-1 > \log_2 fc > 1$  and the specified significance threshold of  $\log_2 fc$  FDR  $q < 0.05$ . C. Venn diagram showing the number of transcription units significantly changed on entry to quiescence, divided into those that go up or down. The overlap illustrates those common to both triggers and defines a murine core quiescence gene set for WT cells.

#### **3.4.1.1 Comparison between murine and human core quiescence genes**

The mCQG are broadly consistent with the core quiescence program identified previously in human foetal lung fibroblasts (Coller et al., 2006). My murine fibroblast program is much larger (1243 genes) compared to the human fibroblast program (149 genes), which may reflect species differences, but could also be due to differences in significance thresholding, the additional quiescence trigger in the human program or variations in quiescence protocols. 28 genes from the human gene set are present in the murine program, this includes 3 genes found under an alternative name and another 3 genes that are present but have other genes mapped to the same loci. Also, in some cases, while the same genes are not present, paralogs or members of the same gene family are (Figure 3.2). This indicates that similar genes are affected by quiescence triggers in both mice and humans.

To identify the most relevant biological pathways represented by the core quiescence genes, the human and murine core gene lists and the genes common to both were subjected to gene set enrichment analysis (GSEA) (Subramanian et al., 2005). The 10 Gene Ontology (GO) terms which returned the most significant overlap with each set are shown in Table 3.1, Table 3.2 and Table 3.3. For mCQG, the top pathways included those related to the cell cycle, which interestingly, were not present in the top 10 GO terms for the human set. Instead, the most significant pathways for the human set included those that are in response to a particular stimulus or its regulation. Nevertheless, none of these pathways are surprising to see, with a mixture of both cell cycle and response pathways represented by the common 28 genes. This further confirms the commonalities between the murine and human quiescence programs.

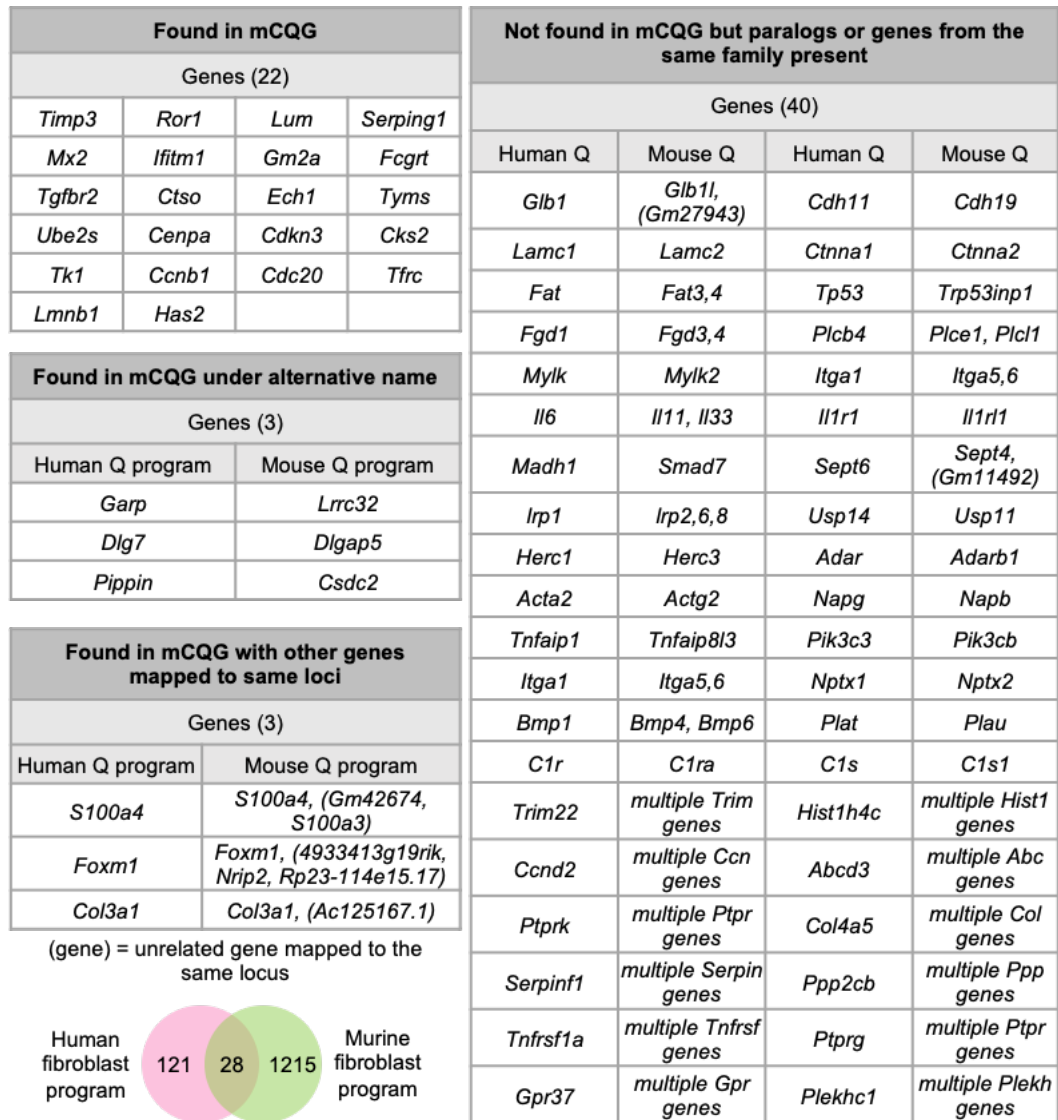


Figure 3.2. **Comparison of the human and murine quiescence programs.**

The gene list described as the murine quiescence program (green) was compared to the gene list described as the human quiescence program (pink). 28 genes were common to both quiescence programs and listed in the tables on the left. The table on the right lists all genes that are part of the human quiescence program that have paralogs or genes from the same family present in the murine quiescence program.

No statistics shown for overlap as there is no appropriate test for this comparison.

Table 3.1. **GSEA of murine core quiescence genes.** The ten most significant overlaps between GO terms and the murine core quiescence genes.

<b>Murine core quiescence genes (mCQG, 1243 genes)</b>				
Set name	Set size	Overlap	p-value	q-value (BH 0.1)
CELL CYCLE	1316	174	1.07E-64	6.34E-61
CELL CYCLE PROCESS	1081	150	5.54E-58	1.64E-54
MITOTIC CELL CYCLE	766	119	2.04E-50	4.03E-47
MITOTIC NUCLEAR DIVISION	361	78	5.10E-42	7.16E-39
REGULATION OF PHOSPHORUS METABOLIC PROCESS	1618	156	6.05E-42	7.16E-39
ORGANELLE FISSION	496	88	2.36E-41	2.33E-38
REGULATION OF PROTEIN MODIFICATION PROCESS	1710	155	1.00E-38	8.45E-36
EXTRACELLULAR SPACE	1376	134	2.18E-36	1.61E-33
CELL DIVISION	460	79	2.47E-36	1.62E-33
CHROMOSOME	880	105	2.50E-35	1.48E-32

Table 3.2. **GSEA of human core quiescence genes.** The ten most significant overlaps between GO terms and the human core quiescence genes.

<b>Human core quiescence genes (149 genes)</b>				
Set name	Set size	Overlap	p-value	q-value (BH 0.1)
RESPONSE TO OXYGEN CONTAINING COMPOUND	1381	34	3.62E-20	1.97E-16
ENZYME BINDING	1737	37	6.65E-20	1.97E-16
EXTRACELLULAR SPACE	1376	32	2.72E-18	5.37E-15
RESPONSE TO EXTERNAL STIMULUS	1821	35	1.81E-17	2.67E-14
REGULATION OF RESPONSE TO STRESS	1468	31	1.36E-16	1.60E-13
REGULATION OF CELL PROLIFERATION	1496	31	2.25E-16	2.22E-13
POSITIVE REGULATION OF RESPONSE TO STIMULUS	1929	34	7.00E-16	5.19E-13
RESPONSE TO ENDOGENOUS STIMULUS	1450	30	7.67E-16	5.19E-13
RESPONSE TO ABIOTIC STIMULUS	1024	26	7.89E-16	5.19E-13
NEGATIVE REGULATION OF RESPONSE TO STIMULUS	1360	29	1.17E-15	6.91E-13

Table 3.3. **GSEA of genes present in both human and murine core quiescence programs.** The ten most significant overlaps between GO terms and the 28 genes present in both the human and murine core quiescence programs.

<b>Both (28 genes)</b>				
Set name	Set size	Overlap	p-value	q-value (BH 0.1)
AGING	264	6	1.31E-08	2.83E-05
MITOTIC CELL CYCLE	766	8	1.43E-08	2.83E-05
CELL CYCLE PROCESS	1081	9	1.05E-08	2.83E-05
DIGESTIVE SYSTEM DEVELOPMENT	148	5	3.53E-08	5.22E-05
CELL CYCLE	1316	9	5.62E-08	6.65E-05
CELL CYCLE PHASE TRANSITION	255	5	4.91E-07	0.0004845
RESPONSE TO EXTERNAL STIMULUS	1821	9	8.53E-07	0.0007214
RESPONSE TO ACID CHEMICAL	319	5	1.45E-06	0.0007792
RESPONSE TO ORGANIC CYCLIC COMPOUND	917	7	1.06E-06	0.0007792
RESPONSE TO OXYGEN CONTAINING COMPOUND	1381	8	1.23E-06	0.0007792

### 3.4.2 Changes in global gene expression on entry to quiescence are not dependent on CIZ1

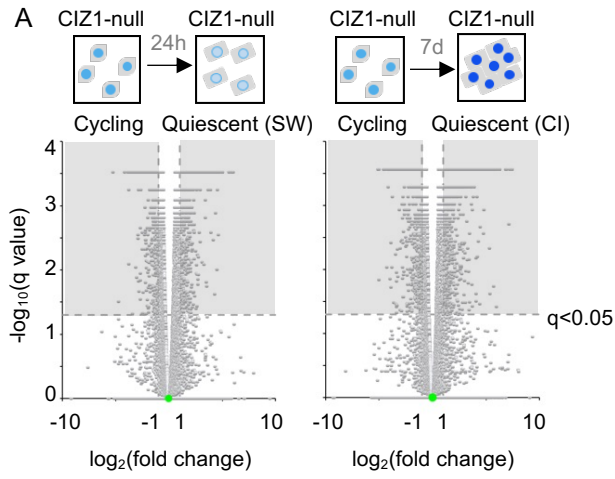
To begin to understand whether CIZ1 impacts the global changes in gene expression that normally take place, genes that significantly changed expression in CIZ1-null PEFs in response to the two quiescence triggers (Figure 3.3A) were compared to those that change in WT PEFs.

Focussing first on each quiescence trigger separately, a comparable number of genes responded in WT and CIZ1-null cells. In WT cells, 4.1% and 4.4% of the genome significantly changed expression ( $-1 > \log_2 \text{foldchange} > 1$ ,  $q < 0.05$ ) following SW and CI, respectively. For CIZ1-null cells, a similar response was recorded with 4.4% and 5.3% following SW and CI (Figure 3.3B).

Like with WT cells, genes common to both SW and CI generated a core quiescence gene set for CIZ1-null cells which follows the same trend as WT but is slightly larger (Figure 3.3C). To investigate the effect of CIZ1 loss on the mCQG, core upregulated and downregulated genes for both genotypes were separately subjected to GSEA. This revealed similar profiles for WT and CIZ1-null cells, with the downregulated sets returning by far the most significant and coherent overlaps with GO terms (Figure 3.3D). Unsurprisingly, these relate to the cell cycle, indicating that CIZ1-null cells, like WT cells, remain capable of executing quiescence-linked gene expression programs.

Notably, for both genotypes, similar numbers of genes are up and down regulated. In fact, slightly more genes increase than decrease, which appears to contradict the widely held notion of global transcriptional repression, though it does support the proposition of quiescence as an actively regulated state (Cheung and Rando, 2013, Cho et al., 2019). When gene expression is expressed in absolute terms (Transcripts Per Million, TPM), it is evident that upregulated genes typically have lower levels in the cycling state than downregulated genes and experience a smaller overall change during quiescence entry (Figure 3.3E). This suggests a greater overall change in the down direction, consistent with the established view of global transcriptional repression during quiescence.

This analysis shows that the loss of CIZ1 does not significantly impact the global changes in gene expression on quiescence entry. However, some genes behave differently (Figure 3.3F) and it is these genes I investigated further.



Threshold	Genes affected			Genes affected		
	Total	Up	Down	Total	Up	Down
$q < 0.05$ $-1 > \log_2 fc > 1$	2078	1071	1007	2514	1357	1157

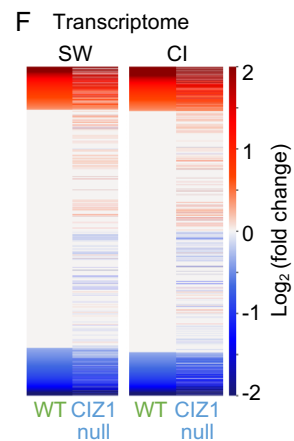
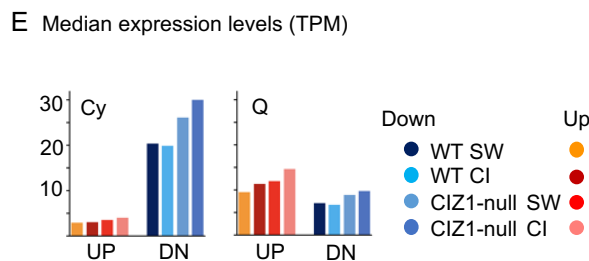
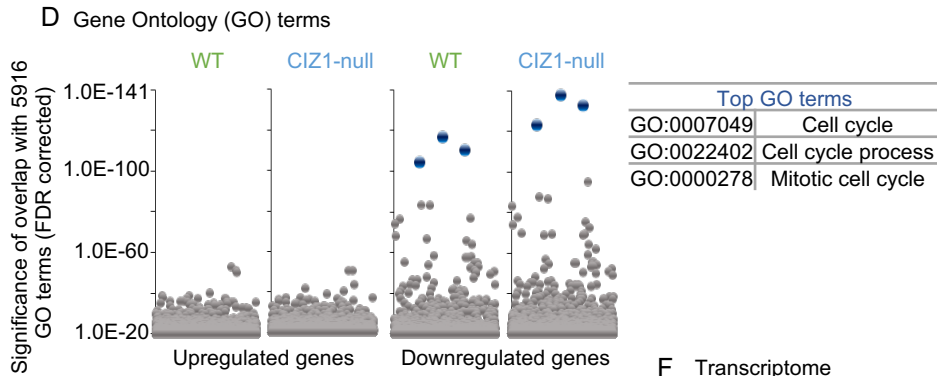
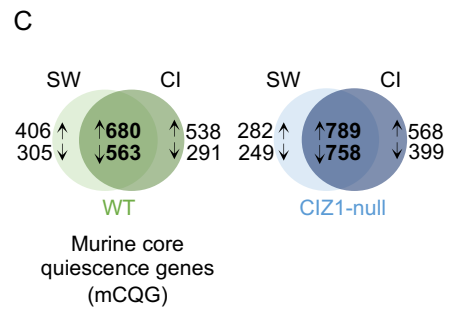
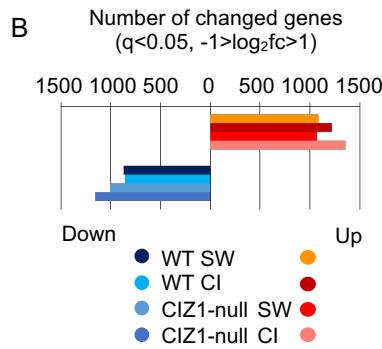


Figure 3.3. **Transcriptomic analysis during entry to quiescence.** A. Volcano plots showing the mean fold change in transcript level against significance (q-value) for all 43834 genes in CIZ1-null PEFs over the quiescence transition for both serum withdrawal (SW) and contact inhibition (CI). CIZ1 is highlighted on each plot in green. Below each plot are the number of genes that reach the threshold  $-1 > \log_2 fc > 1$  and the specified significance threshold of  $\log_2 fc$  FDR  $q < 0.05$ . B. The number of transcription units significantly upregulated ( $\log_2 fc > 1$ , red) or downregulated ( $\log_2 fc < -1$ , blue) on entry to quiescence via SW or CI (FDR  $q < 0.05$ ) for WT and CIZ1-null PEFs, showing a similar number in each class. C. Venn diagrams showing the number of transcription units significantly changed on entry to quiescence, divided into those that go up or down. For WT cells (green) the overlap defines a murine core quiescence gene set. D. Dot plots showing the significance of overlap with all 5916 Gene Ontology (GO) terms for the core quiescence gene sets in C. The most significant GO terms (blue) relate to the cell cycle and are returned by the downregulated genes for both genotypes. E. Median expression level (TPM) of up and downregulated genes shown in B, for cycling and quiescent WT and CIZ1-null cells. Genes that are downregulated during quiescence entry have a higher expression level in the cycling state. F. Heat maps compare fold change in expression during quiescence entry between WT and CIZ1-null PEFs, for the two quiescent methods. Transcription units are ordered by WT fold change; upregulated (red), downregulated (blue), and where  $q > 0.05$  (white).

### 3.4.3 CIZ1-dependent genes during quiescence entry

To explore the CIZ1-dependent genes, both genotypes were compared for the two quiescence triggers separately before finding the overlap between techniques. This allows the gene lists to be divided into four categories; those that fail to go up or down (F-UP, F-DN) in CIZ1-null cells compared to WT cells, and those that go up or down inappropriately (I-UP, I-DN) in CIZ1-null cells (because they did not meet the threshold criteria in WT cells) (Figure 3.4A). All four categories are similarly represented in the CI, SW and overlap lists, indicating no overall bias in the direction of change (Figure 3.4B). However, interrogation of GSEA curated gene sets with the core set for each category (only genes common to both SW and CI) returned by far the most significant overlaps with inappropriately downregulated genes (brown data points) (Figure 3.4C). This shows the I-DN category to be the most coherent in terms of biological role, with the top set representing DREAM complex target genes (Fischer et al., 2016). This is an interesting observation as target genes of the DREAM complex are typically repressed in quiescence, yet they are returned here as part of the I-DN set, suggesting they are only significantly downregulated in CIZ1-null cells and not WT. I therefore decided to investigate the behaviour of the DREAM complex target genes further.

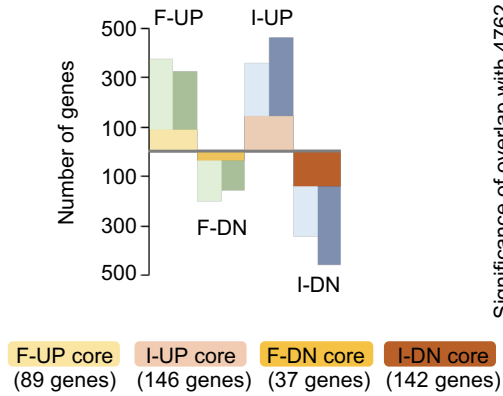
#### 3.4.3.1 DREAM complex targets

Looking specifically at the 929 genes reported to be under the regulation of the DREAM complex (GSEA set M149) (Fischer et al., 2016), differences in the behaviour of a subset during quiescence entry was evident between WT and CIZ1-null cells. As expected, the I-DN gene set is the most populated with 33 genes (Figure 3.4D). When classified by biological process, these high confidence CIZ1-dependent I-DN DREAM target genes revealed striking commonalities. As well as the top-level term of 'cell cycle' the most common GO terms related to DNA metabolism (repair, recombination, replication), and chromatin (Table 3.4). Their high representation makes these biological processes candidates for the underpinning defects in CIZ1-null cells, and therefore the link between CIZ1 and human disease, but they remain representative of a wide range of functions. Further inspection of the mean expression level (TPM values) revealed that all 33 genes follow a downward trend on entry to quiescence, evident in both genotypes. However in all cases, CIZ1-null cells have a higher expression in the cycling state, and in many cases fall further (quiescent state) compared to WT cells (Figure 3.4E, Figure 3.5). The combined effect (magnitude of change) only meets the significance threshold in CIZ1-null cells, and elevated expression in the cycling state appears to be the major contributory factor to their emergence through the applied filters. This led me to explore the cycling state, focussing on the GO terms that were most represented.

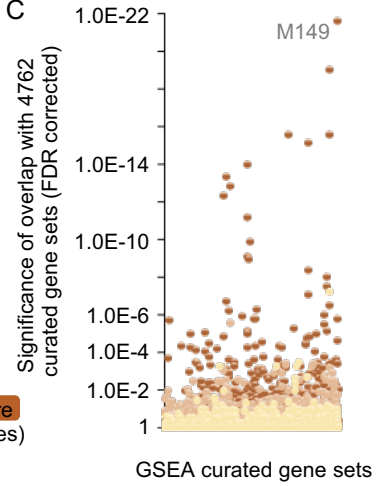
A CIZ1-dependent genes



B



C



D CIZ1- dependent DREAM complex targets

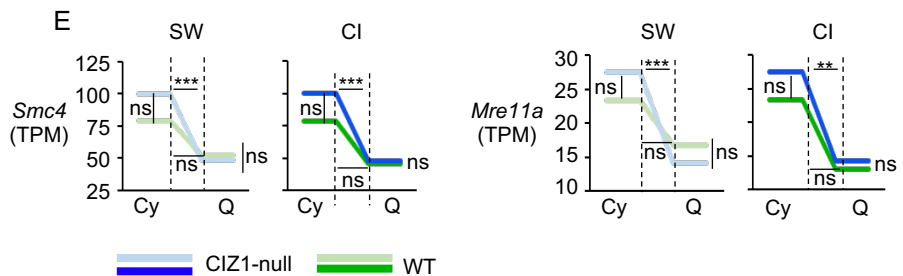
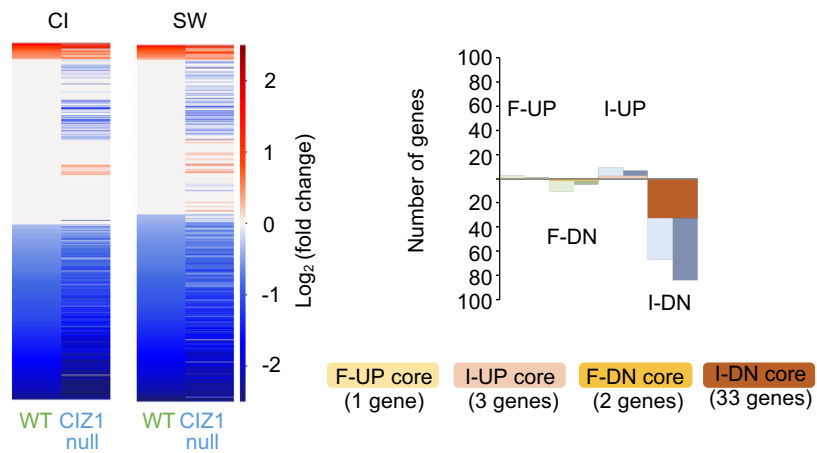


Figure 3.4. **A subset of DREAM complex target genes are modulated by CIZ1.** A. Venn diagrams illustrating CIZ1-dependent genes that are upregulated and downregulated during quiescence entry (intersection shows those that are not CIZ1-dependent). Genes on the left (green) change in WT cells only (FDR  $q < 0.05$ ) and are referred to as genes that ‘fail’ to change in CIZ1-null; genes on the right (blue) change in CIZ1-null cells only (FDR  $q < 0.05$ ) and are referred to as genes that are ‘inappropriately’ changed in CIZ1-null cells. B. Histogram showing the overlap between the two quiescence methods for CIZ1-dependent genes (F-UP; fail to go up, F-DN; fail to go down, I-UP; inappropriately up, I-DN; inappropriately down), highlighted in shades of brown. C. Dot plot showing the significance of overlap between the four core CIZ1-dependent gene sets with 4762 GSEA curated gene sets. I-DN (dark brown) overlap most significantly with Fischer DREAM Targets (systematic name M149). D. Heat maps of 844 DREAM complex target genes defined in M149 (Fischer et al., 2016) showing fold change in expression during quiescence entry in WT and CIZ1-null PEFs, for the two quiescent methods. Genes are ordered by WT fold change. Right, histogram showing the number of DREAM complex target genes that fail to change or are inappropriately changed in CIZ1-null during quiescence entry, for each quiescence trigger separately and the overlap between the two. E. Expression (mean TPM) of *Smc4* (Structural Maintenance of Chromosomes 4) and *Mre11a* (MRE11 Homolog, Double Strand Break Repair Nuclease), before (cycling, Cy) and after (quiescence, Q), by SW (left) and CI (right). \*\* FDR  $q < 0.01$ , \*\*\* FDR  $q < 0.001$  and ns denotes no significant difference. Similar data for all 33 I-DN genes is given in Figure 3.5.

Table 3.4. **Core set of DREAM complex target genes that are inappropriately downregulated during quiescence entry in CIZ1-null cells.** Unique UniProtKB identifiers are shown, along with the overarching GO biological process annotation for each identifier, collected using QuickGO ([www.ebi.ac.uk/QuickGO](http://www.ebi.ac.uk/QuickGO)).

33 DREAM target genes I-DN	UniProtKB identifier	GO-biological process annotations	
<i>Tfdp1</i> : Transcription factor Dp-1	Q08639	15	Cell cycle, regulation of transcription
<i>Haus4</i> : HAUS Augmin like complex subunit 4	Q8BFT2	10	Cell division, centrosome cycle, spindle assembly
<i>Mtbp</i> : MDM2 binding protein	Q8BJS8	9	Cell cycle, regulation of protein ubiquitination, protein localisation to kinetochore
<i>Orc2</i> : Origin recognition complex subunit 2	Q60862	2	DNA replication
<i>Hnrnpab</i> : Heterogeneous nuclear ribonucleoprotein A/B	Q99020	9	Regulation of transcription, regulation of gene expression, mRNA modification
<i>Nup155</i> : Nucleoporin 115	Q99P88	14	mRNA and protein transport, nuclear envelope organisation
<i>Mre11a</i> : Meiotic recombination 11 homolog A	Q61216	49	Double-strand break repair, DNA repair, telomere maintenance, DNA damage checkpoint signalling, cellular response to DNA damage stimulus
<i>Usp1</i> : Ubiquitin carboxyl-terminal hydrolase 1	Q8BJQ2	20	DNA repair, protein deubiquitination, cellular response to DNA damage stimulus
<i>Cacybp</i> : Calcyclin-binding protein	Q9CXW3	6	Negative regulation of cell death, positive regulation of DNA replication
<i>Tipin</i> : TIMELESS-interacting protein	Q91WA1	23	DNA replication checkpoint signalling, replication fork protection/arrest, cell cycle phase transition, positive regulation of cell population proliferation
<i>Gpd2</i> : Glycerol-3-phosphate dehydrogenase	Q64521	8	Glycerol-3-phosphate metabolic process, NADH metabolic process, gluconeogenesis
<i>Fancm</i> : Fanconi anemia group M protein homolog	Q8BGE5	20	Cellular response to DNA damage stimulus, DNA repair, replication fork processing, positive regulation of protein monoubiquitination
<i>Exosc2</i> : Exosome Component 2	Q8VBV3	26	RNA processing, positive regulation of cell growth
<i>Rfwd3</i> : E3 ubiquitin-protein ligase	Q8CIK8	31	Double-strand break repair via HR, protein ubiquitination, mitotic G1 DNA damage checkpoint signalling, replication fork processing, chromosome breakage
<i>Tcof1</i> : Treacle protein	O08784	8	Neural crest cell development/formation, regulation of translation
<i>Nup43</i> : Nucleoporin 43	P59235	7	Protein transport, cell division, mRNA transport, chromosome segregation, cell cycle
<i>Rad51c</i> : RAD51 Paralog C	Q924H5	22	Double-strand break repair via HR, DNA repair, DNA recombination, positive regulation of G2/M transition

<i>Smc4</i> : Structural maintenance of chromosomes protein 4	Q8CG47	20	Chromosome condensation, cell division, cell cycle, single strand break repair, kinetochore organisation, chromosome segregation
<i>Slbp</i> : Histone RNA hairpin-binding protein	P97440	10	mRNA processing/transport, cap-dependent translational initiation
<i>Eri1</i> : 3'-5' exoribonuclease 1	Q7TMF2	5	Histone mRNA catabolic process, rRNA processing, gene silencing by RNA
<i>Zw10</i> : Centromere/kinetochore protein zw10 homolog	O54692	30	Mitotic sister chromatid segregation, regulation of exit from mitosis, mitotic spindle assembly, checkpoint signalling, protein transport, cell division
<i>Ezh2</i> : Enhancer of zeste homolog 2	Q61188	92	Histone H3-K27 methylation, negative regulation of transcription/gene expression, chromatin organisation, positive regulation of MAP kinase activity
<i>Nup85</i> : Nucleoporin 85	Q8R480	14	Protein import into nucleus, mRNA export from nucleus, positive regulation of transcription
<i>Wdr76</i> : WD repeat-containing protein 76	A6PWY4	5	Cellular response to DNA damage stimulus, regulation of DNA damage checkpoint
<i>Gins3</i> : GINS Complex Subunit 3	Q9CY94	12	DNA replication, DNA unwinding involved in DNA replication
<i>Rpa2</i> : Replication protein A	Q62193	29	Double-strand break repair via HR, nucleotide-/base-excision repair, mismatch repair, DNA replication, telomere maintenance, regulation of DNA damage checkpoint, protein localisation to chromosome, DNA recombination
<i>Snrpd1</i> : Small Nuclear Ribonucleoprotein D1	P62315	11	Spliceosomal snRNP assembly, mRNA splicing, RNA processing
<i>Atad5</i> : ATPase family AAA domain-containing protein 5	Q4QY64	25	Positive regulation of DNA replication and cell cycle G2/M phase transition, cellular response to DNA damage stimulus, intrinsic apoptotic signalling pathway in response to DNA damage
<i>Xrcc2</i> : X-Ray repair cross complementing 2	Q9CX47	32	Double-strand break repair via HR, strand invasion, cell cycle, DNA repair, cellular response to DNA damage stimulus, DNA recombination
<i>Palb2</i> : Partner And Localiser Of BRCA2	Q3U0P1	17	Double-strand break repair via HR, cellular response to DNA damage stimulus, DNA recombination, DNA repair
<i>Mnd1</i> : Meiotic Nuclear Divisions 1	Q8K396	4	DNA recombination, cell cycle
<i>Cenpl</i> : Centromere protein L	Q3U3S3	1	Assembly of kinetochore proteins, mitotic progression, chromosome segregation
<i>Hist1h2aj</i> : Histone H2A type 1-J	Q99878	2	Heterochromatin assembly

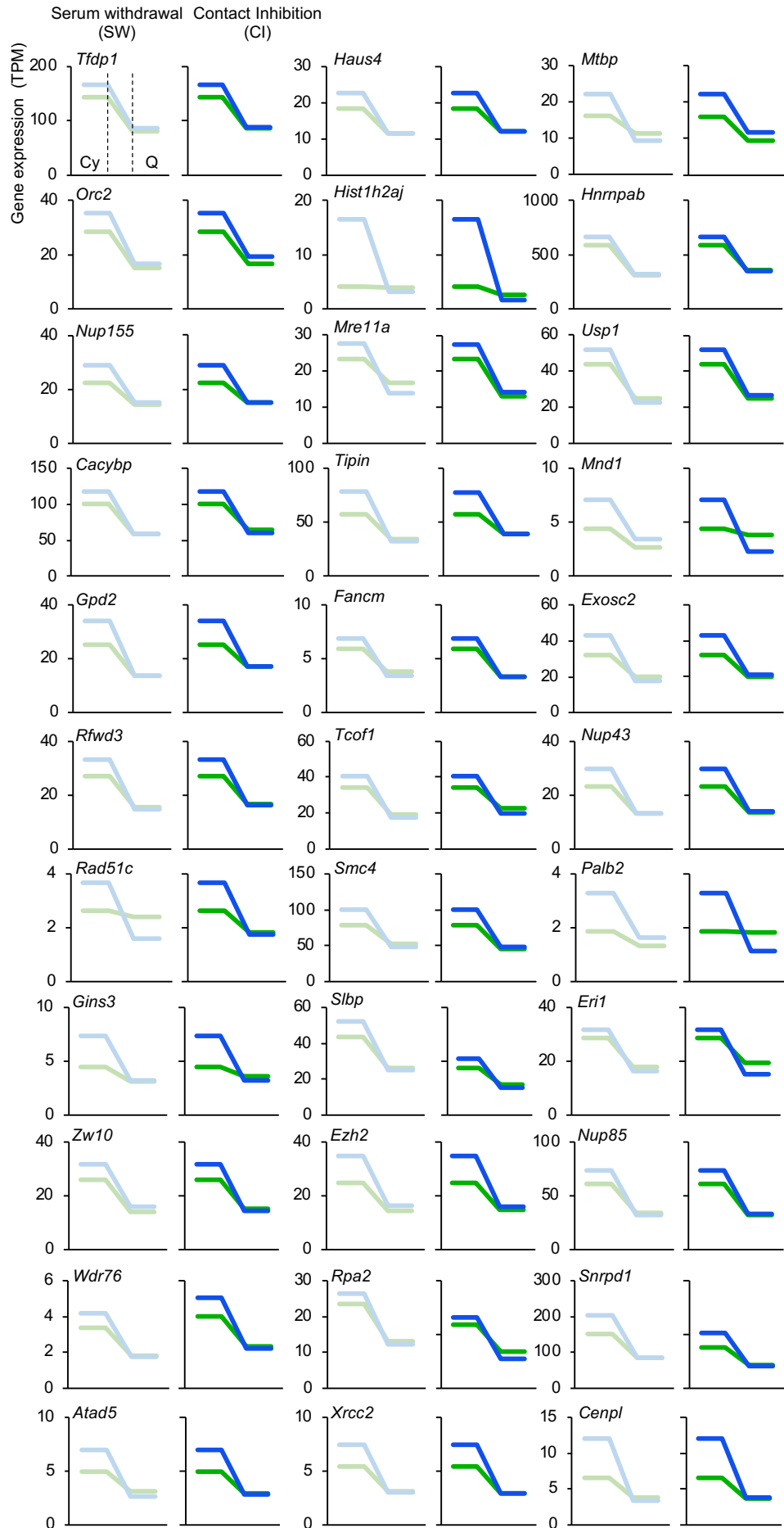


Figure 3.5. **Expression changes for the 33 I-DN DREAM complex target genes during quiescence entry.** Graphs show mean expression levels (Mean Transcripts Per Million, TPM) of all 33 I-DN DREAM complex target genes in WT (green) and CIZ1-null (blue) cells before (cycling, Cy) and after (quiescence, Q); contact inhibition (right) and serum withdrawal (left). All genes see a drop in TPM at the end of both quiescence protocols and in both genotypes, but this fall is only significant for CIZ1-null cells. There is no significant difference between the cycling expression levels for the two genotypes or between the quiescent expression levels, for both protocols and for all genes.

#### 3.4.4 DNA repair and chromatin organisation genes

Direct comparison of the cycling state for the 33 genes returned no significant difference between WT and CIZ1-null cells, so TPM values for all genes described by an implicated GO term were analysed for trends. Focus on the GO terms related to chromatin and DNA repair were chosen due to their high representation by the CIZ1-dependent I-DN DREAM target genes (Figure 3.6A).

In the cycling state, the high-level term 'chromatin organisation' favours higher expression in CIZ1-null cells, a trend that is even more marked for the subordinate term 'chromosome condensation', but not for 'chromosome localization'. The high-level term 'DNA repair' is not overall perturbed by loss of CIZ1 in cycling cells. The subordinate term 'regulation of DNA double-strand break repair by homologous recombination' is slightly skewed while the similar size subordinate term 'mismatch repair' is not (Figure 3.6B). This reinforces the suggestion that chromatin condensation and homology directed repair are both affected by loss of CIZ1. As 'chromatin condensation' has the biggest skew toward higher expression in cycling CIZ1-null cells, the complex associated with this process, the condensin complex, was analysed further.

In eukaryotes the condensin complex exists in two forms, I and II (Figure 3.6C). Both contain the core subunits SMC2 and SMC4, of which SMC4 is represented in the core I-DN set. Condensins have been associated with chromatin compaction during yeast and human quiescence (Coller et al., 2006, Swygert et al., 2019), and condensin II specifically implicated in a thymocyte model (Rawlings et al., 2011). Strikingly, expression of *Smc2*, *Smc4* and the additional subunits *Ncaph*, *Ncapd2*, and *Ncapg* for condensin I, and *Ncaph2*, *Ncapd3*, and *Ncapg2* for condensin II are all skewed towards increased expression in CIZ1-null cycling cells compared to WT. Though the difference is not significant for any one component, the overall trend is significant (Figure 3.6D,E). In contrast, subunits of the closely related cohesin complex are only slightly skewed. Additionally, two similarly sized sets that represent the TOR complex involved in cell proliferation control (Loewith and Hall, 2011), and the CDC73 PAF1 complex involved in survival during long-term quiescence (Oya et al., 2019), are not affected (Figure 3.6E). This suggests that CIZ1-null cells have elevated expression of the chromatin condensation machinery prior to receipt of quiescence triggers.

**A**

	DREAM target genes (I-DN)
Chromatin	<i>Smc4, Ezh2, Hist1h2aj, Nup43, Nup155, Zw10, Cenp1</i>
DNA repair	<i>Mre11a, Usp1, Fancm, Rfwd3, Rad51c, Wdr76, Rpa2, Atad5, Xrcc2, Palb2</i>

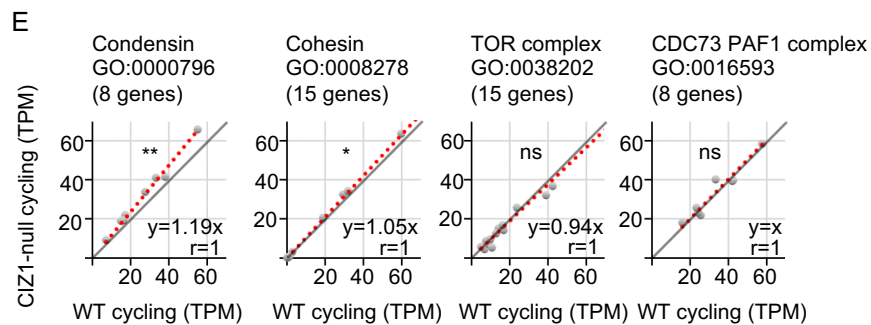
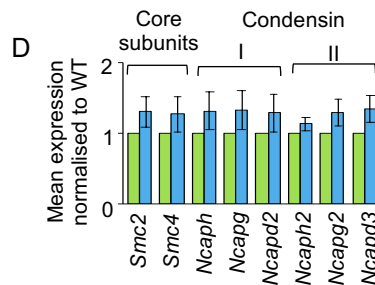
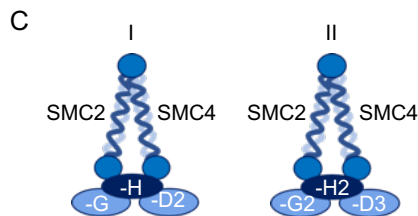
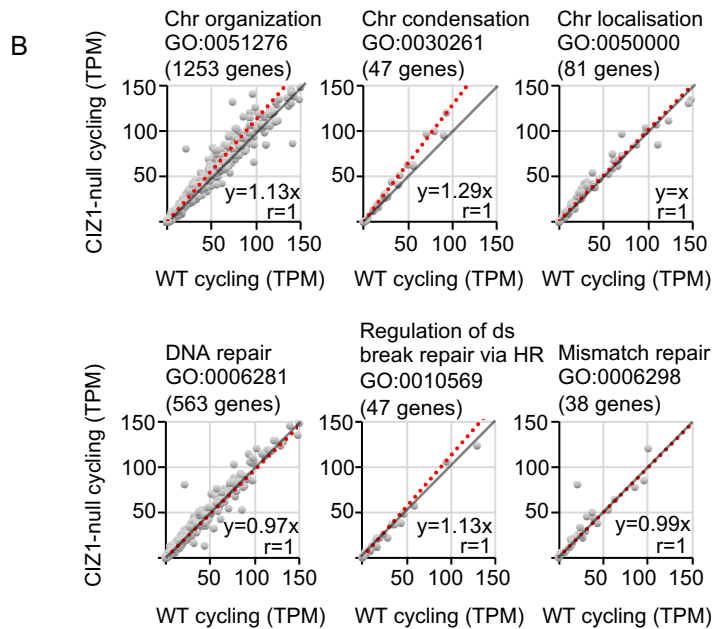
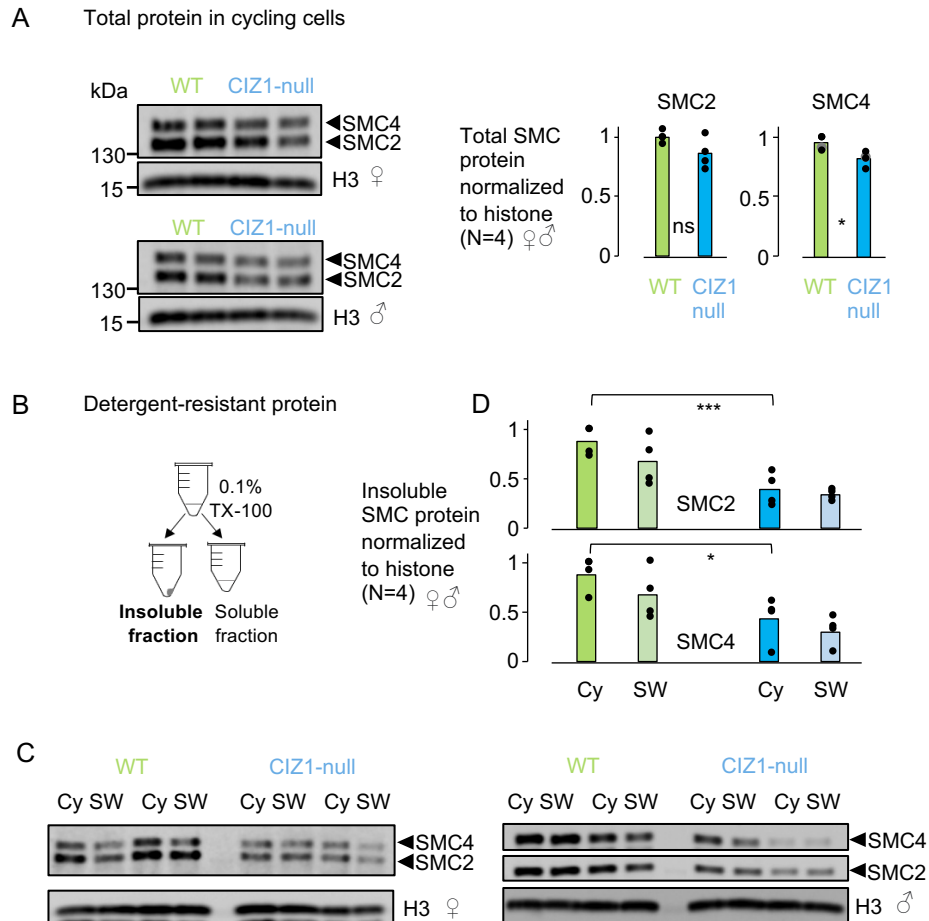


Figure 3.6. **Elevated expression of chromatin condensation genes.** A. Genes that relate to chromatin or DNA repair from the 33 I-DN CIZ1-dependent DREAM targets outlined in Table 3.4. B. Scatter plots comparing expression (mean TPM) in cycling WT and CIZ1-null cells, for all genes within the high-level GO terms; chromosome organisation and DNA repair, plus two subordinate terms for each, as indicated. The grey line ( $y=x$ ) illustrates no difference between WT and CIZ1-null cells and the red line is the best fit to the data calculated in excel, with the slope of the line indicated. A skew towards the y axis indicates a higher expression in CIZ1-null cycling cells. C. Schematic illustrating the subunits of condensin I and II. D. Mean TPM for all condensin subunits in WT (green) and CIZ1-null (blue) PEFs in the cycling state, normalised to WT,  $\pm$ SEM. Individually, no subunit is significantly different between WT and CIZ1-null. E. As in B, for subunits of the condensin complex, the cohesin complex, the TOR complex and the CDC73 PAF1 complex. Expression of the condensin subunit class is significantly affected by loss of CIZ1. Results are compared by the Wilcoxon's signed ranked test where ns denotes no significant difference, \*  $p<0.05$  and \*\*  $p<0.01$ .

#### **3.4.4.1 Core condensin subunits protein levels**

To understand if elevated expression of the condensin subunits in CIZ1-null cells translates to elevated protein levels, I sought to analyse the total protein levels from two female and two male cycling populations for both genotypes. The two core subunits, SMC2 and SMC4, were relatively unchanged between WT and CIZ1-null cells (Figure 3.7A). If anything, CIZ1-null cells have slightly less total protein. This concludes that the elevated transcript does not equal elevated condensin protein.

One possibility is that elevated transcript could reflect compensation for compromised function of the condensin complex. Therefore, the binding ability of the condensin complex in WT and CIZ1-null cells was investigated. Cycling populations and populations following a 1-hour SW were subjected to a 5-minute detergent (0.1% Triton-X-100) incubation to allow cytosolic and nucleosolic proteins to be released prior to centrifugation (Figure 3.7B). Centrifugation created two parts to the sample: pellet (insoluble material including chromatin and nuclear structural proteins) and supernatant (soluble proteins from cytoplasm and nucleus). The two fractions were separated, and the pellet fraction analysed by western blot. This revealed significantly less SMC2 and SMC4 protein in the CIZ1-null insoluble fraction compared to WT, in both the cycling state and after SW. This suggests that their assembly on chromatin is subtly influenced by CIZ1 (Figure 3.7C,D).



**Figure 3.7. Increased solubility of SMC2 and SMC4 in CIZ1-null cells.** A. Whole cell lysates from WT and CIZ1-null cycling populations, female (top) and male (bottom), illustrating the total protein levels for SMC2, SMC4 and Histone H3. For each genotype 4 independent cell populations were examined (2 female, 2 male); WT (13.49, 13.31, 13.20, 13.30) and CIZ1-null (13.42, 13.59, 13.45, 13.38). Right, quantification showing mean for the 4 independent populations with individual values indicated. B. Schematic demonstrating the sample preparation of detergent-resistant (insoluble) protein for subsequent western blot analysis. C. Detergent-resistant fractions from WT and CIZ1-null female (left) and male (right) populations in a cycling state and following a short (1 hour) SW. For each genotype 4 independent cell populations were examined (2 female, 2 male); WT (13.22, 13.32, 13.20, 13.30) and CIZ1-null (41.2fa, 14.2, 13.41, 13.43). D. Quantification showing mean for the 4 independent populations with individual values indicated. Results from the cycling states were compared by t-test where ns denotes no significant change, \*  $p < 0.05$ , \*\*\*  $p < 0.001$ .

### 3.5 Discussion

Whole transcriptome sequencing is a powerful tool that has helped reveal a framework through which CIZ1 impacts gene expression on entry to quiescence. The cell must initially prevent cell cycle progression through downregulation of cell cycle-related genes. Other gene sets are also known to be downregulated including those relating to signal transduction and metabolism. Conversely, in order to aid quiescence entry, cell cycle inhibitors are known to be upregulated. Recent advances have started to propose quiescence as a poised, heterogenous cellular state due to the upregulation of some genes as well as different gene signatures evident depending on the quiescence trigger and the cell type (Cheung and Rando, 2013, Collier et al., 2006, Marescal and Cheeseman, 2020). The data presented here supports these ideas and demonstrates that in the absence of CIZ1, cells retain the ability to downregulate cell cycle genes with no dramatic effect on the number of genes that change expression over the quiescence transition. A similar number of genes are also upregulated compared to downregulated for both genotypes illustrating quiescence is a more complex state than originally believed.

Despite this, a subset of genes appear to be dependent on CIZ1. A defined, coherent set of genes that meet the significance thresholds for downregulation in CIZ1-null cells but not in WT has been established. These are enriched for targets of the DREAM complex. Initially, this data was distracting as it implies that a subset of DREAM target genes are downregulated only in CIZ1-null cells. However, evaluation of TPM values illustrated how these genes emerged through the significance filters. These genes were downregulated in WT cells but did not meet the significance threshold. All 33 genes had a higher expression level in CIZ1-null cycling cells, illustrating a clear trend in behaviour. An elevated expression in the cycling state may be the consequence of many things, including but not limited to, a change in RNA stability and other post-transcriptional controls or a compensation mechanism for a non-functioning pathway.

Another interesting observation is that the CIZ1-dependent I-DN DREAM target genes are involved in common biological processes. Notably, chromosome organisation and DNA double-strand break repair. Genes relating to chromatin condensation and in particular subunits of the condensin complex all have altered gene expression in the absence of CIZ1 and always manifest as increased expression in the cycling state of CIZ1-null cells. Again, this is not significant on an individual gene basis but the trend within the set is. As this is not translated to higher total protein levels in cycling CIZ1-null cells, it can be concluded that the effect of CIZ1 on gene expression does not affect a cell's ability to enter a stable, quiescent state.

However, this analysis has predicted two pathways which are failing in CIZ1-null cells. It suggests failure to organise chromatin and failure to repair DNA damage/breaks. Further analysis of the condensin complex at the protein level begins to suggest compromised function in CIZ1-null cells. With less functionality, the condensin complex may not be able to fulfil its role, making chromatin condensation a candidate process for instability during entry to quiescence in CIZ1-null cells.

## 4 CIZ1-dependent chromatin condensation during quiescence entry

### 4.1 Introduction

The condensation state of chromatin, and the condensation process, is most commonly studied when interphase chromatin is compacted into chromosomal units on entry into mitosis. However, condensation also occurs in other stages of the cell cycle; as cells enter quiescence (Tokuyasu et al., 1968) and after chromatin is replicated in S phase (Li et al., 1998).

Chromatin condensation and reduction of nuclear size on entry to quiescence is well-documented in *Saccharomyces cerevisiae* (Laporte et al., 2016, Swygert et al., 2019), primary human fibroblasts (Evertts et al., 2013) and thymocytes (Rawlings et al., 2011). These studies all implicate a role for the condensin complex over the quiescence transition. Following the transcriptomic study discussed in Chapter 3, chromatin condensation was identified as a potential defective pathway in CIZ1-null cells. In light of this, I sought to investigate the chromatin condensation status of WT and CIZ1-null cells upon quiescence.

How WT nuclei transition to a stable, condensed quiescent state is not fully understood. Therefore, this chapter also investigates the underlying mechanism of chromatin condensation in response to quiescence triggers. During mitosis, the function of the condensin II complex has been linked to the methylation status of histone H4 lysine 20 (H4K20). Normally, dissociation of the demethylase PHF8 leads to emergence of H4K20me1 and recruitment of NCAPD3 and NCAPG2 (Liu et al., 2010), while lack of the mono-methyltransferase SET8, results in mitotic chromosome condensation failure (Houston et al., 2008). As well as mitosis, H4K20 methylation has been implicated in quiescence-linked condensation. During entry to quiescence, H4K20me1 is converted to H4K20me3 and loss of the enzyme responsible, Suv4-20h2, impacts chromatin compaction during this transition (Evertts et al., 2013). As previous analysis of CIZ1 at the Xi has revealed CIZ1-dependent maintenance of two other histone post-translational modifications (PTMs), H3K27me3 and H2AK119Ub1 (Stewart et al., 2019), this raises the possibility of defects in maintenance of H4K20me1.

## 4.2 Aims

The aims of the work described in this chapter were to:

- Profile chromatin condensation during entry to quiescence in WT and CIZ1-null cells.
- Progress understanding of CIZ1 function during entry to quiescence by focussing on its relationship with H4K20me1 and the function of the condensin II complex.

### 4.3 Experimental design

This chapter exploits the same two quiescence protocols used in Chapter 3, with focus on the serum withdrawal (SW) method due to the speed of response and the fact that all cells are subjected to the trigger simultaneously. Analysis at time points over a short (1-2 hours) or long (24 hour) SW period have been carried out to compare the response of WT and CIZ1-null populations. In some experiments SW is followed by a period in which serum is added back (AB) to the medium.

Condensation of chromatin in quiescent cells results in a compacted nucleus when compared to cycling nuclei. Therefore, analysis of nuclear area can be used as a surrogate measurement for chromatin condensation (Swygert et al., 2019). To quantify nuclear area, immunofluorescence images of DAPI stained WT and CIZ1-null primary embryonic fibroblasts (PEFs) were analysed in the image processing package, Fiji. All images were split into the three channels, (red, green and blue) with only the blue channel being of interest here. The region(s) of interest (ROIs) were selected based on the “Otsu Threshold” which outlines all nuclei. Conversion of the threshold image to a mask image enables all particles in the image to be analysed creating a table of numbered ROIs with corresponding area measurement in pixels (Figure 4.1). Results can be converted from pixels to area in microns, and from area to volume, assuming a spherical nucleus (Chapter 2, Methods).

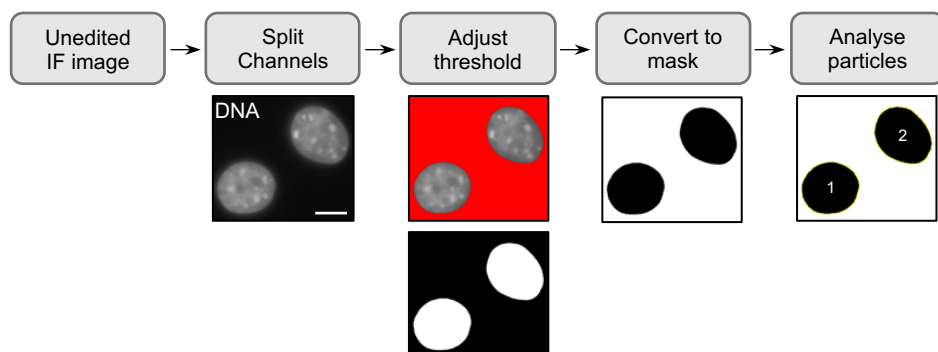


Figure 4.1. **Fiji analysis workflow.** Example workflow for quantification of nuclear area using the Fiji image analysis software.

## 4.4 Results

### 4.4.1 Chromatin condensation on entry to quiescence is impaired in CIZ1-null cells

Experiments conducted here investigate if there are any phenotypic defects in line with the gene sets derived from the transcriptomic analysis outlined in Chapter 3, and whether these underpin the unstable quiescence observed in CIZ1-null cells (Figure 1.8). WT and CIZ1-null cells were exposed to SW and AB and the response of each population analysed for both nuclear size and S phase index.

Before exposure to quiescence stimuli, there was no significant difference in the average nuclear area between WT and CIZ1-null cycling cells (Figure 4.2A) and both populations exhibited the same proportion of cells in S phase (19%). As expected, both WT and CIZ1-null cells responded to 24 hours of SW and stopped cycling, evidenced by a reduced fraction of cells that incorporated EdU (5-ethynyl-2'-deoxyuridine), a marker of cells engaged in DNA synthesis, during a 30-minute pulse. Upon AB, both genotypes are capable of re-entry back into the cell cycle shown by an increase in the number of cells in S phase (Figure 4.2B).

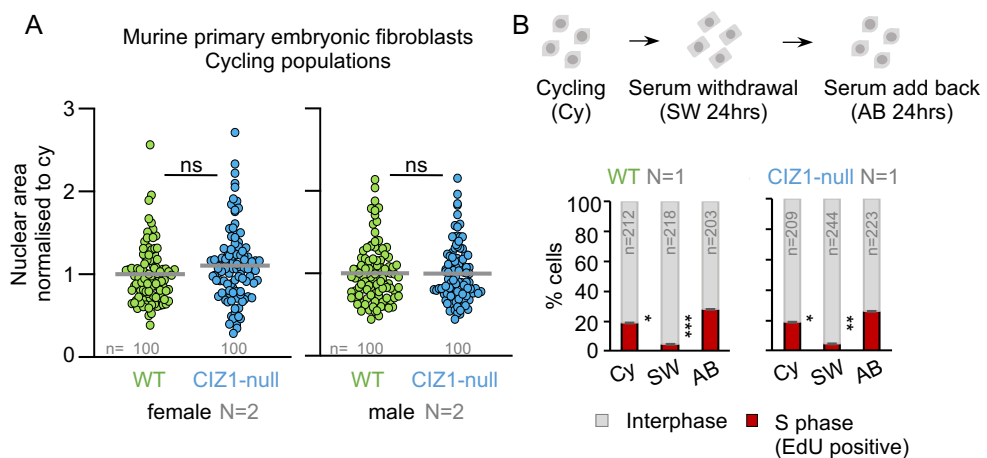


Figure 4.2. **WT and CIZ1-null cells have a reduced S phase index following 24-hour SW.** A. Nuclear area in cycling female and male populations of WT (green) and CIZ1-null (blue) PEFs, demonstrating no difference in nuclear size. Dots represent individual nuclei, with mean (grey bar). B. Serum withdrawal (SW) and add back (AB) strategy and their effect on S phase index. Histograms show the proportion of cells that incorporate EdU during a 30-minute pulse (replicating, red). No difference is detected between WT and CIZ1-null cells in response to SW and AB. Results are compared by either t-test (A) or one-way ANOVA (B), where ns denotes no significant difference, \*  $p < 0.05$ , \*\*  $p < 0.01$ , \*\*\*  $p < 0.001$ .

For WT cells, cell cycle exit is accompanied by successful chromatin condensation measured by an average 25% decrease in nuclear area relative to parent populations, for both male and female PEFs (Figure 4.3A). This parallels previous studies (Evertts et al., 2013, Swygert et al., 2019) and supports chromatin condensation as a phenotypic stage of quiescence entry. However, CIZ1-null cells exhibited a striking failure to condense their nuclei, during the 24 hours following SW, and remained the same size as the cycling population (Figure 4.3B). Surprisingly, upon re-entry to the cell cycle (AB), both WT and CIZ1-null cells remain capable of nuclear decondensation, so that while WT cells returned to the usual size of a cycling population, CIZ1-null nuclei increased in size by an average of 30% compared to their cycling state (Figure 4.3A,B). Considerable heterogeneity was evident in the CIZ1-null population, though even in the most enlarged nuclei, DAPI-dense regions remained, and the nuclear lamina was unperturbed (Figure 4.3C). Thus, CIZ1-null cells are compromised in their ability to condense their chromatin but appear to remain competent at decondensation, strongly implicating CIZ1 in the control or execution of nuclear condensation during quiescence.

Previously, the CIZ1-dependent process of chromatin relocation during replication of the inactive X chromosome was shown to be perturbed in culture adapted cell lines (Stewart et al., 2019). To ask whether chromatin condensation during quiescence entry is also affected by long-term culture, 3T3s (D001 3T3, female mouse fibroblasts (Ridings-Figueroa et al., 2017)) were subjected to SW and AB. Chromatin condensation was evident in this immortalised cell line, unlike other CIZ1-dependent processes, as 3T3 nuclei successfully condensed by 13% in response to SW and returned to the same size as a cycling population upon AB (Figure 4.3D).

Analysis of WT nuclear area after a short SW revealed that the condensation process is in progress as early as one-hour post SW, which implies that CIZ1-dependent chromatin condensation is an early event during quiescence entry (Figure 4.3E).

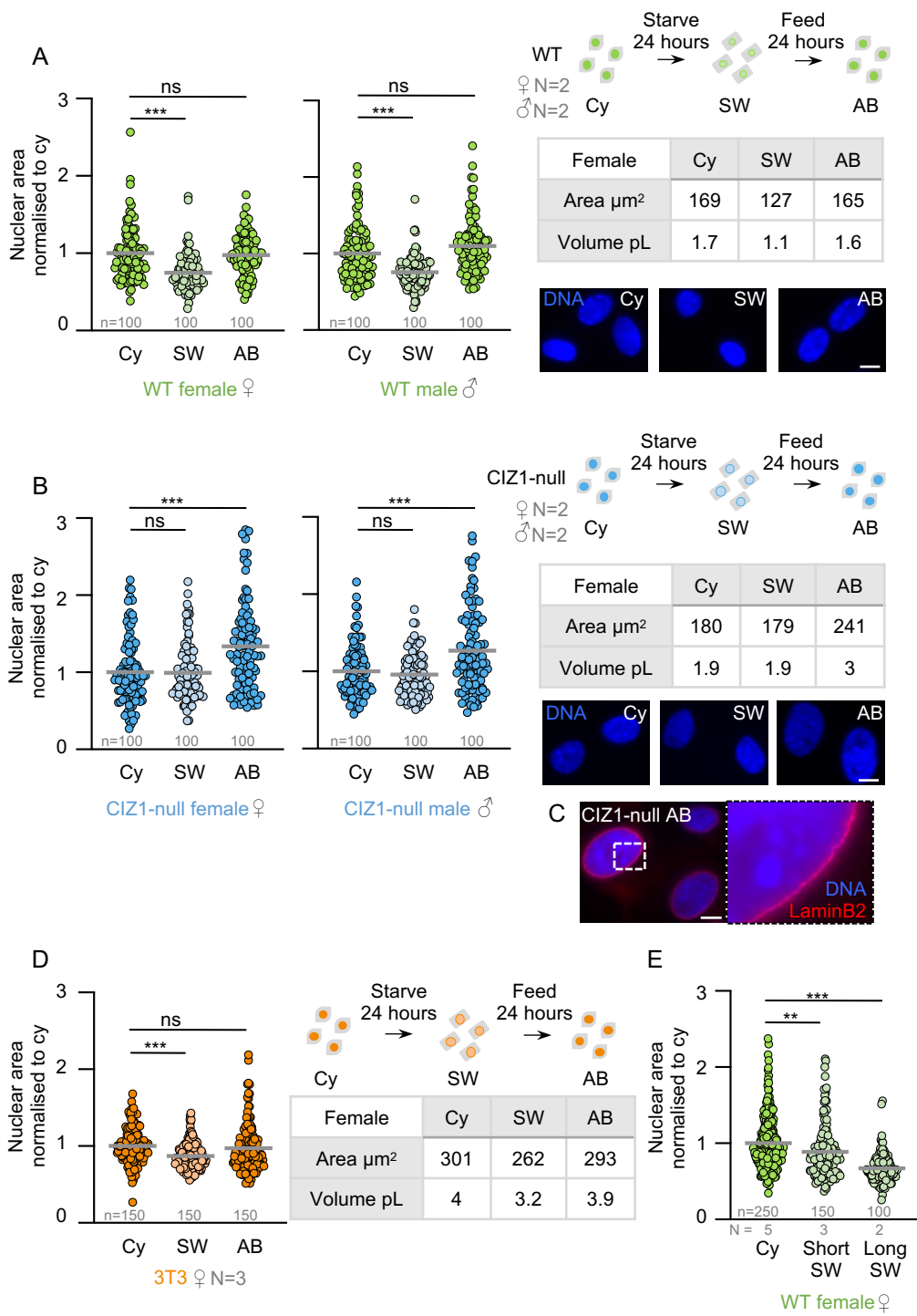


Figure 4.3. **Nuclei from CIZ1-null cells fail to condense during entry to quiescence.** A. Graphs show change in nuclear area over 24-hour SW and AB strategy for male and female WT (green) PEFs, normalised to the means for the cycling control state. Mean areas and calculated volumes, assuming a spherical nucleus, are shown alongside representative images of WT nuclei at each stage. B. As in A but for CIZ1-null (blue) PEFs. C. Immunodetection of the nuclear lamina (Lamin B2, red) in a representative CIZ1-null AB population. D. Nuclear area for the 3T3 cell line (orange) over the SW and AB strategy. E. Nuclear area for female WT PEFs demonstrating a gradual drop in size over a short (1 hour) and long (24 hours) SW window. All results are compared by one-way ANOVA where ns denotes no significant difference, \*\*  $p < 0.01$ , \*\*\*  $p < 0.001$ . DNA is stained with DAPI (blue) and scale bar represents  $10\mu\text{m}$ .

Using the alternative quiescence trigger, contact inhibition (CI), a similar defect was evident in CIZ1-null cells exiting the cell cycle. This methodology takes place across a very different time window, with cells typically reaching 100% confluency after 3 days in culture (d3) followed by a further 4 days (d7) until they reach quiescence. At 100% confluency, WT nuclear area decreased by 27% whereas CIZ1-null nuclei did not change in comparison to the cycling state. This parallels the responses seen following SW. However, after 7 days into the protocol, CIZ1-null nuclei eventually condensed. WT nuclei also condensed further in the extra 4 days of culture and in fact formed a more compact nucleus in comparison to CIZ1-null cells by the end of the time course. There was a 44% and a 33% decrease in nuclear area for WT and CIZ1-null cells, respectively, by day 7 in comparison to the cycling population (Figure 4.4). This analysis confirms that the chromatin condensation pathway is impaired in CIZ1-null cells but suggests that it is not completely dysfunctional. Whether CIZ1-null nuclei eventually condense via the same pathway as WT cells, or through an alternative pathway is not known.

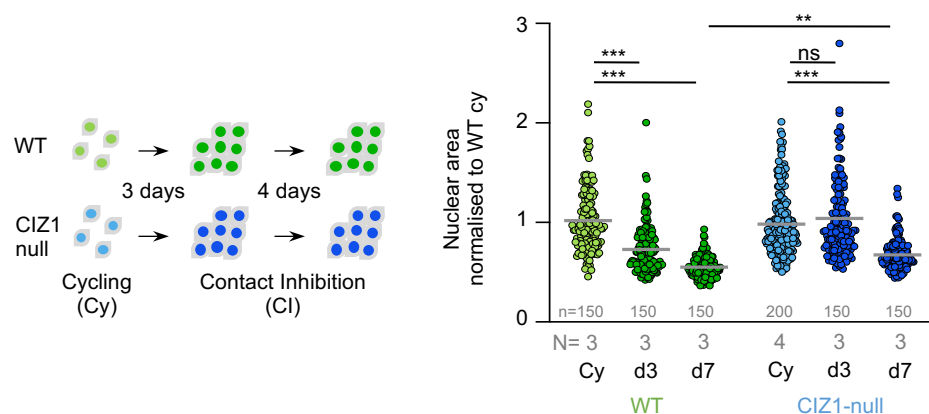


Figure 4.4. **WT and CIZ1-null nuclear area changes in response to contact inhibition.** Nuclear area for WT and CIZ1-null PEFs in a cycling state, at 100% confluency (d3) and 4 days after 100% confluency (d7) with no serum withdrawal. Results are compared by two-way ANOVA where ns denotes no significant difference, \*\*  $p < 0.01$ , \*\*\*  $p < 0.001$ .

#### 4.4.2 Reduced H4K20me1 in CIZ1-null cells

The data presented so far demonstrates a defect in the condensation pathway during quiescence entry. Transcriptomic data analysis and protein quantification suggest a fault in the function of the condensin complex, which is normally dependent on the methylation status of H4K20 during mitotic chromosome formation. Therefore, to understand how CIZ1 may influence condensin function in response to quiescence triggers, H4K20me1 levels in CIZ1-null cells were evaluated.

H4K20me1, like H3K27me3 and H2AK119Ub1, is enriched at the Xi in WT cells. It has been suggested to play a role in the compaction of facultative heterochromatin, but not the initiation of gene silencing, during X chromosome inactivation (Tjalsma et al., 2021, Dixon-McDougall and Brown, 2022). Immunofluorescence analysis in female cells showed H4K20me1 is dramatically compromised in CIZ1-null cells. A clear absence of H4K20me1 assemblies was evident in CIZ1-null cells, with a fall from 35% marked Xi's in WT cycling populations to 3%. This aligns with results for both CIZ1 itself and H3K27me3 as well as previous analysis that included H2AK119Ub1 (Stewart et al., 2019). Notably different between these PTMs is the behaviour of H4K20me1 upon SW. While H3K27me3 and CIZ1 remained high in WT cells, the frequency of H4K20me1 assemblies fall to 14% after 1 hour (short SW) and 3% by 24 hours (long SW) (Figure 4.5A,B). This shows that H4K20me1 enrichment at the Xi is normally modulated during entry to quiescence, unlike that of H3K27me3.

Another difference between H3K27me3 and H4K20me1 is the frequency of Xi assemblies evident in a WT population. As only a subset of cells have enrichment of H4K20me1 at the Xi, WT cycling populations were incubated with the modified base EdU to understand whether this relates to cell cycle stage. Specifically, it can be asked whether ongoing replication of the Xi correlates with H4K20me1 enrichment. This data shows that H4K20me1 accumulation at the Xi does not coincide with replication of the Xi, as the majority of cells with H4K20me1 marked Xi's (99%) were not actively replicating (Figure 4.5C). Unfortunately, one issue with this experiment is that the number of replicating Xi's were very low in the population, so insufficient data on replicating Xi's was collected. This data is inconclusive on whether H4K20me1 assemblies are associated with cell cycle stage and requires more investigation.

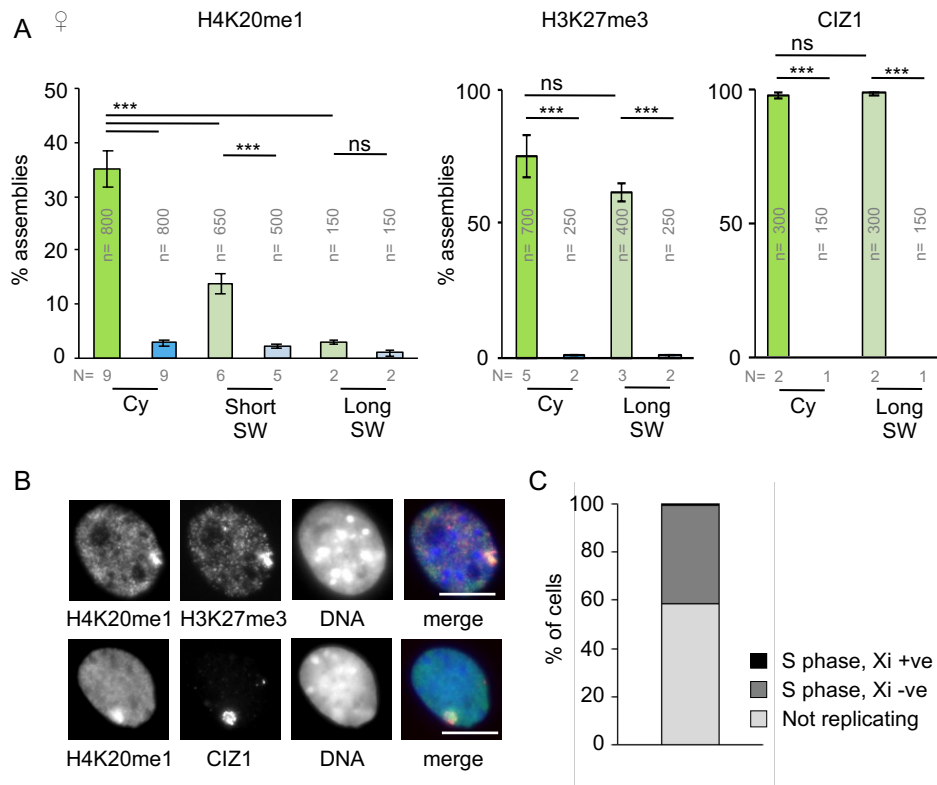
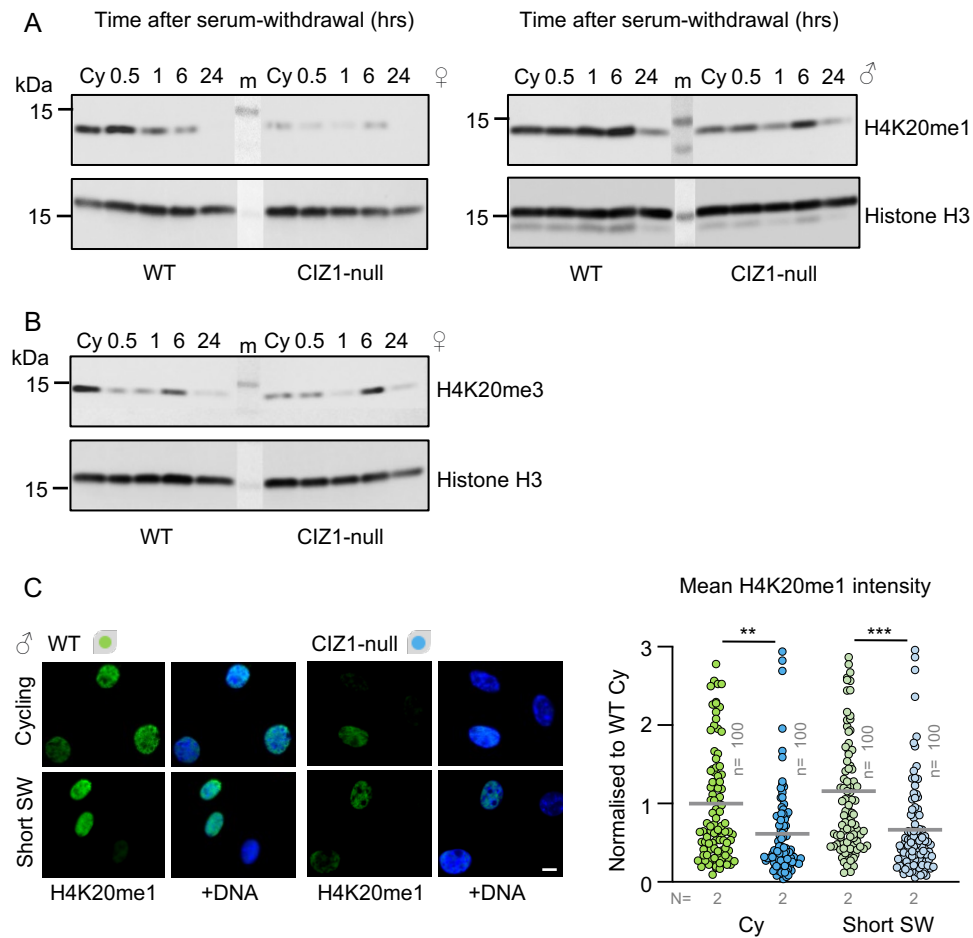


Figure 4.5. **Loss of H4K20me1 assemblies at the Xi in female CIZ1-null PEFs.** A. Frequency of H4K20me1, H3K27me3 and CIZ1 assemblies at the Xi in female WT (green) and CIZ1-null (blue) PEFs, in the cycling state (darker shades) and after a short or long SW (paler shades), with  $\pm$ SEM. n denotes the total number of cells evaluated. Results are compared by two-way ANOVA where ns denotes no significant difference and \*\*\*  $p < 0.001$ . B. Example images of H4K20me1 at H3K27me3-marked Xi and H4K20me1 at CIZ1-marked Xi in WT cells. In merge image, H4K20me1 is green, H3K27me3 or CIZ1 are red and DNA is stained with DAPI (blue). Scale bar represents 10 $\mu$ m. C. Quantification of the replication status of WT cycling cells with H4K20me1 marked Xi's detected after 30 minutes of labelling with EdU. Cells are categorised into those that are in S phase and replicating their Xi (black), in S phase but are not replicating their Xi (dark grey) or those that are not in S phase (light grey). N=2, n=300.

Both SW-induced loss of H4K20me1 in WT cells and overall suppression in CIZ1-null cells, is evident globally in western blot analysis of both female and male populations. This is marked in female cells but moderate in male cells which do not contain Xi-associated enriched assemblies. Over a 24-hour SW window, WT cells showed a gradual loss of H4K20me1, with high levels in both the cycling and 30-minute samples that fall 1-hour post SW until no evidence was left of the mark 24 hours post SW. This analysis mirrors the results attained through calculating H4K20me1-Xi frequencies. In male cells, where the results will be more representative of the entire nucleus, H4K20me1 levels remained high in WT cells from a cycling state to 6 hours post SW, followed by a noticeable drop at 24 hours post SW. For both female and male, H4K20me1 levels in CIZ1-null cells were lower in comparison to WT (Figure 4.6A). However, an interesting observation is the apparent increase in H4K20me1 levels at 6 hours post SW in the absence of CIZ1. Hypotheses can be presented for why this may occur, for example, it may be a response to the condensation failure that occurs in CIZ1-null cells, with a backup mechanism attempting to induce condensation.

H4K20me1 has been reported to be converted to H4K20me3 upon entry to quiescence, therefore, the levels of H4K20me3 were studied over the same time course in the same samples from female cells. This analysis does not confirm a clear transition from monomethylation to trimethylation. High levels of H4K20me3 were also present in WT cycling cells but not in CIZ1-null cells. Levels then dramatically reduced in the WT population only 30 minutes post SW and remained low throughout the window, except for a spike at 6 hours that was seen in both WT and CIZ1-null cells. These high levels were not maintained, as H4K20me3 levels diminished again by the end of the test window at 24 hours (Figure 4.6B). It is also important to note that H4K20me3 does not mark the Xi in either WT or CIZ1-null populations. These analyses imply that H4K20me3 levels peak at 6 hours post SW in both genotypes in a manner unaffected by the absence of CIZ1. Again, these results require confirmation in a fresh set of samples. As this is only a 24-hour window, the time frame may be too short to see emergence of H4K20me3.

H4K20me1 depletion in CIZ1-null cells was further confirmed by immunofluorescence intensity measurements of nucleus-wide H4K20me1 in male cells. Here, a drop in fluorescence intensity was evident between WT and CIZ1-null cycling populations as well as populations exposed to a short SW (Figure 4.6C). Depletion of both Xi-enriched and nucleus-wide H4K20me1 shows that the establishment or the maintenance of H4K20me1 is dependent on CIZ1, and that this defect exists before exposure to quiescence stimuli.



**Figure 4.6. Global depletion of H4K20me1 in CIZ1-null PEFs.**

A. Western blot illustrating H4K20me1 levels over a 24-hour SW time course for WT and CIZ1-null female (left) and male (right) PEFs, and Histone H3. B. Western blot illustrating H4K20me3 levels over a 24-hour SW time course for WT and CIZ1-null female PEFs and Histone H3. C. Example field images of cycling and SW male PEF populations, illustrating lower H4K20me1 (green) levels in CIZ1-null cells compared to WT. DNA is stained with DAPI (blue) and scale bar represents 10 $\mu$ m. Right, mean H4K20me1 immunofluorescence signal in nuclei from male WT and CIZ1-null PEFs in a cycling state and following a short (1 hour) SW. Results are compared by two-way ANOVA where \*\*  $p < 0.01$ , \*\*\*  $p < 0.001$ .

#### **4.4.3 Manipulation of WT and CIZ1-null cells to investigate the role of CIZ1 and H4K20 methylation in chromatin condensation during quiescence entry**

Data presented here show that CIZ1-null cells have compromised H4K20me1 and compromised chromatin condensation. Although methylation of H4K20 has previously been associated with condensation, the experiments described so far only correlate the behaviour between CIZ1, H4K20me1 and condensation. Therefore, using two systems to either manipulate the expression of CIZ1 or the methyltransferase associated with H4K20me1 deposition, the next investigations aim to functionally link CIZ1-dependent H4K20me1 with chromatin condensation during entry to quiescence.

##### **4.4.3.1 Induced expression of ectopic GFP-CIZ1 in CIZ1-null cells**

Expression of full-length GFP-CIZ1 from an integrated transgene was induced by incubating CIZ1-null cells with doxycycline (dox) for 48 hours (Figure 4.7A). All nuclei express GFP-CIZ1, but only a subset form discreet assemblies at the Xi within 48 hours. On average, 18% of the population have detectable CIZ1 assemblies at the Xi throughout my analysis. Therefore, a particular set of criteria had to be created in order to analyse the effect of CIZ1 on H4K20me1 accumulation at the Xi. By analysing the frequency of H4K20me1 assemblies in the presence or absence of a CIZ1 assembly a clear relationship with CIZ1 is evident. 26% of cells with CIZ1 present at the Xi showed enrichment of H4K20me1, compared to only 2% in nuclei with no CIZ1 assemblies (Figure 4.7B). This aligns with previous results which showed coincident accumulation of H3K27me3, H2AK119Ub1 and *Xist* with new ectopic CIZ1 assemblies (Stewart et al., 2019). As well as emergence of H4K20me1 assemblies at the Xi, ectopic GFP-CIZ1 also increased the mean nuclear intensity of H4K20me1 (Figure 4.7C).

With the ability to restore H4K20me1, the next question to address was whether the induced expression of CIZ1 in a CIZ1-null cell restored chromatin condensation following SW. As above, CIZ1-null cycling populations were incubated with or without dox for 48 hours in complete high-serum media (HS +/-dox). For SW populations, media was replaced with low-serum media 24 hours before analysis, which also included dox for induced populations (LS +/-dox) (Figure 4.7D). Importantly, induction of GFP-CIZ1 had no effect on nuclear size in the cycling state but supported partial reversion of the condensation defect after SW. Where CIZ1-null nuclei usually failed to condense upon SW, induced populations successfully condensed their nuclei with the average nuclear size falling by 11% (Figure 4.7E). This reinforces the link between CIZ1 and condensation during entry to quiescence, by showing that the defect can be reversed.

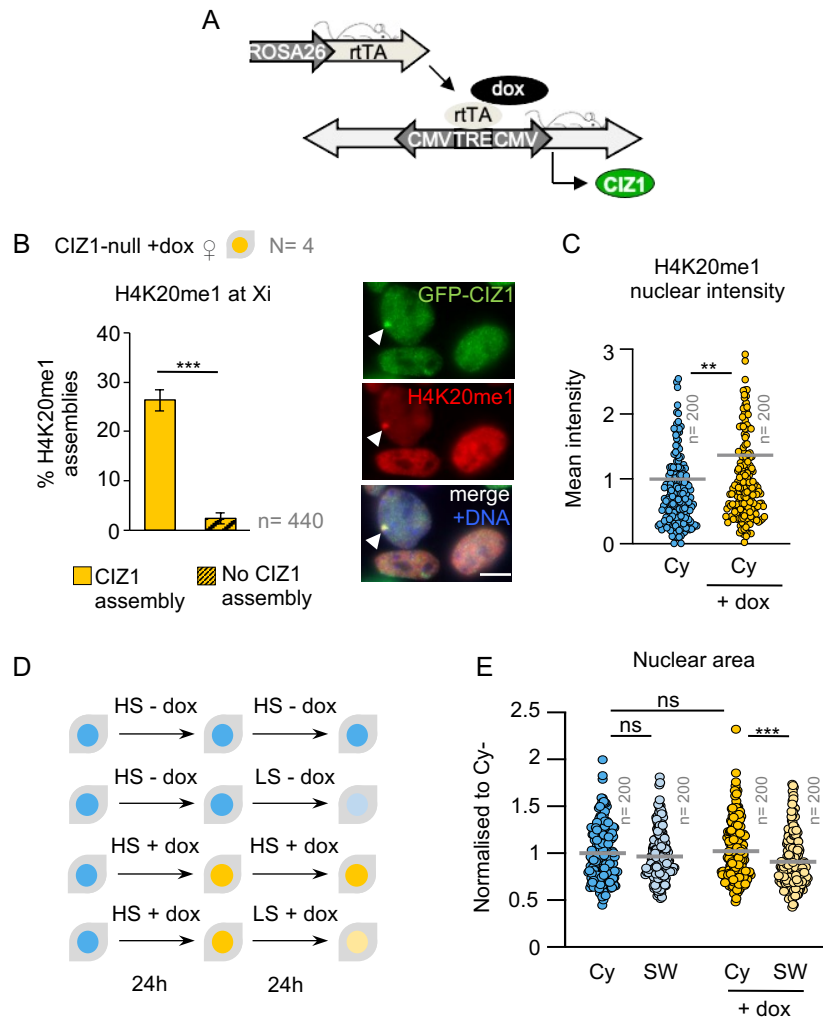


Figure 4.7. **Induction of GFP-CIZ1 in CIZ1-null PEFs.** A. Strategy describing GFP-CIZ1 doxycycline (dox) induction in CIZ1-null PEFs (Ridings-Figueroa et al., 2017). B. Effect on frequency of H4K20me1 assemblies in a dox-induced CIZ1-null female cycling population after 48 hours (yellow), categorised by whether GFP-CIZ1 expressing cells had formed a distinct CIZ1 assembly. Right, representative image illustrating colocalisation of GFP-CIZ1 (green) and H4K20me1 (red) assemblies (white arrow). C. Mean H4K20me1 immunofluorescence signal in nuclei from CIZ1-null cycling PEFs with (+dox, yellow) or without (blue) induction of GFP-CIZ1. DNA is stained with DAPI (blue) and scale bar represents 10 $\mu$ m. D. Strategy describing induction of GFP-CIZ1 and SW. All populations were cultured in complete (high-serum, HS) media with/without dox for 48 hours, except for SW populations where after 24 hours media was replaced with low-serum (LS) media with/without dox. E. Nuclear area for cells in a cycling state or following a long SW with/without dox induction, showing restoration of condensation capability. Results are compared by t-test (B, C) or two-way ANOVA (E) where ns denotes no significant difference, \*\*  $p < 0.01$ , \*\*\*  $p < 0.001$ .

#### **4.4.3.2 Inhibition of the H4K20me1 methyltransferase, SET8, in WT cells**

CIZ1 is known to stabilise multiple histone PTMs, H3K27me3 and H2AK119Ub1 (Stewart et al., 2019), which have the potential to elicit pleiotropic effects on cellular functions. To test whether depletion of H4K20me1 alone can cause the condensation defect observed in CIZ1-null cells, WT cells were incubated with the inhibitor, UNC0379, to specifically suppress formation of H4K20me1. The substrate competitive inhibitor UNC0379 (Ma et al., 2014) selectively inhibits the lysine methyltransferase SET8 (Figure 4.8A), with an  $IC_{50}$  of 7.3 $\mu$ M. At 10 $\mu$ M, UNC0379 was effective at reducing the frequency of H4K20me1 assemblies at the Xi by 48% in female WT PEFs during a 2-hour incubation. There was no effect on the number of H3K27me3 assemblies. In the same cells, a drop in global H4K20me1 levels, but not H3K27me3, was also evident with the mean nuclear intensity falling by 42% in comparison to an untreated control (Figure 4.8B). A short incubation time (2 hours) was chosen for these experiments to minimise complications with the roles of H4K20me1 in mitosis. WT cycling populations incubated with or without UNC0379 displayed no significant difference between S phase index, indicating the short incubation time of UNC0379 did not stop cell cycle progression (Figure 4.8C). The same analysis in male cells also revealed a reduction in the average H4K20me1 nuclear intensity following UNC0379 treatment (Figure 4.8D).

To see if loss of H4K20me1 in WT cells impacted nuclear condensation during quiescence entry, UNC0379 was included in the low-serum media during a 2-hour SW (Figure 4.8E). In the cycling state, the drug treatment had no effect on nuclear size, however, following a short SW, condensation was impaired in UNC0379-treated WT nuclei (Figure 4.8F). This links H4K20me1 with nuclear condensation following SW and implicates depletion of H4K20me1 in CIZ1-null cells as the defect underlying condensation failure.

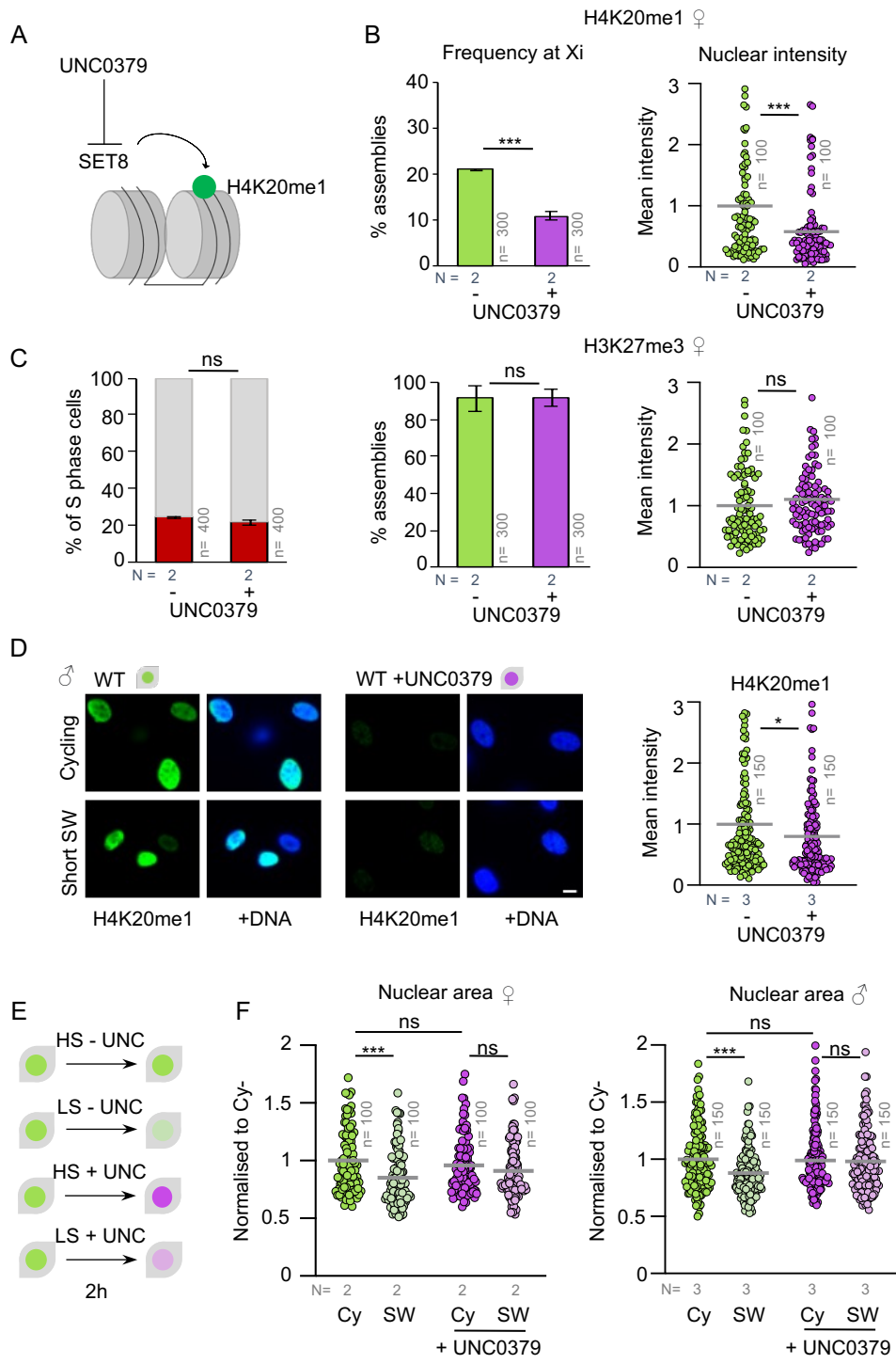


Figure 4.8. **H4K20me1-dependent chromatin condensation following SW.**

A. Schematic of UNC0379 as an inhibitor of SET8. B. Female WT cycling PEFs with (purple) and without (green) UNC0379, showing reduced H4K20me1 assemblies (histogram) and fluorescence intensity (dot plots), but no effect on H3K27me3. C. Histogram shows no effect on the proportion of replicating cells (red), detected after 30 minutes of EdU labelling. D. Example images of male PEF populations, illustrating lower H4K20me1 (green) levels following UNC0379 treatment. DNA is stained with DAPI (blue) and scale bar represents 10 $\mu$ m. Right, mean H4K20me1 nuclear intensity for male WT PEFs in a cycling state with and without UNC0379. E. Strategy describing UNC0379 treatment (UNC) for cycling (high-serum, HS) and SW (low-serum, LS) populations. F. Effect of UNC0379 on nuclear area before and after a short SW, showing loss of function in female (left) and male (right) WT PEFs. Results are compared by t-test (B,C,D) or two-way ANOVA (F) where ns denotes no significant difference, \*  $p < 0.05$ , \*\*\*  $p < 0.001$ .

#### **4.4.4 Overexpansion of CIZ1-null nuclei over multiple rounds of quiescence entry and exit**

Physiologically, many cell types undergo multiple rounds of quiescence entry and exit. As a first step to mimicking their physiological experience, CIZ1-null cells were subjected to two rounds of 24-hour SW followed by two rounds of 24-hour AB and examined at each stage. Further rounds could not be conducted due to increasing cell density and contact inhibition starting to apply an additional trigger to the cells. In CIZ1-null cells, a second round of nuclear expansion is evident, with CIZ1-null nuclei becoming approximately 60% larger than their parent population by the end of the series (Figure 4.9A). CIZ1-null cells have therefore lost their ability to control the extent of their nuclei decondensation, with progressive expansion after each re-feed resulting in overly large nuclei. Interestingly, expansion in nuclear size is also evident over short periods of SW/AB. At the end of three rounds, CIZ1-null nuclei were on average 20% larger than WT (Figure 4.9B). The state of this decondensed chromatin is of interest. It could be hypothesised that the failure to condense chromatin and subsequent overexpansion upon AB would create a fragile chromatin state that is both impaired in its ability to control gene expression and also prone to DNA strand breaks. This section has demonstrated that CIZ1-null cells are defective in condensing their nuclei in response to quiescence triggers but remain capable of decondensation, for which a threshold has not been detected.

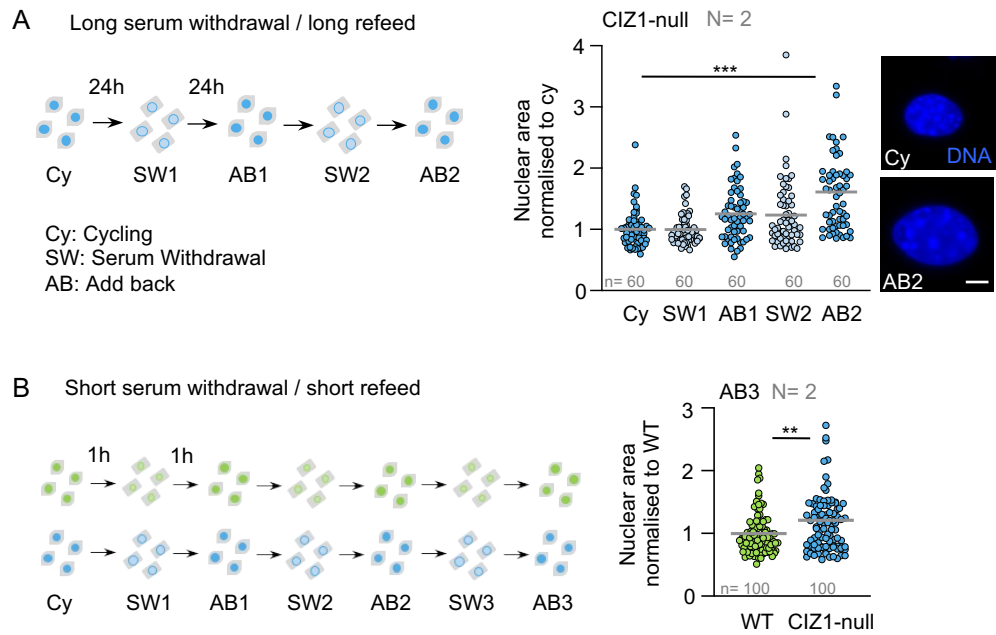


Figure 4.9. **Aberrant decondensation of CIZ1-null nuclei.** A. Nuclear area for CIZ1-null PEFs at each stage over two rounds of long SW and AB, showing failure to condense but stepwise decondensation. Representative images demonstrate the overexpansion of CIZ1-null nuclei where DNA is stained with DAPI (blue) and scale bar represents 10µm. Results are compared by one-way ANOVA where \*\*\*  $p < 0.001$ . B. Nuclear area for WT and CIZ1-null PEFs following three rounds of a short SW and AB (AB3). Results are compared by t-test where \*\*  $p < 0.01$ .

#### **4.4.5 CIZ1-null cells are more susceptible to cell death upon serum withdrawal**

To explore the impact of defective H4K20me1-dependent condensation and inappropriate decondensation the stability of nuclei following SW and AB was compared. Firstly, cell viability over the long treatment series was examined. WT and CIZ1-null cells were stained with trypan blue at each SW and AB stage to distinguish between live (impermeable) and dead (dye permeable) cells (Figure 4.10A). Both WT and CIZ1-null cells are susceptible to cell death upon SW, with the number of permeable cells falling upon AB (Figure 4.10B). This fall is proposed to be a consequence of the media change which removes cells that are detached from the plate surface. Focussing on the initial 24-hour SW window, it is clear that CIZ1-null cells are more vulnerable compared to WT cells, with cell death evident in the CIZ1-null population 17 hours post SW (Figure 4.10C). This implies that CIZ1-null cells may already be in an unstable state and unable to cope with the additional stress of SW compared to WT cells. It is worth considering the impact of cell density in these experiments as CIZ1-null populations appeared sparser compared to WT and it is unknown how this may influence the response of cells to SW.

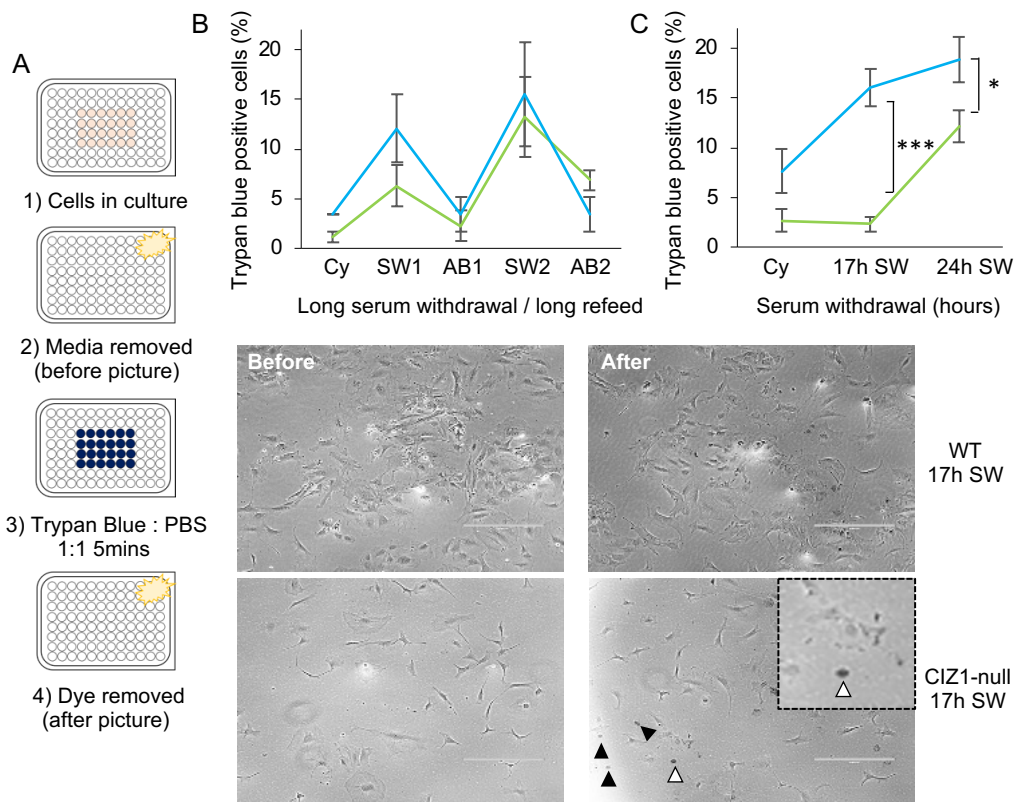


Figure 4.10. **Cell viability over multiple rounds of SW and AB.**

A. Protocol for trypan blue staining. Cells were cultured in a 96-well plated and analysed in the well. B. Mean proportion  $\pm$ SEM of WT (green) and CIZ1-null (blue) cells stained with trypan blue indicating dead cells in each population over two SW and AB cycles. At each stage, for WT N=3 n=174 and for CIZ1-null N=2 n=116. There is no significant difference between WT and CIZ1-null populations. C. Mean proportion  $\pm$ SEM of cells stained with trypan blue in WT and CIZ1-null cycling, 17-hour post SW and 24-hour post SW populations. For all populations N=6 n=600. Results are compared by t-test where \* denotes  $p < 0.05$  and \*\*\*  $p < 0.001$ . Below, example field images before and after trypan blue staining of WT and CIZ1-null populations following 17-hour SW.

#### 4.4.6 Generation of fragile CIZ1-null nuclei

Analysis of nuclear stability itself over one round of SW and AB was also carried out. As defects in the condensation process are seen as early as 1-hour post SW, a short SW/AB cycle was exploited to compare CIZ1-null cells to WT (Figure 4.11A). Shorter times also reduced any effect of cell death that may cause deviation in the results.

One method to measure the fragility of the nucleus is to subject cells to passages through a fine needle (Furusawa et al., 2015). Exposure to mechanical shear and the susceptibility to this stress can then be evaluated microscopically. Cycling and AB populations from both genotypes were passed through a 25G needle 40 times prior to fixation. A reference sample that experienced 0 needle passes was taken from each population in order to calculate the relative fragmentation of nuclei. Samples were stained with DAPI to visualise nuclei, concentrated onto a microscope slide and the number of intact nuclei in each field counted. All populations experienced a significant loss in the relative number of nuclei following passages through a needle, however, CIZ1-null nuclei upon AB demonstrated increased susceptibility to shear force. For WT, the relative number of nuclei in the cycling and AB populations, following 40 needle passes, fell by 36% and 54% respectively. For the CIZ1-null cycling population, the loss of nuclei was not too dissimilar to WT, with the relative number of nuclei falling by 45%. However, the CIZ1-null AB population experienced the biggest loss as the relative number of nuclei fell by 77% after 40 needle passes (Figure 4.11B). This correlated nuclear expansion with nuclear fragility and suggests that CIZ1-null cells undergoing quiescence cycles in the body might be vulnerable to mechanical stress.

Even without mechanical stress, phosphorylation of ataxia telangiectasia mutated (pATM) indicated that cell cycle checkpoints are significantly more activated in CIZ1-null PEFs specifically upon AB. ATM is a protein kinase involved in the DNA damage response (DDR), a conserved mechanism for detecting DNA damage and initiating downstream effector pathways. The DDR can be activated in response to multiple types of DNA damage caused by internal and external factors. ATM is rapidly recruited to sites of double-strand breaks (DSBs) and activated via the Mre11-Rad50-Nbs1 (MRN) complex and autophosphorylation (Paull, 2015). Phosphorylation and activation of ATM, and another protein kinase ATR, results in a cascade of events including phosphorylation of the histone variant ( $\gamma$ H2AX) and other downstream checkpoint kinases. This results in cell cycle arrest to allow time for DNA repair or in the case where DNA cannot be repaired, controlled cell death via apoptosis (Zhou and Elledge, 2000, Harper and Elledge, 2007).

In a cycling state, for both WT and CIZ1-null cells, less than 10% of the population exhibited positive pATM nuclei. Nuclei were considered to be positive for the checkpoint marker if there were three or more distinguishable subnuclear foci. A slight increase in the number of positive nuclei was seen upon SW, for both genotypes, however this difference was not significant. A difference in checkpoint activation between the two genotypes was only evident upon AB. Only 6% of WT AB nuclei were positive for pATM compared to 15% of the CIZ1-null AB population (Figure 4.11C). Apparent checkpoint activation raises the possibility of DNA damage upon AB.

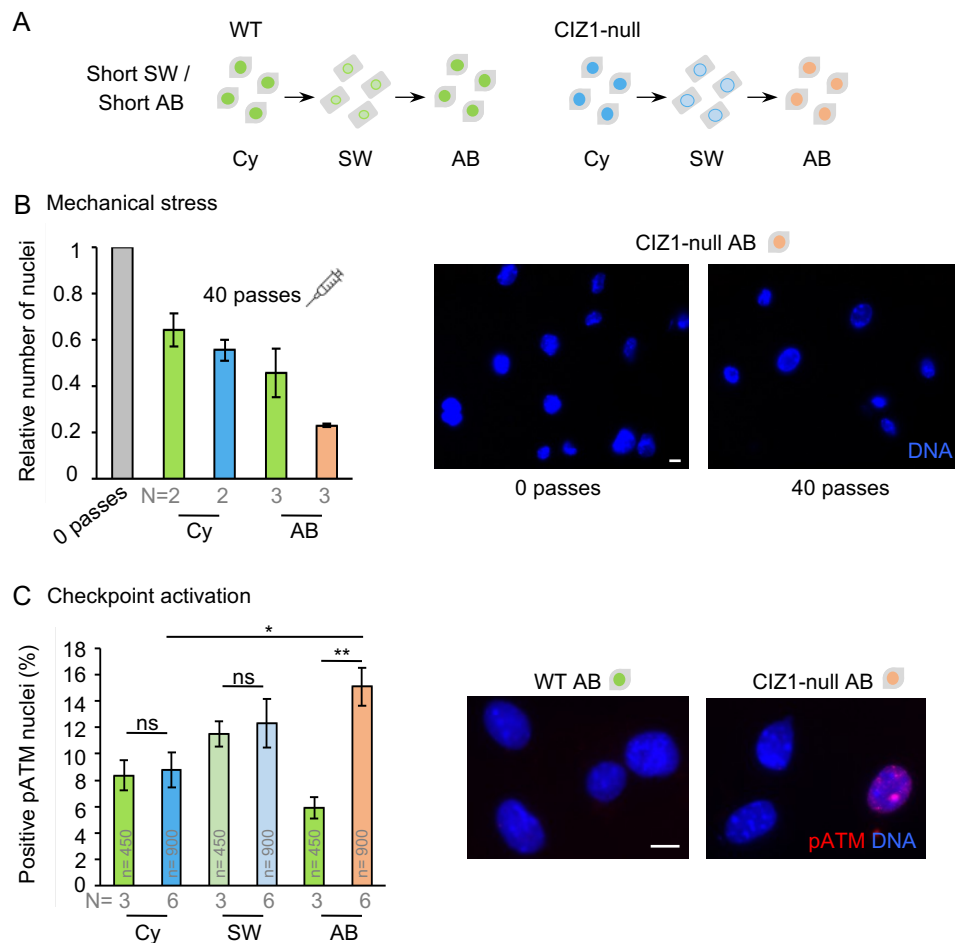


Figure 4.11. **Fragility and checkpoint activation upon AB in CIZ1-null cells.**

A. Short SW and AB strategy used to analyse the response of WT (green) and CIZ1-null (blue) nuclei in B and C. CIZ1-null populations exhibited increased nuclear fragility and checkpoint activation upon AB (orange). B. The relative number of nuclei that survived 40 passes through a 25G needle  $\pm$ SEM. Right, field images of a CIZ1-null AB population before and after 40 passes. C. Frequency of positive pATM nuclei,  $\pm$ SEM. Right, field images of WT and CIZ1-null AB nuclei showing pATM foci (red). Results are compared by two-way ANOVA where ns denotes no significant difference, \*  $p < 0.05$ , \*\*  $p < 0.01$ . DNA is stained with DAPI (blue), and scale bar represents 10  $\mu$ m.

#### 4.4.6.1 Links with the extended contact inhibition strategy

A similar checkpoint activation response was seen using a standardised long-term CI maintenance protocol. This work was carried out previously in the Coverley lab by Rose Wilson and discussed earlier in Figure 1.8. WT and CIZ1-null populations were subjected to a 21-day CI time course with pATM evident within the first week. Other checkpoint activation markers (pCHK1 and  $\gamma$ H2AX) appeared later on in the time course. Part of this methodology required the media to be replenished every three-four days, meaning the cells experienced natural serum-depletion and AB throughout culture (Figure 4.12). These cycles of starvation and feeding parallel the SW/AB strategy discussed above and would be expected to be a cause of stress for the CIZ1-null population.

Proliferating colonies that emerged from the checkpoint activated CIZ1-null monolayers exhibited features characteristic of transformed cells and checkpoint activation remained evident. Both PEF and tail-tip fibroblast (TTF) populations exhibited these focal outgrowths and I have also replicated this with crystal violet staining of WT and CIZ1-null TTF populations at the end of the 21-day CI time course (Figure 4.12). These data suggest that the epigenetic instability caused by deletion of CIZ1 is sufficient to create vulnerable nuclei, and to drive quiescence escape. While these colony populations experienced sustained DNA damage checkpoint activation it remains an open question as to whether their emergent phenotypes reflect DNA damage and genetic mutation.

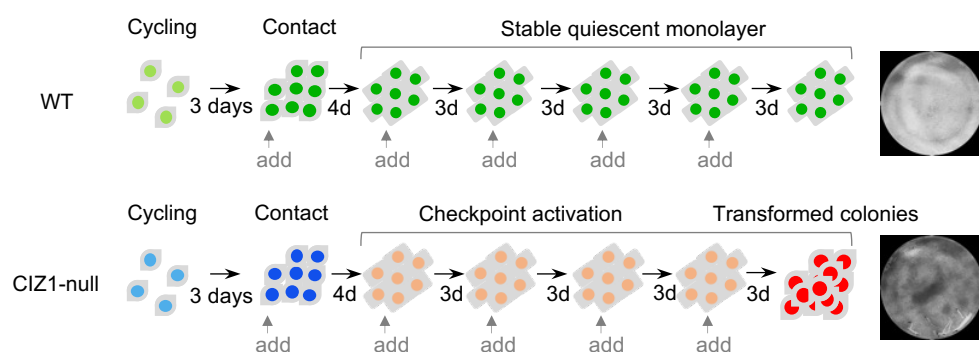


Figure 4.12. **Extended contact inhibition strategy.** Schematic representation of the order of events observed in CIZ1-null cells following contact inhibition and extended culture with media changes indicated. Right, 3cm culture dishes stained with crystal violet showing WT and CIZ1-null TTF populations at the end of the 21-day time course.

## 4.5 Discussion

The work described here links the function of the CIZ1 protein with processes that condense and help guard the genome during establishment of a condensed, quiescent nucleus. Genetically null murine embryonic fibroblasts fail to condense their nuclei on entry to quiescence whilst retaining the capability to decondense. This chapter has built upon previous knowledge to outline a potentially catastrophic series of events that take place in the absence of CIZ1. Here, the function of CIZ1 as a protector of the epigenome has been extended to the histone PTM, H4K20me1. Nuclear condensation failure in the absence of CIZ1, is the consequence of H4K20me1 depletion and manifests during quiescence entry.

My analysis suggests that it is the subsequent inappropriate nuclear decondensation that is most damaging to the cell. How CIZ1-null nuclei remain capable of decondensation is uncertain and the mechanism behind this process is not fully understood. Studies using *Xenopus* eggs indicate that decondensation after mitosis is an active process that involves RuvB-like ATPases (Magalska et al., 2014). The ATPase p97 is also responsible for removing the mitotic kinase Aurora B from chromatin enabling chromatin decondensation (Ramadan et al., 2007). Therefore, the decondensation of chromatin may not be a simple deactivation of condensation proteins and suggests different processes behind condensation and decondensation.

Sustained activation of DNA damage checkpoint kinases precedes the emergence of phenotypically transformed lineages. This suggests that the epigenetic instability experienced in the absence of CIZ1 could be an early (pre-mutation) driver of transformation and is of interest in relation to cancer initiation. The expansion of CIZ1-null nuclei implicates condensin function at some level, though can also be linked with changes in ploidy. I have demonstrated that oversized nuclei can be generated in short-term experiments, with cycles of SW and AB that fall far short of a replication cycle and are therefore not primarily driven by changes in ploidy. Thus, nuclear expansion may be an early event, that precedes genetic and ploidy change in some cancers.

### 4.5.1 Activation of the DNA damage response

A major remaining goal is to link the failed condensation event to activation of checkpoint proteins associated with the DDR. The presence of DNA breaks/damage in CIZ1-null cells is not shown here and is only suggested through monitoring activated checkpoint kinases. While there appears to be a chronological order, there is no direct evidence to show that failure to condense initiates the response.

Understanding the immediate trigger of checkpoint activation is not straightforward. CIZ1-null cells are known to be inefficient in the process of DNA damage repair, as cycling cells are sensitive to replication stress induced by hydroxyurea, suggesting a defect in the resolution of DNA breaks unconnected to quiescence (Nishibe et al., 2013). Similarly, a separate study reported sensitivity to  $\gamma$ -irradiation in fibroblasts and increased DNA breaks in brain tissue, linking the deficit to impaired motor and cognitive functioning in mice (Khan et al., 2018). Therefore, it is likely that any damage which occurs following quiescence triggers takes longer to resolve in the absence of CIZ1. This may describe the chronic checkpoint activation seen following AB. Checkpoint activation could also be a direct response to aberrant condensation (Burgess et al., 2014) possibly detected at decondensation, or it may be initiated by DNA damage resulting from hyper-decondensation. Changes in chromatin have been shown to recruit checkpoint markers in the absence of DNA breaks (Bakkenist and Kastan, 2003, Burgess et al., 2014), and modification of H4K20 has already emerged as a regulator of genomic integrity (Jørgensen et al., 2013). Also, transcriptomic analysis (Chapter 3) detected elevated expression of regulators and executors of homology-directed DNA DSB repair. This could be consistent with either compromised functionality or heavy burden of damage.

The DDR exists to prevent persistent DNA damage and to maintain genome integrity. Defects in the DDR or repair processes have been associated with mutagenesis and disease, including cancer (Volkova et al., 2020). To investigate if CIZ1-null cells and the subsequent breakthrough colonies have experienced DNA damage, DNA from the colony lineages could be sequenced. If present, this will reveal mutational signatures that are common following inaccurate DNA DSB repair.

## **4.5.2 Chromatin condensation**

### ***4.5.2.1 The relationship between gene repression and chromatin condensation***

As CIZ1-null cells fail to condense their nuclei but remain capable of gene repression during quiescence entry, my data argues that repression is not dependent on nuclear condensation in mammals. This does not align with ideas emerging from yeast (Swygert et al., 2019), where condensin-dependent chromatin compaction is a cause of transcriptional repression. This study uses a different methodology to determine gene expression and analyses transcription based on the occupancy of polymerase II in condensin-depleted cells. Therefore, our outcomes may not be directly comparable. It may also suggest that the role of the condensin complex in gene regulation during quiescence is not conserved between yeast and mice.

### ***4.5.2.2 Eventual condensation of CIZ1-null nuclei***

Interestingly, analysis of nuclear condensation via CI suggests that CIZ1-null nuclei do eventually condense. This is a delayed response compared to WT indicating the condensation process is inefficient without CIZ1. This may be due to diminished H4K20me1 levels and therefore slower condensin function or the eventual result of a different, compensatory pathway. Analysis of longer SW times was difficult to monitor due to an increase in cell death in the population, hence it has not been possible to determine if CIZ1-null nuclei would eventually condense via this method. Nevertheless, I have shown that the initial failure to condense upon quiescence triggers is enough to disturb the CIZ1-null quiescent state and subsequent entry back into the cell cycle.

### ***4.5.2.3 Limitations of analysis***

Chromatin condensation has been analysed here based on 2D DAPI-stained immunofluorescence images to calculate nuclear area changes. These nuclear areas can be used to generate predicted changes in nuclear volume, but this does presume the nucleus is a spherical shape which is not always the case. Therefore, it is not definite how the 3D structure of the nucleus changes in response to quiescence triggers. To achieve a more accurate volume calculation, three-dimensional imaging technologies could be exploited for future analysis, though was not practical here because of the number of nuclear required to achieve statistical significance.

#### **4.5.2.4 *When do cells exit the cell cycle?***

Typically, it is believed that cells exit the cell cycle before the restriction point in early G1. However, I see an average reduction in area as early as 1-hour post SW, creating the possibility that cells begin to experience events associated with quiescence exit at other points in the cell cycle. To investigate this further, cell populations could be synchronised prior to SW, however, many of the common synchronisation techniques are not compatible with my experiments. For example, the use of cell cycle inhibitors may affect the chromatin state and interfere with the measured outputs. Also, triggering quiescence is a common synchronisation technique but would not work in this project.

#### **4.5.3 H4K20 methylation**

##### **4.5.3.1 *Other methylated states of H4K20***

H4K20 can either be mono-, di- or tri-methylated. Here, I have primarily focussed on the H4K20me1 modification due to its accumulation at the Xi in female cells and its association with function of the condensin complex in mitosis. However, both the di- and tri- methylated states are shown to be dependent on prior monomethylation of H4K20 (Oda et al., 2009). Therefore, in my analysis where diminished H4K20me1 is seen in CIZ1-null and UNC0379-treated WT populations, other forms of methylated H4K20 may be affected. Whether these also impact nuclear condensation during quiescence requires further investigation but is unlikely due to CIZ1-dependent condensation being an early event following quiescence triggers. At this point H4K20me3 levels are low and the known roles for H4K20me2 are mainly associated with DNA damage repair (Botuyan et al., 2006).

##### **4.5.3.2 *H4K20me1 is a dynamic histone modification***

H4K20me1 levels fluctuate dramatically throughout the cell cycle, with the highest levels associated with mitosis. This made analysis of H4K20me1 nuclear intensity difficult, with a large range of intensities seen in both WT and CIZ1-null populations. To overcome this, I ensured enough replicates were taken and a representative number of nuclei analysed for each population. WT and CIZ1-null cells were also cultured at comparable densities to avoid different proliferation rates. In fact, all WT and CIZ1-null populations are heterogenous in terms of nuclear size and H4K20me1 intensities. One way to enable easier discrimination between my comparisons could have been to synchronise the populations. However, this comes with its own caveats and difficulties when working with primary cells.

#### **4.5.3.3 Role of H4K20me1 in other stages of the cell cycle**

With chromatin condensation on entry to quiescence being CIZ1-dependent, the question surrounding this process in other cell cycle stages remains. H4K20me1 is not completely absent in CIZ1-null nuclei and some cells in the population still have bright immunofluorescence signal. CIZ1-null nuclei are also capable of forming condensed chromosomes during mitosis, indicating that H4K20me1 levels in mitosis may not be affected in CIZ1-null populations. Transcriptomic data, in Chapter 3, suggests defects in the cycling state but this has not yet been explored. There is no significant difference between the nuclear area of cycling WT and CIZ1-null nuclei suggesting that the implications of CIZ1-dependent chromatin condensation are only observed upon quiescence triggers.

#### **4.5.3.4 H4K20me1 and the condensin complex**

My data correlates reduced function and increased solubility of the condensin complex (seen in Chapter 3) with diminished H4K20me1 levels in CIZ1-null cells. Function of the condensin complex has been linked to H4K20 methylation in the literature, however, direct evidence is not shown here. In-depth interaction studies, such as CHIP-SEQ, could confirm that condensation failure, caused by loss of H4K20me1, is a result of non-functioning condensin.

## 5 Dispersal of CIZ1-Xi assemblies: an *in vitro* assay

### 5.1 Introduction

As well as nuclear condensation during quiescence entry, CIZ1 has been shown to effect chromatin state and behaviour in other contexts. It has been associated with replication-linked relocation of the Xi during mid-S phase as the Xi fails to move from its position at the nuclear periphery towards an internal position and back during its replication in CIZ1-null cells (Stewart et al., 2019). Moreover, CIZ1 assemblies are themselves dynamic, and undergo disassembly in late metaphase (Ridings-Figueroa et al., 2017). The timing of disassembly mimics the behaviour of *Xist* RNA (Duthie et al., 1999, Clemson et al., 1996).

Localisation of *Xist* RNA to the Xi has been linked to the phosphorylation state of chromatin based on activity of the Aurora B kinase (AURKB) (Hall et al., 2009). Throughout the cell cycle, levels of protein kinases and phosphatases fluctuate to regulate the transitions between different phases and mostly studied in mitosis. Due to an increase in kinase activity and a decrease in phosphatase activity, protein phosphorylation increases in mitosis (Nasa and Kettenbach, 2018).

Hall *et al*, manipulated the release of *Xist* from the Xi in interphase by inhibiting protein phosphatase 1 (PP1). They suggest this inhibition may inappropriately activate AURKB and go on to show that inhibitors of AURKB in fact block the release of *Xist* usually seen in metaphase. This study has successfully been able to investigate *Xist* localisation through the manipulation of cell cycle enzymes and demonstrates how powerful these experimental approaches can be. Using the same PP1 inhibitors as Hall *et al*, studies in the Coverley lab have also been able to manipulate the dispersal of CIZ1 in interphase (unpublished). The balance of enzymes that deposit and remove post-translational modifications is essential for maintaining homeostasis within a cell and for carrying out the correct functions at the correct time.

## 5.2 Aims

Previous chapters have discussed the importance in regulating histone methylation status. Here, I begin to investigate the balance between protein kinases and phosphatases on the retention and integrity of CIZ1 assemblies. I have designed and validated an *in vitro* assay using permeabilized adherent cells and used it to ask a set of questions. The aims of this piece of work were as follows:

- To develop a permeabilised cell assay to probe the release and subnuclear relocation of CIZ1.
- To exploit the permeabilised cell assay to understand the relationship between CIZ1 assemblies, Xi chromatin and RNA integrity.
- To determine whether CIZ1 disassembly and relocation of CIZ1 particles is an active process
- To determine if the permeabilised cell assay removes an inhibitor of release with specific focus on the phosphatase ACP5.

## 5.3 Experimental design and assay development

To explore how CIZ1 is anchored at the Xi, I developed an *in vitro* assay to manipulate CIZ1 release. Using our standard immunofluorescence protocol (Chapter 2, methods), pre-fixation detergent treatment (0.1% Triton-X-100, 1 minute) does not detach adherent cells or disperse CIZ1 assemblies, which can be seen as a distinct entity at the Xi. Here, addition of a two-minute high salt (500mM NaCl with detergent) incubation was included prior to fixation (Figure 5.1A). Both the detergent and salt steps are applied in cytoskeletal (CSK) buffer, historically used to study the cytoskeleton (Wilson et al., 2016, Lenk et al., 1977). CSK buffer has a basal salt concentration of 100mM, which is close to the physiological level of NaCl, upon which increasing the salt concentrations were tested. By increasing the salt concentration above its physiological level, it is possible to gradually remove soluble or loosely bound proteins and then examine the behaviour of CIZ1 and its binding to the Xi. Exposure to 500mM NaCl triggers CIZ1 release from the Xi and its dispersal across the nucleus (Figure 5.1B). Using antibodies for either the N-terminal or C-terminal domain of CIZ1, any differences in the behaviour between the two can be investigated. In normal WT cells, high salt does not uncouple the two domains and therefore either antibody can be used for CIZ1 analysis. The extent of dispersal across the nucleus can be quantified using Fiji (Chapter 2, methods) (Figure 5.1C). Inhibitors can be included during the detergent and high salt incubations to manipulate the response of CIZ1. This enabled me to investigate requirements of the mechanism behind CIZ1 dispersal.

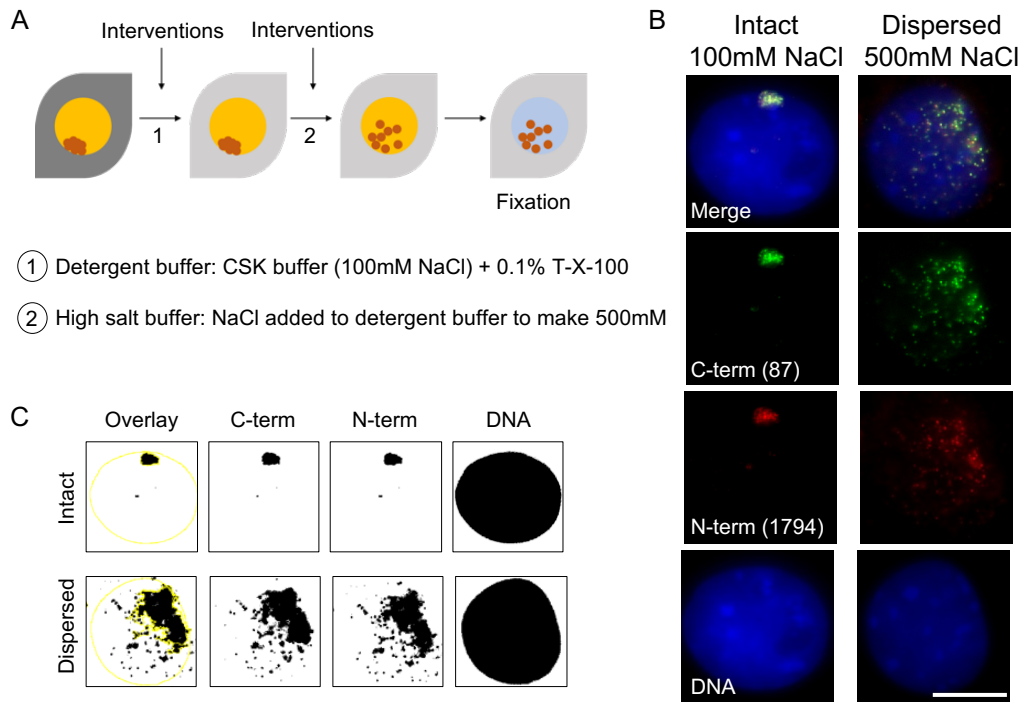


Figure 5.1. ***In vitro* dispersal of CIZ1.** A. Schematic describing the experimental design for the permeabilised cell assay. Cells are exposed to a detergent and high salt incubation prior to fixation. B. Representative images for CIZ1 localisation in 3T3 cells before and after exposure to high salt conditions. Antibodies for the two domains of CIZ1; C-term (87, green) and N-term (1794, red) show the dramatic re-localisation of CIZ1. DNA is stained with DAPI (blue) and scale bar represents 10 $\mu$ m. C. Representative images of masks used in Fiji to measure the extent of CIZ1 dispersal across the nucleus.

## 5.4 Results

### 5.4.1 Requirements for CIZ1 dispersal

It is important to understand the requirements of the release and dispersal event. I explored this using vanadyl ribonucleoside complexes (VRC) and ATP $\gamma$ S (Figure 5.2A).

VRC's are analogues that bind to and block the active sites of many ribonucleases (RNases). With the addition of VRC to both the detergent and salt steps, CIZ1 is no longer released from the Xi by high salt, suggesting that RNase activity is required for CIZ1 dispersal (Figure 5.2B,C). Therefore, treatment with detergent and 500mM NaCl in the presence or absence of an RNase inhibitor reveals an additional requirement of dispersal.

Secondly, I used the ATP analogue ATP $\gamma$ S to block ATP hydrolysis-driven processes in the cell, to ask whether CIZ1 movement requires energy. This could shed light on the type of movement CIZ1 is undergoing. For example, does its release allow passive diffusion away from the Xi site, or is active transport involved. Adding ATP $\gamma$ S (1mM) to treatments, in the same way as VRC, results in a retention of CIZ1 at the Xi in 90% of the population (Figure 5.2B,C), indicating that either the release or translocation of CIZ1 requires energy and that at least one step is an active process mediated by an ATP-dependent enzyme. A subtler observation is that, despite CIZ1 remaining as a distinct entity, the CIZ1 assembly appears slightly larger following high salt in the presence of ATP $\gamma$ S, when compared to the detergent control or high salt with VRC. This larger assembly may be a product of release from chromatin but failure to disperse away due to the lack of hydrolysable ATP.

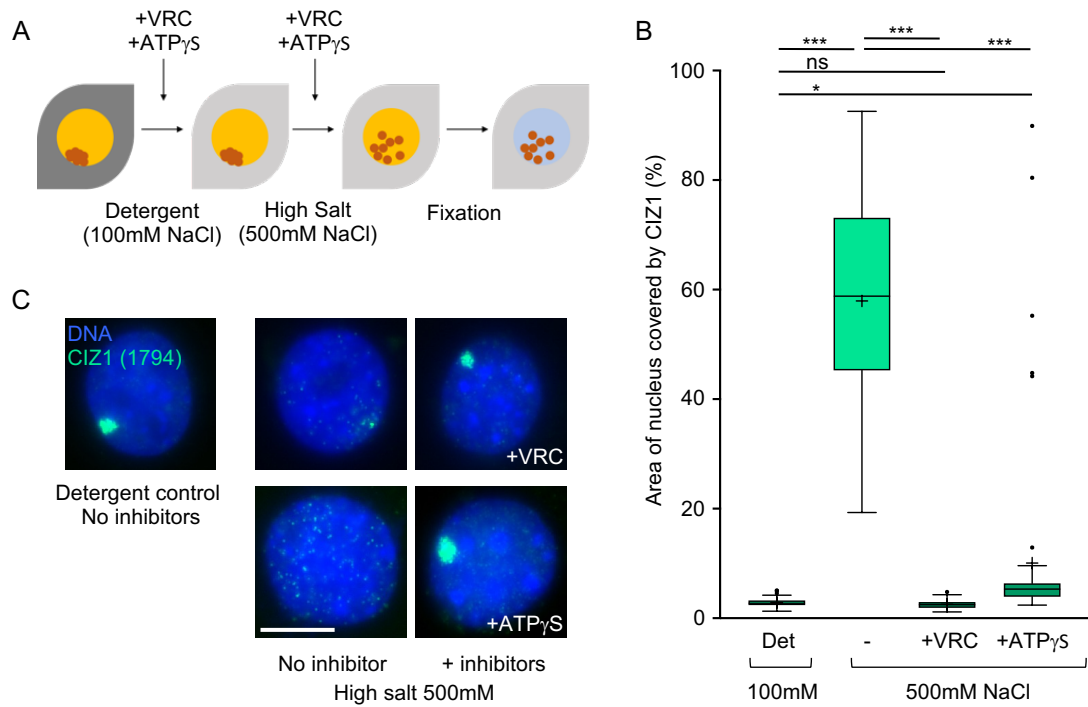


Figure 5.2. **Dispersal of CIZ1 requires RNase activity and is an energy driven process.** A. Schematic describing the experimental design with the addition of VRC or ATP $\gamma$ S in both the detergent and high salt steps. B. Tukey box and whisker plot showing quantification of CIZ1 dispersal following 100mM NaCl (Det), 500mM NaCl, 500mM NaCl +VRC and 500mM NaCl + ATP $\gamma$ S incubation. For each condition N=3, n=60 nuclei analysed. Results are compared by one-way ANOVA where ns denotes no significant difference, \*  $p < 0.05$  and \*\*\*  $p < 0.001$ . C. Representative images for CIZ1 (green) localisation in 3T3 cells before and after exposure to high salt conditions, with or without VRC and ATP $\gamma$ S addition. DNA is stained with DAPI (blue) and scale bar represents 10 $\mu$ m.

#### **5.4.2 Xi chromatin remains localised**

As a high salt environment, without inhibition of RNases, promotes dispersal of CIZ1, this raised the question regarding the behaviour of Xi chromatin under the same conditions.

Using immunofluorescence and a specific antibody to H2AK119Ub1, which is enriched at the Xi and an accepted marker of the location of Xi chromatin, I studied its location following high salt exposure. The Xi is seen to stay as a discrete entity, while in the same cell CIZ1 is dispersed across the nucleus. In the presence of VRC, CIZ1 and H2AK119Ub1 assemblies remain colocalised (Figure 5.3A,B). This shows that high salt and RNases promote release of CIZ1 from the Xi rather than dispersal of Xi chromatin. However, despite not being statistically significant, the Xi chromatin does appear to expand slightly when VRC is absent from the high salt buffer, suggesting some disturbance in its integrity.

With 3T3 cells being an immortalised cell line and with previous work in the lab demonstrating differences in CIZ1 behaviour between 3T3 and primary fibroblasts, it was important to test the permeabilised cell assay in a primary cell context. This experiment was therefore replicated in primary WT fibroblasts, with the same results. (Figure 5.3A,B).

These data show that high salt and RNases promote release of CIZ1 from the Xi rather than dispersal of Xi chromatin, and this can occur in both a primary and non-primary cell.

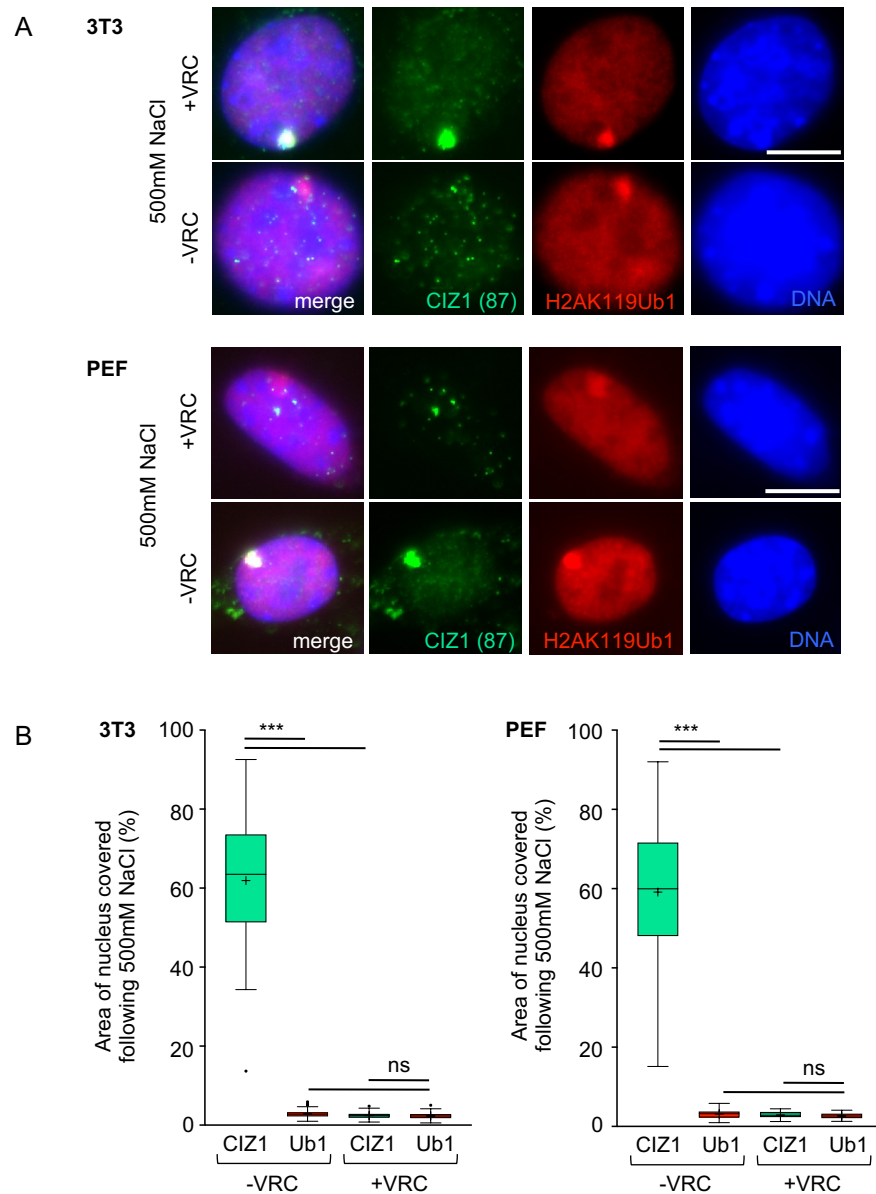


Figure 5.3. **CIZ1 disperses away from Xi chromatin.** A. Representative images for CIZ1 (green) and Xi (H2AK119Ub1, red) localisation in 3T3 cells (top) and WT PEFs (bottom) following high salt incubation with or without VRC. DNA is stained with DAPI (blue) and scale bar represents 10 $\mu$ m. B. Tukey box and whisker plots showing quantification of CIZ1 and H2AK119Ub1 dispersal in 3T3 cells (left) and WT PEFs (right). For each condition in 3T3s N=4, n=75. For PEF -VRC conditions N=3 n=60, +VRC conditions N=2 n=40. All results were compared by two-way ANOVA where ns denotes no significant difference and \*\*\* p<0.001.

### 5.4.3 Titration of NaCl to refine the CIZ1 release assay

The high-salt concentration of 500mM NaCl was originally chosen as this is the concentration regularly used as part of nuclear matrix extractions in the Coverley lab (Stewart and Coverley, 2018). To investigate the threshold concentration of salt needed for dispersal, cells were treated in a step gradient of salt concentrations. Using salt concentrations of 100mM (CSK only) up to 500mM NaCl in 50mM intervals, cells were analysed for the extent of CIZ1 dispersal. CIZ1 patches appeared more dispersed (occupy a greater area) as soon as the salt concentration of the CSK buffer was exceeded (100mM). The number of discrete Xi patches started to fall around 250mM NaCl, and complete dispersal (no CIZ1 at the Xi) in all cells occurred at 300mM (Figure 5.4). This set the salt threshold needed for CIZ1 dispersal at 300mM NaCl.

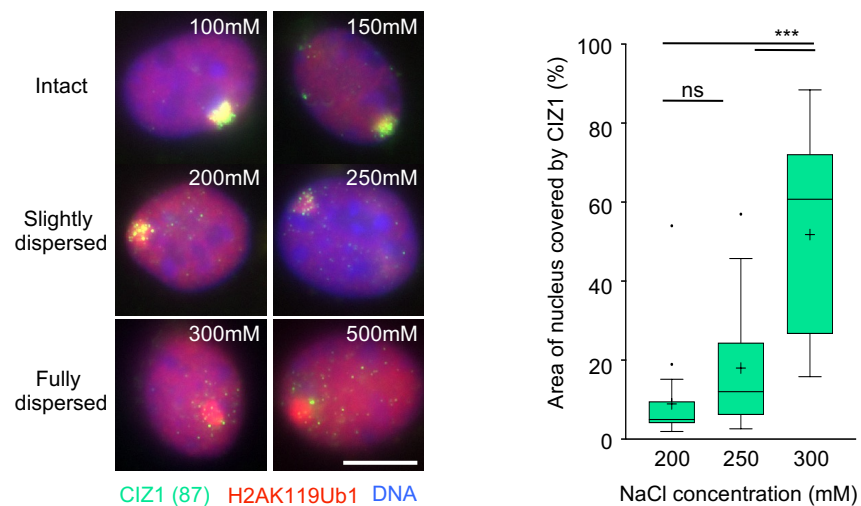


Figure 5.4. **CIZ1 disperses at 300mM NaCl.** Representative images demonstrating CIZ1 dispersal in 3T3 cells over various salt concentrations. Right, quantification of CIZ1 dispersal following 200, 250 and 300mM salt incubation. For each condition N=1, n=20. This experiment has been carried out twice but only one was quantified. Results were compared by one-way ANOVA where ns denotes no significant difference and \*\*\*  $p < 0.001$ . DNA is stained with DAPI (blue) and scale bar represents 10 $\mu$ m.

#### **5.4.4 Extraction of putative catalytic ACP5 between 200-300mM NaCl.**

I have established that the event which causes CIZ1 dispersal is triggered between the increase from 200mM to 300mM NaCl. There are many possible explanations for this as many soluble proteins or those loosely bound to chromatin can be removed between 200 and 300mM NaCl, including an activity that might promote retention. A review of the literature revealed one possible candidate to be a protein phosphatase, due to the established links between PP1, AURKB and *Xist* retention at the Xi (Hall et al., 2009). In this study, and studies in the Coverley lab, PP1 was suspected based on use of broad-spectrum inhibitors so there is the possibility other phosphatases may also be implicated.

Several protein interactions are known for CIZ1 including proteins that regulate cell proliferation and the cell cycle (Pauzaite et al., 2016). One of these protein interactions is with the phosphatase, Tartrate-Resistant Acid Phosphatase 5 (TRAP/ACP5). Its interaction with CIZ1 was found using high-throughput affinity-purification mass spectrometry and published as part of the BioPlex (Huttlin et al., 2015). This study discovered 4 protein interactors for CIZ1 in HEK293T cells, a derivative of the human embryonic kidney cell line HEK293, that include NR2E1, MAPK14, EDA and ACP5. ACP5 is an iron-containing metalloenzyme commonly expressed in osteoclasts and alveolar macrophages (Boorsma et al., 2017). It was reasoned that understanding if the high salt treatment removes an inhibitor of release such as a protein phosphatase like PP1 or ACP5, might shed light on one potential mechanism behind CIZ1 retention at the Xi.

In order to do this, the partitioning of CIZ1 and ACP5 was analysed by western blot. A 3T3 population was subjected to a CSK incubation supplemented with detergent (0.1% Triton-X-100) and VRC. Following centrifugation, this generated two samples; the pellet (p), that contains any insoluble material, and the supernatant (sn), that contains all soluble cellular components (Figure 5.5A). CIZ1 is a complex protein which under denaturing conditions appears as multiple distinct entities, these may represent higher order complexes as well as various splice variants. In the lab we have multiple independently generated antibodies that have been validated to a greater or lesser degree on recombinant CIZ1, synthetic peptides and lysates from WT and CIZ1-null cells. Two of these antibodies have been used here, Nov4 that binds to the extreme C-terminus of CIZ1 and 1794 that binds to the N-terminus (Figure 1.7). The predicted MW of full-length CIZ1 is 100kDa (Coverley et al., 2005). This is detected by Nov4 in both the pellet and supernatant fractions. A faint band at 100kDa is also detected by 1794 but an entity just under 100kDa is more prominent (Figure 5.5B). Preliminary work with recombinant proteins in the Coverley lab has suggested this form to be full-length CIZ1

following a cleavage event at the C-terminal end and is therefore undetected by Nov4. It is important to note that despite a proportion of full-length CIZ1 being detergent-soluble, the majority remains in the detergent-resistant fraction. Excluding the non-specific 250kDa band, that appears to be a biproduct from the secondary antibody (Figure 5.5C), both antibodies also detect a CIZ1 entity at 125kDa in the pellet fraction. This entity has previously been documented (Coverley et al., 2005), with multiple possible reasons behind its existence. Notably, an additional dominant entity at 60kDa is recognised only by 1794 in the supernatant fraction (Figure 5.5B). Currently, it is uncertain what form of CIZ1 this band characterises. It has been well documented that ACP5 exists as two isoforms known as ACP5a and ACP5b. The monomeric form, ACP5a (~37kDa), can be post-translationally cleaved into ACP5b to generate two fragments (~16 and ~25kDa) joined by a disulphide bond. This cleavage event activates and increases the phosphatase activity of ACP5 (Ek-Rylander et al., 1991, Ljusberg et al., 1999, Reithmeier et al., 2017). In my analysis, ACP5 appears as a dominant entity at 60kDa in the supernatant fraction as well as a higher order entity (>250kDa) (Figure 5.5B). These migrations do not correlate with the expected sizes for ACP5 but alternative forms of ACP5 have been documented. For example, a larger ~55kDa complex has been characterised in plants with similar isoforms also identified in humans (Hadler et al., 2008, Flanagan et al., 2006). Therefore, these could be complexes of ACP5 with itself or other proteins. For my analysis I focus on the 60kDa entities detected by ACP5 and 1794.

Next, proteins removed over a serial exposure to increased NaCl concentration, in the absence of VRC, were harvested and analysed by western blot (Figure 5.5D). 1794 detects full-length CIZ1 in the salt supernatants up to 300mM, with higher NaCl concentrations no longer affecting the extractability of CIZ1. Other smaller CIZ1 forms are also extracted between 100-200mM, including the 60kDa entity. ACP5 provides a mechanistically interesting observation over the serial salt extraction. The 60kDa entity is evident in the 100mM supernatant as expected, however, an alternative form of ACP5 is present in the 300mM fraction. This 300mM fraction contains proteins removed between 200-300mM NaCl and where we would expect a potential inhibitor to be released (in line with activation of dispersal of CIZ1 between 200-300mM). Here, the highly enzymatic form of ACP5 is released, seen visually as a band at 16kDa (Figure 5.5E). Thus, ACP5 is a plausible candidate responsible for maintaining CIZ1 assemblies at the Xi. However, more in-depth analysis is required in order to directly associate the loss of ACP5 with CIZ1 dispersal as other proteins also released in this 200-300mM NaCl fraction could alter CIZ1's localisation.

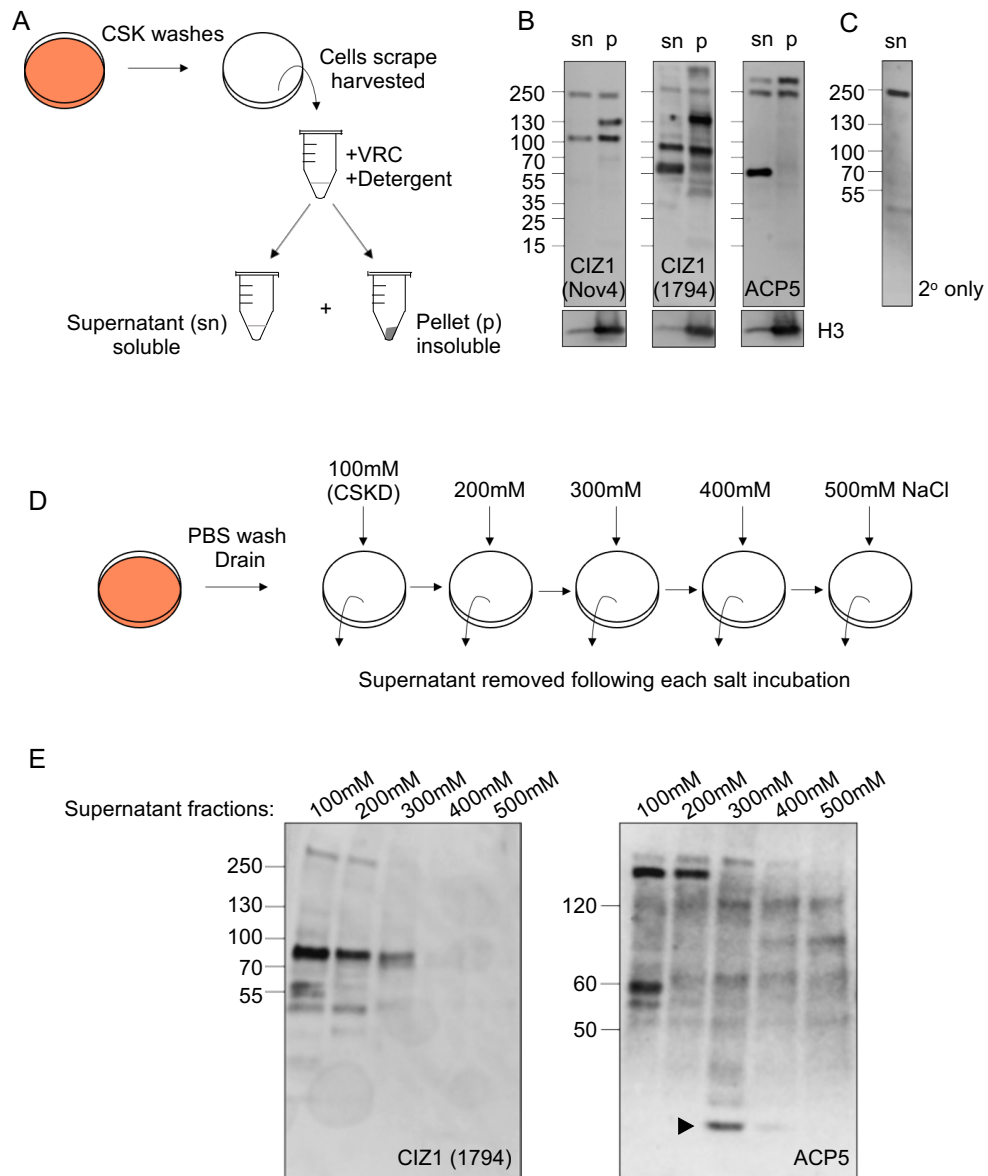


**Figure 5.5. Extractability of CIZ1 and ACP5.** A. Schematic describing the generation of insoluble and soluble fractions following a CSK incubation with detergent and VRC. B. Western blot analysis of the soluble supernatant (sn) and insoluble pellet (p) fractions generated in A for the C-term of CIZ1 (detected by Nov4), the N-term of CIZ1 (detected by 1794) and ACP5. Histone H3 indicates successful separation between the pellet and supernatant. C. Western analysis of the supernatant fraction with no primary antibody and therefore acts as a secondary antibody control. D. Schematic describing the serial salt extraction protocol. To the same population of cells, the salt concentration was gradually increased from 100mM to 500mM with proteins removed at each 100mM step analysed. E. Western analysis of samples generated in D, probed for either CIZ1 (1794) or ACP5.

#### **5.4.5 CIZ1 and ACP5 interaction**

As an interaction between CIZ1 and ACP5 has already been reported (Huttlin et al., 2015), I wanted to see if the 60kDa entity correlated to a denaturation resistant CIZ1:ACP5 complex. In order to see whether this 60kDa band is a complex of the 1794 and ACP5 epitopes, I attempted an immunoprecipitation experiment. Using Protein A/G UltraLink™ Resin, detergent-soluble proteins bound to either 1794 (N-term epitope) or Nov4 (extreme C-term epitope) were pulled down and analysed by western blot (Figure 5.6A). Control loading samples were taken from each reaction following antibody incubation but prior to protein A/G addition. ACP5 probing revealed a faint band at 60kDa in the 1794 pull down lane (Figure 5.6B). This begins to suggest that ACP5 and CIZ1 may exist as one complex. The 60kDa entity is also seen in all loading samples, despite the signal being very weak. As expected, this band isn't present in the Nov4 pulldown and therefore confirms that if CIZ1 and ACP5 are complexed it's not with the full-length form of CIZ1. The higher order ACP5 entity (above 250kDa) is also revealed in the loading samples but not in the test lanes suggesting CIZ1 is not part of this complex. Despite the 60kDa entity being a promising candidate for a CIZ1:ACP5 complex, this experiment has only been run once and with the band not being strikingly obvious, a re-run with some optimisation for detection is required.

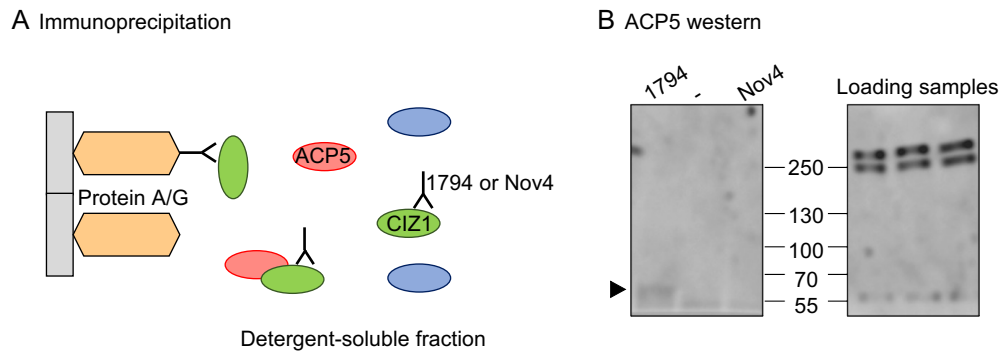


Figure 5.6. **CIZ1 and ACP5 interaction studies.** A. Schematic describing the capture of CIZ1 using the 1794 or Nov4 antibody and Protein A/G UltraLink™ Resin. In the first incubation, 1794 or Nov4 was added to the detergent-soluble fraction and binds to its epitope in either the N-terminal or C-terminal of CIZ1, respectively. Upon addition, Protein A/G interacts with the antibody resulting in CIZ1 (green) and any potential CIZ1:ACP5 complexes to be extracted from unbound ACP5 (red) and other unbound soluble proteins (blue). B. Western blot analysis of 1794, no antibody (-) and Nov4 pulldowns probed with ACP5. Loading samples were taken from each reaction prior to Protein A/G addition. A faint band at 60kDa is seen in the 1794 pull down fraction indicating ACP5 is complexed with the N-terminal of CIZ1.

## 5.5 Discussion

In this chapter, I have shown that CIZ1 particles can be manipulated to separate and disperse from the Xi in the presence of high salt and endogenous RNase activity, with an apparent need for ATP hydrolysis. I chose to pause my work in this area after my first year in favour of that described in Chapters 3 and 4. However, this data raises a set of new questions and below I highlight new direction that could be taken to progress this work.

VRC preserves CIZ1 assemblies at the Xi in the presence of high salt. There are several possibilities for the role of VRC in this context as it acts as an inhibitor of various RNases but its target specificity is unknown (Frazier and Champney, 2012). As *Xist* is known to be required for CIZ1 recruitment to the Xi (Ridings-Figueroa et al., 2017) and interacts directly with CIZ1 (Sofi et al., 2022), VRC could protect the degradation of *Xist* by blocking endogenous RNases. In fact, the GIY-YIG nuclease domain of CIZ1 (Figure 1.7) might itself possess ribonuclease activity. The GIY-YIG superfamily is a group of nucleases which share a domain containing a Glu residue, an Arg residue and two motifs “GIY” and “YIG” in the C-terminal, centre and N-terminal respectively (Dunin-Horkawicz et al., 2006). A metal binding pocket that is conserved throughout GIY-YIG endonucleases is thought to be the active site for cleavage requiring metal ions (Truglio et al., 2005). The GIY-YIG nuclease domain could therefore be responsible for cleaving *Xist* to cause dispersal. Before understanding the action of VRC, the role of *Xist* in CIZ1 dispersal needs to be determined. By exploiting techniques such as RNA-FISH, the response of *Xist* to high salt conditions can be examined. For example, *Xist* could be visualised to see if it disperses away from the Xi along with CIZ1, and whether it is cleaved (possibly into two forms). This is one experiment that could shed considerable light on the mechanism underpinning the release of CIZ1 particles.

As well as understanding the requirements for CIZ1 release, another important question surrounds the nature of CIZ1 movement, and whether it is random diffusion, active translocation set on a tract, or a spring-loaded event. Here, I have provided evidence that CIZ1 dispersal requires energy, though whether this relates to the movement itself or to a prior event remains unclear. Evidence for an active movement mechanism in the nucleus has been documented using a rapamycin-induced system in CHO cells. Two motion states; curvilinear and long-range movements were reported for repositioning of the chromosome sites, which are both directional movements (Chuang et al., 2006). In fact, the Xi itself is known to shuttle between two locations in the nucleus, in a manner that is dependent on CIZ1 (Stewart et al., 2019). Future experiments to investigate *in*

*vitro* CIZ1 dispersal could exploit time lapse imaging of GFP-CIZ1 transfected cells, in which ectopic protein accumulates at the Xi alongside endogenous protein (Ridings-Figueroa et al., 2017). If the permeabilised cell assay is successful at dispersing GFP-CIZ1, a flow cell could be used to flood cells with the high salt buffer whilst on the microscope, enabling analysis of mutated versions. One possible mutation could be introduced into the GIY-YIG domain to understand its role in dispersal.

To understand the mechanism of movement away from the Xi, inhibitors of transport molecules could be used. Nuclear actin and myosin have both been implicated in chromosome movement, in response to serum removal (Mehta et al., 2010) and as part of the rapamycin-induced system (Chuang et al., 2006). The idea of actin and myosin forming filaments in the nucleus and their potential involvement in directional movement of entities has been controversial (Dillon, 2008, de Lanerolle, 2012). However, recent advances are starting to shed light in this area, with evidence of nuclear actin forming short, dynamic filaments aiding chromatin organisation (Bera and Sengupta, 2020). In yeast cells, microtubules are believed to be involved in the nuclear rearrangement needed for successful entry to quiescence, as well as a potential role for tubulins (Laporte and Sagot, 2014). I began some experimentation in this area but was unable to obtain consistent results.

Based on an understanding of phosphatase and kinase activity throughout the cell cycle, and their effect on *Xist* (Hall et al., 2009) and CIZ1 (Unpublished data and (Ridings-Figueroa et al., 2017)), I focussed on the known CIZ1 interactor ACP5 as a candidate inhibitor of release. However, I think it would also be important to profile the behaviour of other phosphatases over the serial salt gradient including PP1. So far, the preliminary data here does not directly link the removal of ACP5 with dispersal of CIZ1. Therefore, further interaction studies and a functional analysis of ACP5 will need to be performed. For example, an important question would be if use of an ACP5 inhibitor has the same effect as high salt. If CIZ1 disperses in the presence of an ACP5 inhibitor, without high salt, this directly involves ACP5 in the mechanism behind CIZ1 retention at the Xi. Other studies in the laboratory have used a broad-spectrum protein phosphatase inhibitor and seen exactly this result (Coverley, Williamson unpublished).

This chapter also starts to investigate the idea of a CIZ1 and ACP5 complex. An uncharacterised entity at 60kDa is detected by both ACP5 and the N-terminal antibody for CIZ1, 1794. I have considered the possibility that this represents a denaturation-resistant complex between ACP5 and a CIZ1 variant. Interestingly, over the salt extraction series, this putative complex is only in the supernatant following low salt incubations (up to 200mM NaCl). Upon increase to 300mM, this complex is no longer observed and instead the lower MW catalytic form of ACP5 is detected in the supernatant fraction. I therefore propose that when the salt concentration exceeds 200mM this dissociates ACP5 from a complexed form, releasing the catalytic phosphatase. It would also be of interest to analyse the insoluble fraction over the serial salt extraction to see the behaviour of proteins that are retained following high salt incubations.

Despite the unknowns about mechanism of release, the data here describes a successful *in vitro* assay to probe the relationship between CIZ1 retention and dispersal from Xi chromatin. Initial findings highlight the importance of RNases, energy and a possible inhibitor of release that can be removed between 200-300mM NaCl.

## 6 Discussion

Entry to and exit from quiescence is an essential part of our physiology, but the mechanisms that control and maintain this cellular state are still not fully understood. It is widely appreciated that the balance between proliferation and quiescence is key to maintaining tissue homeostasis and that dysregulation can underlie various human pathologies. However, it is only recently becoming clear that quiescence is a highly complex state, and its establishment and maintenance involves many factors whose dysregulation could impact the fidelity of the transition, with downstream consequences.

Here, I uncouple the repression of cell cycle genes from chromatin condensation upon quiescence entry by comparing the response of WT and CIZ1-null murine fibroblasts to quiescence triggers. My data solidifies the importance for maintenance of the epigenome and identifies an underpinning role as chromatin organisation changes over this transition. The consequences of failure to regulate gene expression and chromatin organisation in and out of quiescence are presently underappreciated and will likely have a major impact on the cell and viability of the organism. Linking failure to achieve and maintain a stable, quiescent nucleus with potential genome instability may help in the advancement of medical interventions for a range of diseases, including cancer.

### 6.1 CIZ1 as a protector of the epigenome

This data and previously published data (Stewart et al., 2019, Sofi et al., 2022) show that CIZ1 plays a critical role in the maintenance of at least three histone PTMs; H4K20me1, H3K27me3 and H2AK119Ub1, at the Xi in cycling primary murine fibroblasts. Importantly, my work has extended CIZ1 analysis beyond the Xi by quantifying H4K20me1 loss and nuclear condensation deficiency in male cells. How CIZ1 protects these histone PTMs is currently unknown and is an emerging question from this work. Future analysis on the role of CIZ1 in this process may shed light on potential therapeutic targets to help restore or exploit epigenetic stability in disease contexts.

Recent work suggests that absence of histone PTMs at the Xi in CIZ1-null cells may reflect loss of protective CIZ1:RNA assemblies that influence access to chromatin modifying enzymes (Sofi et al., 2022). It is proposed that CIZ1 forms large phase-separated assemblies through its prion-like domains (PLDs, Figure 1.7) and interaction with RNA. There is currently no evidence that indicates a direct interaction between CIZ1 and histone PTMs or their associated modifiers. Upon the re-expression of CIZ1, subsequent reinstatement of these histone modifications at the Xi is seen. This further

emphasizes their CIZ1-dependence and indicates that CIZ1 is essential in preserving the epigenetic landscape.

### **6.1.1 Misbalance of histone modifiers**

Post-translational modification of histones, including H4K20 methylation, have emerged as regulators of genomic integrity (Jørgensen et al., 2013), as have chromatin modifiers whose activity determines histone methylation dynamics (Audia and Campbell, 2016). An imbalance in histone-modifying enzymes have been associated with human disease, for example, in hepatocellular carcinoma the H4K20me1 methyltransferase, SET8, acts as an oncogene. Overexpression of SET8 enhances cancer progression by promoting cell proliferation, migration and invasion (Wu et al., 2020). On the other hand, the H4K20me1 demethylase, PHF8, has also been documented as an oncogene and is associated with progression of colorectal cancer (Lv et al., 2017). This thesis focusses on the importance of H4K20me1 stability and how its loss, in the absence of CIZ1, contributes to transformation, expanding our knowledge on epigenetic disruption and its role in disease.

The enzymatic activities of histone modifiers may offer a route to intervention (Audia and Campbell, 2016, Nepali and Liou, 2021), an idea supported by specific high-frequency point mutations in histone genes in some tumours, notably paediatric cancers (Mohammad and Helin, 2017). Oncohistones alter the epigenetic landscape and are implicated in the genesis of several tumours (Qiu et al., 2018, Flaus et al., 2021), though in most cases how they give rise to cellular dysfunction are not understood. It is therefore important to understand the compromised downstream cellular events and when in the aetiology of cancer they give rise to irreversible genetic change to identify potential therapeutic targets.

I propose that there may be a link between the epigenetic instability, caused by loss of protective CIZ1:RNA assemblies in CIZ1-null cells, and CIZ1 associated cancers. It will therefore be of interest to see if other histone PTMs are influenced by CIZ1 and the consequences of their loss. All my experiments have used murine fibroblasts; therefore it remains to be seen if loss of CIZ1 assemblies and subsequent epigenetic instability is a cause for transformation in humans.

## 6.2 The implication of chromatin condensation in disease

A causative link between compromised DNA repair pathways, genome instability and cancer is very well established and understood in great detail (Jackson and Bartek, 2009), while the contribution of chromatin condensation pathways is much less well developed. Nevertheless, chromatin condensation failure has been implicated in disease, and the condensin complex identified as a mutated subnetwork in a pan-cancer network analysis, linking non-functioning condensin with cancer progression (Leiserson et al., 2015). It has been reported that chromatin compaction is able to protect genomic DNA from radiation damage and other chemical agents highlighting it as an important cellular mechanism for maintaining genomic integrity (Takata et al., 2013).

Altered condensin expression and mutations in condensin II have been reported in colorectal and pancreatic cancers (Weyburne and Bosco, 2021, Baergen et al., 2019, Kim et al., 2019). Similarly in murine models, mice that harbour a missense mutation in the condensin II subunit, NCAPH2, have a defect in T cell development and fail to condense their chromatin during the double-negative to double-positive transition (Gosling et al., 2007, Gosling et al., 2008, Rawlings et al., 2011). These mice further develop T-cell lymphoma with associated DNA damage and mitotic defects. Interestingly, despite this mutation initiating tumour formation, there is no evidence of chromatin decondensation in the interphase nucleus or any major changes in the gene expression programs related to development (Woodward et al., 2016). This parallels the abnormal quiescence of CIZ1-null fibroblasts and the pathology of CIZ1-null mice. Leukaemia (Nishibe et al., 2013) and high penetrance lymphomas (Ridings-Figueroa et al., 2017) are evident in adult mice bearing exon 5 deletion or gene trap insertion into intron 1, respectively. Notably, both lineages originate in progenitors whose maintenance requires quiescence entry and exit cycles (Shin et al., 2020). My data provides a plausible pathway for how a defect in CIZ1 could underpin the emergence of unstable lineages in cell types that undergo cycles of quiescence as part of their normal biology. By profiling the CIZ1 status in these cancers, and their chromatin state, this could provide the opportunity for an early detection biomarker as well as potential therapeutic targets.

Other studies suggest that condensation failure may drive genome instability, a hallmark of cancer (Hanahan and Weinberg, 2011), and disease progression. In colorectal cancer patients, expression of all condensin genes is altered, and reduced expression is linked with poor survival. In this context, it is suggested that reduced condensin complex function results in chromosome instability (CIN) and acts as a driver of disease progression. Key phenotypes associated with CIN that are evident in cells with diminished condensin gene expression include an increase in nuclear area, along with chromosome decompaction and micronucleus formation. Here, SMC2 was identified as a novel CIN gene (Baergen et al., 2019).

As CIZ1 is implicated in various cancers, this proposes that an underlying mechanism promoting genomic instability may be failed CIZ1-dependent regulation of the condensin complex. A similar role for the retinoblastoma protein (pRB) has been associated with mitotic chromosome condensation. In the absence of pRB, loss of condensin II recruitment and association with chromosomes is evident, resulting in failed condensin function (Longworth et al., 2008, Manning et al., 2010). This provides a potential cause for the genomic instability seen in pRB-deficient tumours (Coschi et al., 2010, Coschi et al., 2014) and also describes a possible mechanism for how CIZ1 acts as a tumour suppressor during quiescence cycles.

### **6.3 Clinical application**

Cancer cells are known for their aberrant nuclear architecture with diagnosis of some cancers historically based on increases in nuclear size (Zink et al., 2004, Fischer, 2020). As nuclear size is highly controlled, with any changes being strictly regulated, it was unexpected to see the expanded, oversized CIZ1-null nuclei over multiple rounds of serum withdrawal and addback. It is evident that these nuclei are more fragile when compared to nuclei that can successfully alter their nuclear size, raising the possibility that this may be an exploitable weakness.

It has been shown that fasting during chemotherapy leads to cancer cells being more responsive to treatment whilst normal cells experience a measure of protection. This fasting presents better outcomes in cancer patients in response to treatment as well as reducing the number of relapse patients (Nencioni et al., 2018). Given that CIZ1 expression is altered in many cancers it would be worthwhile to understand whether the aberrant chromatin condensation seen in CIZ1-null cells here might translate to CIZ1-defective cancer cells, and so contribute to their vulnerability during fasting.

## 6.4 Final remarks

My PhD has focussed on the role of CIZ1 during highly regulated transitions through the cell cycle, particularly entry to and exit from quiescence. Previous analysis revealed that maintenance of a stable quiescent state is CIZ1-dependent. Here, I develop our knowledge of CIZ1 as a protector of the epigenome and report on the downstream consequences. By analysing changes in the transcriptome following quiescence triggers, I identified a set of murine core quiescence genes that appear relatively unperturbed by the loss of CIZ1. Nevertheless, a subset of genes relating to chromatin condensation and homology directed repair behaved differently in CIZ1-null cells and therefore highlighted these as potential defective processes in the absence of CIZ1 (**Chapter 3**). Profiling nuclear size during quiescence entry established that chromatin condensation is compromised in CIZ1-null cells and associated with loss of H4K20me1. This implicated epigenetic instability as the primary vulnerability in CIZ1-null cells. Following aberrant chromatin condensation, decondensation still occurs upon cell cycle re-entry resulting in checkpoint activated, vulnerable nuclei (**Chapter 4**). Emergence of inappropriately decondensed nuclei in lineages that experience quiescence entry and exit cycles as part of their aetiology could therefore arise if CIZ1, or other contributors to H4K20me1-dependent condensation, were compromised. For another strand of my project, I developed a permeabilised cell assay to study the dynamics of CIZ1 retention at the Xi (**Chapter 5**). Though separate to my quiescence work, this assay will provide a foundation for future projects in the Coverley lab to further our understanding of CIZ1 in the cell cycle.

## Appendix A

PDF of peer-reviewed book chapter. Proposed publication date: Oct/Nov 2022.

**Dobbs OG** and Coverley D. (2022) Chromatin Dynamics During Entry to Quiescence and Compromised Functionality in Cancer Cells. In Kloc M, Kubiak JZ (editors), Nuclear, Chromosomal, and Genomic Architecture in Biology and Medicine.

# **Chromatin dynamics during entry to quiescence and compromised functionality in cancer cells**

Olivia Grace Dobbs\* and Dawn Coverley

Department of Biology, University of York, York, YO10 5DD, United Kingdom

\*grace.dobbs@york.ac.uk

## **Abstract**

Quiescence is a vital cellular state where cells can reversibly exit the cell cycle and cease proliferation in unfavourable conditions. Cells can undergo multiple transitions in and out of quiescence during their lifetime, and an imbalance in this highly regulated process can promote tumorigenesis and disease. The nucleus experiences vast changes during entry to quiescence, including changes in gene expression and a reduction in size due to increased chromatin compaction. Studies into these changes have highlighted the importance of a core quiescence gene expression programme, reorganisation of nuclear structures and the action of the condensin complex in creating a stable, quiescent nucleus. However, the underpinning mechanisms behind the formation of a quiescent nucleus are still not fully understood. This chapter explores the current literature surrounding chromatin dynamics during entry to quiescence, the association between quiescence and disease, and accentuates the need for further studies to understand this transition. Linking failure to maintain a stable, quiescent state with potential genome instability may help in the advancement of medical interventions for a range of diseases, including cancer.

Keywords: Quiescence, Chromatin, Nuclear condensation, Condensin complex, H4K20me.

## **1. Introduction**

The majority of cells in the human body are not actively cycling but in a poised, non-proliferating state known as quiescence. Quiescence has been described as a reversible, stress-resistant state in which chromatin is compacted, and gene expression suppressed as cells exit the cell cycle (Coller et al., 2006). Some cells can experience multiple rounds of entry and exit from quiescence, for example, fibroblasts in the process of tissue repair, lymphocytes as a part of the immune response, and

the reactivation of stem cells (Yao, 2014). It is this reversibility of quiescence that is essential for maintaining tissue homeostasis, making it a highly controlled cellular state, with a range of factors determining entry and exit. Imbalances in the transition between proliferation and quiescence in multicellular organisms can underlie a range of diseases, including excess proliferation associated with cancer (Cho et al., 2019), as well as too little proliferation that may result in cell loss and accelerated ageing and degeneration (Pack et al., 2019). As quiescence is an essential part of our normal physiology, it is important to understand the mechanisms controlling successful quiescence entry and exit and what happens when these processes go wrong.

To study the quiescent state *in vitro* a number of techniques have been developed to stimulate the anti-proliferative triggers that cells experience in the body (Mitra et al., 2018). Two well-established protocols include mitogen withdrawal (serum starvation) and cell contact inhibition. When a cell experiences such anti-proliferative cues, intracellular signalling (reviewed extensively elsewhere (Duronio and Xiong, 2013, Cho et al., 2019, Ricard et al., 2021)), instigates global changes in both gene expression and chromatin organisation to ensure a stable transition to a quiescent state. This chapter focuses on these two nuclear processes in relation to quiescence entry and their compromised functionality in cancer cells.

## **2. Gene expression changes during quiescence entry**

The prevailing view of quiescence is as a dormant phase of the cell cycle with little activity. However, recent advances have altered this view of the quiescent state to one that is actively regulated to allow for rapid re-entry to the cell cycle when needed. Transcriptional profiling studies have been conducted to follow the changes in gene expression that occur during entry to quiescence and, therefore, better our understanding of this “resting” cellular state.

As expected, when a cell exits the cell cycle, there is a global suppression of cell-cycle genes. These include cyclin A2, cyclin B, cyclin E2, and survivin, as well as genes involved in DNA replication to ensure a halt to cell cycle progression. Quiescent cells also exhibit a low metabolic activity; therefore genes relating to mitochondrial function are downregulated (Cheung and Rando, 2013).

Despite quiescent cells being recognised for what they do not do, studies into quiescence are beginning to show that it remains an active state with upregulation of gene sets involved in transcriptional regulation and stem cell fate decisions (Cheung and Rando, 2013, Cho et al., 2019). Transient upregulation of stress-related genes is also seen upon entry to quiescence before becoming repressed, enabling a successful response to the quiescent trigger. Interestingly, the corresponding proteins remain at a high level despite eventual gene repression (Marguerat et al., 2012).

Using a yeast model, studies have quantified the transcriptome and proteome of proliferating and quiescent populations. They revealed that quiescent *Schizosaccharomyces pombe* cells have a smaller transcriptome compared to cells that were cycling but the proteome remained at a similar size. Even though comparable in size, the proteome in quiescent cells is remodelled in a way that reflects the change in gene expression and is adapted for maintenance rather than cell growth (Marguerat et al., 2012).

While most studies focus on the widespread repression of transcription during quiescence entry and the downregulation of essential genes involved in proliferation, translation, and metabolite biogenesis, it is clear that the transition to quiescence is not a simple shut down. Quiescent cells need to have a basal level of transcription in order to survive, and active regulation is required to maintain the quiescent cell in a state that is ready to re-enter the cell cycle when instructed (Marguerat et al., 2012, McKnight et al., 2015, Roche et al., 2017).

### ***Core quiescence program***

As exit from the cell cycle can be initiated by a range of different triggers, one question that surrounds quiescence is whether one or multiple quiescent states exist. By distinguishing whether a gene expression change is the result of the specific trigger instructing cell cycle arrest or central to quiescence itself will help understand the functionality of quiescent cells.

To begin to address this, some studies have compared quiescence triggers and profiled the expression changes that occur. In human fibroblasts, the initial gene expression changes are dependent on the trigger (serum starvation or contact inhibition), but the changes have common functions that are essential to quiescence entry, such as downregulation of pro-proliferation genes. This suggests that each trigger is capable of creating a subtly different quiescent state, possibly resulting in a heterogeneous quiescent population (Coller et al., 2006, Yao, 2014). Interestingly, adult neural stem cells (NSCs) also demonstrate a range of quiescent states. A deeper, dormant quiescent state and a primed quiescent state have been modelled based on whether the cells receive BMP or BMP/FGF treatment, respectively. These two states have distinct signalling pathways and transcriptional programs with an increase in the LRIG1 protein evident in the primed quiescent state. This data suggests that the level of LRIG1 expression is an important regulator of the transition between the cell cycle and quiescence in NSCs (Marqués-Torrejón et al., 2021).

Focussing on the serum starvation method, 135 serum deprivation early response genes (SDERGs) have been identified in human fibroblasts. These include two tumour suppressor genes, SALL2 and MXI1, that also have a unique role in regulating other SDERGs. Silencing of these two genes during quiescence entry results in

failed cell cycle exit and continued progression of the cell cycle (Liu et al., 2007), evidencing a clear hierarchy.

Following such initial signal-dependent changes, cells eventually develop a common quiescence programme. This is a set of gene expression changes vital to the maintenance of the long-term quiescent state and is not specific to the initial trigger. The quiescence program includes genes involved in the regulation of cell growth and division, suppression of apoptosis, suppression of differentiation, and intercellular communication. These are candidate genes that could be required for maintaining cells in a reversible, viable arrested state (Coller et al., 2006, Liu et al., 2007). What is becoming clear is that different genes are involved in the transition to quiescence compared to the maintenance of the quiescent state.

### ***The DREAM complex***

Repression of cell cycle genes is essential for quiescence entry and requires strict regulation. The dimerization partner, RB-like, E2F, and multi-vulval class B (DREAM) complex is best known for its role in quiescent cells where it is involved in the repression of pro-proliferation genes (Sadasivam and DeCaprio, 2013).

The DREAM complex is made up of a MuvB core complex along with the additional subunits p130 or p107, E2F4, and dimerization partner 1 (DP1). The MuvB core consists of five MuvB-like proteins; LIN9, LIN37, LIN52, LIN54, and RBBP4. Phosphorylation of the LIN52 subunit at Ser28 by the kinase DYRK1A is needed for binding of p130/E2F4 to the MuvB core and subsequent assembly of the DREAM complex (Litovchick et al., 2011). In other stages of the cell cycle, the MuvB core can assemble and function with other transcription factors such as BMYB and FOXM1 (Sadasivam and DeCaprio, 2013). The balance between different complex assemblies in response to proliferative/anti-proliferative triggers determines DREAM complex activity and the extent to which it can repress cell-cycle genes by binding to CHR promoter elements (Müller and Engeland, 2010, Müller et al., 2014) and E2F target genes (Litovchick et al., 2007).

### ***Epigenetic status in quiescence***

The methylation status of DNA and post-translational modification of histones determine chromatin state, whether it is in a receptive conformation for transcription factor binding and transcriptional activation or a closed conformation resulting in transcriptional suppression. Thus, chromatin state in quiescence requires consideration.

DNA methylation occurs at cytosines in CpG sequences and plays an important role in mammalian development by modulating gene expression, typically

suppressing it. However, in human fibroblasts, constant levels of DNA methylation are observed through all phases of the cell cycle, with no global changes evident in the quiescent state (Vandiver et al., 2015). Similarly, no difference in CpG methylation was observed between naive and activated T cells, further supporting the hypothesis that DNA methylation is not significantly altered in quiescence (Rawlings et al., 2011).

In contrast, specific histone post-translational modifications have been linked with the quiescent state. Most notably, on entry to quiescence, *Saccharomyces cerevisiae* exhibit a global reduction in histone acetylation as the lysine deacetylase, Rpd3, targets gene promoters of at least 50% of genes, resulting in their hypoacetylation and repression (McKnight et al., 2015). Moreover, while similar levels of H3K4me2, H3K36me2, and H3K36me3 were observed between proliferating and quiescent yeast cell populations, H3K4me3 falls upon quiescence entry. As H3K4me3 is associated with active chromatin this is not surprising, though it is also worth noting that even in quiescent cells, H3K4me3 levels are still relatively high, suggesting that features associated with transcriptionally active chromatin remain (Young et al., 2017).

In human cells, the picture is still emerging. While similar global levels of histone methylation were observed between proliferating and quiescent fibroblasts (Evertts et al., 2013), in lymphocytes and hair follicle stem cells, quiescence coincided with reduced levels of H3 lysine methylation (Baxter et al., 2004, Lee et al., 2016).

One histone post-translational modification that is highly dynamic through the cell cycle, and attracting investigation in the context of quiescence, is methylation of histone H4 at lysine 20 (H4K20). H4K20 can exist without methylation or in a mono-, di-, or tri-methylated state. H4K20me2 is present throughout the cell cycle and is the most abundant state, with H4K20me1 and H4K20me3 present at much lower levels (Pesavento et al., 2008). H4K20me1 levels fluctuate throughout the cell cycle, with the highest levels in the G2/M phase, while H4K20me3 is associated with quiescence, heterochromatic regions, and transcriptional silencing. The upregulation of H4K20me3 was found to be the most widespread change in histone modification status in quiescent human fibroblasts (Evertts et al., 2013, Jørgensen et al., 2013).

### ***Other post-transcriptional controls***

Additional mechanisms implicated in differential regulation of gene expression in quiescence include RNA stability, expression and function of specific microRNAs, and RNA polymerase II (RNA Pol II). RNA Pol II remains relatively high in quiescent cells, but levels of the initiating and elongating forms become depressed (Young et al., 2017).

Several microRNAs, non-coding RNA molecules that can bind to mRNAs, have been linked with entry to quiescence. For example, miR-29 is downregulated resulting in increased expression of its target genes, including those that code for extracellular matrix proteins (Suh et al., 2012). Another microRNA, miR-489, is upregulated in quiescent muscle stem cells and prevents cell proliferation by targeting the oncogene Dek mRNA (Cheung et al., 2012). Thus, microRNAs have been linked with both the maintenance of the quiescent state and the prevention of uncontrolled exit.

The widely accepted global reduction in RNA levels in quiescent cells disguises the fact that many RNAs are still highly expressed. This reflects a combination of active transcription and an increase in RNA stability. In fact, quiescent cells can store important RNAs that are vital to their survival when transcribed during active proliferation or the transition to the quiescent state (Young et al., 2017). Extracellular matrix organisation genes are among those that have increased stability in quiescent human fibroblasts compared to proliferating fibroblasts (and which are also upregulated) (Johnson et al., 2017).

The diverse mechanisms that regulate gene expression in quiescent cells, the sequestration of RNA as well as the histone modifications associated with active transcription, suggest that quiescent cells are in a poised state and are adapted for a quick response to environmental change, ensuring tissue homeostasis.

### **3. Nuclear reorganisation and chromosome positioning**

Packaging of chromatin in the nucleus is highly versatile and in quiescent cells exists in a compact, condensed form that appears different to interphase (Tokuyasu et al., 1968). Changes have been seen in both the facultative heterochromatin, which can adapt between active euchromatin and condensed heterochromatin, and in gene-poor constitutive heterochromatin (Grigoryev et al., 2004). Moreover, the spatial organization of chromatin in the nucleus is not random and adopts configurations that are specific to quiescent cells. Condensation of chromatin in quiescent cells results in a reduced nuclear size when compared to cycling nuclei. Analysis of nuclear area/volume can be used as a surrogate measurement for chromatin condensation (Swygert et al., 2019).

The spatial organisation of chromatin plays a key role in gene expression by influencing the maintenance of epigenetic marks and the long-range interaction of inter- and intra- chromosomal domains. As disruption of this organisation, and other features of nuclear architecture, are closely associated with disease phenotypes such as cancer (Zink et al., 2004, Foster and Bridger, 2005), the rearrangements that occur in quiescence, and the mechanism by which they are achieved, require a more thorough and detailed analysis than they have received so far. A few pioneering papers have begun to shed light on this area.

### ***The role of microtubules during quiescence entry***

Microtubules, formed of  $\alpha$ - and  $\beta$ -tubulin, are dynamic and the largest type of filament that contribute to the cell's cytoskeletal network. Their ability to polymerise and depolymerise underpins multiple cell processes, notably chromosome segregation during mitosis in all eukaryotes (Wade, 2009). However, in *S. cerevisiae* their role in the conversion of a G1 nucleus to a quiescent nucleus has been described and highlights their importance in nuclear reorganisation events. The short nuclear microtubules originating from the spindle pole body in G1, termed the 'Rabl' configuration, elongate to form a stable array across the nucleus in quiescence. As they grow, the nucleus undergoes a dramatic rearrangement, with the nucleolus moving from a position opposite the spindle pole body to one at the side of the microtubule array. Cells that are defective in forming the array have poor survival during extended periods in the quiescent state but remain able to exit the cell cycle (Laporte et al., 2013). Overall, many of the changes experienced by yeast cells as they enter quiescence are similar in mammalian cells (Laporte and Sagot, 2014) though whether this reorganisation event is conserved remains unknown.

### ***The role of nuclear myosin during quiescence entry***

Studies of nuclear reorganisation events during quiescence entry in human fibroblasts have implicated nuclear myosin. In primary interphase nuclei, chromosomes are located in discrete chromosome territories, and their position is strictly regulated. Gene-poor chromosomes are typically located at the periphery of the nucleus, but move to a more internal position in quiescence (Bridger et al., 2000). In fact, ten chromosomes have been shown to change their position in the nucleus upon exit from the cell cycle. Repositioning is a rapid response to quiescence triggers (serum starvation), with chromosomes evident in their new position after only 15 minutes. This rapid, manipulable transition has allowed evaluation of the effect of small molecule inhibitors and has implicated nuclear myosin 1 $\beta$  in the relocation process, suggesting that chromosome movement is an active process (Mehta et al., 2010).

## **4. Chromatin condensation during quiescence entry**

Whilst the compaction of chromatin into mitotic chromosomes is well understood, the chromatin condensation that takes place upon entry to quiescence remains relatively underexplored. Chromatin condensation is clearly evident in quiescent *S. cerevisiae* (Laporte et al., 2016, Swygert et al., 2019), quiescent primary human fibroblasts (Everetts et al., 2013), and during thymocyte development (Rawlings et

al., 2011). However, how nuclei transition to this stable, condensed state is not understood.

### ***The Condensin complex***

Two major protein complexes that play a role in chromatin organisation are cohesin and condensin, both structural maintenance of chromosomes (SMC) complexes important in chromatid cohesion and chromatin condensation, respectively (Hirano, 2012, Uhlmann, 2016). In eukaryotes, two forms of the condensin complex, condensin I and II, exist (Hirano, 2012) both consisting of the two core subunits SMC2 and SMC4, plus three different additional subunits; NCAPH, NCAPD2 and NCAPG for condensin I and NCAPH2, NCAPD3 and NCAPG2 for condensin II (Gerlich et al., 2006). The two SMC core subunits exist as a V-shaped complex and, when associated with the non-SMC subunits, form a ring-shaped structure (Yuen and Gerton, 2018). The prevailing model describing the mechanism by which condensin compacts chromatin is the ‘Loop Extrusion’ model, in which DNA is pushed through the ring structure from both directions to form a DNA loop that extends as more DNA is pushed through (Uhlmann, 2016, Terakawa et al., 2017). In quiescent *S. cerevisiae*, condensin has been shown to bind large chromosomal interaction domains (L-CIDs), which resemble topologically associated domains (TADs) in metazoans, forming chromatin loops between the domains, which is consistent with the loop extrusion model (Swygert et al., 2019). However, other studies are beginning to suggest that the condensin complex binds to DNA itself through DNA binding domains in the non-SMC subcomplex creating a ‘safety belt’ mechanism (Kschonsak et al., 2017).

Condensin complexes play a key role in chromatin condensation, which was first reported in 1997 (Hirano et al., 1997), and since then immunofluorescence studies have shown that condensin I and II are sequestered in different locations of the cell. While condensin II is located in the nucleus during interphase, condensin I is found in the cytoplasm and only able to access chromosomes after nuclear envelope breakdown in mitosis (Maeshima and Laemmli, 2003, Hirota et al., 2004). The difference in location has been theorised to underpin independent functions, with nuclear exclusion limiting the action of condensin I to a specific point in the cell cycle (Hirano, 2012). As condensin II is located in the nucleus throughout the cell cycle, it would be able to impact chromosomes during prophase before nuclear envelope breakdown, and consistent with this, deletion of NCAPD3 (Hirota et al., 2004), NCAPG2, and NCAPH2 (Ono et al., 2004) all have a dramatic effect on the prophase nucleus, with chromatin unable to condense. Condensin I then binds to chromosomes in prometaphase and anaphase and remains there throughout mitosis, contributing to their stability until after segregation (Gerlich et al., 2006). While condensin I and II work together to ensure stable condensation of chromatin into chromosomes, they

can also function independently of each other, as neither complex needs the other to associate with chromosomes (Hirota et al., 2004).

### ***The role of the Condensin complex in quiescence***

Condensation of interphase chromatin into chromosomes at mitosis and the compaction of nuclei in quiescence are different events with different endpoints, yet it is plausible that the same condensation machinery underpins them both.

In quiescent yeast cells, the promotion of loops between TAD/L-CID boundaries by condensin is known to lead to the compaction of chromatin. In the same study, knockdown of the core condensin subunit SMC2 in human foreskin fibroblasts prevented chromatin condensation during entry to quiescence, demonstrating a role for condensin in both yeast and human quiescence (Swygert et al., 2019). Furthermore, a specific role for condensin II has been established in thymocyte development. Mice lacking the Kleisin- $\beta$  subunit, NCAPH2, are unable to condense their chromatin, a defect that is proposed to underlie heightened apoptosis and reduced numbers of double-positive thymocytes (Gosling et al., 2007, Gosling et al., 2008, Rawlings et al., 2011).

Interestingly, condensin has also been closely associated with the changes in gene expression that occur during quiescence entry. In condensin-depleted *S. cerevisiae*, an increase in polymerase II occupancy is seen compared to controls that remain capable of chromatin compaction. The authors suggest that the effect of nuclear compaction in quiescence is to repress transcription and that in its absence, transcriptional de-repression can occur in quiescent cells (Swygert et al., 2019, Swygert et al., 2021).

### ***H4K20 methylation and condensation***

H4K20 exists in a mono-, di- and tri- methylated state, and the di- and tri- modifications have been shown to be dependent on the presence of monomethylation (Oda et al., 2009). These post-translational modifications of H4K20 have been associated with the regulation of chromatin compaction and also with DNA damage repair and DNA replication (Jørgensen et al., 2013). During prophase, the H4K20me1 demethylase, PHF8, is phosphorylated and removed from chromatin resulting in the accumulation of H4K20me1. H4K20me1 is thought to play a role in mitotic chromosome condensation by providing a platform for condensin II complex binding via HEAT repeat clusters in two subunits, NCAPD3 and NCAPG2 (Liu et al., 2010). Similarly, the role of H4K20me1 in cell cycle progression was illustrated by manipulating its methyltransferase, PR-Set7/SET8. Lack of SET8 and

reduced H4K20me1 levels prevent cells from passing to mitosis from G2 with global chromosome condensation failure (Houston et al., 2008, Oda et al., 2009).

Importantly, H4K20 methylation impacts chromatin structure in other stages of the cell cycle, as well as in mitosis, and because condensin II is present in the nucleus throughout the cell cycle, it is the most likely candidate for H4K20-dependent interphase roles. Loss of SET8 in embryonic stem cells results in chromatin decondensation in interphase nuclei (Oda et al., 2009), while SET8-mediated H4K20 methylation is thought to regulate chromatin decompaction during the transition from mitosis to G1, helping to guard against loss of genome integrity (Shoaib et al., 2018).

While there is a lack of information on the role of H4K20me1 during entry to quiescence, once in quiescence H4K20me3 has a documented role and has been associated with an increase in chromatin compaction (Lu et al., 2008, Evertts et al., 2013). H4K20me3 becomes more prominent in quiescent cells, and upon depletion of both SUV4-20H1 and SUV4-20H2, the enzymes responsible for converting H4K20me1 to H4K20me2 and H4K20me3, respectively, a decrease in chromatin compaction is observed along with failure to exit the cell cycle (Lu et al., 2008, Evertts et al., 2013).

Overall, the available evidence, largely based on manipulating enzymes that modify H4K20, reveals a range of effects on cell cycle progression and chromatin condensation, some of which can be linked to quiescence.

## 5. Quiescence and disease

Quiescence is a stress-resistant state which the cell can enter as part of its normal physiology to avoid the accumulation of DNA damage and over proliferation in unfavourable conditions. The cell experiences major reorganisation events during the transition from an interphase nucleus to a condensed, quiescent nucleus. Therefore, it is unsurprising that defects in the players that drive and regulate this transition have been linked with human diseases such as cancer and other diseases of ageing.

Over their lifespan, ageing stem cells can begin to lose their function and cause a misbalance between proliferation and quiescence. Hematopoietic stem cells (HSCs) can demonstrate how ageing affects functional capacity as the majority of aged HSCs have lost their regenerative capabilities and remain quiescent. This results in reduced levels of adaptive immune cells and an increased risk of anaemia and myeloid leukaemia (Pietras et al., 2011). Ageing in the muscle stem cell niche results in the cells losing their ability to remain in a quiescent state, reducing the stem cell population and thereby impacting the regenerative capacity of the muscle (Chakkalakal et al., 2012). Long-lived HSCs also accumulate sites of DNA damage over the ageing process that poses a risk to their genome integrity (Beerman et al., 2014). DNA damage response (DDR) pathways exist to efficiently manage DNA

damage in all cells and promote damage repair or cell death to maintain healthy cell populations. DNA damage is particularly detrimental in quiescence as cells are unable to repair strand breaks by the accurate process of homologous recombination (HR) and instead rely on the error-prone mechanism of non-homologous end joining (NHEJ). This inaccurate form of repair leaves quiescent HSCs susceptible to mis-repaired breaks, mutations, genomic instability, and may underly haematological disorders including leukaemia (Mohrin et al., 2010, Pietras et al., 2011). Upon re-entry to the cell cycle, HSCs have been shown to upregulate DDR pathways and repair damage accumulated during quiescence to avoid further downstream effects during proliferation (Beerman et al., 2014).

Cancer cells are defined by their inability to sustain quiescence and no longer respond to anti-proliferative signals. Along with the evasion of controlled cell death by apoptosis, this results in uncontrolled cell proliferation (Roche et al., 2017). SDERGs, tumour suppressor genes that normally play a role in cell cycle exit, are downregulated, and breast cancer patients who have a reduced expression of SDERGs have a worse survival rate as well as an increased chance of cancer metastasis (Liu et al., 2007). Therefore, the global regulation of gene expression that occurs during quiescence entry is vital for the restraint of tumour cell growth. Dysregulation of the DREAM complex and its target genes have also been associated with cancer. Upregulation of the subunits that associate with the MuvB core during the active cell cycle is commonly observed in cancer, tipping the balance towards a proliferative competent state (Iness and Litovchick, 2018, Iness et al., 2019). Similarly, inhibition of DREAM complex formation by the PCNA-associated factor (PAF), which is upregulated in various cancers, including lung adenocarcinoma, leads to failure of cell-cycle gene repression and failure to establish a quiescent state (Kim et al., 2021). In contrast, quiescence can be beneficial to cancer cell survival as a way to avoid the cytotoxic effects of chemotherapy, which typically targets actively cycling cells (Sadasivam and DeCaprio, 2013, Iness and Litovchick, 2018). This is evident in glioblastoma, an aggressive brain tumour, which consists of both proliferating and quiescent cells. Quiescence in this context allows for regrowth of the tumour following cytotoxic therapy. A risk allele associated with LRIG1 has been identified for glioblastoma and it has been proposed that these quiescent cancer cells may be in a primed state, with a high level of LRIG1, that enables cell cycle re-entry and cancer progression. However, loss of LRIG1 altogether results in failed quiescence entry and hyperproliferation of normal NSCs. This requirement for balanced expression is an important demonstration of the fine-tuning required for homeostasis (Marqués-Torrejón et al., 2021).

Chromatin condensation failure has also been implicated in disease, and the condensin complex identified as a mutated subnetwork in a pan-cancer network analysis, linking non-functioning condensin with cancer progression (Leiserson et al., 2015). Mutations in condensin subunits can, in fact, drive cancer. Notably, a missense mutation in NCAPH2 leads to T-cell lymphoma in mice, with associated DNA damage and mitotic defects. Interestingly, despite this mutation initiating tumour formation, there is no evidence of chromatin decondensation in the interphase

nucleus or any major changes in the gene expression programs related to development (Woodward et al., 2016). Other studies suggest that condensation failure may drive genome instability, a hallmark of cancer (Hanahan and Weinberg, 2011). In colorectal cancer patients, expression of all condensin genes is altered, and reduced expression is linked with poor survival. In this context, it is suggested that reduced condensin complex function results in chromosome instability (CIN) and acts as a driver of disease progression. Key phenotypes associated with CIN that are evident in cells with diminished condensin gene expression include an increase in nuclear area, along with chromosome decompaction and micronucleus formation. Here, SMC2 was identified as a novel CIN gene (Baergen et al., 2019).

## **6. Concluding remarks**

Entry to and exit from quiescence is an essential part of our physiology, but the mechanisms that control and maintain this cellular state are still not fully understood. It is widely appreciated that the balance between proliferation and quiescence is key to maintaining tissue homeostasis and that dysregulation can underlie human pathologies (Fig. 1). However, it is only recently becoming clear that quiescence is a highly complex state, and its establishment and maintenance involves many factors whose dysregulation could impact the fidelity of the transition, with downstream consequences. Advances focussing on gene expression and chromatin organisation in both yeast models and human studies demonstrate the dramatic remodelling that occurs when a cell exits the cell cycle (Fig. 2). This requires coordinated downregulation of genes involved in cell cycle progression, which has been the main hallmark of quiescent cells for many years. However, quiescent cells are not merely resting. They exist in a highly regulated, actively maintained state for preparation to re-enter the cell cycle when instructed. Moreover, quiescent cells are not in one simple cell state but, in fact, exist as a heterogeneous population dependent on the initiating trigger. Alongside the vast changes seen at the level of gene expression, the significant changes in chromatin organisation, that result in a visibly more compact nucleus, also need to be tightly controlled. Exactly how quiescent cells form a condensed chromatin state is still uncertain, but studies suggest that the condensin complex, most likely condensin II, plays a role modulated by the methylation status of H4K20. The consequences of failure in these processes and the potential for genome instability are presently underappreciated and will likely have a major impact on the cell and viability of the organism.

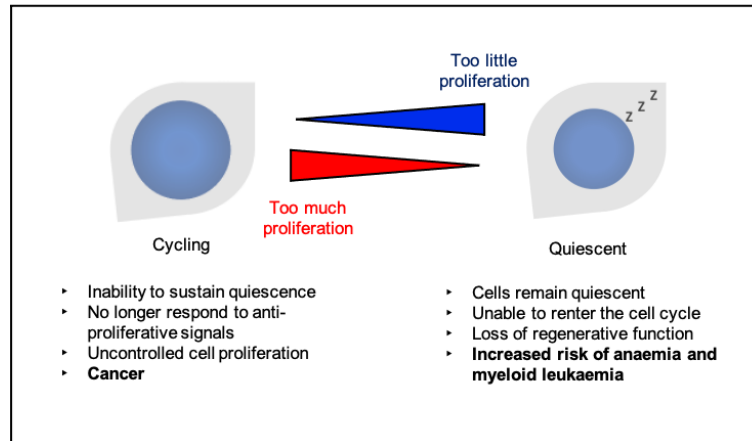


**Figure 1. Consequences of imbalance between a cycling and quiescent state.** Dysregulation of the quiescence transition can result in too much or too little cell proliferation and is linked with various pathologies. This highlights the importance of an accurate, regulated transition between these two states to maintain tissue homeostasis.

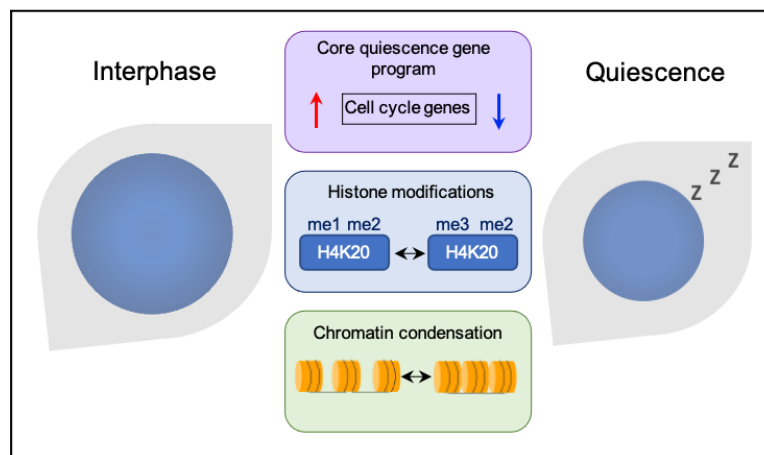


**Figure 2. Summary of three key cellular changes during the reversible quiescence transition.** As a cell exits the cell cycle and enters quiescence it undergoes dramatic changes, including in global gene expression, histone modifications and chromatin dynamics.

- Baergen, A. K., Jeusset, L. M., Lichtensztejn, Z. & Mcmanus, K. J. 2019. Diminished Condensin Gene Expression Drives Chromosome Instability That May Contribute to Colorectal Cancer Pathogenesis. *Cancers (Basel)*, 11.
- Baxter, J., Sauer, S., Peters, A., John, R., Williams, R., Caparros, M. L., Arney, K., Otte, A., Jenuwein, T., Merckenschlager, M. & Fisher, A. G. 2004. Histone hypomethylation is an indicator of epigenetic plasticity in quiescent lymphocytes. *EMBO J*, 23, 4462-72.
- Beeraman, I., Seita, J., Inlay, M. A., Weissman, I. L. & Rossi, D. J. 2014. Quiescent hematopoietic stem cells accumulate DNA damage during aging that is repaired upon entry into cell cycle. *Cell Stem Cell*, 15, 37-50.
- Bridger, J. M., Boyle, S., Kill, I. R. & Bickmore, W. A. 2000. Re-modelling of nuclear architecture in quiescent and senescent human fibroblasts. *Curr Biol*, 10, 149-52.
- Chakkalakal, J. V., Jones, K. M., Basson, M. A. & Brack, A. S. 2012. The aged niche disrupts muscle stem cell quiescence. *Nature*, 490, 355-60.
- Cheung, T. H., Quach, N. L., Charville, G. W., Liu, L., Park, L., Edalati, A., Yoo, B., Hoang, P. & Rando, T. A. 2012. Maintenance of muscle stem-cell quiescence by microRNA-489. *Nature*, 482, 524-8.
- Cheung, T. H. & Rando, T. A. 2013. Molecular regulation of stem cell quiescence. *Nat Rev Mol Cell Biol*, 14, 329-40.
- Cho, I. J., Lui, P. P., Obajdin, J., Riccio, F., Stroukov, W., Willis, T. L., Spagnoli, F. & Watt, F. M. 2019. Mechanisms, Hallmarks, and Implications of Stem Cell Quiescence. *Stem Cell Reports*, 12, 1190-1200.
- Coller, H. A., Sang, L. & Roberts, J. M. 2006. A new description of cellular quiescence. *PLoS Biol*, 4, e83.
- Duronio, R. J. & Xiong, Y. 2013. Signaling pathways that control cell proliferation. *Cold Spring Harb Perspect Biol*, 5, a008904.
- Evertts, A. G., Manning, A. L., Wang, X., Dyson, N. J., Garcia, B. A. & Coller, H. A. 2013. H4K20 methylation regulates quiescence and chromatin compaction. *Mol Biol Cell*, 24, 3025-37.
- Foster, H. A. & Bridger, J. M. 2005. The genome and the nucleus: a marriage made by evolution. Genome organisation and nuclear architecture. *Chromosoma*, 114, 212-29.
- Gerlich, D., Hirota, T., Koch, B., Peters, J. M. & Ellenberg, J. 2006. Condensin I stabilizes chromosomes mechanically through a dynamic interaction in live cells. *Curr Biol*, 16, 333-44.
- Gosling, K. M., Goodnow, C. C., Verma, N. K. & Fahrner, A. M. 2008. Defective T-cell function leading to reduced antibody production in a kleisin-beta mutant mouse. *Immunology*, 125, 208-17.
- Gosling, K. M., Makaroff, L. E., Theodoratos, A., Kim, Y. H., Whittle, B., Rui, L., Wu, H., Hong, N. A., Kennedy, G. C., Fritz, J. A., Yates, A. L., Goodnow, C. C. & Fahrner, A. M. 2007. A mutation in a chromosome condensin II subunit, kleisin beta, specifically disrupts T cell development. *Proc Natl Acad Sci U S A*, 104, 12445-50.

- Grigoryev, S. A., Nikitina, T., Pehrson, J. R., Singh, P. B. & Woodcock, C. L. 2004. Dynamic relocation of epigenetic chromatin markers reveals an active role of constitutive heterochromatin in the transition from proliferation to quiescence. *J Cell Sci*, 117, 6153-62.
- Hanahan, D. & Weinberg, R. A. 2011. Hallmarks of cancer: the next generation. *Cell*, 144, 646-74.
- Hirano, T. 2012. Condensins: universal organizers of chromosomes with diverse functions. *Genes Dev*, 26, 1659-78.
- Hirano, T., Kobayashi, R. & Hirano, M. 1997. Condensins, chromosome condensation protein complexes containing XCAP-C, XCAP-E and a *Xenopus* homolog of the *Drosophila* Barren protein. *Cell*, 89, 511-21.
- Hirota, T., Gerlich, D., Koch, B., Ellenberg, J. & Peters, J. M. 2004. Distinct functions of condensin I and II in mitotic chromosome assembly. *J Cell Sci*, 117, 6435-45.
- Houston, S. I., Mcmanus, K. J., Adams, M. M., Sims, J. K., Carpenter, P. B., Hendzel, M. J. & Rice, J. C. 2008. Catalytic function of the PR-Set7 histone H4 lysine 20 monomethyltransferase is essential for mitotic entry and genomic stability. *J Biol Chem*, 283, 19478-88.
- Iness, A. N., Felthousen, J., Ananthapadmanabhan, V., Sesay, F., Saini, S., Guiley, K. Z., Rubin, S. M., Dozmorov, M. & Litovchick, L. 2019. The cell cycle regulatory DREAM complex is disrupted by high expression of oncogenic B-Myb. *Oncogene*, 38, 1080-1092.
- Iness, A. N. & Litovchick, L. 2018. MuvB: A Key to Cell Cycle Control in Ovarian Cancer. *Front Oncol*, 8, 223.
- Johnson, E. L., Robinson, D. G. & Collier, H. A. 2017. Widespread changes in mRNA stability contribute to quiescence-specific gene expression patterns in a fibroblast model of quiescence. *BMC Genomics*, 18, 123.
- Jørgensen, S., Schotta, G. & Sørensen, C. S. 2013. Histone H4 lysine 20 methylation: key player in epigenetic regulation of genomic integrity. *Nucleic Acids Res*, 41, 2797-806.
- Kim, M. J., Cervantes, C., Jung, Y. S., Zhang, X., Zhang, J., Lee, S. H., Jun, S., Litovchick, L., Wang, W., Chen, J., Fang, B. & Park, J. I. 2021. PAF remodels the DREAM complex to bypass cell quiescence and promote lung tumorigenesis. *Mol Cell*, 81, 1698-1714.e6.
- Kschonsak, M., Merkel, F., Bisht, S., Metz, J., Rybin, V., Hassler, M. & Haering, C. H. 2017. Structural Basis for a Safety-Belt Mechanism That Anchors Condensin to Chromosomes. *Cell*, 171, 588-600.e24.
- Laporte, D., Courtout, F., Salin, B., Ceschin, J. & Sagot, I. 2013. An array of nuclear microtubules reorganizes the budding yeast nucleus during quiescence. *J Cell Biol*, 203, 585-94.
- Laporte, D., Courtout, F., Tollis, S. & Sagot, I. 2016. Quiescent *Saccharomyces cerevisiae* forms telomere hyperclusters at the nuclear membrane vicinity through a multifaceted mechanism involving Esc1, the Sir complex, and chromatin condensation. *Mol Biol Cell*, 27, 1875-84.

- Laporte, D. & Sagot, I. 2014. Microtubules move the nucleus to quiescence. *Nucleus*, 5, 113-8.
- Lee, J., Kang, S., Lilja, K. C., Colletier, K. J., Scheitz, C. J., Zhang, Y. V. & Tumber, T. 2016. Signalling couples hair follicle stem cell quiescence with reduced histone H3 K4/K9/K27me3 for proper tissue homeostasis. *Nat Commun*, 7, 11278.
- Leiserson, M. D., Vandin, F., Wu, H. T., Dobson, J. R., Eldridge, J. V., Thomas, J. L., Papoutsaki, A., Kim, Y., Niu, B., McLellan, M., Lawrence, M. S., Gonzalez-Perez, A., Tamborero, D., Cheng, Y., Ryslik, G. A., Lopez-Bigas, N., Getz, G., Ding, L. & Raphael, B. J. 2015. Pan-cancer network analysis identifies combinations of rare somatic mutations across pathways and protein complexes. *Nat Genet*, 47, 106-14.
- Litovchick, L., Florens, L. A., Swanson, S. K., Washburn, M. P. & Decaprio, J. A. 2011. DYRK1A protein kinase promotes quiescence and senescence through DREAM complex assembly. *Genes Dev*, 25, 801-13.
- Litovchick, L., Sadasivam, S., Florens, L., Zhu, X., Swanson, S. K., Velmurugan, S., Chen, R., Washburn, M. P., Liu, X. S. & Decaprio, J. A. 2007. Evolutionarily conserved multisubunit RBL2/p130 and E2F4 protein complex represses human cell cycle-dependent genes in quiescence. *Mol Cell*, 26, 539-51.
- Liu, H., Adler, A. S., Segal, E. & Chang, H. Y. 2007. A transcriptional program mediating entry into cellular quiescence. *PLoS Genet*, 3, e91.
- Liu, W., Tanasa, B., Tyurina, O. V., Zhou, T. Y., Gassmann, R., Liu, W. T., Ohgi, K. A., Benner, C., Garcia-Bassets, I., Aggarwal, A. K., Desai, A., Dorrestein, P. C., Glass, C. K. & Rosenfeld, M. G. 2010. PHF8 mediates histone H4 lysine 20 demethylation events involved in cell cycle progression. *Nature*, 466, 508-12.
- Lu, X., Simon, M. D., Chodaparambil, J. V., Hansen, J. C., Shokat, K. M. & Luger, K. 2008. The effect of H3K79 dimethylation and H4K20 trimethylation on nucleosome and chromatin structure. *Nat Struct Mol Biol*, 15, 1122-4.
- Maeshima, K. & Laemmli, U. K. 2003. A two-step scaffolding model for mitotic chromosome assembly. *Dev Cell*, 4, 467-80.
- Marguerat, S., Schmidt, A., Codlin, S., Chen, W., Aebersold, R. & Bähler, J. 2012. Quantitative analysis of fission yeast transcriptomes and proteomes in proliferating and quiescent cells. *Cell*, 151, 671-83.
- Marqués-Torrejón, M., Williams, C. a. C., Southgate, B., Alfazema, N., Clements, M. P., García-Díaz, C., Blin, C., Arranz-Emparan, N., Fraser, J., Gammoh, N., Parrinello, S. & Pollard, S. M. 2021. LRIG1 is a gatekeeper to exit from quiescence in adult neural stem cells. *Nat Commun*, 12, 2594.
- Mcknight, J. N., Boerma, J. W., Breeden, L. L. & Tsukiyama, T. 2015. Global Promoter Targeting of a Conserved Lysine Deacetylase for Transcriptional Shutoff during Quiescence Entry. *Mol Cell*, 59, 732-43.
- Mehta, I. S., Amira, M., Harvey, A. J. & Bridger, J. M. 2010. Rapid chromosome territory relocation by nuclear motor activity in response to serum removal in primary human fibroblasts. *Genome Biol*, 11, R5.
- Mitra, M., Ho, L. D. & Collier, H. A. 2018. An In Vitro Model of Cellular Quiescence in Primary Human Dermal Fibroblasts. *Methods Mol Biol*, 1686, 27-47.

- Mohrin, M., Bourke, E., Alexander, D., Warr, M. R., Barry-Holson, K., Le Beau, M. M., Morrison, C. G. & Passegué, E. 2010. Hematopoietic stem cell quiescence promotes error-prone DNA repair and mutagenesis. *Cell Stem Cell*, 7, 174-85.
- Müller, G. A. & Engeland, K. 2010. The central role of CDE/CHR promoter elements in the regulation of cell cycle-dependent gene transcription. *FEBS J*, 277, 877-93.
- Müller, G. A., Wintsche, A., Stangner, K., Prohaska, S. J., Stadler, P. F. & Engeland, K. 2014. The CHR site: definition and genome-wide identification of a cell cycle transcriptional element. *Nucleic Acids Res*, 42, 10331-50.
- Oda, H., Okamoto, I., Murphy, N., Chu, J., Price, S. M., Shen, M. M., Torres-Padilla, M. E., Heard, E. & Reinberg, D. 2009. Monomethylation of histone H4-lysine 20 is involved in chromosome structure and stability and is essential for mouse development. *Mol Cell Biol*, 29, 2278-95.
- Ono, T., Fang, Y., Spector, D. L. & Hirano, T. 2004. Spatial and temporal regulation of Condensins I and II in mitotic chromosome assembly in human cells. *Mol Biol Cell*, 15, 3296-308.
- Pack, L. R., Daigh, L. H. & Meyer, T. 2019. Putting the brakes on the cell cycle: mechanisms of cellular growth arrest. *Curr Opin Cell Biol*, 60, 106-113.
- Pesavento, J. J., Yang, H., Kelleher, N. L. & Mizzen, C. A. 2008. Certain and progressive methylation of histone H4 at lysine 20 during the cell cycle. *Mol Cell Biol*, 28, 468-86.
- Pietras, E. M., Warr, M. R. & Passegué, E. 2011. Cell cycle regulation in hematopoietic stem cells. *J Cell Biol*, 195, 709-20.
- Rawlings, J. S., Gatzka, M., Thomas, P. G. & Ihle, J. N. 2011. Chromatin condensation via the condensin II complex is required for peripheral T-cell quiescence. *EMBO J*, 30, 263-76.
- Ricard, N., Bailly, S., Guignabert, C. & Simons, M. 2021. The quiescent endothelium: signalling pathways regulating organ-specific endothelial normalcy. *Nat Rev Cardiol*, 18, 565-580.
- Roche, B., Arcangioli, B. & Martienssen, R. 2017. Transcriptional reprogramming in cellular quiescence. *RNA Biol*, 14, 843-853.
- Sadasivam, S. & Decaprio, J. A. 2013. The DREAM complex: master coordinator of cell cycle-dependent gene expression. *Nat Rev Cancer*, 13, 585-95.
- Shoaib, M., Walter, D., Gillespie, P. J., Izard, F., Fahrenkrog, B., Lleres, D., Lerdrup, M., Johansen, J. V., Hansen, K., Julien, E., Blow, J. J. & Sørensen, C. S. 2018. Histone H4K20 methylation mediated chromatin compaction threshold ensures genome integrity by limiting DNA replication licensing. *Nat Commun*, 9, 3704.
- Suh, E. J., Remillard, M. Y., Legesse-Miller, A., Johnson, E. L., Lemons, J. M., Chapman, T. R., Forman, J. J., Kojima, M., Silberman, E. S. & Coller, H. A. 2012. A microRNA network regulates proliferative timing and extracellular matrix synthesis during cellular quiescence in fibroblasts. *Genome Biol*, 13, R121.
- Swygert, S. G., Kim, S., Wu, X., Fu, T., Hsieh, T. H., Rando, O. J., Eisenman, R. N., Shendure, J., Mcknight, J. N. & Tsukiyama, T. 2019. Condensin-Dependent Chromatin Compaction Represses Transcription Globally during Quiescence. *Mol Cell*, 73, 533-546.e4.

- Swygert, S. G., Lin, D., Portillo-Ledesma, S., Lin, P. Y., Hunt, D. R., Kao, C. F., Schlick, T., Noble, W. S. & Tsukiyama, T. 2021. Local chromatin fiber folding represses transcription and loop extrusion in quiescent cells. *Elife*, 10.
- Terakawa, T., Bisht, S., Eeftens, J. M., Dekker, C., Haering, C. H. & Greene, E. C. 2017. The condensin complex is a mechanochemical motor that translocates along DNA. *Science*, 358, 672-676.
- Tokuyasu, K., Madden, S. C. & Zeldis, L. J. 1968. Fine structural alterations of interphase nuclei of lymphocytes stimulated to growth activity in vitro. *J Cell Biol*, 39, 630-60.
- Uhlmann, F. 2016. SMC complexes: from DNA to chromosomes. *Nat Rev Mol Cell Biol*, 17, 399-412.
- Vandiver, A. R., Idrizi, A., Rizzardi, L., Feinberg, A. P. & Hansen, K. D. 2015. DNA methylation is stable during replication and cell cycle arrest. *Sci Rep*, 5, 17911.
- Wade, R. H. 2009. On and around microtubules: an overview. *Mol Biotechnol*, 43, 177-91.
- Woodward, J., Taylor, G. C., Soares, D. C., Boyle, S., Sie, D., Read, D., Chathoth, K., Vukovic, M., Tarrats, N., Jamieson, D., Campbell, K. J., Blyth, K., Acosta, J. C., Ylstra, B., Arends, M. J., Kranc, K. R., Jackson, A. P., Bickmore, W. A. & Wood, A. J. 2016. Condensin II mutation causes T-cell lymphoma through tissue-specific genome instability. *Genes Dev*, 30, 2173-2186.
- Yao, G. 2014. Modelling mammalian cellular quiescence. *Interface Focus*, 4, 20130074.
- Young, C. P., Hillyer, C., Hokamp, K., Fitzpatrick, D. J., Konstantinov, N. K., Welty, J. S., Ness, S. A., Werner-Washburne, M., Fleming, A. B. & Osley, M. A. 2017. Distinct histone methylation and transcription profiles are established during the development of cellular quiescence in yeast. *BMC Genomics*, 18, 107.
- Yuen, K. C. & Gerton, J. L. 2018. Taking cohesin and condensin in context. *PLoS Genet*, 14, e1007118.
- Zink, D., Fischer, A. H. & Nickerson, J. A. 2004. Nuclear structure in cancer cells. *Nat Rev Cancer*, 4, 677-87.

## Appendix B

PDF of manuscript currently in the submission process.

**Dobbs OG**, Wilson RHC, Newling K, Ainscough JFX, Coverley D. Epigenetic instability caused by absence of CIZ1 drives transformation during quiescence cycles. 2022.

# Epigenetic instability caused by absence of CIZ1 drives transformation during quiescence cycles

Olivia G. Dobbs<sup>1,2</sup>, Rosemary H. C. Wilson<sup>1,3</sup>, Katherine Newling<sup>1,4</sup>, Justin F-X Ainscough<sup>1</sup>, Dawn Coverley<sup>1,2</sup>,

<sup>1</sup> Department of Biology, University of York, UK, YO10 5DD.

<sup>2</sup> York Biomedical Research Institute, University of York, York, UK.

<sup>3</sup> Exact Sciences Innovation, The Sherard Building, Oxford Science Park, Edmund Halley Rd, Oxford OX4 4DQ.

<sup>4</sup> Genomics and bioinformatics laboratory, Bioscience Technology Facility, University of York, UK, YO10 5DD.

Correspondence should be addressed to OGD.

Key words: Quiescence, CIZ1, Nuclear condensation, H4K20me1, Condensin complex, Epigenetic instability

Cip1-interacting zinc finger protein 1 (CIZ1) forms RNA-dependent protein assemblies that stabilise epigenetic state, notable at the inactive X chromosome in females. Here we show that male and female CIZ1-null primary murine fibroblasts have reduced H4K20me1 and that this compromises nuclear condensation on entry to quiescence. Global transcriptional repression remains intact in condensation-deficient CIZ1-null cells, however a subset of genes linked with chromatin condensation and homology-directed DNA repair are perturbed. Failure to condense is phenotypically mimicked by manipulation of the H4K20me1 methyltransferase, SET8, in WT cells and partially reverted in CIZ1-null cells upon re-expression of CIZ1. Crucially, during exit from quiescence nuclear decondensation remains active, so that repeated entry and exit cycles give rise to expanded nuclei susceptible to mechanical stress, DNA damage checkpoint activation, and downstream emergence of transformed proliferative colonies. Together, the data show that CIZ1's protection of the epigenome guards against genome instability during quiescence cycles.

**Introduction** Quiescence is a reversible, stress-resistant state in which cells experience global transcriptional changes, chromatin condensation and reduction in nuclear size. In the body, most cells are quiescent and can remain in this stabilised state for years. Some cell types undergo multiple rounds of entry to and exit from quiescence as they execute differentiation programs or adaptive responses. The reversibility of quiescence is essential for maintaining tissue homeostasis and well-studied in the contexts of tissue repair, immune response, and stem cell reactivation, while failure is implicated in tumorigenesis<sup>1</sup>. Cultured mammalian cells can be driven into reversible quiescence by established protocols that impose extrinsic cues to drive signalling, including contact inhibition and nutrient deprivation<sup>2</sup>. Both lead to global gene expression changes and reduce the proliferation rate of cells through repression of cell cycle genes via the DREAM complex<sup>3</sup>. In human fibroblasts, pathway-specific genes have been identified, as well as core quiescence genes, that are both independent of the specific quiescence trigger and vital to maintenance of a long-term quiescent state<sup>4,5</sup>.

Cip1-interacting zinc finger protein 1 (CIZ1) is a nuclear protein implicated in DNA replication<sup>6</sup>, cell cycle<sup>7,8</sup>, apoptosis<sup>9,10</sup>, transcriptional regulation<sup>11,12,13</sup>, and maintenance of repressive chromatin at the inactive X chromosome (Xi)<sup>14,15</sup>. It has been linked with human pathologies including paediatric<sup>16,17</sup> and common adult-onset cancers<sup>10,11,13,18-20</sup>, and with late onset neurological conditions<sup>21</sup> and Alzheimer's disease<sup>22</sup>, often as aberrant alternatively spliced variants<sup>23</sup>. A convincing mechanistic basis for the links with this diverse set of conditions is lacking, and there is no consensus on the underpinning defect or affected pathway. Analysis of the role of CIZ1 at the Xi in differentiated somatic cells identified a functional interaction with the long non-coding RNA (lncRNA) *Xist*, which drives localised formation of CIZ1:RNA assemblies in a manner dependent on its intrinsically disordered regions<sup>24</sup>. Time-resolved high-resolution imaging further suggests that CIZ1:RNA complexes are at the heart of the macromolecular assembly that drives formation of the Xi during early development<sup>25</sup>. Absence of CIZ1 assemblies in differentiated fibroblasts results in failure to enrich histone post-translational modifications (PTMs) that are characteristic of facultative heterochromatin which, along with *Xist* enrichment, can be reinstated upon expression of ectopic CIZ1<sup>24</sup>. Together, the data argue that CIZ1 assemblies may be part of a phase-separated molecular shield<sup>26</sup> that promotes or protects a subset of histone PTMs by influencing access to chromatin by modifying enzymes, with possible pleiotropic consequences. Although most of the biochemical evidence around CIZ1 function is derived from analysis at the Xi, its loss is felt at loci across the genome<sup>27</sup>, and smaller assemblies are distributed throughout the nucleus in male and female cells<sup>28</sup>.

Here, we report the striking observation that loss of CIZ1 combined with quiescence, is sufficient to drive formation of proliferative, phenotypically transformed cell lineages. Potential relevance to the earliest, pre-mutation stages of cancer aetiology, focussed our analysis on the immediate response of CIZ1-null cells to the quiescence triggers, rather than the downstream events or resulting lineages. We find that H4K20me1 is depleted in CIZ1-null cells and that this is sufficient to compromise chromatin condensation during quiescence entry and to give rise to a persistent checkpoint activated state from which new cell lineages emerge. Together the data describe a pathway from epigenetic instability to cellular transformation initiated by a single gene defect and identifies CIZ1 as a protector of the epigenome relevant to human disease.

## Results

**Nuclear condensation on entry to quiescence is dependent on CIZ1** Chromatin condensation and reduction of nuclear size on entry to quiescence is well-documented in *Saccharomyces cerevisiae*<sup>29,30</sup>, primary human fibroblasts<sup>31</sup> and thymocytes<sup>32</sup>. Here we compared the behaviour of WT murine primary embryonic fibroblasts (PEFs) with that of age-matched PEFs from mice lacking CIZ1 (CIZ1-null)<sup>14</sup>. In a cycling state, no significant difference in average nuclear area was evident (Fig.1A), however upon exposure to a trigger of quiescence entry (serum withdrawal, SW) and exit (serum add back, AB) WT and CIZ1-null populations behaved differently. For both, S phase index fell and recovered as expected (Fig.1B) but only WT cells exhibited a significant 25% decrease in nuclear area relative to parent populations (Fig.1C). A similar defect was evident in cells exiting cycle in response to contact inhibition (CI); at 100% confluency WT nuclear area decreased by 27% whereas CIZ1-null nuclei did not change (Fig.1D). Despite condensation failure CIZ1-null cells still decondensed their nuclei on cell cycle re-entry (AB), increasing in size by an average of 30% compared to their cycling state (Fig.1C), while WT nuclei returned to normal size. Considerable heterogeneity was evident in the CIZ1-null population, though even in the most enlarged nuclei DAPI-dense regions remained and the nuclear lamina was unperturbed (Fig.1E). Similar results were derived from independent primary cell isolates for each genotype (male and female), strongly implicating CIZ1 in the control or execution of nuclear condensation during quiescence. Strikingly,

repeated cycles of SW and AB leads to progressive nuclear expansion with CIZ1-null nuclei becoming approximately 60% larger than their parent population following 2 rounds (Fig.1F).

**Global gene expression changes on entry to quiescence are not dependent on CIZ1** We asked whether CIZ1 impacts the transcriptional program that normally takes place during quiescence entry<sup>4,5</sup>. We minimised the effects of pathway-specific signalling and increased focus on common downstream events by comparing changes in the transcriptome in response to two quiescence triggers (SW or CI), in three independently derived populations of PEFs from both WT and CIZ1-null female embryos (Fig.2A). For WT cells this generated a gene set that is broadly consistent with the core quiescence program identified previously in human foetal lung fibroblasts (SFig.1)<sup>4</sup>. We refer to these as murine core quiescence genes (mCQG).

In WT cells 4.1% and 4.4% of the genome significantly changed expression ( $-1 > \log_2 \text{foldchange} > 1$ ,  $q < 0.05$ ) following SW and CI, respectively. For CIZ1-null cells a similar response was recorded with 4.4% and 5.3% following SW and CI (Fig.2B, SFig.2). Full gene lists are given in SData sets 1 and 2.

mCQG sets generated by integration of quiescence triggers (Fig.2C) returned similar profiles in gene set enrichment analysis (GSEA)<sup>33</sup>, with the downregulated component for both WT and CIZ1-null cells returning by far the most significant and coherent overlap with Gene Ontology (GO) terms (Fig.2D). Unsurprisingly these relate to the cell cycle, indicating that CIZ1-null cells, like WT cells, remain capable of executing quiescence-linked gene expression programs. This argues that repression is not dependent on nuclear condensation in mammals, which does not align with ideas emerging from analysis in yeast where condensin-dependent chromatin compaction is a cause of transcriptional repression<sup>30</sup>.

Notably, slightly more genes increased than decreased (Fig.2B) which appears to contradict the widely held notion of global transcriptional repression, though it does support the proposition of quiescence as an actively regulated state<sup>1,34</sup>. However, when gene expression is expressed in absolute terms (Transcripts Per Million, TPM), it is evident that upregulated genes are typically lower in the cycling state than downregulated genes, which results in greater overall change in the down direction (Fig.2E). This is consistent with the established view of global transcriptional repression during quiescence.

**A subset of DREAM complex target genes are elevated in CIZ1-null cells** Even though CIZ1-null cells follow the same trend as WT cells, some genes behaved differently (Fig.2F). These are divided into four categories; those that fail to go up (F-UP) or down (F-DN) in CIZ1-null cells compared to WT cells, and those that go up or down inappropriately (I-UP, I-DN) in CIZ1-null cells (because they did not meet the threshold criteria in WT cells, SData Set 3). Interrogation of GSEA curated gene sets with the core set for each category (only genes common to both SW and CI, Fig.2G) showed that core I-DN genes (brown data points in Fig.2G and H) are the most coherent in biological role, with the top set being DREAM complex target genes<sup>3</sup>. The dimerization partner, RB-like, E2F and multi-vulval class B (DREAM) complex is best known for its role in quiescence where it is involved in repression of pro-proliferation genes. Looking at the 929 genes normally under the regulation of the DREAM complex (GSEA M149), we saw differences in the behaviour of a subset during quiescence entry (Fig.2I) with 33 of them represented in our core I-DN set. When classified by biological process, the most common GO terms returned by these high-confidence CIZ1-dependent I-DN DREAM target genes relate to DNA metabolism (repair, recombination, replication, and chromatin, STable1, Fig3A). TPM values revealed that all 33 follow a downward trend on entry to quiescence in both genotypes, but start higher (cycling state), and in many cases fall further (quiescent state) in CIZ1-null cells. The combined effect (magnitude of change) only meets the significance threshold in CIZ1-null cells (Fig.3B and SFig.3), and elevated expression in the cycling state appears to be the major contributory factor to their emergence through our filters. This led us to explore the cycling state, focussing on the GO terms that were most represented.

The high-level term 'chromatin organisation' slightly favours higher expression in CIZ1-null cells, and this trend is even more marked for the subordinate term 'chromosome condensation', but not for 'chromosome localisation'. Similarly, 'regulation of DNA double-strand break repair by homologous recombination' is slightly skewed while the similar size term 'mismatch repair' and their parent term 'DNA repair' are not (Fig.3C). This suggests that chromatin condensation and homology directed repair are both affected by loss of CIZ1, offering candidate processes underpinning the links between CIZ1 and disease. Here we have focused on chromatin condensation because of the clarity of the result.

**Compromised condensin binding in CIZ1-null cells** In eukaryotes the condensin complex exists in two forms, I and II. Both contain the core subunits SMC2 and SMC4, of which SMC4 is represented in our core I-DN set. Condensins have been associated with chromatin compaction during yeast and human quiescence<sup>4,30</sup>, and condensin II specifically implicated in a thymocyte model<sup>32</sup>. Strikingly, expression of *Smc2*, *Smc4* and the additional subunits *Ncaph*, *Ncapd2*, and *Ncapg* for condensin I, and *Ncaph2*, *Ncapd3*, and *Ncapg2* for condensin II are all skewed towards increased expression in CIZ1-null cycling cells compared to WT. Though the difference is not significant for any one component, the overall trend is significant (Fig.3D,E). In contrast, subunits of the closely related cohesin complex are less affected. Additionally, two similarly sized sets that represent the TOR complex involved in cell proliferation control<sup>35</sup>, and the CDC73 PAF1 complex involved in survival during long-term quiescence<sup>36</sup>, are not affected (Fig.3D). Thus, the observed deficit in nuclear condensation during entry to quiescence (Fig.1) correlates with *elevated* expression of the condensation machinery prior to receipt of quiescence triggers.

Elevated transcript could reflect compensation for compromised function, which led us to look at condensin proteins. SMC2 and SMC4 total protein levels were relatively unchanged (Fig.3F). However, we detected a reproducible decrease in the insoluble fraction of both proteins in CIZ1-null cells across four biological replicates, both in the cycling state and after serum withdrawal (Fig.3G). This suggests that their assembly on chromatin is influenced by CIZ1.

**Reduced H4K20me1 in CIZ1-null cells** Function of the condensin II complex has been linked to the methylation status of histone H4 lysine 20 (H4K20). Normally, dissociation of the demethylase PHF8 leads to emergence of H4K20me1 at mitosis and recruitment of NCAPD3 and NCAPG2<sup>37</sup>, while lack of the mono-methyltransferase SET8, results in mitotic chromosome condensation failure<sup>38</sup>. As well as mitosis, H4K20 methylation has been implicated in quiescence-linked condensation through loss of Suv4-20h2<sup>31</sup>.

Our previous analysis of CIZ1 at the Xi revealed CIZ1-dependent maintenance of H3K27me3 and H2AK119Ub1<sup>27</sup>. As H4K20me1 is also known to be enriched at the Xi and suggested to play a role in its compaction (though not its repression)<sup>39</sup>, we evaluated H4K20me1 in CIZ1-null cells (Fig.4A). This showed a dramatic reduction in frequency of H4K20me1-enriched Xi's in female CIZ1-null cycling populations (3%) compared to WT (35%) and aligns with results for both CIZ1 itself and H3K27me3 (Fig.4B), and with previous analysis of H2AK119Ub1<sup>27</sup>. Notably different is the behaviour of H4K20me1 upon SW. While CIZ1 and H3K27me3 remained high in WT cells, the frequency of H4K20me1-enriched Xi's fell to 14% after 1 hour (short SW) and 3% by 24 hours (long SW). Therefore, H4K20me1 enrichment at the Xi is normally modulated during entry to quiescence (Fig.4A,B) and is coincident with nuclear condensation (Fig.4C). Both SW-induced loss of H4K20me1 in WT cells and overall suppression in CIZ1-null cells, is evident globally in western blot analysis. This is marked in female cells (Fig.4D) but moderate in male cells which do not contain Xi-associated enriched zones (SFig.4A). H4K20me1 depletion was further confirmed in male cells by immunofluorescence (SFig.4B). Depletion of both Xi-enriched and nucleus-wide H4K20me1 confirms that the establishment or maintenance of H4K20me1 is dependent on CIZ1, and that this defect exists before exposure to quiescence stimuli.

To confirm the link between CIZ1 assemblies and accumulation of H4K20me1 at the Xi, we rescued the phenotype in CIZ1-null cells by induced expression of ectopic GFP-CIZ1 from an integrated vector (Fig.4E)<sup>14</sup>. All nuclei express GFP-CIZ1, but only a subset form new discrete assemblies within 48 hours (18% in the population analysed here). For these cells, 26% show enrichment of H4K20me1, compared to only 2% in nuclei with no CIZ1 assemblies (Fig.4E). This aligns with previous results which showed coincident accumulation of H3K27me3, H2AK119Ub1 and *Xist* with new CIZ1 assemblies<sup>27</sup>. Ectopic GFP-CIZ1 also increased the mean nuclear intensity of H4K20me1, and importantly supported partial reversion of the condensation defect after SW (Fig.4F), reinforcing the link between CIZ1 and condensation during entry to quiescence.

**Inhibition of SET8 is sufficient to compromise nuclear condensation in quiescence** CIZ1 stabilises multiple PTMs which have the potential to cause pleiotropic effects. Therefore, we tested whether depletion of H4K20 methylation alone can mimic the CIZ1-null condensation defect in WT cells. The substrate competitive inhibitor UNC0379 selectively inhibits SET8<sup>40</sup> and was effective at reducing the frequency of H4K20me1-enriched Xi's and nucleus-wide H4K20me1 levels in WT PEFs during a two-hour incubation, with no effect on H3K27me3, S phase index (Fig.4G), or nuclear size in cycling populations (Fig.4H, SFig.4C). However, following a short SW condensation was impaired in UNC0379-treated WT nuclei (Fig.4H, SFig.4C), which implicates depletion of H4K20me1 as the defect underlying failure to condense.

**Epigenetic instability to nuclear vulnerability and spontaneous transformation** To explore the impact of defective H4K20me1-dependent condensation and inappropriate decondensation we compared the properties of nuclei at SW and AB. Susceptibility to shear forces induced by passage through a fine needle<sup>41</sup> was increased in CIZ1-null nuclei upon AB (Fig.5A,B), correlating nuclear expansion with nuclear fragility. This suggests that CIZ1-null cells undergoing quiescence cycles in the body might be vulnerable to mechanical stress. However, even without mechanical stress, increased phosphorylation of ataxia telangiectasia mutated (pATM) indicates that cell cycle checkpoints are significantly more activated in CIZ1-null PEFs specifically upon AB (Fig.5C), and so raises the possibility of DNA damage. A similar response was seen following CI using a standardised long-term maintenance protocol in which media is replenished every three to four days (natural SW by depletion). Under these conditions checkpoint activation (pATM) was evident within the first week, while phosphorylated checkpoint kinase 1 (pCHK1) and phosphorylated histone H2AX ( $\gamma$ H2AX) emerged later. For all markers there was no difference between the two genotypes at the start of the time course (cycling), but all became progressively activated, reaching 60-90% of the CIZ1-null population (Fig.5D). This suggests that CIZ1-null cells are either impaired in their ability to resolve DNA damage or associated signalling, or that they experience repeated assault.

By the end of the 21-day CI time course, proliferating colonies emerged from checkpoint activated CIZ1-null monolayers (at a rate of approximately 1 per 5,000-10,000 cells plated), while WT cells established a stable monolayer (Fig.5E). This was replicated in independent isolates of both PEFs and dermal fibroblasts from tail tips (TTF's). Cell proliferation is evidenced by incorporation of the nucleotide analogue EdU into approximately 15% of colony cells, but not the surrounding monolayer (Fig.5F). Checkpoint activation ( $\gamma$ H2AX) remained evident, and colony cells exhibited features characteristic of transformed cells, encroaching on surrounding monolayers (SFig.4D,E). A spontaneously immortalised TTF line also presented with substantially enlarged nuclei compared to parent cells (SFig.4F). These data show that the epigenetic vulnerability caused by CIZ1 deletion is sufficient to create vulnerable nuclei, and to drive quiescence escape (Fig.5G).

**Discussion** We have identified a requirement for CIZ1 during the formation of a quiescent nucleus and outlined a potentially catastrophic series of events that take place in its absence. Previous biochemical analysis showed that CIZ1-*Xist* assemblies modulate H3K27me3 and H2AK119Ub1 at the Xi<sup>24,27</sup>, extended here to include H4K20me1. Thus, CIZ1 is emerging as a protector of the epigenetic landscape, with likely pleiotropic and context-specific effects. One of these, nuclear condensation failure, is the consequence of H4K20me1 depletion and manifests during quiescence entry.

However, the data suggest that it is subsequent inappropriate decondensation on re-entry to cycle that is most damaging as it is accompanied by nuclear fragility and sustained activation of the DNA damage response. Crucially, this precedes the emergence of phenotypically transformed lineages, suggesting that the epigenetic instability experienced in the absence of CIZ1 could be a driver of genome instability, and possibly therefore an early (pre-mutation) driver of cancer initiation. In fact, aberrant nuclear architecture is a long-established feature of cancer cells, with diagnosis of some cancers historically based on increases in nuclear size or the condensation state of chromatin<sup>42</sup>. This implicates condensin function, though is also linked with changes in ploidy. In our protocols oversized nuclei can be generated in short-term experiments, with cycles of SW and AB that fall far short of a replication cycle (one hour) and are therefore not primarily driven by changes in ploidy. Thus, we propose that nuclear expansion may be an early event, that precedes genetic and ploidy change in some cancers.

Aberrant condensin expression and mutations in condensin II have been reported in colorectal and pancreatic cancers<sup>43-45</sup> and linked with chromosome instability and disease progression. In murine models, mutations in condensin II subunits cause defects in T cell development, failure to condense and development of T-cell lymphoma<sup>32,46</sup>. This parallels the abnormal quiescence of CIZ1-null fibroblasts in this study, and the pathology of CIZ1-null mice. Leukemias<sup>47</sup> and high penetrance lymphomas<sup>14</sup> are evident in adult mice bearing exon 5 deletion or gene trap insertion into intron 1, respectively. Notably, both cell types originate in progenitors whose maintenance requires quiescence entry and exit cycles<sup>48</sup>. This aligns with the idea that a defect in CIZ1 could underpin the emergence of unstable lineages in cell types that undergo quiescence cycles as part of their normal biology.

The balance between histone modifiers that add and remove PTMs and determine the methylation dynamics of H4K20me1 are also implicated in cancer; SET8 with hepatocellular carcinoma<sup>49</sup> and PHF8 with colorectal cancer<sup>50</sup>. Therefore, their inhibition may offer a route to intervention. This idea is supported by high-frequency point mutations in histone genes in several

tumours, notably paediatric cancers<sup>51,52</sup>. However, before exploitation of such findings it will be necessary to understand the downstream cellular events that are compromised, and crucially when in the aetiology of cancer, they give rise to irreversible genetic change. Here, we have uncovered one such consequence, and identified quiescence entry and exit as a vulnerable cellular transition.

Our data does not show that CIZ1-null cells experience DNA damage prior to phenotypic transformation. However, it does show persistent activation of the checkpoint kinases that arrest the cell cycle in response to DNA damage. In pre-malignancies, chronic checkpoint activation is a well-established concept that offers a selection pressure in favour of checkpoint escape, and the subsequent emergence of unprotected hypermutable cells<sup>53,54</sup>. Thus, quiescence cycles are emerging as a point of vulnerability, and possible intrinsic driver of transformation.

Understanding the immediate trigger of checkpoint activation is not straightforward. It could be a direct response to aberrant condensation<sup>55</sup> possibly detected at decondensation. However, it seems more likely that it is initiated by DNA damage resulting from hyper-decondensation. We also cannot rule out other CIZ1-dependent chromatin deficiencies that directly compromise DNA repair. CIZ1-null cycling cells are sensitive to replication stress induced by hydroxyurea, suggesting a defect in the resolution of DNA breaks unconnected to quiescence<sup>47</sup>, however these CIZ1-null cells could have already experienced quiescence cycles and developed susceptible nuclei. Similarly, a separate study reported sensitivity to  $\gamma$ -irradiation in fibroblasts and increased DNA breaks in brain tissue, linking the deficit to impaired motor and cognitive functioning in mice<sup>21</sup>. Here again, the source of the DNA breaks is not known and could have arisen from a condensation defect. Finally, our transcriptomic study detected elevated expression of regulators and executors of homology-directed DNA double-strand break repair, which could reflect either compromised functionality, or heavy burden of damage.

Whether compromised CIZ1 assemblies and the associated epigenetic instability is ever a primary cause for transformation outside of genetically manipulated murine models remains to be seen. However, the data described here outline a pathway which, through aberrant quiescence cycles, translates epigenetic instability to cellular transformation, and so identifies CIZ1 as a guardian of the epigenome with implications for human disease.

**Acknowledgments** This work was supported by BBSRC doctoral training grants to OD (BB/M011151/1) and RW (BB/F016751/1), and by MR/R008981/1. We are grateful to Jonathan Godwin and Louisa Williamson for support with cell isolation, to Sally James for library preparation and Emma Stewart for transcriptomic analysis support.

## Materials and Methods

**Cells and cell culture** CIZ1-null mice were generated as described<sup>14</sup> from C57BL/6 ES clone IST13830B6 (TIGM) harbouring a neomycin resistance gene trap inserted into intron 1. Murine primary embryonic fibroblasts (PEFs) were derived from individual embryos at day 13-14 of gestation, and murine tail-tip fibroblasts (TTFs) at 3-4 weeks (Supplemental Table 2). Both were maintained in Dulbecco's Modified Eagle Medium (DMEM), GlutaMAX, high glucose (4.5g/l) and low glucose (1g/l) (Gibco), respectively, and grown on Nunc™ Cell Culture Dishes (ThermoFisher Scientific, 150350) with 0.13-0.16mm thick glass coverslips. Media was supplemented with 10% FBS (PAA) and 1% Pen/Strep/Glutamine (PSG, Gibco) referred to here as high-serum media. Cells were maintained in a rapidly cycling state at 37°C with 5% CO<sub>2</sub> and split to avoid cell contact. All cell populations were used at passage 2-4. For inducible cells harbouring transactivator and responder transgenes, addition of doxycycline (dox) to media (5-10 µg/ml) was used to induce GFP-CIZ1 over 48 hours.

**Ethics** All work with animal models is compliant with UK ethical regulations. Breeding and genetic modification of mice was carried out under UK Home Office license, and with approval of the Animal Welfare and Ethical Review Body at the host institution. Analysis on cells and tissues derived from these mice was carried out with approval of the Animal Welfare and Ethical Review Body at the University of York.

**Quiescence** For quiescence by serum withdrawal, cells were plated at 70-80% confluency in high-serum media. After 24 hours, media was removed, cells washed in warmed PBS, and low-serum media added (DMEM, 0.01% FBS and 1% PSG)<sup>2</sup> for either a short (up to two hours) or a long (24 hours) serum withdrawal. To achieve contact inhibition, fibroblasts were plated at 70-80% confluency and cultured to 100% confluency (typically 3 days). At the point of 100% confluency, media was changed (fresh, high-serum media) and cells were incubated for a further four days (quiescent). For foci formation, quiescent cells were maintained for a further 2 weeks with high-serum media changed twice a week.

**Detection of foci formation** Plates with adherent cells were washed twice in room temperature (RT) PBS (Dulbecco's Phosphate Buffered Saline, 14190-094), followed by fixation with 4% paraformaldehyde (PFA) for 20 minutes, then stained with 0.05% filtered crystal violet for 30 minutes, and washed to reveal stained foci. Analysis was in triplicate, imaged using bright-field microscopy, and foci scored manually and expressed as a function of cells plated.

**Inhibitors** UNC0379 (Sigma, sml1465) a selective, substrate competitive inhibitor of SET8 (IC<sub>50</sub> of 7.3 µM<sup>40</sup>), was used at 10µM for two hours (in high-serum media for cycling cells or low-serum media for cells subject to serum withdrawal).

**S phase labelling** Adherent cells on coverslips were incubated with 5-ethynyl-2'-deoxyuridine (EdU, 10µM) for a 30-minute pulse period, or extended time periods where indicated, under standard growth conditions. To visualize newly synthesized DNA, coverslips were washed briefly in cytoskeletal buffer (CSK; 10mM PIPES/KOH pH 6.8, 100mM NaCl, 300mM sucrose, 1mM EGTA, 1mM MgCl<sub>2</sub>, 1mM DTT, 1 cOmplete™ Protease Inhibitor Cocktail per 50ml) with 0.1% Triton-X-100 before fixation with 4% paraformaldehyde (PFA) for 15 minutes. Coverslips were then washed in PBS and EdU detected using the Click-iT® EdU Alexa Fluor® 555 kit (ThermoFisher), as recommended. Briefly, coverslips were blocked with BSA Antibody buffer (0.02% SDS, 0.1% TX100, 10 mg/ml nuclease-free BSA in PBS) before incubation in a light-proof humidified chamber with Click-iT® reaction cocktail for 60 minutes. Coverslips were then washed and mounted using VectaShield with DAPI (Vector Labs).

**Immunofluorescence** Adherent cells grown on glass coverslips were subjected to a 1-minute detergent wash (0.1% Triton-X-100 in PBS) and then fixed for 15 minutes in 4% PFA. After fixation, cells were rinsed twice with RT PBS then incubated for 30 minutes in BSA antibody buffer. Coverslips were incubated for 1-2 hours at 37 °C with primary antibody (in BSA antibody buffer), followed by three washes in BSA antibody buffer before incubating with anti-species secondary antibodies (Alexa Fluor 488 or 568) for one hour. Cells were washed a further three times in BSA antibody buffer prior to mounting in VectaShield with DAPI (Vector labs, H-1200). For DNA damage response antibodies (pATM, pH2AX, pChk1), PBS was substituted by TBS in all buffers. Antibodies are listed in Supplementary Table 3.

**Imaging and image analysis** Fluorescence was captured using a Zeiss Axiovert 200M fitted with a 63X/1.40 Plan-Apochromat objective and Zeiss filter sets 2, 10, 15 (G365 FT395 LP420, BP450-490 FT510 BP515-565, BP546/12 FT580 LP590), using Axiocam 506 mono and Axiovision image acquisition software (SE64 release 4.9.1). For images where intensity differences are quantified, all samples were analysed as a set, with constant image acquisition parameters, and no image manipulation. For presentation purposes images were enhanced using Fiji V1.0<sup>56</sup>, and where intensity differences are being illustrated, all images in the set were manipulated identically. All quantification was conducted on unedited images.

For measurements of nuclear area typically 30-50 cells from each population were analysed using Fiji V1.0<sup>56</sup>. Channels were split to show blue, green and red output separately, and thresholds for nuclear area identified using the Otsu setting in the blue (DAPI) channel. Thresholds were converted to masks and all particles within size 0.01-Infinity analysed and returned as area in pixels. Conversion to area in  $\mu\text{m}^2$ , then to volume was calculated based on the 10 $\mu\text{m}$  scale bar and assumes a spherical nucleus. Where intensity measures for other channels were required, the DAPI mask was overlaid onto the relevant image and pixel density within the mask returned as maximum, minimum or mean density in the selected area.

**Sub-cellular fractionation and analysis by western blot** Adherent cells were scrape harvested following two cold washes in PBS supplemented with 2mM PMSF, then either denatured by heating to 90°C in SDS-PAGE sample buffer (2% SDS, 15% glycerol, 1.7% betamercaptoethanol, 75mM Tris pH 6.8 with bromophenol blue) to generate whole cell lysate or supplemented to 0.1% Triton-X-100. After incubation for 3-5 minutes on ice, samples were centrifuged for 2 minutes at 5000rpm, to generate a pellet fraction (insoluble material including chromatin). Fractions were denatured in SDS-PAGE sample buffer for subsequent analysis by western blot after separation through a 4-15% gradient gel (BioRad) and transfer to nitrocellulose membrane using iBlot gel transfer stacks (Invitrogen) or a semi-dry transfer. Membranes were blocked with 5% BSA or 10% milk, in PBS with 0.1% Tween20, for 30 minutes before primary antibody incubation for 2 hours at RT or overnight at 4 °C depending on antibody, with gentle agitation. Blots were washed three times with blocking buffer then probed with HRP-conjugated anti-species secondary antibody (Jackson Immunochemicals 115-035-174 and 211-032-171) for 1 hour at RT and imaged using EZ-ECL (Biological Industries) and Syngene PXi chemiluminescence imaging system. Image quantification was performed on unedited images with background subtracted and normalised to histone for loading.

**Nuclear fragility** Method was adapted from Furusawa, T. *et al*<sup>41</sup>. Adherent cells were harvested by trypsinisation then pelleted at 2000rpm and resuspended in 200 $\mu\text{l}$  PBS/Hoechst (1:1000). Before subjecting cells to mechanical shear, a reference sample (0 passes) was taken and fixed in 4% PFA to generate a measure of cell count and integrity. Using a 1ml syringe, the remaining cell suspension was passed through a 25G needle 40 times, then fixed. Equal volumes of treated and untreated fixed cells were concentrated onto microscope slides using a cytospin and mounted in Vectashield (Vector Labs, H-1000). The number of intact stained nuclei in 2-7 fields per independent experiment were counted, averaged and expressed relative to control.

**Graphical presentation and statistical analysis** Experiments were designed to use the minimum number of animals (independently derived PEF or TTF populations) while achieving statistically valid data, with N representing the number of independent experiments. Unless stated otherwise for nuclear area measurements, 30-50 cells from three independent coverslips were analysed at the indicated treatment times. For scoring histone PTMs, or protein at the Xi, each replicate is an average of 3 independent counts or measurements per coverslip (30-50 cells each), with the average of all replicates shown. Unless stated otherwise, values represent the means  $\pm$  SEM. Asterisks indicate statistical significance (ns not significant, \*p < 0.05; \*\*p < 0.01; \*\*\*p < 0.001). Statistical analysis was carried out in GraphPad Prism using a two-tailed Student's t test, one-way ANOVA or two-way ANOVA. Significance for expression level differences between WT and CIZ1-null cycling cells for subunits of the condensin complex, cohesin complex, TOR complex and CDC73 PAF1 complex were calculated using the Wilcoxon signed rank test. Graphs were generated using GraphPad Prism Version 9.1.0 (216) or Microsoft Excel and, where indicated, measurements normalised to the relevant internal control.

**Transcriptome analysis** Primary (before passage 4) murine embryonic fibroblasts 13.1, 13.8 and 14.4 (female WT PEFs) and 13.15, 13.17 and 14.2 (female CIZ1-null PEFs) were grown to 80% confluency. For each cell line, RNA was extracted with TRIzol (Ambion, 15596-026), from cycling

cells, 24 hours following serum withdrawal (SW), or 4 days after 100% confluency (CI). Briefly, adherent cells were washed twice with PBS, drained on a shallow angle for 2 minutes and excess PBS removed. 1mL of TRIzol was added per 28cm<sup>2</sup> and incubated for 3-5 minutes at RT with periodic agitation. Lysates were collected in clean Eppendorf tubes. Chloroform was added to lysates at a ratio of 1:5 and lysates were shaken vigorously for 15 seconds before incubation at RT for 3 minutes before centrifugation at 12,000g for 15 minutes. The aqueous phase was transferred into a clean Eppendorf and mixed with equal volume of isopropanol through gentle inversion and incubated at RT for 10 minutes followed by a 10-minute centrifugation at 12,000g. Supernatant was removed, and the RNA pellet washed with an equal volume of 75% ethanol to the volume of TRIzol used. Sample was centrifuged for 5 minutes at 12,000g and the supernatant removed. RNA pellet was allowed to dry for 30 seconds before resuspension in nuclease-free water. Isolated RNA was then treated with DNase (Roche, 04716728001), and purified (RNA Clean & Concentrator-5 kit, R1015, Zymo Research), before quality analysis by agarose gel, NanoDrop spectrophotometer and Agilent 2100 Bioanalyzer. Libraries were prepared with NEBNext® Ultra™ RNA library Prep Kit for Illumina®, and enriched for mRNA using NEBNext Poly(A) mRNA Magnetic Isolation Module, which is optimized for production of libraries with 250-400bp inserts. Enriched mRNA was fragmented by heating to 95°C for 12 minutes, cDNA synthesised from random primers, followed by end repair, dA-tailing, adaptor ligation and PCR enrichment. Libraries were sequenced at the Leeds Institute for Molecular Medicine (LIMM) using Illumina 3000 system, using paired-end sequencing to generate ~50 million reads per sample. Sequence reads were trimmed to remove any adapter sequences using Cutadapt version 1.8.3<sup>57</sup> then aligned to version GRCm38 of the mouse genome using HISAT2<sup>58</sup>. Transcriptomes were assembled and gene expression quantified using the Tuxedo pipeline (version 2.2.1)<sup>59</sup>. Cufflinks was used to assemble transcriptomes for each sample using the GTF annotation file for the GRCm38 mouse genome (*C57BL/6*), followed by Cuffmerge to merge individual sample transcriptomes. Quantification, normalisation and differential expression was carried out using Cuffquant, Cuffnorm, and Cuffdiff, respectively. False discovery rate (FDR) was controlled using the Benjamini-Hochberg method in the StatsModels library (v.0.8.0), to generate q-values. Genes are stated to differ in expression level when the average log<sub>2</sub>(fold change) between two states, passes the significance threshold, FDR q<0.05, and is either above 1 or below -1. Thresholds are illustrated in the volcano plots in SFig.2. Volcano plots were generated in Excel. Heat maps were generated using Spyder (v.4.1.4), accessed via Anaconda Navigator (v.1.9.12), using the pandas, seaborn and matplotlib modules. Transcription units which did not have a numerical value for log<sub>2</sub>(fold change), due to mean expression of 0 in one condition, were manually removed before generating the plots. Individual transcripts per million (TPM) were extracted for biological replicates (independent PEF lines) enabling calculation of means and SEM, and comparison between genotypes. Gene Set Enrichment Analysis<sup>33</sup> was performed in Python 3.6 using one-sided Fisher's Exact tests as part of the SciPy library (v.0.19.0).

## References

1. Cho, I.J. *et al.* Mechanisms, Hallmarks, and Implications of Stem Cell Quiescence. *Stem Cell Reports* **12**, 1190-1200 (2019).
2. Mitra, M., Ho, L.D. & Collier, H.A. An In Vitro Model of Cellular Quiescence in Primary Human Dermal Fibroblasts. *Methods Mol Biol* **1686**, 27-47 (2018).
3. Fischer, M., Grossmann, P., Padi, M. & DeCaprio, J.A. Integration of TP53, DREAM, MMB-FOXM1 and RB-E2F target gene analyses identifies cell cycle gene regulatory networks. *Nucleic Acids Res* **44**, 6070-6086 (2016).
4. Collier, H.A., Sang, L. & Roberts, J.M. A new description of cellular quiescence. *PLoS Biol* **4**, e83 (2006).
5. Liu, H., Adler, A.S., Segal, E. & Chang, H.Y. A transcriptional program mediating entry into cellular quiescence. *PLoS Genet* **3**, e91 (2007).
6. Coverley, D., Marr, J. & Ainscough, J. Ciz1 promotes mammalian DNA replication. *J Cell Sci* **118**, 101-112 (2005).
7. Copeland, N.A., Sercombe, H.E., Wilson, R.H. & Coverley, D. Cyclin-A-CDK2-mediated phosphorylation of CIZ1 blocks replisome formation and initiation of mammalian DNA replication. *J Cell Sci* **128**, 1518-1527 (2015).
8. Mitsui, K., Matsumoto, A., Ohtsuka, S., Ohtsubo, M. & Yoshimura, A. Cloning and characterization of a novel p21(Cip1/Waf1)-interacting zinc finger protein, ciz1. *Biochem Biophys Res Commun* **264**, 457-464 (1999).
9. Sun, G., Ding, X.A., Argaw, Y., Guo, X. & Montell, D.J. Akt1 and dCIZ1 promote cell survival from apoptotic caspase activation during regeneration and oncogenic overgrowth. *Nat Commun* **11**, 5726 (2020).
10. Chen, X. *et al.* CIZ1 knockdown suppresses the proliferation of bladder cancer cells by inducing apoptosis. *Gene* **719**, 143946 (2019).
11. den Hollander, P., Rayala, S.K., Coverley, D. & Kumar, R. Ciz1, a Novel DNA-binding coactivator of the estrogen receptor alpha, confers hypersensitivity to estrogen action. *Cancer Res* **66**, 11021-11029 (2006).
12. Thacker, U. *et al.* Identification of DHX9 as a cell cycle regulated nucleolar recruitment factor for CIZ1. *Sci Rep* **10**, 18103 (2020).
13. Lei, L., Wu, J., Gu, D., Liu, H. & Wang, S. CIZ1 interacts with YAP and activates its transcriptional activity in hepatocellular carcinoma cells. *Tumour Biol* (2016).
14. Ridings-Figueroa, R. *et al.* The nuclear matrix protein CIZ1 facilitates localization of Xist RNA to the inactive X-chromosome territory. *Genes Dev* **31**, 876-888 (2017).
15. Sunwoo, H., Colognori, D., Froberg, J.E., Jeon, Y. & Lee, J.T. Repeat E anchors Xist RNA to the inactive X chromosomal compartment through CDKN1A-interacting protein (CIZ1). *Proc Natl Acad Sci U S A* **114**, 10654-10659 (2017).
16. Rahman, F., Ainscough, J.F., Copeland, N. & Coverley, D. Cancer-associated missplicing of exon 4 influences the subnuclear distribution of the DNA replication factor CIZ1. *Hum Mutat* **28**, 993-1004 (2007).
17. Warder, D.E. & Keherly, M.J. Ciz1, Cip1 interacting zinc finger protein 1 binds the consensus DNA sequence ARYSR(0-2)YYAC. *J Biomed Sci* **10**, 406-417 (2003).
18. Higgins, G. *et al.* Variant Ciz1 is a circulating biomarker for early-stage lung cancer. *Proc Natl Acad Sci U S A* **109**, E3128-3135 (2012).
19. Liu, T. *et al.* Ciz1 promotes tumorigenicity of prostate carcinoma cells. *Front Biosci (Landmark Ed)* **20**, 705-715 (2015).
20. Swarts, D.R.A., Stewart, E.R., Higgins, G.S. & Coverley, D. CIZ1-F, an alternatively spliced variant of the DNA replication protein CIZ1 with distinct expression and localisation, is overrepresented in early stage common solid tumours. *Cell Cycle*, 1-16 (2018).
21. Khan, M.M., Xiao, J., Patel, D. & LeDoux, M.S. DNA damage and neurodegenerative phenotypes in aged Ciz1 null mice. *Neurobiol Aging* **62**, 180-190 (2018).
22. Dahmcke, C.M., Buchmann-Moller, S., Jensen, N.A. & Mitchelmore, C. Altered splicing in exon 8 of the DNA replication factor CIZ1 affects subnuclear distribution and is associated with Alzheimer's disease. *Mol Cell Neurosci* **38**, 589-594 (2008).
23. Rahman, F.A., Aziz, N. & Coverley, D. Differential detection of alternatively spliced variants of Ciz1 in normal and cancer cells using a custom exon-junction microarray. *BMC Cancer* **10**, 482 (2010).
24. Sofi, S. *et al.* Prion-like domains drive CIZ1 assembly formation at the inactive X chromosome. *J Cell Biol* **221** (2022).

25. Markaki, Y. *et al.* Xist nucleates local protein gradients to propagate silencing across the X chromosome. *Cell* **184**, 6174-6192.e6132 (2021).
26. Mészáros, B. *et al.* PhaSePro: the database of proteins driving liquid-liquid phase separation. *Nucleic Acids Res* **48**, D360-D367 (2020).
27. Stewart, E.R. *et al.* Maintenance of epigenetic landscape requires CIZ1 and is corrupted in differentiated fibroblasts in long-term culture. *Nat Commun* **10**, 460 (2019).
28. Ainscough, J.F. *et al.* C-terminal domains deliver the DNA replication factor Ciz1 to the nuclear matrix. *Journal of Cell Science* **120**, 115-124 (2007).
29. Laporte, D., Courtout, F., Tollis, S. & Sagot, I. Quiescent *Saccharomyces cerevisiae* forms telomere hyperclusters at the nuclear membrane vicinity through a multifaceted mechanism involving Esc1, the Sir complex, and chromatin condensation. *Mol Biol Cell* **27**, 1875-1884 (2016).
30. Swygert, S.G. *et al.* Condensin-Dependent Chromatin Compaction Represses Transcription Globally during Quiescence. *Mol Cell* **73**, 533-546 e534 (2019).
31. Evertts, A.G. *et al.* H4K20 methylation regulates quiescence and chromatin compaction. *Mol Biol Cell* **24**, 3025-3037 (2013).
32. Rawlings, J.S., Gatzka, M., Thomas, P.G. & Ihle, J.N. Chromatin condensation via the condensin II complex is required for peripheral T-cell quiescence. *EMBO J* **30**, 263-276 (2011).
33. Subramanian, A. *et al.* Gene set enrichment analysis: a knowledge-based approach for interpreting genome-wide expression profiles. *Proc Natl Acad Sci U S A* **102**, 15545-15550 (2005).
34. Cheung, T.H. & Rando, T.A. Molecular regulation of stem cell quiescence. *Nat Rev Mol Cell Biol* **14**, 329-340 (2013).
35. Loewith, R. & Hall, M.N. Target of rapamycin (TOR) in nutrient signaling and growth control. *Genetics* **189**, 1177-1201 (2011).
36. Oya, E. *et al.* Leo1 is essential for the dynamic regulation of heterochromatin and gene expression during cellular quiescence. *Epigenetics Chromatin* **12**, 45 (2019).
37. Liu, W. *et al.* PHF8 mediates histone H4 lysine 20 demethylation events involved in cell cycle progression. *Nature* **466**, 508-512 (2010).
38. Houston, S.I. *et al.* Catalytic function of the PR-Set7 histone H4 lysine 20 monomethyltransferase is essential for mitotic entry and genomic stability. *J Biol Chem* **283**, 19478-19488 (2008).
39. Tjalsma, S.J.D. *et al.* H4K20me1 and H3K27me3 are concurrently loaded onto the inactive X chromosome but dispensable for inducing gene silencing. *EMBO Rep* **22**, e51989 (2021).
40. Ma, A. *et al.* Discovery of a selective, substrate-competitive inhibitor of the lysine methyltransferase SETD8. *J Med Chem* **57**, 6822-6833 (2014).
41. Furusawa, T. *et al.* Chromatin decompaction by the nucleosomal binding protein HMGN5 impairs nuclear sturdiness. *Nat Commun* **6**, 6138 (2015).
42. Fischer, E.G. Nuclear Morphology and the Biology of Cancer Cells. *Acta Cytol* **64**, 511-519 (2020).
43. Weyburne, E. & Bosco, G. Cancer-associated mutations in the condensin II subunit CAPH2 cause genomic instability through telomere dysfunction and anaphase chromosome bridges. *J Cell Physiol* **236**, 3579-3598 (2021).
44. Baergen, A.K., Jeusset, L.M., Lichtensztejn, Z. & McManus, K.J. Diminished Condensin Gene Expression Drives Chromosome Instability That May Contribute to Colorectal Cancer Pathogenesis. *Cancers (Basel)* **11** (2019).
45. Kim, J.H., Youn, Y., Kim, K.T., Jang, G. & Hwang, J.H. Non-SMC condensin I complex subunit H mediates mature chromosome condensation and DNA damage in pancreatic cancer cells. *Sci Rep* **9**, 17889 (2019).
46. Gosling, K.M. *et al.* A mutation in a chromosome condensin II subunit, kleisin beta, specifically disrupts T cell development. *Proc Natl Acad Sci U S A* **104**, 12445-12450 (2007).
47. Nishibe, R. *et al.* CIZ1, a p21Cip1/Waf1-interacting protein, functions as a tumor suppressor in vivo. *FEBS Lett* **587**, 1529-1535 (2013).
48. Shin, J.J. *et al.* Controlled Cycling and Quiescence Enables Efficient HDR in Engraftment-Enriched Adult Hematopoietic Stem and Progenitor Cells. *Cell Rep* **32**, 108093 (2020).
49. Wu, J. *et al.* Downregulation of histone methyltransferase SET8 inhibits progression of hepatocellular carcinoma. *Sci Rep* **10**, 4490 (2020).

50. Lv, Y., Shi, Y., Han, Q. & Dai, G. Histone demethylase PHF8 accelerates the progression of colorectal cancer and can be regulated by miR-488 in vitro. *Mol Med Rep* **16**, 4437-4444 (2017).
51. Flaus, A., Downs, J.A. & Owen-Hughes, T. Histone isoforms and the oncohistone code. *Curr Opin Genet Dev* **67**, 61-66 (2021).
52. Mohammad, F. & Helin, K. Oncohistones: drivers of pediatric cancers. *Genes Dev* **31**, 2313-2324 (2017).
53. Bartkova, J. *et al.* DNA damage response as a candidate anti-cancer barrier in early human tumorigenesis. *Nature* **434**, 864-870 (2005).
54. Gorgoulis, V.G. *et al.* Activation of the DNA damage checkpoint and genomic instability in human precancerous lesions. *Nature* **434**, 907-913 (2005).
55. Burgess, R.C., Burman, B., Kruhlak, M.J. & Misteli, T. Activation of DNA damage response signaling by condensed chromatin. *Cell Rep* **9**, 1703-1717 (2014).
56. Schindelin, J. *et al.* Fiji: an open-source platform for biological-image analysis. *Nat Methods* **9**, 676-682 (2012).
57. Martin, M. Cutadapt removes adapter sequences from high-throughput sequencing reads. *Bioinformatics in Action* **17**, 10-12 (2012).
58. Kim, D., Langmead, B. & Salzberg, S.L. HISAT: a fast spliced aligner with low memory requirements. *Nat Methods* **12**, 357-360 (2015).
59. Trapnell, C. *et al.* Differential gene and transcript expression analysis of RNA-seq experiments with TopHat and Cufflinks. *Nat Protoc* **7**, 562-578 (2012).

## Figure legends.

**Figure 1. Nuclei from CIZ1-null cells fail to condense on entry to quiescence.** **A.** Nuclear area in cycling female and male populations of WT (green) and CIZ1-null (blue) primary embryonic fibroblasts (PEFs), demonstrating no difference in nuclear size. Dots represent individual nuclei, with mean (grey bar). Right, example workflow for quantification of nuclear area using Fiji image analysis, see methods. **B.** Serum withdrawal (SW) and add back (AB) strategy and their effect on S phase index. Histograms show the proportion of cells that incorporate EdU during a 30-minute pulse (replicating, red). No difference is detected between WT and CIZ1-null cells. **C.** Graphs show change in nuclear area over the SW and AB strategy for male and female WT and CIZ1-null PEFs, normalised to the means for the cycling control state. Representative images of WT and CIZ1-null nuclei at each stage are shown. *Below*, mean areas and calculated volumes assuming a spherical nucleus, see methods. **D.** Nuclear area for WT and CIZ1-null PEFs in a cycling state (day 0) and at 100% confluency (day 3) with no SW. **E.** Immunodetection of the nuclear lamina (Lamin B2, red) in a representative CIZ1-null AB population. **F.** Nuclear area for CIZ1-null PEFs over two rounds of SW and AB, showing failure to condense but stepwise decondensation. Representative images demonstrate the overexpansion of CIZ1-null nuclei. All results are either compared by t-test (A), one-way ANOVA (B,C,F) or two-way ANOVA (D) where ns denotes no significant difference, \*  $p < 0.05$ , \*\*  $p < 0.01$ , \*\*\*  $p < 0.001$ . DNA is stained with DAPI (blue) and scale bar represents  $10\mu\text{m}$ .

**Figure 2. Transcriptome analysis on entry to quiescence.** **A.** Schematic describing two strategies for inducing quiescence, serum withdrawal (SW, 24 hours) and contact inhibition (CI, 7 days), each applied to triplicate cell populations from independent day 13 embryos, from WT or CIZ1-null female mice. **B.** The number of transcription units significantly upregulated ( $\log_2\text{fc} > 1$ , red) or downregulated ( $\log_2\text{fc} < -1$ , blue) upon entry to quiescence via SW or CI (FDR  $q < 0.05$ ) for WT and CIZ1-null PEFs, showing a similar number in each class. **C.** Venn diagrams showing the number of transcription units significantly changed upon entry to quiescence (FDR  $q < 0.05$ ) that are common to both quiescence methods, divided into those that go up or down. For WT cells (green) this defines a murine core quiescence gene set. **D.** Dot plots showing the significance of overlap with all 5916 Gene Ontology (GO) terms for the core quiescence gene sets in C. The most significant GO terms (blue) relate to the cell cycle and are returned by the downregulated genes for both genotypes. **E.** Median expression level (TPM) of upregulated and downregulated genes shown in B, for cycling WT and CIZ1-null cells. Genes that are downregulated during quiescence entry have a higher expression level in the cycling state. **F.** Heat maps compare fold change in expression during quiescence entry between WT and CIZ1-null PEFs, for the two quiescent methods. Transcription units are ordered by WT fold change; upregulated (red), downregulated (blue), and where  $q > 0.05$  (white). **G.** Venn diagrams illustrating CIZ1-dependent genes that are upregulated and downregulated during quiescence entry (intersection shows those that are not CIZ1-dependent). Genes on the left (green) change in WT cells only (FDR  $q < 0.05$ ) and are referred to as genes that 'fail' to change in CIZ1-null; genes on the right (blue) change in CIZ1-null cells only (FDR  $q < 0.05$ ) and are referred to as genes that are 'inappropriately' changed in CIZ1-null cells. Right, histogram showing the overlap between the two quiescence methods for CIZ1-dependent genes (F-UP; fail to go up, F-DN; fail to go down, I-UP; inappropriately up, I-DN; inappropriately down), highlighted in shades of brown. **H.** Dot plot showing the significance of overlap between the four core CIZ1-dependent gene sets with 4762 GSEA Curated Gene Sets. I-DN (dark brown) overlap most significantly with Fischer DREAM Targets (systematic name M149). **I.** Heat maps of all 844 DREAM complex target genes defined in M149 (Fischer et al., 2016) showing fold change in expression during quiescence entry in WT and CIZ1-null PEFs, for the two quiescent methods. Genes are ordered by WT fold change. Data underpinning this analysis is given in Sdata sets.

**Figure 3. Perturbation of the condensin complex.** **A.** Genes that relate to chromatin or DNA repair from the 33 I-DN CIZ1-dependent DREAM targets outlined in STable 1. **B.** Expression (mean TPM) of *Smc4* (Structural Maintenance of Chromosomes 4) and *Mre11a* (MRE11 Homolog, Double Strand Break Repair Nuclease), before (cycling, Cy) and after (quiescence, Q), by SW (left) and CI (right). Similar data for all 33 I-DN genes is given in SFig.3. **C.** Scatter plots comparing expression (mean TPM) in cycling WT and CIZ1-null cells, for all genes within high level GO terms chromosome organisation and DNA repair, plus two subordinate terms for each, as indicated. The grey line ( $y=x$ ) illustrates no difference between WT and CIZ1-null cells and the red line is the best fit to the data calculated in excel, with the slope of the line indicated. A skew towards the y axis indicates a higher expression in CIZ1-null cycling cells. **D.** As in C, for subunits of the condensin complex, the cohesin

complex, the TOR complex and the CDC73 PAF1 complex. Expression of the condensin subunit class is significantly affected by loss of CIZ1. **E.** Mean TPM for all condensin subunits in WT (green) and CIZ1-null (blue) PEFs in the cycling state, normalised to WT,  $\pm$ SEM. *Smc2* and *Smc4* are the two core subunits common to both condensin I and II. Individually, no subunit is significantly different between WT and CIZ1-null. **F.** Whole cell lysates from WT and CIZ1-null cycling populations, female (top) and male (bottom), illustrating the total protein levels for SMC2, SMC4 and Histone H3. Below, quantification showing mean for the 4 independent populations (2 female, 2 male) with individual values indicated. **G.** Detergent-resistant fractions from WT and CIZ1-null male populations in a cycling state and following a short (1 hour) SW. Below, quantification showing mean for 4 independent populations (2 female, 2 male) with individual values indicated. Results are compared by t-test (B,E,F,G), or the Wilcoxon's signed ranked test (D) where ns denotes no significant difference, \*  $p < 0.05$ , \*\*  $p < 0.01$ , \*\*\*  $p < 0.001$ .

**Figure 4. H4K20me1 depletion in CIZ1-null PEFs.** **A.** Frequency of H4K20me1, H3K27me3 and CIZ1 assemblies at the Xi in female WT (green) and CIZ1-null (blue) PEFs, in the cycling state (darker shades) and after a short or long SW (paler shades), with  $\pm$ SEM. n denotes the total number of cells evaluated. **B.** Example images of H4K20me1 (green) at H3K27me3-marked (red) Xi and H4K20me1 at CIZ1-marked (red) Xi in WT cells. **C.** Nuclear area for female WT PEFs demonstrating a gradual drop in size over a short and long SW window. **D.** Western blot illustrating H4K20me1 levels over a 24 hour SW time course for WT and CIZ1-null female PEFs, and Histone H3. **E.** Strategy describing GFP-CIZ1 doxycycline (dox) induction in CIZ1-null PEFs<sup>14</sup>. Right, effect on frequency of H4K20me1 assemblies in a dox-induced CIZ1-null female cycling population (yellow) after 48 hours, categorised by whether GFP-CIZ1 expressing cells had formed a distinct CIZ1 assembly. Below, representative image illustrating colocalisation of GFP-CIZ1 (green) and H4K20me1 (red) assemblies (white arrow). **F.** Mean H4K20me1 immunofluorescence signal in nuclei from CIZ1-null cycling PEFs with (yellow) or without (blue) induction of GFP-CIZ1 (+dox). Right, nuclear area in the same cells following a long SW, showing restoration of condensation capability. **G.** WT cycling PEFs before (green) and after a 2 hour incubation with 10 $\mu$ M UNC0379 (purple), showing reduced H4K20me1 assemblies (histogram) and fluorescence intensity (dot plots), but no effect on H3K27me3. Right, Histogram shows no effect on the proportion of replicating cells (red), detected after 30 minutes of EdU labelling. **H.** Effect of UNC0379 on nuclear area before and after a short SW, showing loss of function in female WT PEFs. Results are compared by t-test (E, F(left),G), one-way ANOVA (C) or two-way ANOVA (A,B,F(right),H) where ns denotes no significant difference, \*  $p < 0.05$ , \*\*  $p < 0.01$ , \*\*\*  $p < 0.001$ . DNA is stained with DAPI (blue) and scale bars represent 10 $\mu$ m.

**Figure 5. Fragility, checkpoint activation and instability induced by quiescence in CIZ1-null cells.** **A.** Short SW and AB strategy used to analyse the response of WT (green) and CIZ1-null (blue) nuclei in B and C. **B.** The relative number of nuclei that survived 40 passes through a 25G needle<sup>41</sup>  $\pm$ SEM, where N represents the number of independent experiments, each with 2-7 fields analysed. **C.** Frequency of cells with activated checkpoint kinase (pATM),  $\pm$ SEM. Right, representative images showing pATM foci (red) in WT and CIZ1-null AB nuclei. **D.** Checkpoint activation (pATM, pCHK1,  $\gamma$ H2AX) in WT and CIZ1-null cells after CI and extended culture, where day 0 represents cycling cells. Below, representative images show foci in contact inhibited CIZ1-null cells at the end of the 21-day time course. **E.** 6cm culture dishes stained with crystal violet showing primary fibroblasts (tail-tip, TTF and embryonic, PEF) populations from WT and CIZ1-null mice, at the end of the 21-day CI time course. Bar is 1cm. Right, quantification of macroscopically visible foci in CIZ1-null TTF populations and a PEF population, compared to WT. Histograms show mean foci incidence  $\pm$ SD at 21 days after plating  $4.5 \times 10^5$  cells. N represents the number of plates counted **F.** Field images of WT and CIZ1-null monolayers 21 days post-plating, detected after a 16-hour pulse with EdU. Monolayer cells remain unlabeled however CIZ1-null focal outgrowths contain S phase cells. Scale bar 200 $\mu$ m. **G.** Schematic representation of the order of events observed in CIZ1-null cells following CI and extended culture. Results are compared by t-test (D, E), or two-way ANOVA (C) where ns denotes no significant difference, \*  $p < 0.05$ , \*\*  $p < 0.01$ , \*\*\*  $p < 0.001$ . DNA is stained with DAPI (blue), and scale bar represents 10 $\mu$ m unless otherwise stated.

**Fig.1**

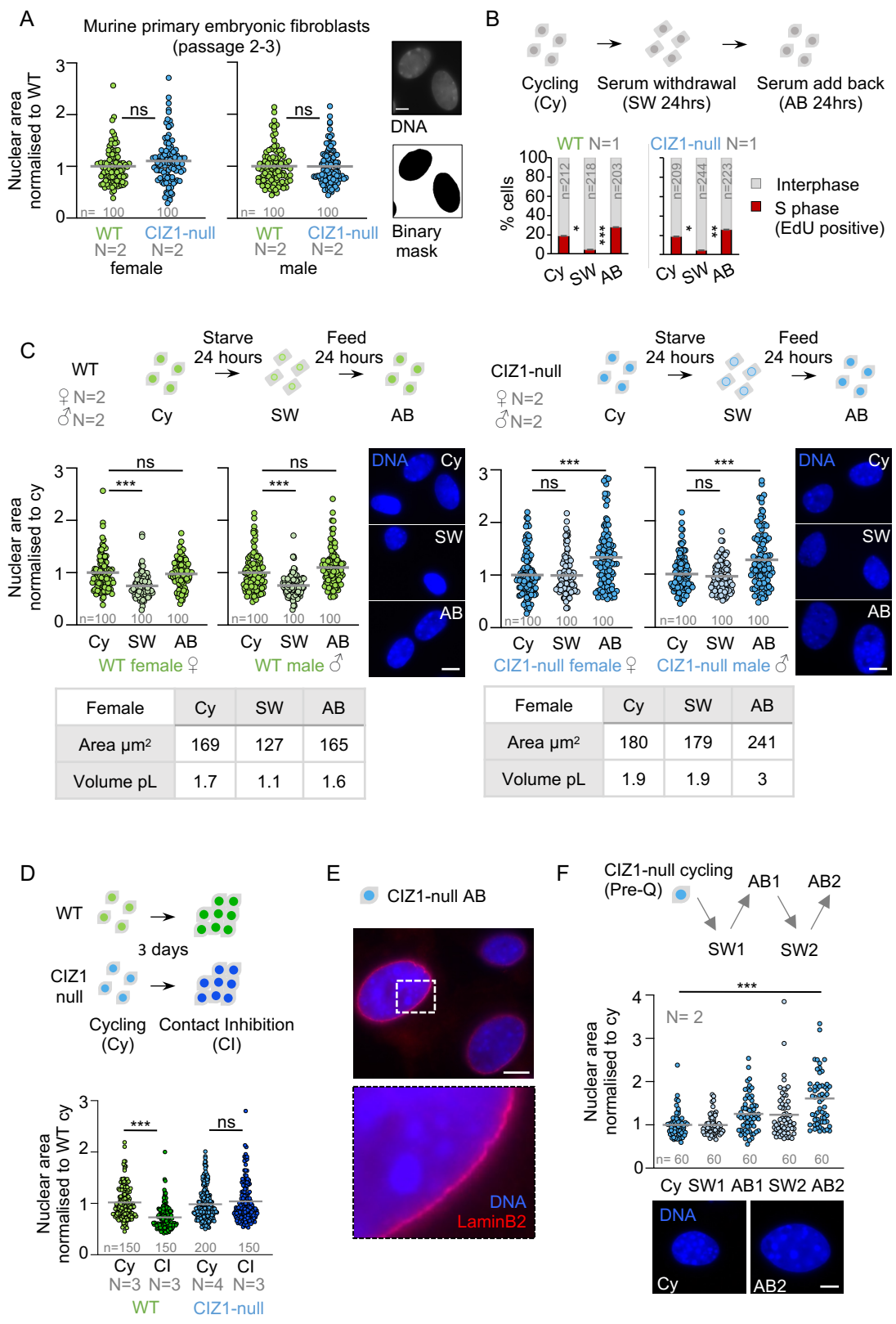


**Fig.2**

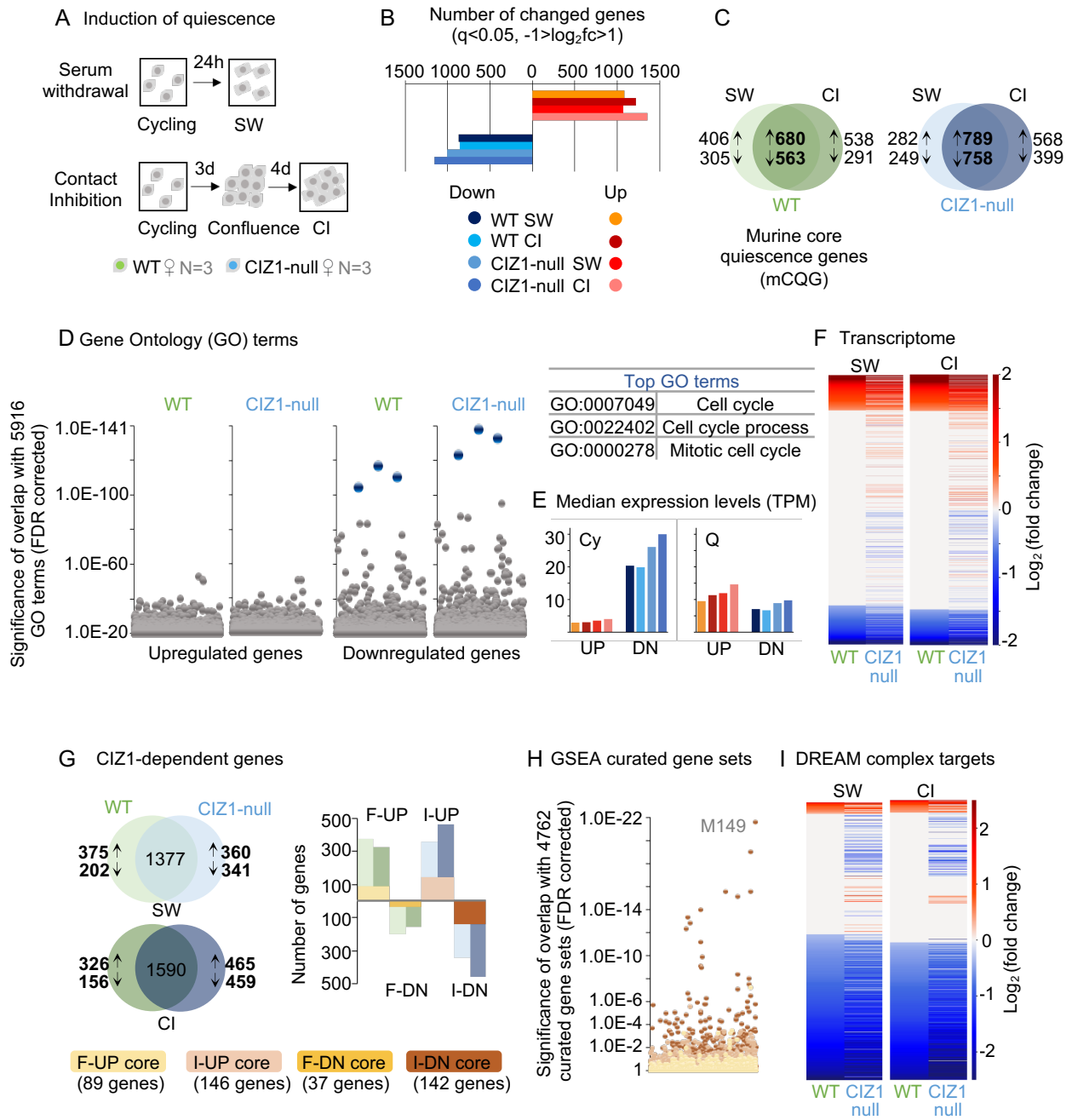


**Fig. 3**

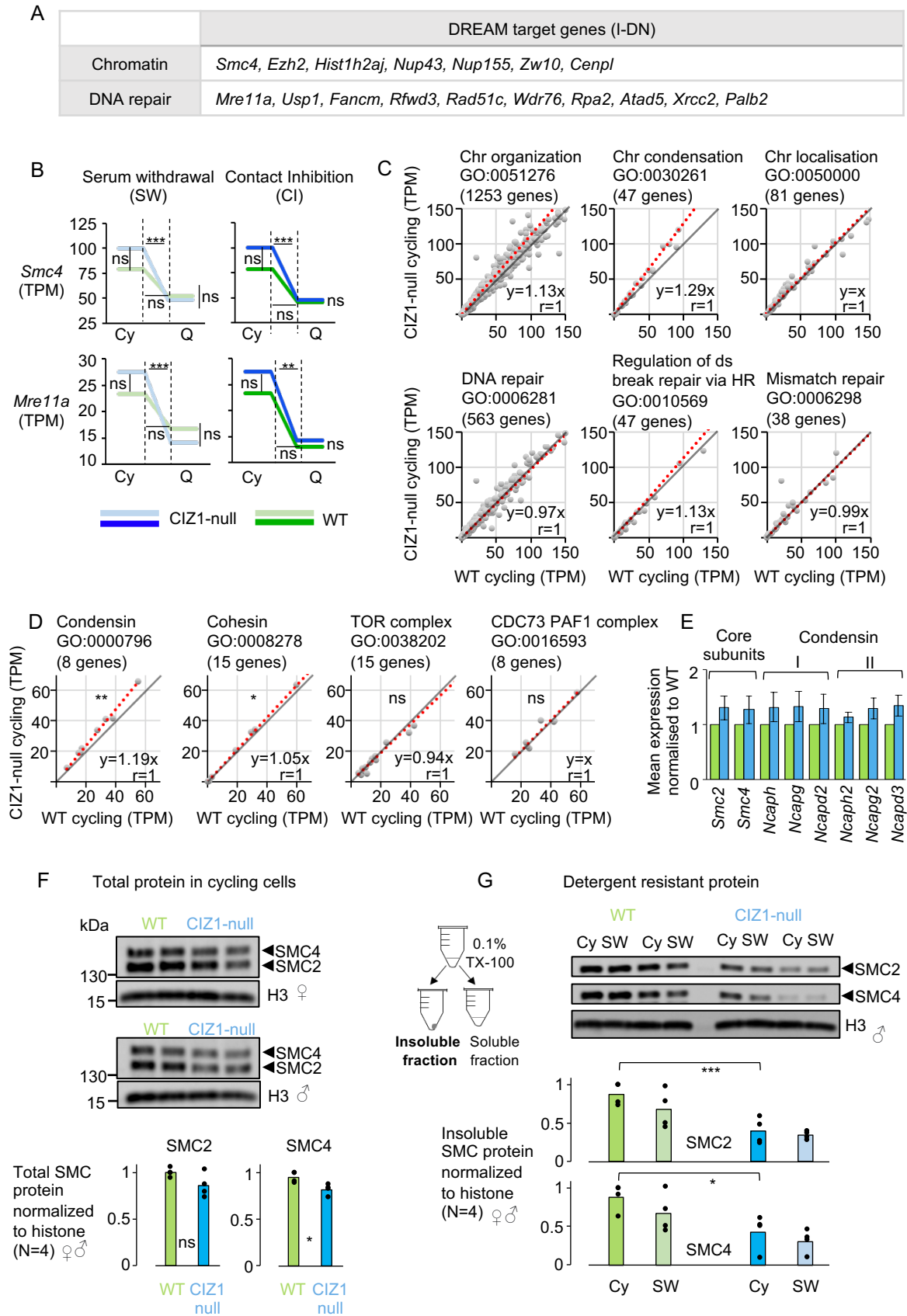


**Fig.4**

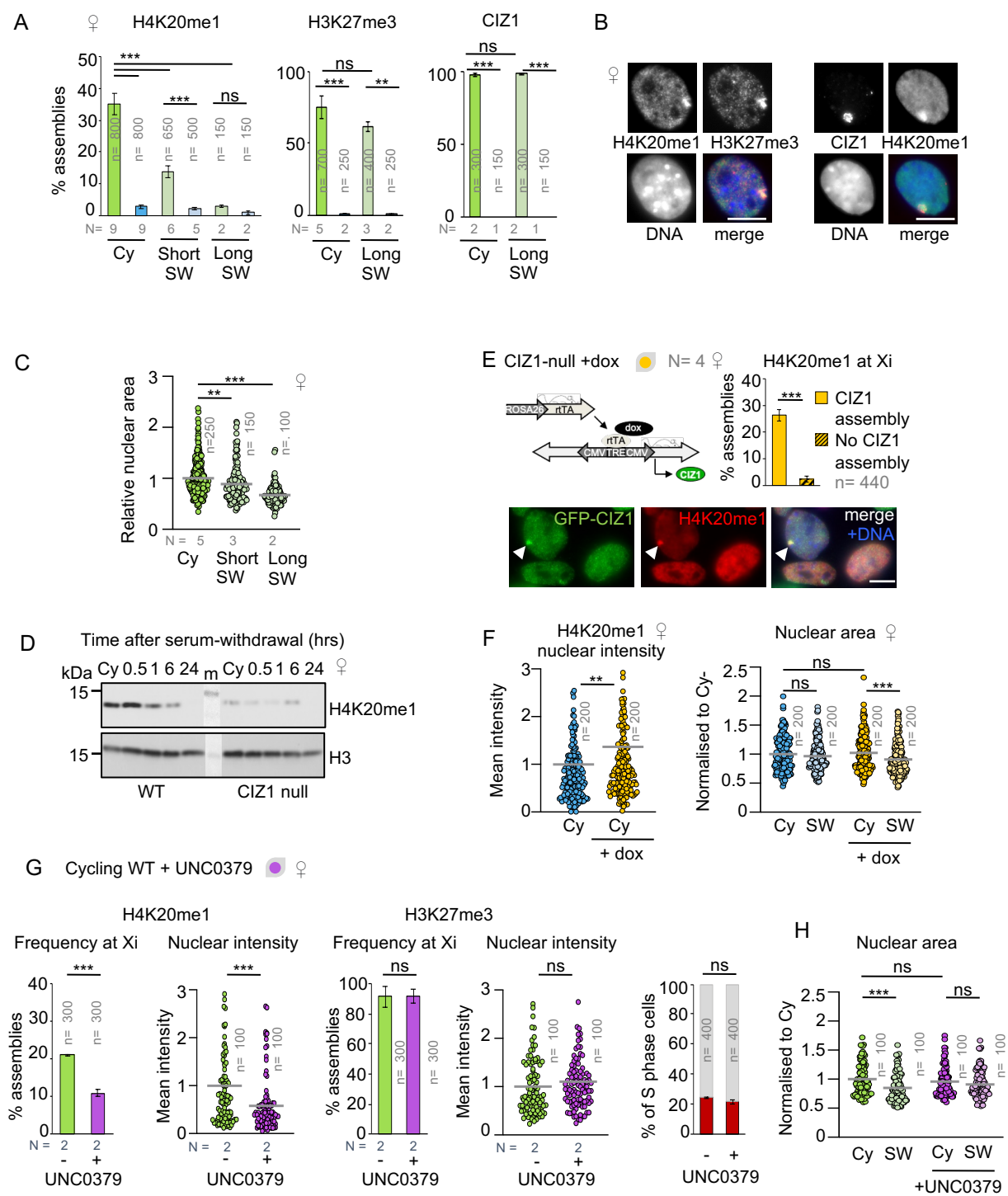
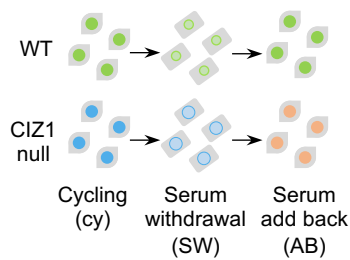
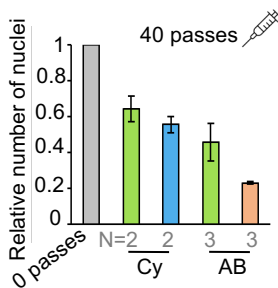


**Fig.5**

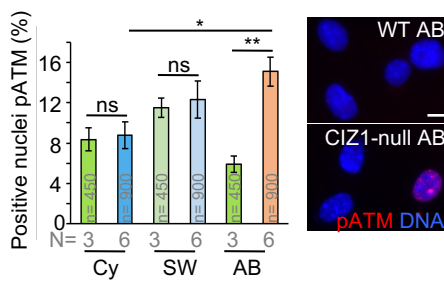
**A Short serum withdrawal / short add back**



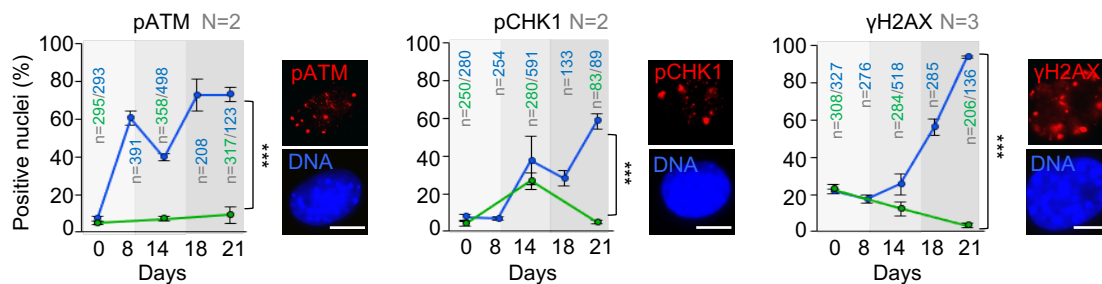
**B Mechanical stress**



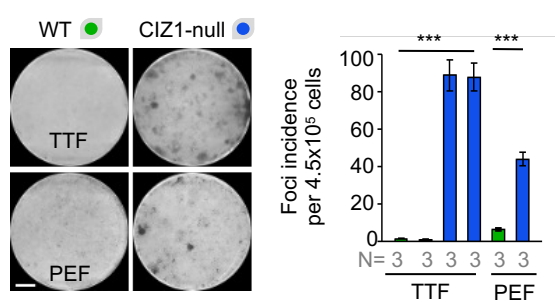
**C Checkpoint activation**



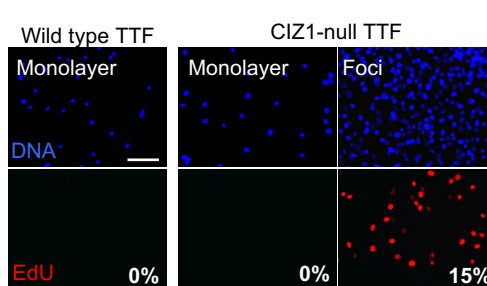
**D Contact Inhibition (extended culture)**



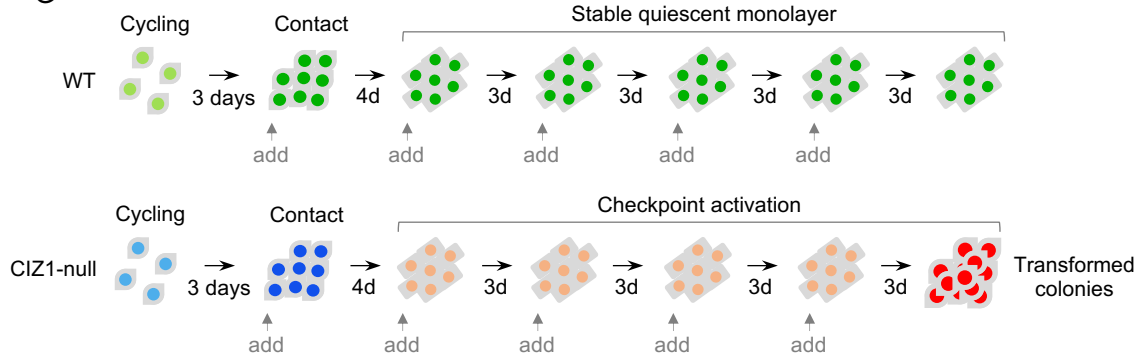
**E**



**F**



**G**



## Appendix C

Gene lists generated from transcriptomic analysis. Provided as separate excel files.

These excel files are part of the supplemental information associated with the manuscript in Appendix B.

Data set 1. Excel file showing mean data with significance indicators for all transcription units that are changed upon entry to quiescence in WT PEFs.

Data set 2. Excel file showing mean data with significance indicators for all transcription units that are changed upon entry to quiescence in CIZ1-null PEFs.

Data set 3. Excel file showing change with significance indicators for all transcription units between a cycling and quiescent state. Includes gene lists that are common to both genotypes as well as the F-UP, F-DN, I-UP and I-DN sets.

Data set 4. Excel file showing GSEA output for the four core gene sets from Data set 3.

Data set 5. Excel file showing mean data and the size of change with significance indicators for all transcription units from the curated gene set “M149, Fischer DREAM targets” that are inappropriately downregulated in CIZ1-null PEFs during entry to quiescence by both methods (serum withdrawal and contact inhibition).

## Abbreviations

AB	Serum add-back
Ac	Acidic domain
ACP5	Tartrate-Resistant Acid Phosphatase 5
ANOVA	Analysis of variance
ATP	Adenosine triphosphate
AURKB	Aurora B kinase
BMP	Bone morphogenetic protein
BrdU	Bromodeoxyuridine
BSA	Bovine serum albumin
CDK	Cyclin-dependent kinase
CDKi	Cyclin-dependent kinase inhibitor
CI	Contact inhibition
CIN	Chromosome instability
CIZ1	Cip1-interacting zinc finger 1
CSK	Cytoskeletal buffer
Cy	Cycling
D-PBS	Dulbecco's phosphate buffered saline
DAPI	4',6-diamidino-2-phenylindole
DDR	DNA damage response
DMEM	Dulbecco's modified Eagle's medium
DNA	Deoxyribonucleic acid
dox	Doxycycline
DP1	Dimerization partner 1
DREAM	Dimerization partner, RB-like, E2F and multi-vulval class B
DSB	Double-strand break
DTT	Dithiothreitol
EDTA	Ethylenediaminetetraacetic acid
EdU	5-ethynyl-2'-deoxyuridine
F-DN	Fail to go down
F-UP	Fail to go up
FDR	False discovery rate
FGF	Fibroblast growth factor
FITC	Fluorescein isothiocyanate
FPKM	Fragment counts per million

G0	Quiescence
G1	Growth 1 phase
G2	Growth 2 phase
GFP	Green fluorescent protein
GO	Gene ontology
GSEA	Gene set enrichment analysis
H2AK119Ub1	Ubiquitylation of histone H2A at lysine 119
H3	Histone H3
H3K27me3	Tri-methylation of histone H3 at of lysine 27
H4K20	Histone H4 lysine 20
H4K20me1	Mono-methylation of histone H4 at lysine 20
H4K20me2	Di-methylation of histone H4 at lysine 20
H4K20me3	Tri-methylation of histone H4 at lysine 20
HR	Homologous recombination
HS	High serum
HSCs	Hematopoietic stem cells
I-DN	Inappropriately downregulated
I-UP	Inappropriately upregulated
kDa	Kilodalton
L-CIDs	Large chromosomal interaction domains
lncRNA	Long non-coding RNA
LS	Low serum
M	Mitosis
mCQG	Murine core quiescence genes
MRN	Mre11-Rad50-Nbs1
MuSCs	Skeletal muscle stem cells
NaCl	Sodium chloride
NHEJ	Non-homologous end joining
NLS	Nuclear localisation signal
NM	Nuclear matrix
NSCs	Neural stem cells
°C	Degrees centigrade
p	Pellet
PAGE	Polyacrylamide Gel Electrophoresis
pATM	Phosphorylated ataxia telangiectasia mutated protein
PBS	Phosphate buffered saline

pCHK1	Phosphorylated checkpoint kinase 1
PEF	Primary embryonic fibroblast
PFA	Paraformaldehyde
PHF8	PHD Finger Protein 8
PIPES	Piperazine-N,N'bis(2-ethanesulfonic acid)
PLD	Prion-like domains
PMSF	Phenylmethanesulfonylfluoride
PP1	Protein phosphatase 1
pRB	The retinoblastoma protein
PSG	Penicillin streptomycin glutamine
PTM	Post-translational modification
Q	Quiescent
q-value	False detection rate corrected p value
RNA	Ribonucleic acid
RNA pol II	RNA polymerase II
ROI	Region of interest
RT	Room temperature
S phase	DNA synthesis phase
<i>S. cerevisiae</i>	<i>Saccharomyces cerevisiae</i>
<i>S. pombe</i>	<i>Schizosaccharomyces pombe</i>
SDERGs	Serum deprivation early response genes
SDS	Sodium dodecyl sulphate
SEM	Standard error of the mean
SMC	Structural maintenance of chromosomes
Sn	Supernatant
SW	Serum withdrawal
TADs	Topologically associated domains
TBS	Tris buffered saline
TPM	Transcripts per million
TTF	Tail-tip fibroblast
VRC	Vanadyl ribonucleoside complex
WT	Wild-type
Xi	Inactive X chromosome
<i>Xist</i>	X-inactive specific transcript
ZF	Zinc finger
$\gamma$ H2AX	Phosphorylated histone H2AX

## References

- Ainscough, J. F., Rahman, F. A., Sercombe, H., Sedo, A., Gerlach, B. & Coverley, D. 2007. C-terminal domains deliver the DNA replication factor Ciz1 to the nuclear matrix. *J Cell Sci*, 120, 115-24.
- Amani, J., Gorjizadeh, N., Younesi, S., Najafi, M., Ashrafi, A. M., Irian, S. & Azizian, K. 2021. Cyclin-dependent kinase inhibitors (CDKIs) and the DNA damage response: The link between signaling pathways and cancer. *DNA Repair (Amst)*, 102, 103103.
- Audia, J. E. & Campbell, R. M. 2016. Histone Modifications and Cancer. *Cold Spring Harb Perspect Biol*, 8, a019521.
- Baergen, A. K., Jeusset, L. M., Lichtensztejn, Z. & McManus, K. J. 2019. Diminished Condensin Gene Expression Drives Chromosome Instability That May Contribute to Colorectal Cancer Pathogenesis. *Cancers (Basel)*, 11.
- Bakkenist, C. J. & Kastan, M. B. 2003. DNA damage activates ATM through intermolecular autophosphorylation and dimer dissociation. *Nature*, 421, 499-506.
- Barnum, K. J. & O'Connell, M. J. 2014. Cell cycle regulation by checkpoints. *Methods Mol Biol*, 1170, 29-40.
- Baxter, J., Sauer, S., Peters, A., John, R., Williams, R., Caparros, M. L., Arney, K., Otte, A., Jenuwein, T., Merckenschlager, M. & Fisher, A. G. 2004. Histone hypomethylation is an indicator of epigenetic plasticity in quiescent lymphocytes. *EMBO J*, 23, 4462-72.
- Beerman, I., Seita, J., Inlay, M. A., Weissman, I. L. & Rossi, D. J. 2014. Quiescent hematopoietic stem cells accumulate DNA damage during aging that is repaired upon entry into cell cycle. *Cell Stem Cell*, 15, 37-50.
- Bera, M. & Sengupta, K. 2020. Nuclear filaments: role in chromosomal positioning and gene expression. *Nucleus*, 11, 99-110.
- Berezney, R. & Coffey, D. S. 1974. Identification of a nuclear protein matrix. *Biochem Biophys Res Commun*, 60, 1410-7.
- Bertoli, C., Skotheim, J. M. & de Bruin, R. A. 2013. Control of cell cycle transcription during G1 and S phases. *Nat Rev Mol Cell Biol*, 14, 518-28.
- Bloom, J. & Cross, F. R. 2007. Multiple levels of cyclin specificity in cell-cycle control. *Nat Rev Mol Cell Biol*, 8, 149-60.
- Bonitto, K., Sarathy, K., Atai, K., Mitra, M. & Collier, H. A. 2021. Is There a Histone Code for Cellular Quiescence? *Front Cell Dev Biol*, 9, 739780.
- Boonsanay, V., Zhang, T., Georgieva, A., Kostin, S., Qi, H., Yuan, X., Zhou, Y. & Braun, T. 2016. Regulation of Skeletal Muscle Stem Cell Quiescence by Suv4-20h1-Dependent Facultative Heterochromatin Formation. *Cell Stem Cell*, 18, 229-42.

- Boorsma, C. E., van der Veen, T. A., Putri, K. S. S., de Almeida, A., Draijer, C., Mauad, T., Fejer, G., Brandsma, C. A., van den Berge, M., Bossé, Y., Sin, D., Hao, K., Reithmeier, A., Andersson, G., Olinga, P., Timens, W., Casini, A. & Melgert, B. N. 2017. A Potent Tartrate Resistant Acid Phosphatase Inhibitor to Study the Function of TRAP in Alveolar Macrophages. *Sci Rep*, 7, 12570.
- Botuyan, M. V., Lee, J., Ward, I. M., Kim, J. E., Thompson, J. R., Chen, J. & Mer, G. 2006. Structural basis for the methylation state-specific recognition of histone H4-K20 by 53BP1 and Crb2 in DNA repair. *Cell*, 127, 1361-73.
- Bridger, J. M., Boyle, S., Kill, I. R. & Bickmore, W. A. 2000. Re-modelling of nuclear architecture in quiescent and senescent human fibroblasts. *Curr Biol*, 10, 149-52.
- Brockdorff, N. 2017. Polycomb complexes in X chromosome inactivation. *Philos Trans R Soc Lond B Biol Sci*, 372.
- Brockdorff, N., Ashworth, A., Kay, G. F., McCabe, V. M., Norris, D. P., Cooper, P. J., Swift, S. & Rastan, S. 1992. The product of the mouse Xist gene is a 15 kb inactive X-specific transcript containing no conserved ORF and located in the nucleus. *Cell*, 71, 515-26.
- Brown, C. J., Hendrich, B. D., Rupert, J. L., Lafrenière, R. G., Xing, Y., Lawrence, J. & Willard, H. F. 1992. The human XIST gene: analysis of a 17 kb inactive X-specific RNA that contains conserved repeats and is highly localized within the nucleus. *Cell*, 71, 527-42.
- Burgess, R. C., Burman, B., Kruhlak, M. J. & Misteli, T. 2014. Activation of DNA damage response signaling by condensed chromatin. *Cell Rep*, 9, 1703-1717.
- Chakkalakal, J. V., Jones, K. M., Basson, M. A. & Brack, A. S. 2012. The aged niche disrupts muscle stem cell quiescence. *Nature*, 490, 355-60.
- Chen, X., Wang, P., Wang, S., Li, J., Ou, T. & Zeng, X. 2019. CIZ1 knockdown suppresses the proliferation of bladder cancer cells by inducing apoptosis. *Gene*, 719, 143946.
- Cheung, T. H., Quach, N. L., Charville, G. W., Liu, L., Park, L., Edalati, A., Yoo, B., Hoang, P. & Rando, T. A. 2012. Maintenance of muscle stem-cell quiescence by microRNA-489. *Nature*, 482, 524-8.
- Cheung, T. H. & Rando, T. A. 2013. Molecular regulation of stem cell quiescence. *Nat Rev Mol Cell Biol*, 14, 329-40.
- Cho, I. J., Lui, P. P., Obajdin, J., Riccio, F., Stroukov, W., Willis, T. L., Spagnoli, F. & Watt, F. M. 2019. Mechanisms, Hallmarks, and Implications of Stem Cell Quiescence. *Stem Cell Reports*, 12, 1190-1200.
- Chuang, C. H., Carpenter, A. E., Fuchsova, B., Johnson, T., de Lanerolle, P. & Belmont, A. S. 2006. Long-range directional movement of an interphase chromosome site. *Curr Biol*, 16, 825-31.
- Clemson, C. M., McNeil, J. A., Willard, H. F. & Lawrence, J. B. 1996. XIST RNA paints the inactive X chromosome at interphase: evidence for a novel RNA involved in nuclear/chromosome structure. *J Cell Biol*, 132, 259-75.
- Coller, H. A., Sang, L. & Roberts, J. M. 2006. A new description of cellular quiescence. *PLoS Biol*, 4, e83.
- Cope, N. F., Fraser, P. & Eskiw, C. H. 2010. The yin and yang of chromatin spatial organization. *Genome Biol*, 11, 204.

- Copeland, N. A., Sercombe, H. E., Ainscough, J. F. & Coverley, D. 2010. Ciz1 cooperates with cyclin-A-CDK2 to activate mammalian DNA replication in vitro. *J Cell Sci*, 123, 1108-15.
- Copeland, N. A., Sercombe, H. E., Wilson, R. H. & Coverley, D. 2015. Cyclin-A-CDK2-mediated phosphorylation of CIZ1 blocks replisome formation and initiation of mammalian DNA replication. *J Cell Sci*, 128, 1518-27.
- Coschi, C. H., Ishak, C. A., Gallo, D., Marshall, A., Talluri, S., Wang, J., Cecchini, M. J., Martens, A. L., Percy, V., Welch, I., Boutros, P. C., Brown, G. W. & Dick, F. A. 2014. Haploinsufficiency of an RB-E2F1-Condensin II complex leads to aberrant replication and aneuploidy. *Cancer Discov*, 4, 840-53.
- Coschi, C. H., Martens, A. L., Ritchie, K., Francis, S. M., Chakrabarti, S., Berube, N. G. & Dick, F. A. 2010. Mitotic chromosome condensation mediated by the retinoblastoma protein is tumor-suppressive. *Genes Dev*, 24, 1351-63.
- Costello, G., Rodgers, L. & Beach, D. 1986. Fission yeast enters the stationary phase G0 state from either mitotic G1 or G2. *Current Genetics*, 11, 119-125.
- Coverley, D., Marr, J. & Ainscough, J. 2005. Ciz1 promotes mammalian DNA replication. *J Cell Sci*, 118, 101-12.
- Dahmcke, C. M., Buchmann-Moller, S., Jensen, N. A. & Mitchelmore, C. 2008. Altered splicing in exon 8 of the DNA replication factor CIZ1 affects subnuclear distribution and is associated with Alzheimer's disease. *Mol Cell Neurosci*, 38, 589-94.
- de Lanerolle, P. 2012. Nuclear actin and myosins at a glance. *J Cell Sci*, 125, 4945-9.
- den Hollander, P., Rayala, S. K., Coverley, D. & Kumar, R. 2006. Ciz1, a novel DNA-binding coactivator of the estrogen receptor  $\alpha$ , confers hypersensitivity to estrogen action. *Cancer Research*, 66, 11021-11030.
- Dillon, N. 2008. The impact of gene location in the nucleus on transcriptional regulation. *Dev Cell*, 15, 182-6.
- Dixon-McDougall, T. & Brown, C. J. 2022. Multiple distinct domains of human XIST are required to coordinate gene silencing and subsequent heterochromatin formation. *Epigenetics Chromatin*, 15, 6.
- Drewinko, B., Yang, L. Y., Barlogie, B. & Trujillo, J. M. 1984. Cultured human tumour cells may be arrested in all stages of the cycle during stationary phase: demonstration of quiescent cells in G1, S and G2 phase. *Cell Tissue Kinet*, 17, 453-63.
- Dunin-Horkawicz, S., Feder, M. & Bujnicki, J. M. 2006. Phylogenomic analysis of the GIY-YIG nuclease superfamily. *BMC Genomics*, 7, 98.
- Duronio, R. J. & Xiong, Y. 2013. Signaling pathways that control cell proliferation. *Cold Spring Harb Perspect Biol*, 5, a008904.
- Duthie, S. M., Nesterova, T. B., Formstone, E. J., Keohane, A. M., Turner, B. M., Zakian, S. M. & Brockdorff, N. 1999. Xist RNA exhibits a banded localization on the inactive X chromosome and is excluded from autosomal material in cis. *Hum Mol Genet*, 8, 195-204.
- Ek-Rylander, B., Bill, P., Norgård, M., Nilsson, S. & Andersson, G. 1991. Cloning, sequence, and developmental expression of a type 5, tartrate-resistant, acid phosphatase of rat bone. *J Biol Chem*, 266, 24684-9.

- Evertts, A. G., Manning, A. L., Wang, X., Dyson, N. J., Garcia, B. A. & Collier, H. A. 2013. H4K20 methylation regulates quiescence and chromatin compaction. *Mol Biol Cell*, 24, 3025-37.
- Fang, J., Feng, Q., Ketel, C. S., Wang, H., Cao, R., Xia, L., Erdjument-Bromage, H., Tempst, P., Simon, J. A. & Zhang, Y. 2002. Purification and functional characterization of SET8, a nucleosomal histone H4-lysine 20-specific methyltransferase. *Curr Biol*, 12, 1086-99.
- Fischer, E. G. 2020. Nuclear Morphology and the Biology of Cancer Cells. *Acta Cytol*, 64, 511-519.
- Fischer, M., Grossmann, P., Padi, M. & DeCaprio, J. A. 2016. Integration of TP53, DREAM, MMB-FOXO1 and RB-E2F target gene analyses identifies cell cycle gene regulatory networks. *Nucleic Acids Res*, 44, 6070-86.
- Flanagan, J. U., Cassady, A. I., Schenk, G., Guddat, L. W. & Hume, D. A. 2006. Identification and molecular modeling of a novel, plant-like, human purple acid phosphatase. *Gene*, 377, 12-20.
- Flaus, A., Downs, J. A. & Owen-Hughes, T. 2021. Histone isoforms and the oncohistone code. *Curr Opin Genet Dev*, 67, 61-66.
- Foster, H. A. & Bridger, J. M. 2005. The genome and the nucleus: a marriage made by evolution. Genome organisation and nuclear architecture. *Chromosoma*, 114, 212-29.
- Frazier, A. D. & Champney, W. S. 2012. The vanadyl ribonucleoside complex inhibits ribosomal subunit formation in *Staphylococcus aureus*. *J Antimicrob Chemother*, 67, 2152-7.
- Furusawa, T., Rochman, M., Taher, L., Dimitriadis, E. K., Nagashima, K., Anderson, S. & Bustin, M. 2015. Chromatin decompaction by the nucleosomal binding protein HMGN5 impairs nuclear sturdiness. *Nat Commun*, 6, 6138.
- Gerlich, D., Hirota, T., Koch, B., Peters, J. M. & Ellenberg, J. 2006. Condensin I stabilizes chromosomes mechanically through a dynamic interaction in live cells. *Curr Biol*, 16, 333-44.
- Gosling, K. M., Goodnow, C. C., Verma, N. K. & Fahrner, A. M. 2008. Defective T-cell function leading to reduced antibody production in a kleisin-beta mutant mouse. *Immunology*, 125, 208-17.
- Gosling, K. M., Makaroff, L. E., Theodoratos, A., Kim, Y. H., Whittle, B., Rui, L., Wu, H., Hong, N. A., Kennedy, G. C., Fritz, J. A., Yates, A. L., Goodnow, C. C. & Fahrner, A. M. 2007. A mutation in a chromosome condensin II subunit, kleisin beta, specifically disrupts T cell development. *Proc Natl Acad Sci U S A*, 104, 12445-50.
- Grigoryev, S. A., Nikitina, T., Pehrson, J. R., Singh, P. B. & Woodcock, C. L. 2004. Dynamic relocation of epigenetic chromatin markers reveals an active role of constitutive heterochromatin in the transition from proliferation to quiescence. *J Cell Sci*, 117, 6153-62.
- Guidi, M., Ruault, M., Marbouty, M., Loiodice, I., Cournac, A., Billaudeau, C., Hocher, A., Mozziconacci, J., Koszul, R. & Taddei, A. 2015. Spatial reorganization of telomeres in long-lived quiescent cells. *Genome Biol*, 16, 206.
- Hadler, K. S., Huber, T., Cassady, A. I., Weber, J., Robinson, J., Burrows, A., Kelly, G., Guddat, L. W., Hume, D. A., Schenk, G. & Flanagan, J. U. 2008. Identification of

a non-purple tartrate-resistant acid phosphatase: an evolutionary link to Ser/Thr protein phosphatases? *BMC Res Notes*, 1, 78.

- Hall, L. L., Byron, M., Pageau, G. & Lawrence, J. B. 2009. AURKB-mediated effects on chromatin regulate binding versus release of XIST RNA to the inactive chromosome. *J Cell Biol*, 186, 491-507.
- Hanahan, D. & Weinberg, R. A. 2011. Hallmarks of cancer: the next generation. *Cell*, 144, 646-74.
- Harper, J. W. & Elledge, S. J. 2007. The DNA damage response: ten years after. *Mol Cell*, 28, 739-45.
- Hartwell, L. H. & Kastan, M. B. 1994. Cell cycle control and cancer. *Science*, 266, 1821-8.
- Higgins, G., Roper, K. M., Watson, I. J., Blackhall, F. H., Rom, W. N., Pass, H. I., Ainscough, J. F. & Coverley, D. 2012. Variant Ciz1 is a circulating biomarker for early-stage lung cancer. *Proc Natl Acad Sci U S A*, 109, E3128-35.
- Hirano, T. 2012. Condensins: universal organizers of chromosomes with diverse functions. *Genes Dev*, 26, 1659-78.
- Hirano, T., Kobayashi, R. & Hirano, M. 1997. Condensins, chromosome condensation protein complexes containing XCAP-C, XCAP-E and a Xenopus homolog of the Drosophila Barren protein. *Cell*, 89, 511-21.
- Hirota, T., Gerlich, D., Koch, B., Ellenberg, J. & Peters, J. M. 2004. Distinct functions of condensin I and II in mitotic chromosome assembly. *J Cell Sci*, 117, 6435-45.
- Houston, S. I., McManus, K. J., Adams, M. M., Sims, J. K., Carpenter, P. B., Hendzel, M. J. & Rice, J. C. 2008. Catalytic function of the PR-Set7 histone H4 lysine 20 monomethyltransferase is essential for mitotic entry and genomic stability. *J Biol Chem*, 283, 19478-88.
- Huang, J., Gujar, M. R., Deng, Q., Y Chia, S., Li, S., Tan, P., Sung, W. K. & Wang, H. 2021. Histone lysine methyltransferase Pr-set7/SETD8 promotes neural stem cell reactivation. *EMBO Rep*, 22, e50994.
- Huttlin, E. L., Ting, L., Bruckner, R. J., Gebreab, F., Gygi, M. P., Szpyt, J., Tam, S., Zarraga, G., Colby, G., Baltier, K., Dong, R., Guarani, V., Vaites, L. P., Ordureau, A., Rad, R., Erickson, B. K., Wühr, M., Chick, J., Zhai, B., Kolippakkam, D., Mintseris, J., Obar, R. A., Harris, T., Artavanis-Tsakonas, S., Sowa, M. E., De Camilli, P., Paulo, J. A., Harper, J. W. & Gygi, S. P. 2015. The BioPlex Network: A Systematic Exploration of the Human Interactome. *Cell*, 162, 425-440.
- Iness, A. N., Felthousen, J., Ananthapadmanabhan, V., Sesay, F., Saini, S., Guiley, K. Z., Rubin, S. M., Dozmorov, M. & Litovchick, L. 2019. The cell cycle regulatory DREAM complex is disrupted by high expression of oncogenic B-Myb. *Oncogene*, 38, 1080-1092.
- Iness, A. N. & Litovchick, L. 2018. MuvB: A Key to Cell Cycle Control in Ovarian Cancer. *Front Oncol*, 8, 223.
- Jackson, S. P. & Bartek, J. 2009. The DNA-damage response in human biology and disease. *Nature*, 461, 1071-8.
- Johnson, E. L., Robinson, D. G. & Collier, H. A. 2017. Widespread changes in mRNA stability contribute to quiescence-specific gene expression patterns in a fibroblast model of quiescence. *BMC Genomics*, 18, 123.

- Jørgensen, S., Schotta, G. & Sørensen, C. S. 2013. Histone H4 lysine 20 methylation: key player in epigenetic regulation of genomic integrity. *Nucleic Acids Res*, 41, 2797-806.
- Khan, M. M., Xiao, J., Patel, D. & LeDoux, M. S. 2018. DNA damage and neurodegenerative phenotypes in aged Ciz1 null mice. *Neurobiol Aging*, 62, 180-190.
- Kim, D., Langmead, B. & Salzberg, S. L. 2015. HISAT: a fast spliced aligner with low memory requirements. *Nat Methods*, 12, 357-60.
- Kim, J. H., Youn, Y., Kim, K. T., Jang, G. & Hwang, J. H. 2019. Non-SMC condensin I complex subunit H mediates mature chromosome condensation and DNA damage in pancreatic cancer cells. *Sci Rep*, 9, 17889.
- Kim, M. J., Cervantes, C., Jung, Y. S., Zhang, X., Zhang, J., Lee, S. H., Jun, S., Litovchick, L., Wang, W., Chen, J., Fang, B. & Park, J. I. 2021. PAF remodels the DREAM complex to bypass cell quiescence and promote lung tumorigenesis. *Mol Cell*, 81, 1698-1714.e6.
- Kschonsak, M., Merkel, F., Bisht, S., Metz, J., Rybin, V., Hassler, M. & Haering, C. H. 2017. Structural Basis for a Safety-Belt Mechanism That Anchors Condensin to Chromosomes. *Cell*, 171, 588-600.e24.
- Kwon, J. S., Everetts, N. J., Wang, X., Wang, W., Della Croce, K., Xing, J. & Yao, G. 2017. Controlling Depth of Cellular Quiescence by an Rb-E2F Network Switch. *Cell Rep*, 20, 3223-3235.
- Laporte, D., Courtout, F., Salin, B., Ceschin, J. & Sagot, I. 2013. An array of nuclear microtubules reorganizes the budding yeast nucleus during quiescence. *J Cell Biol*, 203, 585-94.
- Laporte, D., Courtout, F., Tollis, S. & Sagot, I. 2016. Quiescent *Saccharomyces cerevisiae* forms telomere hyperclusters at the nuclear membrane vicinity through a multifaceted mechanism involving Esc1, the Sir complex, and chromatin condensation. *Mol Biol Cell*, 27, 1875-84.
- Laporte, D., Lebaudy, A., Sahin, A., Pinson, B., Ceschin, J., Daignan-Fornier, B. & Sagot, I. 2011. Metabolic status rather than cell cycle signals control quiescence entry and exit. *J Cell Biol*, 192, 949-57.
- Laporte, D. & Sagot, I. 2014. Microtubules move the nucleus to quiescence. *Nucleus*, 5, 113-8.
- Lee, J., Kang, S., Lilja, K. C., Colletier, K. J., Scheitz, C. J., Zhang, Y. V. & Tumber, T. 2016. Signalling couples hair follicle stem cell quiescence with reduced histone H3 K4/K9/K27me3 for proper tissue homeostasis. *Nat Commun*, 7, 11278.
- Lei, L., Wu, J., Gu, D., Liu, H. & Wang, S. 2016. CIZ1 interacts with YAP and activates its transcriptional activity in hepatocellular carcinoma cells. *Tumour Biol*.
- Leiserson, M. D., Vandin, F., Wu, H. T., Dobson, J. R., Eldridge, J. V., Thomas, J. L., Papoutsaki, A., Kim, Y., Niu, B., McLellan, M., Lawrence, M. S., Gonzalez-Perez, A., Tamborero, D., Cheng, Y., Ryslik, G. A., Lopez-Bigas, N., Getz, G., Ding, L. & Raphael, B. J. 2015. Pan-cancer network analysis identifies combinations of rare somatic mutations across pathways and protein complexes. *Nat Genet*, 47, 106-14.
- Lenk, R., Ransom, L., Kaufmann, Y. & Penman, S. 1977. A cytoskeletal structure with associated polyribosomes obtained from HeLa cells. *Cell*, 10, 67-78.

- Li, G., Sudlow, G. & Belmont, A. S. 1998. Interphase cell cycle dynamics of a late-replicating, heterochromatic homogeneously staining region: precise choreography of condensation/decondensation and nuclear positioning. *J Cell Biol*, 140, 975-89.
- Litovchick, L., Florens, L. A., Swanson, S. K., Washburn, M. P. & DeCaprio, J. A. 2011. DYRK1A protein kinase promotes quiescence and senescence through DREAM complex assembly. *Genes Dev*, 25, 801-13.
- Litovchick, L., Sadasivam, S., Florens, L., Zhu, X., Swanson, S. K., Velmurugan, S., Chen, R., Washburn, M. P., Liu, X. S. & DeCaprio, J. A. 2007. Evolutionarily conserved multisubunit RBL2/p130 and E2F4 protein complex represses human cell cycle-dependent genes in quiescence. *Mol Cell*, 26, 539-51.
- Liu, H., Adler, A. S., Segal, E. & Chang, H. Y. 2007. A transcriptional program mediating entry into cellular quiescence. *PLoS Genet*, 3, e91.
- Liu, T., Ren, X., Li, L., Yin, L., Liang, K., Yu, H., Ren, H., Zhou, W., Jing, H. & Kong, C. 2015. Ciz1 promotes tumorigenicity of prostate carcinoma cells. *Front Biosci (Landmark Ed)*, 20, 705-15.
- Liu, W., Tanasa, B., Tyurina, O. V., Zhou, T. Y., Gassmann, R., Liu, W. T., Ohgi, K. A., Benner, C., Garcia-Bassets, I., Aggarwal, A. K., Desai, A., Dorrestein, P. C., Glass, C. K. & Rosenfeld, M. G. 2010. PHF8 mediates histone H4 lysine 20 demethylation events involved in cell cycle progression. *Nature*, 466, 508-12.
- Ljusberg, J., Ek-Rylander, B. & Andersson, G. 1999. Tartrate-resistant purple acid phosphatase is synthesized as a latent proenzyme and activated by cysteine proteinases. *Biochem J*, 343 Pt 1, 63-9.
- Loewith, R. & Hall, M. N. 2011. Target of rapamycin (TOR) in nutrient signaling and growth control. *Genetics*, 189, 1177-201.
- Longworth, M. S., Herr, A., Ji, J. Y. & Dyson, N. J. 2008. RBF1 promotes chromatin condensation through a conserved interaction with the Condensin II protein dCAP-D3. *Genes Dev*, 22, 1011-24.
- Lu, X., Simon, M. D., Chodaparambil, J. V., Hansen, J. C., Shokat, K. M. & Luger, K. 2008. The effect of H3K79 dimethylation and H4K20 trimethylation on nucleosome and chromatin structure. *Nat Struct Mol Biol*, 15, 1122-4.
- Lv, Y., Shi, Y., Han, Q. & Dai, G. 2017. Histone demethylase PHF8 accelerates the progression of colorectal cancer and can be regulated by miR-488 in vitro. *Mol Med Rep*, 16, 4437-4444.
- Lyon, M. F. 1961. Gene action in the X-chromosome of the mouse (*Mus musculus* L.). *Nature*, 190, 372-3.
- Ma, A., Yu, W., Li, F., Bleich, R. M., Herold, J. M., Butler, K. V., Norris, J. L., Korboukh, V., Tripathy, A., Janzen, W. P., Arrowsmith, C. H., Frye, S. V., Vedadi, M., Brown, P. J. & Jin, J. 2014. Discovery of a selective, substrate-competitive inhibitor of the lysine methyltransferase SETD8. *J Med Chem*, 57, 6822-33.
- Maeshima, K. & Laemmli, U. K. 2003. A two-step scaffolding model for mitotic chromosome assembly. *Dev Cell*, 4, 467-80.
- Magalska, A., Schellhaus, A. K., Moreno-Andrés, D., Zanini, F., Schooley, A., Sachdev, R., Schwarz, H., Madlung, J. & Antonin, W. 2014. RuvB-like ATPases function in chromatin decondensation at the end of mitosis. *Dev Cell*, 31, 305-318.

- Manning, A. L., Longworth, M. S. & Dyson, N. J. 2010. Loss of pRB causes centromere dysfunction and chromosomal instability. *Genes Dev*, 24, 1364-76.
- Marescal, O. & Cheeseman, I. M. 2020. Cellular Mechanisms and Regulation of Quiescence. *Dev Cell*, 55, 259-271.
- Marguerat, S., Schmidt, A., Codlin, S., Chen, W., Aebersold, R. & Bähler, J. 2012. Quantitative analysis of fission yeast transcriptomes and proteomes in proliferating and quiescent cells. *Cell*, 151, 671-83.
- Markaki, Y., Gan Chong, J., Wang, Y., Jacobson, E. C., Luong, C., Tan, S. Y. X., Jachowicz, J. W., Strehle, M., Maestrini, D., Banerjee, A. K., Mistry, B. A., Dror, I., Dossin, F., Schöneberg, J., Heard, E., Guttman, M., Chou, T. & Plath, K. 2021. Xist nucleates local protein gradients to propagate silencing across the X chromosome. *Cell*, 184, 6174-6192.e32.
- Marqués-Torrejón, M., Williams, C. A. C., Southgate, B., Alfazema, N., Clements, M. P., Garcia-Diaz, C., Blin, C., Arranz-Emparan, N., Fraser, J., Gammoh, N., Parrinello, S. & Pollard, S. M. 2021. LRIG1 is a gatekeeper to exit from quiescence in adult neural stem cells. *Nat Commun*, 12, 2594.
- Martin, M. 2012. Cutadapt removes adapter sequences from high-throughput sequencing reads. *Bioinformatics in Action*, 17, 10-12.
- Massagué, J. 2004. G1 cell-cycle control and cancer. *Nature*, 432, 298-306.
- McKnight, J. N., Boerma, J. W., Breeden, L. L. & Tsukiyama, T. 2015. Global Promoter Targeting of a Conserved Lysine Deacetylase for Transcriptional Shutoff during Quiescence Entry. *Mol Cell*, 59, 732-43.
- Mehta, I. S., Amira, M., Harvey, A. J. & Bridger, J. M. 2010. Rapid chromosome territory relocation by nuclear motor activity in response to serum removal in primary human fibroblasts. *Genome Biol*, 11, R5.
- Mitra, M., Ho, L. D. & Collier, H. A. 2018. An In Vitro Model of Cellular Quiescence in Primary Human Dermal Fibroblasts. *Methods Mol Biol*, 1686, 27-47.
- Mitsui, K., Matsumoto, A., Ohtsuka, S., Ohtsubo, M. & Yoshimura, A. 1999. Cloning and characterization of a novel p21(Cip1/Waf1)-interacting zinc finger protein, ciz1. *Biochem Biophys Res Commun*, 264, 457-64.
- Mohammad, F. & Helin, K. 2017. Oncohistones: drivers of pediatric cancers. *Genes Dev*, 31, 2313-2324.
- Mohrin, M., Bourke, E., Alexander, D., Warr, M. R., Barry-Holson, K., Le Beau, M. M., Morrison, C. G. & Passegué, E. 2010. Hematopoietic stem cell quiescence promotes error-prone DNA repair and mutagenesis. *Cell Stem Cell*, 7, 174-85.
- Morgan, D. O. 1997. Cyclin-dependent kinases: engines, clocks, and microprocessors. *Annu Rev Cell Dev Biol*, 13, 261-91.
- Moser, J., Miller, I., Carter, D. & Spencer, S. L. 2018. Control of the Restriction Point by Rb and p21. *Proc Natl Acad Sci U S A*, 115, E8219-E8227.
- Müller, G. A. & Engeland, K. 2010. The central role of CDE/CHR promoter elements in the regulation of cell cycle-dependent gene transcription. *FEBS J*, 277, 877-93.
- Müller, G. A., Wintsche, A., Stangner, K., Prohaska, S. J., Stadler, P. F. & Engeland, K. 2014. The CHR site: definition and genome-wide identification of a cell cycle transcriptional element. *Nucleic Acids Res*, 42, 10331-50.

- Nasa, I. & Kettenbach, A. N. 2018. Coordination of Protein Kinase and Phosphoprotein Phosphatase Activities in Mitosis. *Front Cell Dev Biol*, 6, 30.
- Nencioni, A., Caffa, I., Cortellino, S. & Longo, V. D. 2018. Fasting and cancer: molecular mechanisms and clinical application. *Nat Rev Cancer*, 18, 707-719.
- Nepali, K. & Liou, J. P. 2021. Recent developments in epigenetic cancer therapeutics: clinical advancement and emerging trends. *J Biomed Sci*, 28, 27.
- Nishibe, R., Watanabe, W., Ueda, T., Yamasaki, N., Koller, R., Wolff, L., Honda, Z., Ohtsubo, M. & Honda, H. 2013. CIZ1, a p21Cip1/Waf1-interacting protein, functions as a tumor suppressor in vivo. *FEBS Lett*, 587, 1529-35.
- Oda, H., Okamoto, I., Murphy, N., Chu, J., Price, S. M., Shen, M. M., Torres-Padilla, M. E., Heard, E. & Reinberg, D. 2009. Monomethylation of histone H4-lysine 20 is involved in chromosome structure and stability and is essential for mouse development. *Mol Cell Biol*, 29, 2278-95.
- Ono, T., Fang, Y., Spector, D. L. & Hirano, T. 2004. Spatial and temporal regulation of Condensins I and II in mitotic chromosome assembly in human cells. *Mol Biol Cell*, 15, 3296-308.
- Oya, E., Durand-Dubief, M., Cohen, A., Maksimov, V., Schurra, C., Nakayama, J. I., Weisman, R., Arcangioli, B. & Ekwall, K. 2019. Leo1 is essential for the dynamic regulation of heterochromatin and gene expression during cellular quiescence. *Epigenetics Chromatin*, 12, 45.
- Pack, L. R., Daigh, L. H. & Meyer, T. 2019. Putting the brakes on the cell cycle: mechanisms of cellular growth arrest. *Curr Opin Cell Biol*, 60, 106-113.
- Pardee, A. B. 1974. A restriction point for control of normal animal cell proliferation. *Proc Natl Acad Sci U S A*, 71, 1286-90.
- Paull, T. T. 2015. Mechanisms of ATM Activation. *Annu Rev Biochem*, 84, 711-38.
- Pauzaite, T., Thacker, U., Tollitt, J. & Copeland, N. A. 2016. Emerging Roles for Ciz1 in Cell Cycle Regulation and as a Driver of Tumorigenesis. *Biomolecules*, 7.
- Pavletich, N. P. 1999. Mechanisms of cyclin-dependent kinase regulation: structures of Cdk, their cyclin activators, and Cip and INK4 inhibitors. *J Mol Biol*, 287, 821-8.
- Pearl Mizrahi, S., Gefen, O., Simon, I. & Balaban, N. Q. 2016. Persistence to anti-cancer treatments in the stationary to proliferating transition. *Cell Cycle*, 15, 3442-3453.
- Pesavento, J. J., Yang, H., Kelleher, N. L. & Mizzen, C. A. 2008. Certain and progressive methylation of histone H4 at lysine 20 during the cell cycle. *Mol Cell Biol*, 28, 468-86.
- Pietras, E. M., Warr, M. R. & Passegué, E. 2011. Cell cycle regulation in hematopoietic stem cells. *J Cell Biol*, 195, 709-20.
- Qiu, L., Hu, X., Jing, Q., Zeng, X., Chan, K. M. & Han, J. 2018. Mechanism of cancer: Oncohistones in action. *J Genet Genomics*, 45, 227-236.
- Rahman, F. A., Ainscough, J. F.-X., Copeland, N. & Coverley, D. 2007. Cancer-associated missplicing of exon 4 influences the subnuclear distribution of the DNA replication factor Ciz1. *Human Mutation*, 28, 993-1004.
- Rahman, F. A., Aziz, N. & Coverley, D. 2010. Differential detection of alternatively spliced variants of Ciz1 in normal and cancer cells using a custom exon-junction microarray. *BMC Cancer*, 10, 482.

- Ramadan, K., Bruderer, R., Spiga, F. M., Popp, O., Baur, T., Gotta, M. & Meyer, H. H. 2007. Cdc48/p97 promotes reformation of the nucleus by extracting the kinase Aurora B from chromatin. *Nature*, 450, 1258-62.
- Rawlings, J. S., Gatzka, M., Thomas, P. G. & Ihle, J. N. 2011. Chromatin condensation via the condensin II complex is required for peripheral T-cell quiescence. *EMBO J*, 30, 263-76.
- Reithmeier, A., Panizza, E., Krumpel, M., Orre, L. M., Branca, R. M. M., Lehtiö, J., Ek-Rylander, B. & Andersson, G. 2017. Tartrate-resistant acid phosphatase (TRAP/ACP5) promotes metastasis-related properties via TGF $\beta$ 2/T $\beta$ R and CD44 in MDA-MB-231 breast cancer cells. *BMC Cancer*, 17, 650.
- Ricard, N., Bailly, S., Guignabert, C. & Simons, M. 2021. The quiescent endothelium: signalling pathways regulating organ-specific endothelial normalcy. *Nat Rev Cardiol*, 18, 565-580.
- Ridings-Figueroa, R., Stewart, E. R., Nesterova, T. B., Coker, H., Pintacuda, G., Godwin, J., Wilson, R., Haslam, A., Lilley, F., Ruigrok, R., Bageghni, S. A., Albadrani, G., Mansfield, W., Roulson, J. A., Brockdorff, N., Ainscough, J. F. X. & Coverley, D. 2017. The nuclear matrix protein CIZ1 facilitates localization of Xist RNA to the inactive X-chromosome territory. *Genes Dev*, 31, 876-888.
- Roche, B., Arcangioli, B. & Martienssen, R. 2017. Transcriptional reprogramming in cellular quiescence. *RNA Biol*, 14, 843-853.
- Sadasivam, S. & DeCaprio, J. A. 2013. The DREAM complex: master coordinator of cell cycle-dependent gene expression. *Nat Rev Cancer*, 13, 585-95.
- Schafer, K. A. 1998. The cell cycle: a review. *Vet Pathol*, 35, 461-78.
- Schindelin, J., Arganda-Carreras, I., Frise, E., Kaynig, V., Longair, M., Pietzsch, T., Preibisch, S., Rueden, C., Saalfeld, S., Schmid, B., Tinevez, J. Y., White, D. J., Hartenstein, V., Eliceiri, K., Tomancak, P. & Cardona, A. 2012. Fiji: an open-source platform for biological-image analysis. *Nat Methods*, 9, 676-82.
- Schotta, G., Lachner, M., Sarma, K., Ebert, A., Sengupta, R., Reuter, G., Reinberg, D. & Jenuwein, T. 2004. A silencing pathway to induce H3-K9 and H4-K20 trimethylation at constitutive heterochromatin. *Genes Dev*, 18, 1251-62.
- Sherr, C. J. & Roberts, J. M. 2004. Living with or without cyclins and cyclin-dependent kinases. *Genes Dev*, 18, 2699-711.
- Shin, J. J., Schroder, M. S., Caiado, F., Wyman, S. K., Bray, N. L., Bordi, M., Dewitt, M. A., Vu, J. T., Kim, W. T., Hockemeyer, D., Manz, M. G. & Corn, J. E. 2020. Controlled Cycling and Quiescence Enables Efficient HDR in Engraftment-Enriched Adult Hematopoietic Stem and Progenitor Cells. *Cell Rep*, 32, 108093.
- Shin, Y. & Brangwynne, C. P. 2017. Liquid phase condensation in cell physiology and disease. *Science*, 357.
- Shoaib, M., Walter, D., Gillespie, P. J., Izard, F., Fahrenkrog, B., Lleres, D., Lerdrup, M., Johansen, J. V., Hansen, K., Julien, E., Blow, J. J. & Sørensen, C. S. 2018. Histone H4K20 methylation mediated chromatin compaction threshold ensures genome integrity by limiting DNA replication licensing. *Nat Commun*, 9, 3704.
- Sofi, S., Williamson, L., Turvey, G. L., Scoynes, C., Hirst, C., Godwin, J., Brockdorff, N., Ainscough, J. & Coverley, D. 2022. Prion-like domains drive CIZ1 assembly formation at the inactive X chromosome. *J Cell Biol*, 221.

- Spencer, S. L., Cappell, S. D., Tsai, F. C., Overton, K. W., Wang, C. L. & Meyer, T. 2013. The proliferation-quiescence decision is controlled by a bifurcation in CDK2 activity at mitotic exit. *Cell*, 155, 369-83.
- Stewart, E. R. & Coverley, D. 2018. Visualization of Hidden Epitopes at the Inactive X Chromosome. *Methods Mol Biol*, 1861, 103-112.
- Stewart, E. R., Turner, R. M. L., Newling, K., Ridings-Figueroa, R., Scott, V., Ashton, P. D., Ainscough, J. F. X. & Coverley, D. 2019. Maintenance of epigenetic landscape requires CIZ1 and is corrupted in differentiated fibroblasts in long-term culture. *Nat Commun*, 10, 460.
- Subramanian, A., Tamayo, P., Mootha, V. K., Mukherjee, S., Ebert, B. L., Gillette, M. A., Paulovich, A., Pomeroy, S. L., Golub, T. R., Lander, E. S. & Mesirov, J. P. 2005. Gene set enrichment analysis: a knowledge-based approach for interpreting genome-wide expression profiles. *Proc Natl Acad Sci U S A*, 102, 15545-50.
- Suh, E. J., Remillard, M. Y., Legesse-Miller, A., Johnson, E. L., Lemons, J. M., Chapman, T. R., Forman, J. J., Kojima, M., Silberman, E. S. & Collier, H. A. 2012. A microRNA network regulates proliferative timing and extracellular matrix synthesis during cellular quiescence in fibroblasts. *Genome Biol*, 13, R121.
- Sun, G., Ding, X. A., Argaw, Y., Guo, X. & Montell, D. J. 2020. Akt1 and dCIZ1 promote cell survival from apoptotic caspase activation during regeneration and oncogenic overgrowth. *Nat Commun*, 11, 5726.
- Sutcu, H. H. & Ricchetti, M. 2018. Loss of heterogeneity, quiescence, and differentiation in muscle stem cells. *Stem Cell Investig*, 5, 9.
- Swygert, S. G., Kim, S., Wu, X., Fu, T., Hsieh, T. H., Rando, O. J., Eisenman, R. N., Shendure, J., McKnight, J. N. & Tsukiyama, T. 2019. Condensin-Dependent Chromatin Compaction Represses Transcription Globally during Quiescence. *Mol Cell*, 73, 533-546.e4.
- Swygert, S. G., Lin, D., Portillo-Ledesma, S., Lin, P. Y., Hunt, D. R., Kao, C. F., Schlick, T., Noble, W. S. & Tsukiyama, T. 2021. Local chromatin fiber folding represses transcription and loop extrusion in quiescent cells. *Elife*, 10.
- Takata, H., Hanafusa, T., Mori, T., Shimura, M., Iida, Y., Ishikawa, K., Yoshikawa, K., Yoshikawa, Y. & Maeshima, K. 2013. Chromatin compaction protects genomic DNA from radiation damage. *PLoS One*, 8, e75622.
- Takeo, K., Tanaka, R., Miyaji, M. & Nishimura, K. 1995. Unbudded G2 as well as G1 arrest in the stationary phase of the basidiomycetous yeast *Cryptococcus neoformans*. *FEMS Microbiol Lett*, 129, 231-5.
- Terakawa, T., Bisht, S., Eeftens, J. M., Dekker, C., Haering, C. H. & Greene, E. C. 2017. The condensin complex is a mechanochemical motor that translocates along DNA. *Science*, 358, 672-676.
- Thacker, U., Pauzaite, T., Tollitt, J., Twardowska, M., Harrison, C., Dowle, A., Coverley, D. & Copeland, N. A. 2020. Identification of DHX9 as a cell cycle regulated nucleolar recruitment factor for CIZ1. *Sci Rep*, 10, 18103.
- Tjalsma, S. J. D., Hori, M., Sato, Y., Bousard, A., Ohi, A., Raposo, A. C., Roensch, J., Le Saux, A., Nogami, J., Maehara, K., Kujirai, T., Handa, T., Bagés-Arnal, S., Ohkawa, Y., Kurumizaka, H., da Rocha, S. T., Żylicz, J. J., Kimura, H. & Heard, E. 2021. H4K20me1 and H3K27me3 are concurrently loaded onto the inactive X chromosome but dispensable for inducing gene silencing. *EMBO Rep*, 22, e51989.

- Tokuyasu, K., Madden, S. C. & Zeldis, L. J. 1968. Fine structural alterations of interphase nuclei of lymphocytes stimulated to growth activity in vitro. *J Cell Biol*, 39, 630-60.
- Topacio, B. R., Zatulovskiy, E., Cristea, S., Xie, S., Tambo, C. S., Rubin, S. M., Sage, J., Kõivomägi, M. & Skotheim, J. M. 2019. Cyclin D-Cdk4,6 Drives Cell-Cycle Progression via the Retinoblastoma Protein's C-Terminal Helix. *Mol Cell*, 74, 758-770.e4.
- Trapnell, C., Roberts, A., Goff, L., Pertea, G., Kim, D., Kelley, D. R., Pimentel, H., Salzberg, S. L., Rinn, J. L. & Pachter, L. 2012. Differential gene and transcript expression analysis of RNA-seq experiments with TopHat and Cufflinks. *Nat Protoc*, 7, 562-78.
- Trojer, P., Li, G., Sims, R. J., Vaquero, A., Kalakonda, N., Bocconi, P., Lee, D., Erdjument-Bromage, H., Tempst, P., Nimer, S. D., Wang, Y. H. & Reinberg, D. 2007. L3MBTL1, a histone-methylation-dependent chromatin lock. *Cell*, 129, 915-28.
- Truglio, J. J., Rhau, B., Croteau, D. L., Wang, L., Skorvaga, M., Karakas, E., DellaVecchia, M. J., Wang, H., Van Houten, B. & Kisker, C. 2005. Structural insights into the first incision reaction during nucleotide excision repair. *EMBO J*, 24, 885-94.
- Uhlmann, F. 2016. SMC complexes: from DNA to chromosomes. *Nat Rev Mol Cell Biol*, 17, 399-412.
- Vandiver, A. R., Idrizi, A., Rizzardi, L., Feinberg, A. P. & Hansen, K. D. 2015. DNA methylation is stable during replication and cell cycle arrest. *Sci Rep*, 5, 17911.
- Volkova, N. V., Meier, B., González-Huici, V., Bertolini, S., Gonzalez, S., Vöhringer, H., Abascal, F., Martincorena, I., Campbell, P. J., Gartner, A. & Gerstung, M. 2020. Mutational signatures are jointly shaped by DNA damage and repair. *Nat Commun*, 11, 2169.
- Wade, R. H. 2009. On and around microtubules: an overview. *Mol Biotechnol*, 43, 177-91.
- Wang, D. Q., Wang, K., Yan, D. W., Liu, J., Wang, B., Li, M. X., Wang, X. W., Liu, J., Peng, Z. H., Li, G. X. & Yu, Z. H. 2014. Ciz1 is a novel predictor of survival in human colon cancer. *Exp Biol Med (Maywood)*, 239, 862-870.
- Warder, D. E. & Keherly, M. J. 2003. Ciz1, Cip1 interacting zinc finger protein 1 binds the consensus DNA sequence ARYSR(0-2)YYAC. *Journal of Biomedical Science*, 10, 406-417.
- Weyburne, E. & Bosco, G. 2021. Cancer-associated mutations in the condensin II subunit CAPH2 cause genomic instability through telomere dysfunction and anaphase chromosome bridges. *J Cell Physiol*, 236, 3579-3598.
- Wilson, R. 2013. *Organisation of the initiation of DNA replication*. PhD, York University.
- Wilson, R. H., Hesketh, E. L. & Coverley, D. 2016. Preparation of the Nuclear Matrix for Parallel Microscopy and Biochemical Analyses. *Cold Spring Harb Protoc*, 2016, pdb.prot083758.
- Woodward, J., Taylor, G. C., Soares, D. C., Boyle, S., Sie, D., Read, D., Chathoth, K., Vukovic, M., Tarrats, N., Jamieson, D., Campbell, K. J., Blyth, K., Acosta, J. C., Ylstra, B., Arends, M. J., Kranc, K. R., Jackson, A. P., Bickmore, W. A. & Wood, A. J. 2016. Condensin II mutation causes T-cell lymphoma through tissue-specific genome instability. *Genes Dev*, 30, 2173-2186.

- Wu, J., Lei, L., Gu, D., Liu, H. & Wang, S. 2016. CIZ1 is upregulated in hepatocellular carcinoma and promotes the growth and migration of the cancer cells. *Tumour Biol*, 37, 4735-42.
- Wu, J., Qiao, K., Du, Y., Zhang, X., Cheng, H., Peng, L. & Guo, Z. 2020. Downregulation of histone methyltransferase SET8 inhibits progression of hepatocellular carcinoma. *Sci Rep*, 10, 4490.
- Xiao, J., Vemula, S. R. & LeDoux, M. S. 2014. Recent advances in the genetics of dystonia. *Curr Neurol Neurosci Rep*, 14, 462.
- Yao, G. 2014. Modelling mammalian cellular quiescence. *Interface Focus*, 4, 20130074.
- Yao, G., Lee, T. J., Mori, S., Nevins, J. R. & You, L. 2008. A bistable Rb-E2F switch underlies the restriction point. *Nat Cell Biol*, 10, 476-82.
- Yin, J., Wang, C., Tang, X., Sun, H., Shao, Q., Yang, X. & Qu, X. 2013. CIZ1 regulates the proliferation, cycle distribution and colony formation of RKO human colorectal cancer cells. *Mol Med Rep*, 8, 1630-4.
- Young, C. P., Hillyer, C., Hokamp, K., Fitzpatrick, D. J., Konstantinov, N. K., Welty, J. S., Ness, S. A., Werner-Washburne, M., Fleming, A. B. & Osley, M. A. 2017. Distinct histone methylation and transcription profiles are established during the development of cellular quiescence in yeast. *BMC Genomics*, 18, 107.
- Yuen, K. C. & Gerton, J. L. 2018. Taking cohesin and condensin in context. *PLoS Genet*, 14, e1007118.
- Zhou, B. B. & Elledge, S. J. 2000. The DNA damage response: putting checkpoints in perspective. *Nature*, 408, 433-9.
- Zink, D., Fischer, A. H. & Nickerson, J. A. 2004. Nuclear structure in cancer cells. *Nat Rev Cancer*, 4, 677-87.